

British Columbia Geological Survey
Ministry of Energy, Mines and Natural Gas
www.empr.gov.bc.ca/geology

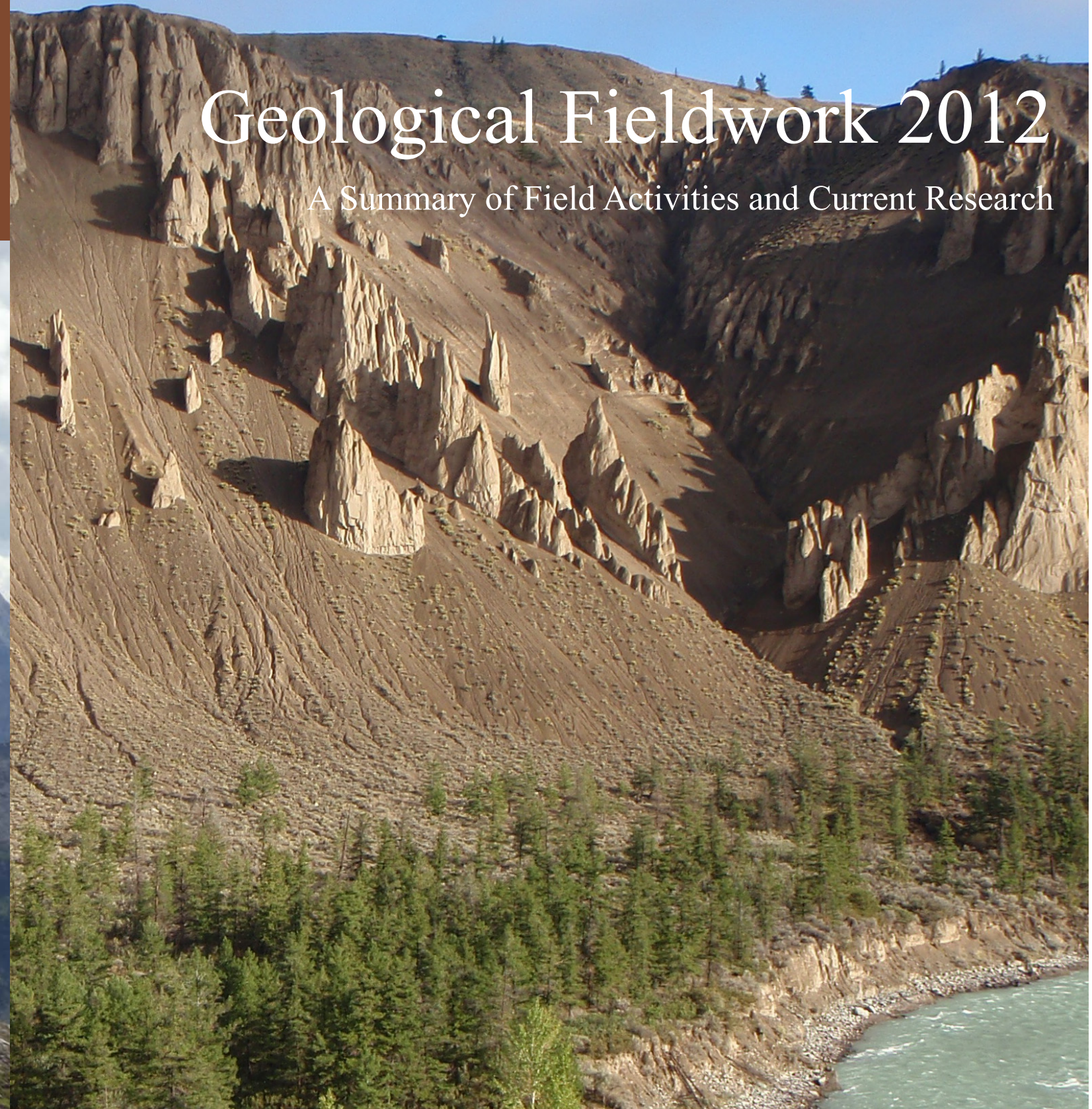


Ministry of
Energy, Mines
and Natural Gas



Geological Fieldwork 2012

A Summary of Field Activities and Current Research



B.C. Ministry of Energy, Mines and Natural Gas, British Columbia Geological Survey Paper 2013-1



Ministry of
Energy, Mines
and Natural Gas



Geological Fieldwork 2012

A Summary of Field Activities and Current Research

Ministry of Energy, Mines and Natural Gas
British Columbia Geological Survey

Paper 2013-1

Ministry of Energy, Mines and Natural Gas

Mines and Mineral Resources Division

British Columbia Geological Survey

Recommended citation format for individual papers:

Nelson, J., Diakow, L., van Staal, C. and Chipley, D., 2013. Ordovician volcanogenic sulphides in the southern Alexander terrane, coastal NW British Columbia: geology, Pb isotopic signature, and a case for correlation with Appalachian and Scandinavian deposits. In: Geological Fieldwork 2012, British Columbia Ministry of Energy, Mines and Natural Gas, British Columbia Geological Survey Paper 2013-1, pp. 13-33.

Front Cover: Hoodoos from erosion of Quaternary glaciolacustrine deposits on the north side of the Chilcotin River, near Farwell canyon, in southern British Columbia. Photo by Paul Schiarizza.

Back Cover: Cambrian to Middle Silurian carbonate rocks of the McKay Group and Beaverfoot Formation at Chrysler Peak (foreground), east of Kimberley, in the western Rocky Mountains. Photo by Fiona Katay.

This publication is available, free of charge, from the British Columbia Geological Survey website:
<http://www.empr.gov.bc.ca/Mining/Geoscience/PublicationsCatalogue/Fieldwork>

British Columbia Cataloguing in Publication Data

Main entry under title:

Geological Fieldwork: - 1974 -

Annual.

Issuing body varies

Vols. for 1978-1996 issued in series: Paper / British Columbia. Ministry of Energy, Mines and Petroleum Resources; vols. for 1997 - 1998, Paper / British Columbia. Ministry of Employment and Investment; vols. for 1999-2004, Paper / British Columbia. Ministry of Energy and Mines; vols. for 2005-2009, Paper / British Columbia. Ministry of Energy, Mines and Petroleum Resources; vols. for 2010, Paper / British Columbia. Ministry of Forests, Mines and Lands; vols. for 2011, Paper / British Columbia. Ministry of Energy and Mines; vols. for 2012- , Paper / British Columbia. Ministry of Energy, Mines and Natural Gas.

Includes Bibliographical references.

ISSN 0381-243X=Geological Fieldwork

1. Geology - British Columbia - Periodicals. 2. Mines and mineral resources - British Columbia - Periodicals. 3. Geology - Fieldwork - Periodicals. 4. Geology, Economic - British Columbia - Periodicals. 5. British Columbia. Geological Survey Branch - Periodicals. I. British Columbia. Geological Division. II. British Columbia. Geological Survey Branch. III. British Columbia. Geological Survey Branch. IV. British Columbia. Dept. of Mines and Petroleum Resources. V. British Columbia. Ministry of Energy, Mines and Petroleum Resources. VI. British Columbia. Ministry of Employment and Investment. VII. British Columbia Ministry of Energy and Mines. VIII. Series: Paper (British Columbia. Ministry of Energy, Mines and Petroleum Resources). IX. Series: Paper (British Columbia. Ministry of Employment and Investment). X. Series: Paper (British Columbia Ministry of Energy and Mines). XI. Series: Paper (British Columbia Ministry of Energy, Mines and Petroleum Resources). XII. Series: Paper (British Columbia Ministry of Forests, Mines and Lands). XIII. Series: Paper (British Columbia Ministry of Energy and Mines). XIV. Series: Paper (British Columbia Ministry of Energy, Mines and Natural Gas).

QE187.46 622.1'09711 C76-083084-3 (Rev.)

Victoria
British Columbia
Canada

January 2013

Foreword

Geological Fieldwork 2012

This is the thirty-eighth edition of **Geological Fieldwork**, a volume of peer-reviewed papers that present the results of geological research conducted by the **British Columbia Geological Survey (BCGS)** and its partners in 2012. The papers address different aspects of British Columbia's geology, highlighting the enormous mineral wealth of the Province. The BCGS helps to unlock this mineral wealth by providing comprehensive, objective, and up-to-date geoscience information, advice, and knowledge to the minerals industry. The annual Geological Fieldwork publication is an important way that the BCGS delivers this help.

In late 2012, the Government of British Columbia expanded the name of the Ministry of Energy and Mines (MEM) to the Ministry of Energy, Mines and Natural Gas (MEMNG). This expansion was accompanied by the return of some employees from the Ministry of Forests, Lands and Natural Resource Operations (MFLNRO). Importantly for the BCGS, the five geologists that deliver the Regional Geologists Program rejoined the Mines and Mineral Resources Division in MEMNG.

British Columbia Geological Survey activity highlights

Research

- Three “Edges” field mapping projects in their 4th and final years were completed. These projects were delivered with the Geological Survey of Canada (GSC) under the auspices of the Geo-mapping for Energy and Minerals program (2009-2013).
- Fieldwork continued on four projects, as part of the GSC's Targeted Geoscience Initiative program (TGI4).
- BCGS geologists published seven Open Files, nine Geofiles, and ten external papers.

Outreach at conferences and workshops

- Survey geologists presented at conferences and workshops including Roundup, PDAC, KEG, GACMAC, CIM, Goldschmidt, Minerals South, Yukon Geoscience Forum, Minerals North, and the Smithers Rock Talk.
- The BCGS co-hosted the 38th annual Cordilleran Tectonics Workshop in Victoria. It was attended by 110 scientists who delivered 50 talks and posters.
- The BCGS Open House was held in Victoria and attracted over 130 geoscientists.
- Staff of the BC Mineral Development Office in Vancouver hosted various investor delegations and participated in the Asia Investment Mission to China and Korea, the Pan-Canadian Mining Session in London (England), and the China Mining Conference in Beijing.

Data archiving and access

- Over 870 heritage COALFILE paper documents were inventoried to locate missing components and ensure complete online access.
- The Property File database now features more than 34 270 documents online.
- MINFILE continues to expand: over 1560 occurrences were updated and 1035 occurrences were added.

Renewal

- Six permanent and four temporary positions were filled.
- The Survey's in-house geochemical laboratory was completely refurbished with new rock saws, fume hoods, a Linkam THMS 600 fluid inclusion heating/freezing stage, and a portable bench-top Thermo Scientific Niton XRF analyzer.
- A new rock storage facility and archive was constructed to accommodate over 600,000 geochemical pulps and rock and soil samples.

Awards

- Dr. Ray Lett (BCGS Emeritus Scientist) was a finalist for a 2012 “Premier's Award”, in the Legacy category.
- Thirteen past and present BCGS geoscientists who worked on creating MapPlace were finalists for a 2012 “Premier's Award”, in the Innovation category.

Stephen M. Rowins
Chief Geologist & Executive Director
British Columbia Geological Survey

Table of Contents

Hickin, A.S., Jones, L.D., Rowins, S.M. and Madu, B.: British Columbia Geological Survey Activities in 2012	1
Nelson, JoAnne, Diakow, Larry, van Staal, Cees and Chipley, Don: Ordovician volcanogenic sulphides in the southern Alexander terrane, coastal NW British Columbia: geology, Pb isotopic signature, and a case for correlation with Appalachian and Scandinavian deposits	13
Massey, N.W.D., Gabites, J.E. and Mortensen, J.K.: LA-ICP-MS geochronology of the Greenwood gabbro, Knob Hill complex, southern Okanagan, British Columbia	35
Massey, N.W.D. and Dostal, J.: Geochemistry of metabasalts from the Knob Hill complex and Anarchist Group in the Paleozoic basement to southern Quesnellia	45
Schiarizza, Paul: The Wineglass assemblage, lower Chilcotin River, south-central British Columbia: Late Permian volcanic and plutonic rocks that correlate with the Kutcho assemblage of northern British Columbia	53
Logan, James M. and Mihalynuk, Mitchell G.: Bonaparte gold: another 195 Ma porphyry Au-Cu deposit in southern British Columbia?	71
Mihalynuk, Mitchell G. and Logan, James M.: Geological setting of Late Triassic porphyry Cu-Au mineralization at Miner Mountain, Princeton, southern British Columbia	81
Mihalynuk, Mitchell G. and Logan, James M.: Geological setting of Late Triassic porphyry Cu-Au mineralization at the Dillard Creek property near Merritt, southern British Columbia	97
Zagorevski, A., Dziawa, C., Friedman, R.M. and Mihalynuk, M.G.: Geology, U-Pb geochronology, and geochemistry of the Miocene Pheno Mountain complex, Hoodoo Mountain area, British Columbia	115
Simandl, G.J., Reid, H.M. and Ferri, F.: Geological setting of the Lonnie niobium deposit, British Columbia, Canada	127
Trofanenko, J., Williams-Jones, A.E., Simandl, G.J. and Reid, H.M.: The Riddle Creek prospect, an unusual example of Sr-Ba-REE-F mineralization outside the Alkaline Province, British Columbia, Canada	139

British Columbia Geological Survey Activities in 2012

A.S. Hickin^{1,a}, L.D. Jones¹, S.M. Rowins¹ and B. Madu²

¹ British Columbia Geological Survey, Ministry of Energy, Mines and Natural Gas, Victoria, BC, V8W 9N3

² British Columbia Geological Survey, Ministry of Energy, Mines and Natural Gas, Vancouver, BC, V6Z 2G3

^a corresponding author: Adrian.Hickin@gov.bc.ca

Recommended citation: Hickin, A.S., Jones, L.D., Rowins, S.M. and Madu, B., 2013. British Columbia Geological Survey Activities in 2012. In: Geological Fieldwork 2012, British Columbia Ministry of Energy, Mines and Natural Gas, British Columbia Geological Survey Paper 2013-1, pp. 1-11.

Abstract

Established in 1895, the British Columbia Geological Survey (BCGS) maintains its tradition of providing geological data and expertise to diverse clients. In 2012, BCGS field geologists, in collaboration with geoscientists from industry, universities, and other government agencies: 1) completed projects to determine the evolution and mineral potential of terranes on the northwestern flank of the Cordillera (as part of the Geo-mapping for Energy and Minerals program, GEM-Edges); 2) continued investigating specialty metals, rare earth elements, and Ni-Cu-PGE-Cr ore systems (as part of the Targeted Geoscience Initiative, TGI4), working on compilations to better understand tectonic controls on Cordilleran metallogeny, and researching porphyry deposits, which constitute a significant part of British Columbia's mineral wealth; and 3) started studies evaluating the use of mineral and geochemical indicators for detecting buried porphyry-style mineralization in drift-covered areas (TGI4). Results from these research projects were published extensively in the provincial, national, and international literature. The BCGS continues its web-based archiving and public access function via its MapPlace portal, Property File, MINFILE, and ARIS databases, and collection of Survey publications, all of which are available free of charge. Staff renewal included hiring a geologist to rebuild capacity in coal geology and GIS experts to revise and enhance the digital geology map of the Province. The Survey's in-house geochemical laboratory was completely refurbished, and a new archive was constructed to house over 600,000 samples. Through technical marketing campaigns that highlighted the Province's mineral and coal endowment, geoscience expertise, geological knowledge, and business climate, the Mineral Development Office in Vancouver (MDO) promoted industry domestically and abroad. Through the work of five Regional Geologists, the MDO monitored and reported the year's exploration and mining activities. From a pool of 118 nominations submitted by 16 BC Public Service agencies representing 27,000 civil servants, BCGS Emeritus Scientist Dr. Ray Lett was selected as a finalist for a 2012 "Premier's Award" in the Legacy category, and thirteen past and present BCGS staff who contributed to developing MapPlace were selected in the Innovation category.

Keywords: British Columbia Geological Survey, Cordilleran geology, Cordilleran tectonics, provincial geoscience, federal-provincial agreements

1. Introduction

Founded in 1895, the British Columbia Geological Survey (BCGS) is the oldest scientific agency in British Columbia. A primary mandate of the BCGS is to provide objective geoscience expertise and data to government, industry, and the general public. This helps to create safe, thriving, and sustainable provincial mineral exploration and mining industries.

The BCGS maintains the flexibility to respond to changing priorities of government and changing market conditions driving the minerals industry. Organizational flexibility and expertise are reflected in a mix of short- and long-term, generally field-based, geoscience projects. The short-term projects typically last for one or two years, and focus on immediate industry needs. Such projects produce new and updated geological and geochemical maps, and generate new knowledge about specific commodities or mineral deposit types. Recent market interest in "hot" commodities (e.g., rare earth elements, metallurgical coal, copper) has led to renewed focus on the Province's rare earth element and coal potential, and a

re-examination of its many past-producing porphyry copper-gold mines and undeveloped deposits. Short-term projects are frequently completed through partnerships with industry, universities, and other public geoscience organizations. Longer term geoscience projects, ranging from two to five years, are typically collaborations with the Geological Survey of Canada (GSC). These projects generate fundamental geoscience knowledge, have a greater national focus, and are designed to achieve common strategic objectives of the federal and provincial governments. Recent long-term strategic partnerships include the GSC's Geo-mapping for Energy and Minerals (GEMs) program and the Targeted Geoscience Initiative program (TGI4). All geoscience products generated through these partnerships are made available online at no cost to the public via MapPlace, the internet portal of the BCGS. In 2012, the MapPlace team was selected for a "Premier's Award" in the Innovation category. These are the highest awards given to employees of the BC Public Service.

British Columbia's mineral exploration and mining industry performed well in 2012, despite the global

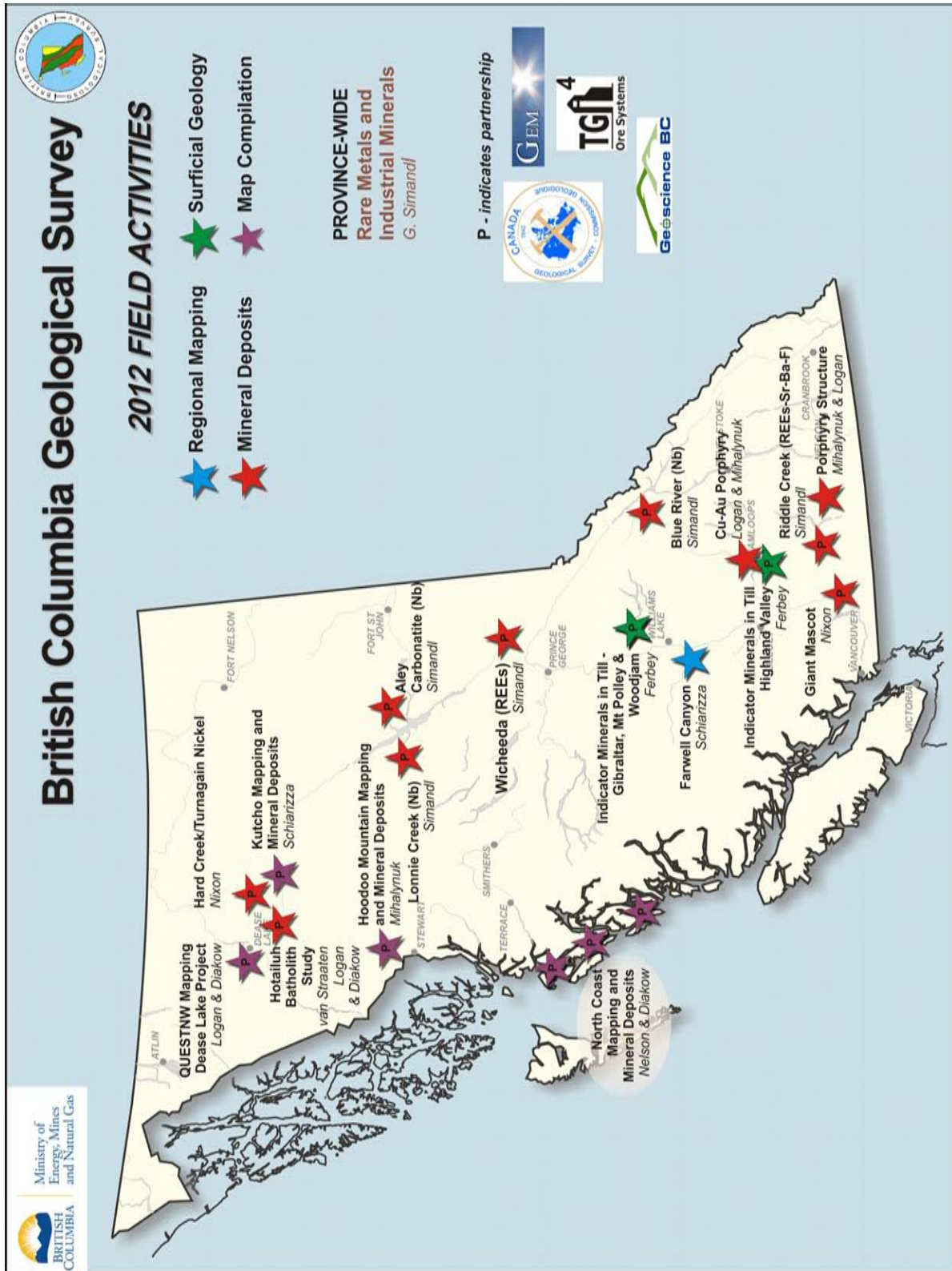


Fig. 1. British Columbia Geological Survey field activities in 2012.

economic slowdown that occurred mid-year. The total value of solid mineral production for 2012 was \$7.4 billion, and mineral exploration spending was \$680 million, up from the \$463 million spent in 2011. Core funding levels for the BCGS in 2012 remained similar to those in previous years. The BCGS continued its long and productive collaboration with the GSC by participating in seven joint projects in 2012. It was the fourth and final year for three GEMs “Edges” projects that targeted parts of northwestern and north-central British Columbia, where existing geological maps are either several decades out of date or at scales inadequate to evaluate mineral potential. Activity this year focused on data synthesis, write-up, and publication. A TGI4 “Specialty Metals” project that started in 2010 under the leadership of George Simandl continued in 2012. Its overall objective is to develop new exploration methods and technologies in the search for specialty metals. Another TGI4 project targeted Ni-Cu-PGE-Cr deposits associated with ultramafic intrusions in BC’s orogenic belts. These “orogenic” Ni-Cu-PGE-Cr deposits are poorly understood, and new models are needed. This initiative includes researchers from the BCGS, the GSC, and the University of British Columbia. Two new TGI4 projects in 2012 (Intrusion-Related Ore Systems) involved surficial mapping and till sampling for porphyry indicator minerals and bedrock mapping of regional structures in porphyry districts of central BC. As in past years, university students were employed as co-op interns and geoscience assistants to help deliver our field programs and improve our digital geoscience databases.

2. Cordilleran Geoscience Section

The Cordillera Geoscience Section collects, synthesizes, and interprets geological data, thereby creating new knowledge. We disseminate both raw and interpreted data to diverse clients through provincial, national, and international presentations and publications. Staffed by twelve full-time geologists with extensive knowledge of Cordilleran geoscience and particular expertise in regional mapping, tectonics, mineral deposits, rock and environmental geochemistry, Quaternary geology, and coal geology, much of the Section’s work is field based.

The Section partners in numerous provincial and inter-agency projects, many of which are multi-year initiatives (Fig. 1). In addition to the GEMs and TGI4 initiatives, the Section is also collaborating with Geoscience BC and organizing fieldtrips for the Society of Economic Geologists (SEG) Fall 2013 meeting in Whistler, BC. Provincial initiatives include updating the Provincial COALFILE database, revitalizing the Provincial geochemical laboratory, and reorganizing and cataloging the 600 000 geochemical and rock sample archive.

2.1. Projects 2012

2.1.1. GEM-Edges: Modeling the Evolution of the Northern Cordillera Resource Environment from the Edges of Exotic Terranes

The GEM-Edges Project is multi-year geological mapping collaboration between the Government of Canada, the Province of British Columbia, Yukon Territory, Geoscience BC, the United States Geological Survey and the Alaska Divisions of the Geological and Geophysical surveys. Initiated in 2009, the project included three field seasons in north-central and northwestern British Columbia and is currently in its final year. It consists of several components, including the North Coast Region Mapping and Metallogeny Project, Iskut River/Hoodoo Mountain Project, and the Kutcho Project, all of which were directed at determining the geological framework and evaluating the mineral potential of the outer terranes of the northern Cordillera.

2.1.1.1. The North Coast Region Mapping and Metallogeny Project

The North Coast component of Edges focused on regional geological mapping of the southern part of the Alexander terrane along the north coast of British Columbia, between Bella Coola and Prince Rupert. This is an area known to host several volcanogenic massive sulphide (VMS) and mesothermal Au deposits. JoAnne Nelson and Larry Diakow compiled and synthesized three field seasons (2009-2011) of data, creating a 1:150 000-scale geological map (Fig. 2) that will be published separately and integrated into the online digital geology of British Columbia atlas. Building on discoveries reported in previous Geological Fieldwork articles, Nelson et al., (this volume) link Ordovician VMS deposits in the Alexander terrane to those of the Caledonides and Appalachians, including deposits in New Brunswick, Newfoundland, Quebec, and Norway.



Fig. 2. Larry Diakow with the first paper draft of the North Coast Open File map (to be released in 2013).

2.1.1.2. Iskut River/Hoodoo Mountain Project

Mitch Mihalynuk and Jim Logan (BCGS) and Alex Zagorevski (GSC) collaborated on the Iskut River/Hoodoo Mountain component of the Edges

partnership, in the region between the Galore Creek porphyry Cu-Au camp and the past-producing Bronson Au camp on the Iskut River. Receding snow and glaciers in the area have uncovered extensive sections of bimodal Carboniferous volcanic rocks with VMS mineralization, and Late Triassic feldspar porphyry intrusions with copper mineralization. Fieldwork was completed in 2011, but geochronological and geochemical studies are ongoing, as aids to map compilation and, ultimately, mineral exploration. In this volume, Zagorevski et al., report a Miocene U-Pb zircon crystallization age (7.78 ± 0.01 Ma) for the Pheno Mountain volcanic complex (discovered by Mihalynuk et al., 2012) supporting inclusion of the complex as part of the Neogene to Quaternary Northern Cordilleran Volcanic Province. Digital geological maps at 1:50 000 scale of 104B/14E and 14W, are being prepared for anticipated release in 2013.

2.1.1.3. Kutcho Project, Wineglass Assemblage

The Kutcho Project was a two-year mapping study completed in 2011 by Paul Schiarizza as part of the Edges Project and in partnership with Kutcho Mining Corporation. This project was directed at gaining a better understanding of the Permo-Triassic Kutcho assemblage, which hosts the Kutcho Creek VMS deposit. Bedrock mapping was completed in 2011 and was released as Open File map 2012-08 (see section 4.2.1 below). Paul's 2012 activities built on his experience in the Sitlika assemblage and work at Kutcho Creek to examine the Wineglass assemblage in the lower reaches of the Chilcotin River, southwest of Williams Lake (Schiarizza, this volume). He concludes that the Wineglass assemblage correlates with the Kutcho assemblage and the volcanic unit of the Sitlika assemblage, on the basis of a remarkable similarity in lithologic components, overlapping ages, similar structural relationships to Cache Creek terrane, and similar unconformable relationships with overlying Upper Triassic-Jurassic sedimentary rocks.

2.1.2. Specialty Metals (TG14)

George Simandl is leading a BCGS-GSC collaboration on a multi-year national and Province-wide study of specialty metals and rare earth elements. Specialty metals are uncommon, nonferrous metals used in small quantities (typically <150 000 tonnes/year) or that are mined from geographically restricted areas. The Specialty Metals Program started in 2010 and will continue until 2015 with two major components: 1) reviewing ore deposits and their mineral economics in Canada; and 2) developing techniques to guide exploration towards ore-grade zones in host deposits. The project is expected to help the Canadian exploration and mining industry be more effective at locating and developing these strategic resources. A number of publications were released in 2012 (see section 4.2. below); the most recent studies focus on unusual Sr-Ba-REE-F mineralization in the Okanagan Valley, well beyond the limits of the British Columbia alkaline province, at the Riddle Creek prospect (Trofanenko et al.,

this volume) and the geological setting of the Lonnie Nb deposit in north-central British Columbia (Simandl et al., this volume).

2.1.3. Till Porphyry Indicator Mineral Study (TG14)

In 2012, Travis Ferbey initiated a field program to develop geochemical and mineralogical methods for detecting buried porphyry-style mineralization in drift-covered areas (Fig. 3). Carried out in collaboration with colleagues at the GSC, and as part of the Till Porphyry Indicator Mineral Study, this investigation is part of the GSC's Intrusion Related Ore Systems TG14 Program, scheduled for completion in 2015. The study is using the trace element compositions and mineral assemblages of basal till samples to characterize dispersal from known deposits such as Highland Valley (calcalkalic Cu-Mo), Gibraltar (calcalkalic Cu-Mo), and Mount Polley (alkalic Cu-Au) mines, and mineralized zones at the Woodjam developed prospect (calcalkalic Cu-Mo-Au). The objective is to help define which components of till are enriched near such deposits, and document which porphyry indicator minerals (PIMs) survive erosion, glacial transport, and near-surface oxidative weathering. This project also incorporates biogeochemistry as a tool to explore for buried porphyry-style mineralization.



Fig. 3. Till sampling as part of the Till Porphyry Indicator Mineral Study (TG14).

2.1.4. Ni-Cu-PGE-Cr Ore Systems (TG14)

The Ni-Cu-PGE-Cr Ore Systems project is a national initiative of the GSC. The BC component, lead by Graham Nixon (BCGS), Doreen Ames (GSC), and James Scoates (UBC), is examining the potential for "orogenic" Ni-Cu-PGE-Cr associated with supra-subduction zone ultramafic-mafic intrusions, exclusive of ophiolites and accreted large igneous provinces. The aim is to establish mineral deposit models and exploration criteria for two poorly understood magmatic sulphide deposits: 1) Giant Mascot, BC's only past-producing Ni mine (1958-74); and 2) the Turnagain Alaskan-type intrusion, which has a substantial resource of low-grade Ni. In 2012, Graham Nixon released a new geological map of the Turnagain

ultramafic intrusion (Open File 2012-05; see section 4.2.1 below). A short field program in 2012 oriented two University of British Columbia graduate students who will be supported by the project to carry out studies of the Turnagain and Giant Mascot deposits.

2.1.5. Update of Cordilleran tectonics and metallogeny

In partnership with the Society of Economic Geology (SEG), and in anticipation of the SEG conference in Whistler (September, 2013), JoAnne Nelson and Maurice Colpron (Yukon Geological Survey) are updating their Cordilleran tectonic and metallogeny synthesis (Nelson and Colpron, 2007). This update, to be released at the meeting in Whistler, describes the tectonic evolution of the Cordillera since the Middle Precambrian and explains how tectonics has governed metallogenesis through time.

2.1.6. Porphyry deposits

British Columbia is known for hosting porphyry deposits, which make up a significant component of British Columbia's mineral wealth. Hence, understanding the geological controls and timing of porphyry deposit emplacement and mineralization remain important fields of research (e.g., Logan and Mihalynuk, in press). The eastward migration of Mesozoic arc magmatism in southern Quesnellia led to the growth of three temporally distinct, north-trending, plutonic belts (from west to east): Late Triassic; Late Triassic-Early Jurassic; and Early Jurassic. Three porphyry copper mineralization events are directly linked to each of these calcalkaline (Cu-Mo±Au) and alkaline (Cu-Au±Ag) magmatic episodes. In 2012, Jim Logan and Mitch Mihalynuk continued their long-standing investigation of assessing the age, geological setting, and stratigraphic-structural controls of porphyry deposits across the Province. In two papers, Mihalynuk and Logan (this volume) report on studies of Late Triassic porphyry Cu-Au mineralization at Miner Mountain and Dillard Creek, in the Nicola belt of southern British Columbia. In a third contribution, Logan and Mihalynuk (this volume) examine the Bonaparte deposit near Kamloops, and consider if historical quartz vein network gold targets might represent an upper level of a buried porphyry system.

Jim Logan, in partnership with the SEG, spent part of 2012 developing a field trip guidebook for the SEG meeting being held at Whistler in September 2013. The field trip ("Porphyry Systems of Central and Southern British Columbia") will present the geological setting and structural history of the central Intermontane belt (a composite of Late Triassic to Early Jurassic volcanic and plutonic arc rocks), and focus on porphyry-related mineral deposits that developed on the fringes of ancestral North America, before terrane accretion in late Early Jurassic time. The trip comprises transects of southern Stikine, Cache Creek, and Quesnel terranes, with visits to six operating mines including Endako (Thompson Creek Metals Company), Gibraltar (Taseko Mines Limited), Mount Polley (Imperial Metals Corporation), Highland Valley (Teck Resources Limited), New Afton (New Gold

Incorporated), and Copper Mountain (Copper Mountain Mining Corporation). The architecture of the Nicola arc, its calcalkaline and alkaline mineral deposits, and the relationship between cospatial early calcalkaline and later alkaline volcanism, plutonism, and mineralization (Cu-Mo±Au vs. Cu-Au) will be presented and highlighted by mine geologists through deposit overviews and onsite tours over the course of this 5-day post-conference trip.

2.1.8. British Columbia coal geology

Janet Riddell was appointed Senior Coal Geologist in March, 2012, a position that was vacant for some years (Fig. 4). Work priorities are directed at updating and maintaining coal exploration databases, establishing contacts with the coal exploration industry, and rebuilding coal geology expertise in the Ministry. The Survey, through Purple Rock Inc. conducted an inventory of 873 existing COALFILE paper documents, locating missing documents, and ensuring that all components of the documents were available online. Janet audited the Coal Assessment Reports for exploration projects conducted since 2002, and contacted exploration and development companies to replace missing data. She will continue to work with industry and the MDO to profile coal geology and exploration opportunities in British Columbia.



Fig. 4. Janet Riddell, the new BCGS Senior Minerals Coal Geologist, at Fording River Coal Mine.

2.1.9. Geochemical laboratory revitalization

Alexei Rukhlov joined the Survey in January 2012 as the new Senior Geochemist. He has been working to revitalize the Geological Survey's in-house geochemical laboratory, and inventory British Columbia's extensive geochemical and rock sample archive. The laboratory is a preparation and analytical facility for ministry geologists and their partners. In 2012, the Ministry invested significant funds in updating the laboratory facility and refurbishing laboratory equipment. New equipment includes a rock saw, a Linkam THMS 600 fluid inclusion stage linked to an Olympus BX microscope modified for infrared studies, and a Thermo portable bench top Niton XRF analyzer. The BCGS Geochemical and Rock Archive was upgraded with a new storage library to accommodate over 600 000 geochemical samples analyzed during national and provincial geochemical surveys since the 1970s. This multi-million dollar archive includes till, silt, and other media samples, and representative rock samples from deposits and geological environments across British Columbia. The samples have been stored, cataloged, and incorporated into a corporate database for querying and retrieval.

In June, the Province recognized Dr. Ray Lett as a Premier's Award Finalist in the Legacy category for his contribution in developing British Columbia's national and provincial geochemical databases (Fig. 5). Ray, now retired, is an Emeritus Scientist at the BCGS.

2.1.10. BCGS Emeritus Scientists

Nominally retired Emeritus Scientists Ray Lett and Nick Massey maintain their contributions to BCGS activities by continuing their research and collaborating with staff. Following up on fieldwork initiated in 2005 to better characterize lithological and geochemical variations of Paleozoic successions in the southern Okanagan region along the Canada-USA border (Boundary Project), Nick Massey and co-workers provide geochronologic (Massey et al., this volume) and geochemical (Massey and Dostal, this volume) data from the Knob Hill complex. This research supports the concept that Paleozoic basement to southern Quesnellia lacks a Laurentian heritage and is entirely exotic to North America. A complete set of geochemical data from the Knob Hill complex and Anarchist Group will be released as a GeoFile in 2013.

3. Resource Information Section

3.1. MapPlace

Since 1995, the MapPlace web service has provided industry and government agencies with comprehensive tools and open geoscience data to aid in the discovery of mineral potential in British Columbia. The mineral industry recognizes MapPlace as innovative and indispensable, with unique and interactive applications and tools to assist in investment decision making. MapPlace continues to provide clients with efficiencies in research time, data costs, and analysis. Data themes and applications available on MapPlace include mineral

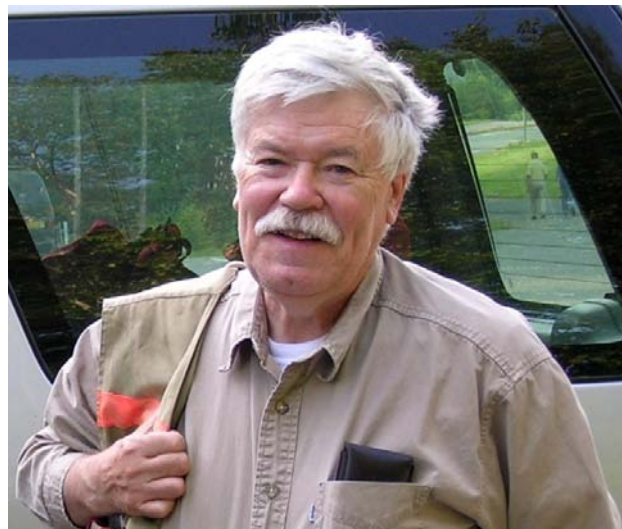


Fig. 5. BCGS Emeritus Scientist Ray Lett received a Premier's Finalist Award in the Legacy Category.

potential, bedrock and surficial geology, publications, mineral and petroleum tenure, MINFILE, assessment reports, geochemistry, and geophysical surveys. Yao Cui and Pat Desjardins contributed geomatic expertise to MapPlace enhancements and the integration of servers. Major technical advances have taken place since the inception of MapPlace 17 years ago, including growing databases, adding better servers, increasing bandwidth, and using affordable advanced database software. Pat and co-op students Thomas Edgehill and Stephen Zhao worked with the next generation of internet mapping and reviewed data modeling and architecture aspects to provide continued delivery of data for the exploration community.

3.2. Property File, MINFILE, and ARIS

During 2012, Property File, a collection of about 98 000 industry documents, continued to grow. As of December 2012, more than 34 270 Property File documents are available online, including those from Falconbridge, Cyprus-Anvil, Chevron, Placer Dome, Rimfire, Mine Plans, Library File items, RGS Maps and Tom Schroeter Project files. A recent collection from the late Dr. Rodney Kirkham is being indexed and scanned. Property File documents can be retrieved through the search application (propertyfile.gov.bc.ca) or through links from MINFILE (minfile.ca). Kirk Hancock is the Property File contact and is currently accepting donations to be included. Kirk works with the Property File contractor, Nicole Barlow, whose team indexes and delivers these valuable documents. Review of Property File documents has identified over 40 new occurrences, which have been added to the MINFILE database.

MINFILE contains geological, location, and economic information on more than 13 050 metallic, industrial mineral, and coal mines, deposits and occurrences in BC. The BCGS has been allocated extra funding to update MINFILE and to add new discoveries by reviewing mineral assessment reports, recent

publications, press releases, Property File, and company websites. Sarah Meredith-Jones is the MINFILE contact; contractors and staff updated over 1560 occurrences, and added 1035 new occurrences.

In compliance with the Mineral Tenure Act (MTA) Regulations, results of mineral exploration programs conducted on mineral claims in British Columbia are submitted to the Ministry of Energy, Mines and Natural Gas. These assessment reports contain information on geology, geophysics, geochemistry, drilling, prospecting and physical work. After a one-year confidentiality period, the reports become an open resource for planning mineral exploration investment, research, land-use planning, and resource management. Users can now access more than 32 600 company mineral assessment reports using the online ARIS database. More than \$1.9 billion of exploration expenditures have been recorded in assessment reports since 1947. The value of expenditures on 2010 exploration programs reported in 742 assessment reports, moved to off-confidential status in 2011, was \$155.0 million. The mining industry is encouraged to submit assessment reports in digital form (PDF by email, CD-ROM, DVD, or USB drive) to the Mineral Titles Branch. Benefits include higher quality digital reports; faster approval; and lower costs for printing, mailing, storage, scanning, and processing. In 2012, 866 reports were submitted, of which 793 were approved. Of these, 690 (87%) were submitted digitally, which is up 2% from the previous year. Allan Wilcox and Ted Fuller work with clients to approve reports. Approval rates increase if: adequate details are provided in cost statements; geochemical values are accurately located and plotted; full-scale geophysical maps are submitted; and cross sections and proper scales accompany drillhole data.

During the past year, Kirk Hancock provided mineral resource assessments of different areas of BC for the Ministry of Aboriginal Relations and Reconciliation to assist with treaty negotiations and other government business. Staff worked with the Mineral Policy and Regional Geology staff to develop economic and social assessments and exploration activity products. Laura de Groot continues to manage 11 000 web pages and keeps staff on track with database management plans and needs.

3.3. BC's Digital Bedrock Geology Map: BCGeology Map

The digital geological map of BC is important for mineral exploration and assessing mineral potential. Over the last couple of years, Yao Cui has been designing and implementing a sustainable and streamlined approach to integrate and deliver digitally seamless geological maps. Yao developed the Geology Operational Database Environment (GODE), using the spatial database PostgreSQL/PostGIS and the Geology Application Database Environment (GADE), using Microsoft® SQL Server 2008 (with spatial extension). Working with JoAnne Nelson, Yao and his team defined the geological framework data model as the base to maintain and edit contact and fault line work. The notion of anchored lines

and points will simplify data integration and reduce data boundary issues. Geological polygons are automatically generated from the line work and bedrock attributes are stored in the database as a point file (Fig. 6). With assistance from co-op students Graham Green and Victoria Francis, extensive initial data quality assurance work was carried out last year on the Province-wide geological framework data before and after its loading into the operational GODE database. This helped categorize and document a set of data quality specifications for the framework data. The approach was put into practice, with Fiona Katay and Leigh Sinclair joining the team this year to complete the recent data quality assurance and integration of updated framework data from North Coast, Terrace and QUEST. Tian Han developed scripts to check contact and fault linework, initially in the QUEST area. Yao and Fiona are working with JoAnne to review and standardize the lexicon and stratigraphic units in BC.

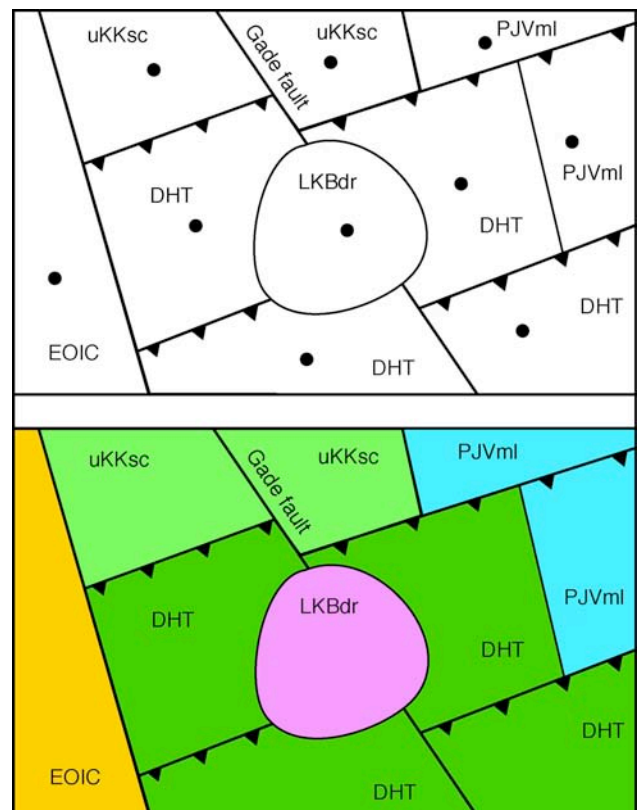


Fig. 6. Framework data showing linework and bedrock attributes stored in points or centroids (top), leading to a final bedrock geological map consisting of polygons, line work, and labels (bottom).

4. Conferences and publications

4.1. Conferences

Continuing a long-standing tradition, geoscientists of the British Columbia Geological Survey presented their research at national and international conferences, including meetings of the: Association for Mineral Exploration British Columbia (Mineral Exploration Roundup); Prospectors and Developer's Association of

Canada; Geological Association of Canada; Geological Society of America; Geochemical Society (22nd V.M. Goldschmidt Conference); International Union of Geological Sciences (34th International Geological Congress); Metallurgy and Materials Society of the Canadian Institute of Mining, Metallurgy and Petroleum (51st Conference of Metallurgists); and 47th Forum on the Geology of Industrial Minerals (Fig. 7). They also represented the Survey at provincial meetings in Kamloops (Kamloops Exploration Group) and Nelson (Minerals South).

In February, the British Columbia Geological Survey and the Pacific Section of the Geological Association of Canada co-hosted the 38th annual Cordilleran Tectonics Workshop (Fig. 8). Organized by JoAnne Nelson, and attended by 110 scientists from universities, government, and industry, the workshop highlighted 50 talks and posters devoted to past, ongoing, and future Cordilleran research. The workshop was capped by a field trip focused on the accretionary tectonics of southern Vancouver Island and led by Stephen Johnston and Dante Canil (School of Earth and Ocean Sciences, University of Victoria).

In November, the British Columbia Geological Survey and Pacific Section of the Geological Association of Canada joined forces again and co-sponsored the 2012 BCGS Open House (Fig. 9). Showcasing the work of BCGS geoscientists, the Open House featured a full day of presentations dedicated to the geology and mineral deposits of British Columbia. In addition to those by geologists from the BCGS, several talks were given by researchers from the School of Earth and Ocean Sciences (University of Victoria) and the Pacific Geoscience Centre (Geological Survey of Canada). The Open House was attended by over 130 geoscientists, with strong industry and student participation. Given its past success in 2009, and again in 2012, it is anticipated that this will become an annual BCGS event.

4.2. Publications

In addition to the annual Geological Fieldwork volume, BCGS geologists published Open Files, GeoFiles, and papers in external peer-reviewed journals. All BCGS publications can be downloaded, free of charge, from www.empr.gov.bc.ca/mining/geoscience/publicationscatalogue/pages/default.aspx.

4.2.1. Open files

Britton, J., DeGrace, J., Grieve, D., Jago, P., Kyba, J., Madu, B., Northcote B., and Chu, R., 2012. Operating mines and selected major exploration projects in BC, 2011. British Columbia Ministry of Energy, Mines and Natural Gas, British Columbia Geological Survey, Open File 2012-01.

Ferbey, T., Levson, V.M., and Lett, R.E., 2012. Till geochemistry of the Huckleberry Mine area, west-central British Columbia (NTS 093E/11). British Columbia Ministry of Energy, Mines and Natural Gas, British Columbia Geological Survey, Open File 2012-02, 52 p.



Fig. 7. British Columbia Geological Survey booth at the Mineral Exploration Roundup, Vancouver, January, 2012.

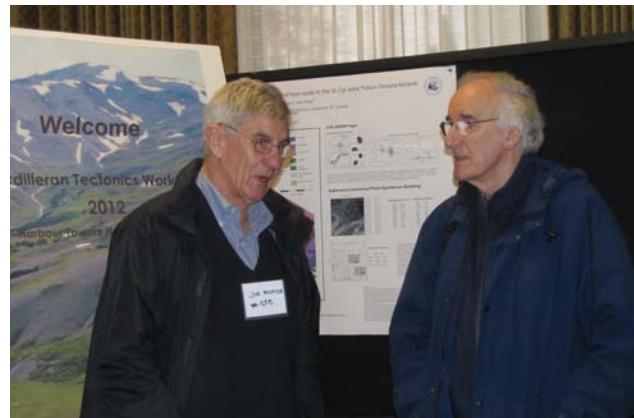


Fig. 8. Jim Monger (left) and Chris Barnes at the 38th annual Cordilleran Tectonics Workshop, Victoria, 2012.

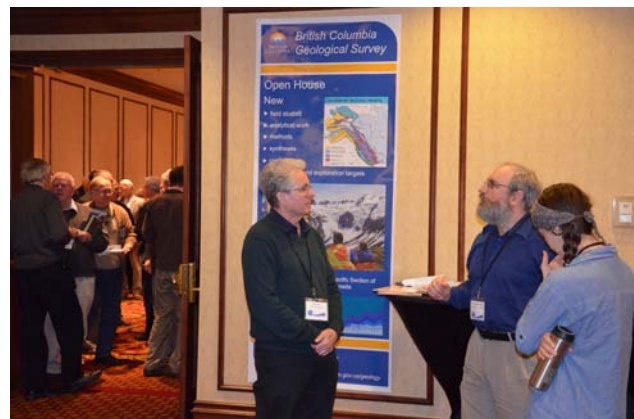


Fig. 9. The open house, sponsored by the British Columbia Geological Survey and the Pacific Section of the Geological Association of Canada and held in Victoria, is anticipated to become an annual event.

Logan, J.M., Moynihan, D.P., Diakow, L.J., and van Straaten, B.I., 2012. Dease Lake - Little Tuya River Geology (NTS 104J/08 & 7E). British Columbia Ministry of Energy, Mines and Natural Gas, British Columbia Geological Survey, Open File 2012-04, scale 1:50 000.

Nixon, G.T., Hitchins, A.C., and Ross, G.P., 2012. Geology of the Turnagain ultramafic intrusion, northern British Columbia (parts of NTS 104I/07 and 10). British Columbia Ministry of Energy, Mines and Natural Gas, British Columbia Geological Survey, Open File 2012-05, scale, 1:10 000.

Simandl, G.J., E.A. Prussin, E.A., and N. Brown, N., 2012. Specialty metals in Canada. British Columbia Ministry of Energy, Mines and Natural Gas, British Columbia Geological Survey, Open File 2012-07, 48 p.

Schiarizza, P., 2012. Bedrock geology of the upper Kutcho Creek area (parts of NTS 104-I/01, 02). British Columbia Ministry of Energy, Mines and Natural Gas, British Columbia Geological Survey, 2012-08 (also released as GSC Open File 7234), scale 1:40 000.

van Straaten, B.I, Logan, J.M., and Diakow, L.J., 2012. Geology of the Hotailuh Batholith, northwestern British Columbia. British Columbia Ministry of Energy, Mines, and Natural Gas British Columbia Geological Survey, Open File 2012-06 and Geoscience BC Report 2012-10, 77 p.

4.2.2. GeoFiles

Cui, Y., 2012. A KML file to display producing mines in British Columbia at any range or point of time in the last 160 years. British Columbia Ministry of Energy, Mines and Natural Gas, British Columbia Geological Survey, GeoFile 2012-03, 3 p.

Cui, Y., 2012. Using regionated KML files to display the status of a large number of mineral occurrences in British Columbia. British Columbia Ministry of Energy, Mines and Natural Gas, British Columbia Geological Survey, GeoFile 2012-04, 2 p.

Cui, Y., 2012. Using regionated KML files to speed up the display of a large number of regional geochemical survey sites in British Columbia. British Columbia Ministry of Energy, Mines and Natural Gas, British Columbia Geological Survey, GeoFile 2012-05, 2 p.

Han, T., Nelson, J.L., and Kyba, J., 2012. Mapping BC's Golden Triangle using ASTER imagery. British Columbia Ministry of Energy, Mines and Natural Gas, British Columbia Geological Survey, GeoFile 2012-06.

Logan, J., Diakow, L., van Straaten, B., Moynihan, D., and O. Iverson, O., 2012. QUEST-Northwest mapping: BC Geological Survey Dease Lake Geoscience Project (NTS 104J, 104I), northern British Columbia. British Columbia Ministry of Energy, Mines and Natural Gas, British Columbia Geological Survey, GeoFile 2012-07.

Simandl, G.J., Fajber, R., Prussin, E.A., Paradis, S., and Grattan, K., 2012. Use of portable XRF in evaluation of rare earth element-bearing phosphate. British Columbia Ministry of Energy, Mines and Natural Gas, British Columbia Geological Survey, GeoFile 2012-01.

Simandl, G.J., Prussin, E.A., Hancock, K., and S. Meredith-Jones, S., 2012. Rare metal-bearing deposits in British Columbia with selected examples. British

Columbia Ministry of Energy, Mines and Natural Gas, British Columbia Geological Survey, GeoFile 2012-02.

Turner, R.J.W., Anderson, R.J., Franklin, R., Ceh, M., Hastings, N., and Wagner, C.L., 2012. Southern British Columbia: Geological landscapes highway map. Geological Survey of Canada Popular Geoscience 98E and British Columbia Ministry of Energy, Mines and Natural Gas, British Columbia Geological Survey, Geofile 2012-09.

Van Straaten, B., and Diakow, L., 2012. Mesozoic magmatic history and metallogeny of the Hotailuh Batholith (NW BC). British Columbia Ministry of Energy, Mines and Natural Gas, British Columbia Geological Survey, GeoFile 2012-08.

4.2.3. External journal publications

Beranek, L.P., van Staal, C.R., McClelland, W.C., Israel, S., and Mihalynuk, M.G., in press. Detrital zircon Hf isotopic compositions indicate a northern Caledonian connection for the Alexander terrane. *Lithosphere*.

Gagnon, J.-F., Barresi, T., Waldron, J.F., Nelson, J.L., Polton, T.P., and Cordey, F., 2012. Stratigraphy of the upper Hazelton Group and the Jurassic evolution of the Stikine terrane, British Columbia. *Canadian Journal of Earth Sciences*, 49, 1027-1052.

Logan, J., and Mihalynuk, M.G., in press. Tectonic controls on paired alkaline porphyry deposit belts (Cu-Au ±Ag-Pt-Pd-Mo) within the Canadian Cordillera. *Economic Geology*, 108.

Rowins, S., 2012. The leading role of the GAC (Geological Association of Canada) in Canadian geoscience, *International Innovation Magazine*, June, 2012, 66-67.

Rowins, S., 2012. Geoscientists and Rodney Dangerfield: Neither gets any respect. Geological Association of Canada Presidential Address. *Geoscience Canada*, 39, 47-51.

Rukhlov, A.S., Blinova, A.I., and Pawlowicz, J.G., in press. Geochemistry, mineralogy and petrology of the Eocene potassic magmatism from the Milk River area, southern Alberta, and Sweet Grass Hills, northern Montana. *Chemical Geology*.

Simandl, G. J., Fajber, R., Paradis, S., in press. Handheld X-ray fluorescence analyser in the assessment of rare earth element-enriched phosphate rocks: methodology, results and data enhancement. *Geochemistry: Exploration, Environment, Analysis*.

Simandl, G. J., Stone, R. S., Paradis, S., Fajber, R., Kressall, R., Grattan, K., Crozier, J., in press. Applicability of handheld X-ray fluorescence spectrometers in the exploration and development of carbonatite-related niobium deposits – a case study of Aley carbonatite, British Columbia, Canada. *Geochemistry: Exploration, Environment, Analysis*.

Sigloch, K., and Mihalynuk, M.G., in press. Terrane Stations: intra-oceanic subduction assembled Cordilleran North America. *Nature Geoscience*.

Smith, C.M., Canil, D., Rowins, S.M., and Friedman, R., 2012. Reduced granitic magmas in an arc setting: The Catface porphyry Cu-Mo deposit of the Paleogene Cascade Arc. *Lithos*, 154, 361-373.

5. Mineral Development Office

The role of the BC Mineral Development Office (MDO) in Vancouver is to provide mineral and coal resource information to industry and government, promote the Province's minerals and coal industry domestically and abroad, and form a point of contact for industry on issues impacting the exploration and mining industries.

A primary output is the delivery of a technical marketing campaign that highlights the Province's mineral and coal potential, geoscience database and expertise, and attractive business climate. This includes developing publications aimed at a variety of audiences, from large foreign investors through to independent domestic entrepreneurs. These publications are distributed widely at conferences, business meetings, over the counter, and online.

This year saw the reformatting and release of "Opportunities to Explore" a popular publication geared to new investors with little knowledge of the Province's mineral resources. Financial and technical input from the Association for Mineral Exploration British Columbia, Mining Association of British Columbia, Geoscience BC and partner agencies have led to two print runs in two languages totaling 2000 copies, and wide access to the online versions. A daughter product of the publication includes a single page Infographic. In response to numerous coal inquiries a "Coal Industry Overview 2011" document was prepared; regular updating of this document is a priority of the Coal Geologist. Increased interest in the jade industry led to a new jade Information Circular, which updated a previous pamphlet.

The MDO coordinates the annual summary documents from the regional geologist program. Two products that represent a significant output from the program include a provincial overview and a regional summary. These publications maintain a reporting legacy that dates back to 1874, with the Annual Reports of the Minister of Mines.

In the past, the map "Communities that Benefit from Mining" was produced to illustrate the relationship between exploration expenditures and benefits to communities. It gained broad appeal from local government, area government representatives, and other parties that wanted to demonstrate the positive aspects of the exploration industry. Although the map has not been produced in recent years, a new version is under development. In an effort to capture the full effect of the industry beyond key exploration projects, the map now will include information about the tenure system and

claimed assessment work. The concept map will divide the Province into benefit 'watersheds'; however, because the map will have a GIS structure, its data can be viewed in a variety of perspectives.

The MDO interacts continuously with the mining and investment industry, including executive management, geologists, and prospectors at conferences, business meetings, trade missions and over the counter contacts. Significant events attended this year include: the Asia Investment Mission to China and Korea; the Pan-Canadian Mining Session in London, England; the Mineral Exploration Roundup, Vancouver; the Prospectors and Developers Association of Canada Convention, Toronto; the China Mining Conference, Beijing; the Sparwood Coal Symposium, Sparwood; and the KEG annual conference, Kamloops (Fig. 10).

The MDO works closely with other government agencies and the professional associations as part of a wider marketing effort. Using the resources of the BCGS, the office provides most of the technical expertise and professional delegates for presentations and meetings with inbound investment interest.

Given the location of the MDO in Vancouver, it is a natural point of contact for members of BC's mineral exploration and mining community. It plays an important role in flagging issues that impact the industry in BC and listening to their concerns.

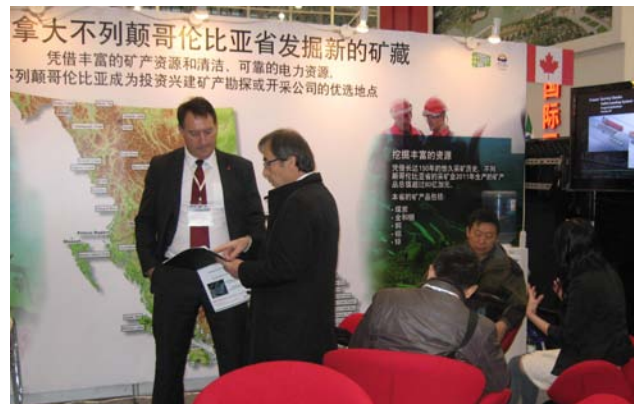


Fig. 10. Bruce Madu at the China Mining Conference held in Beijing.

6. Regional Geologists

In November, the British Columbia Regional Geologists were reassigned to the Ministry of Energy, Mines and Natural Gas from the Ministry Forests, Lands, and Natural Resource Operations. They are vital to government's ability to provide detailed geological knowledge at a regional level, and collate information on industry exploration and mining activity. Within their communities they are recognized experts on matters of exploration trends and successes. They support investment attraction initiatives, land-use processes, First Nation capacity building, and industry and public outreach. The MDO works closely with the Regional Geologists, helping them achieve their defined roles, and

profiling their important connection to the industry and the BCGS.

Regional Geologist	Office	Region
Jeff Kyba	Smithers	Skeena
Paul Jago	Prince George	Omineca and NE
Jim Britton	Kamloops	Thompson/ Okanagan/ Cariboo
Vacant (formerly Dave Grieve)	Cranbrook	Kootenay/ Boundary
Bruce Northcote	Vancouver	South/West Coast

7. Staff Update

The BCGS saw many staff changes in 2012 (Fig. 11). In January, Alexei Rukhlov joined the BCGS as the new Senior Geochemist. Alexei was recruited from the Alberta Geological Survey, where he conducted bedrock mapping and mineral deposit studies. He replaced Ray Lett who retired in October 2011 after more than 20 years of service as the Province’s Senior Geochemist. In March, Janet Riddell (Senior Coal Geologist), Lawrence Aspler (Editor and Publications Geoscientist), and Fiona Katay (GIS Geologist) filled temporary positions in the BCGS that were created to address critical backlog issues identified in the new BC Mineral Exploration and Mining Strategy. Holly Arnold (Junior Geoscientist) also joined in the Fall as part of the same backlog initiative. In May, Adrian Hickin arrived as the new Director of the Cordilleran Geoscience Section, a position vacated in November 2011 when Steve Rowins became the Chief Geologist and Executive Director. Adrian was previously the Director of Oil and Gas Geoscience in the Oil and Gas Division of the BC Ministry of Energy and Mines. In August, Melanie Mitchell, previously an Administrative Assistant with the Survey in Victoria, was promoted to the new position of Survey Branch Coordinator. Betty Chow joined the MDO in Vancouver as Administrative Assistant, shared with Mineral Titles Branch.



Fig. 11. British Columbia Geological Survey staff, 2012.

Finally, the Survey takes pleasure in recognizing Dave Grieve, the Regional Geologist for Cranbrook

(Southeast Region), who is retiring in early 2013, after more than 35 years of dedicated service to the Province (Fig. 12). We wish Dave a happy retirement.

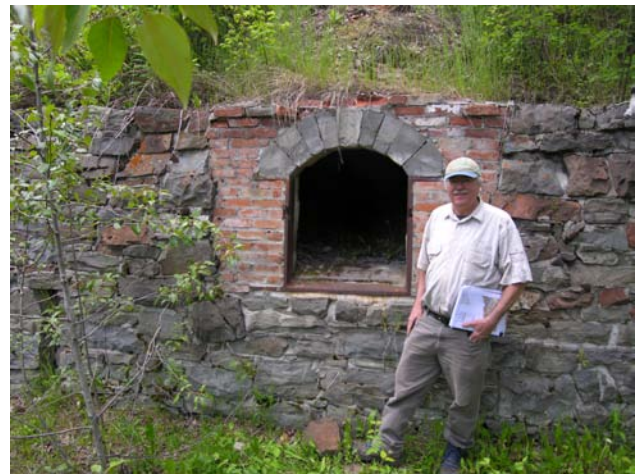
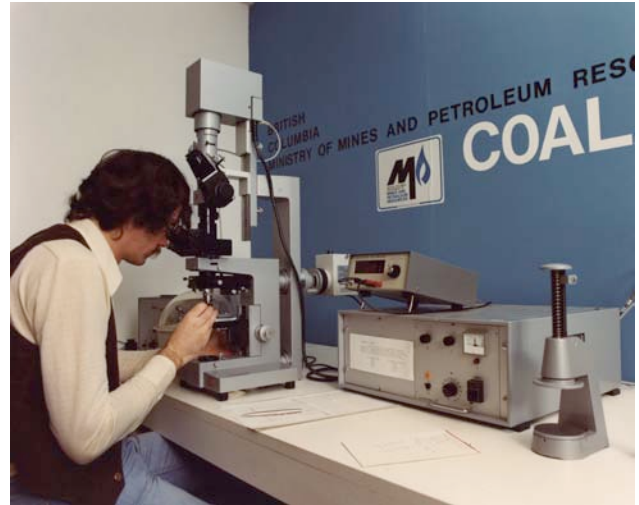


Fig. 12. Dave Grieve at the coal lab in 1977 (top) and at the Hosmer coke ovens in 2012 (bottom).

Acknowledgment

We thank George Owsiacki of Total Earth Science Services for desktop publishing.

References cited

- Logan, J., and Mihalynuk, M.G., in press. Tectonic controls on paired alkaline porphyry deposit belts (Cu-Au ±Ag-Pt-Pd-Mo) within the Canadian Cordillera. *Economic Geology*, 108.
- Mihalynuk, M., Zagorevski, A., and Cordey, F. 2012. Geology of the Hoodoo Mountain area (NTS 104B/14). *Geological Fieldwork 2011, British Columbia Ministry of Energy and Mines, British Columbia Geological Survey Paper 2012-1*, pp. 45-67.
- Nelson, J., and Colpron, M., 2007. Tectonics and metallogeny of the British Columbian, Yukon, and Alaskan Cordillera, 1.8 Ga to present. In: Goodfellow, W.D. (Ed.), *Mineral Deposits of Canada: a Synthesis of Major Deposit-Types, District Metallogeny, the Evolution of Geological Provinces, and Exploration Methods: Geological Association of Canada, Mineral Deposits Division, Special Publication No. 5*, pp. 755-791.

Ordovician volcanogenic sulphides in the southern Alexander terrane, coastal NW British Columbia: geology, Pb isotopic signature, and a case for correlation with Appalachian and Scandinavian deposits

JoAnne Nelson^{1,a}, Larry Diakow¹, Cees van Staal² and Don Chipley³

¹ British Columbia Geological Survey, Ministry of Energy, Mines and Natural Gas, Victoria, BC, V8W 9N3

² Geological Survey of Canada, Vancouver, BC, V6B 5J3

³ Department of Geological Sciences, Queen's University, Kingston, ON, K7L 3N6

^a corresponding author: JoAnne.Nelson@gov.bc.ca

Recommended citation: Nelson, J., Diakow, L., van Staal, C. and Chipley, D., 2013. Ordovician volcanogenic sulphides in the southern Alexander terrane, coastal NW British Columbia: geology, Pb isotopic signature, and a case for correlation with Appalachian and Scandinavian deposits. In: Geological Fieldwork 2012, British Columbia Ministry of Energy, Mines and Natural Gas, British Columbia Geological Survey Paper 2013-1, pp. 13-33.

Abstract

The southern part of the Craig subterrane of the Alexander terrane, which extends from Prince of Wales Island southward into coastal British Columbia, contains an Ordovician volcanic-sedimentary-intrusive suite of probable back-arc affinity, the Moira Sound unit. Mapping, prospecting, and geochronological work as part of the GEM-Edges project in 2009-2011 identified small sulphide occurrences within and adjacent to Ordovician rhyolites and rhyolite breccias of this unit. The previously known Pitt VMS occurrence on Pitt Island consists of a 3.5 kilometre-long trend of base-metal sulphide bodies aligned along a major shear zone that marks the southwestern limit of ductile shearing related to the mid-Cretaceous Grenville Channel fault. Deformation of the sulphides and their host quartz-muscovite schists is so intense that an epigenetic, synkinematic origin cannot be ruled out on geological grounds. However, chalcopyrite and sphalerite separates from the main Pitt showing yield lead isotopic ratios of $^{206}\text{Pb}/^{204}\text{Pb}$: 18.1701-18.1911; $^{207}\text{Pb}/^{204}\text{Pb}$: 15.5643-15.5660 and $^{208}\text{Pb}/^{204}\text{Pb}$: 38.1015-38.0893. These values, in particular the $^{206}\text{Pb}/^{204}\text{Pb}$ ratio, are significantly lower than those of Cretaceous syngenetic and epigenetic deposits elsewhere in the Coast belt (ca. 18.4 – 18.7) and are thus incompatible with an epigenetic origin linked to the Grenville Channel fault or its splays, the spatial association notwithstanding. Instead, they closely match leads from Ordovician volcanogenic deposits of New Brunswick, Newfoundland, Quebec, and Norway. In terms of $^{208}\text{Pb}/^{204}\text{Pb}$ vs. $^{206}\text{Pb}/^{204}\text{Pb}$, the Pitt lead is identical to that of the Bathurst camp. Current tectonic models place the Alexander terrane near the northern end of the Caledonide chain in early to mid-Paleozoic time, based on faunal affinities and Baltican-Caledonian detrital zircon patterns. The Pitt Pb isotopic data support these models. They indicate that Ordovician volcanogenic massive sulphides in the Alexander terrane may link to a chain of deposits that originated in now dismembered arcs and back arcs that constituted a circum-lapetus ocean ring of fire.

Keywords: Alexander terrane, volcanogenic massive sulphides, Ordovician, Pb isotopes, Pitt prospect

1. Introduction

The Alexander terrane is a composite allochthonous crustal fragment that extends for over 1500 kilometres, from the St. Elias Range in southwestern Yukon, through northwestern British Columbia and southeastern Alaska, and into the coastal area of British Columbia (Fig. 1). The history of the Alexander terrane, as recorded by Neoproterozoic to Triassic rocks, differs profoundly from that of more inboard, peri-Laurentian terranes and the adjacent Laurentian continental margin (Nelson and Colpron, 2007; Colpron and Nelson, 2009). Its early history more closely resembles terranes in the Caledonides. For example, Silurian limestones in the southern part of the terrane contain unusual microbial-aphrosalpingid sponge reef faunas (rather than the more common coralline reefs); the only known coeval and correlative faunas are in the western Baltican Urals and

near Salair in northern Siberia (Soja, 1994; Soja and Antoshkina, 1997).

Furthermore, the Devonian Karheen Formation and the Silurian Heceta Formation contain coarse alluvial deposits similar to the Old Red Sandstone of the northern Caledonides (Bazard et al., 1995; Soja and Krutikov, 2008). Based on the Uralian faunas, evidence of a low-latitude Devonian paleopole, and preliminary detrital zircon data, Bazard et al. (1995) proposed that the Alexander terrane lay close to the Scandinavian Baltic margin in mid-Paleozoic time (Fig. 2). If this is correct, then the Alexander terrane should have a shared history with the pericratonic and oceanic allochthons of the Scandinavian Caledonides. In particular, Neoproterozoic and early Paleozoic VMS deposits in the Alexander terrane may be a continuation of metallogenetic belts of the northern Caledonides and Baltica. Herein we present

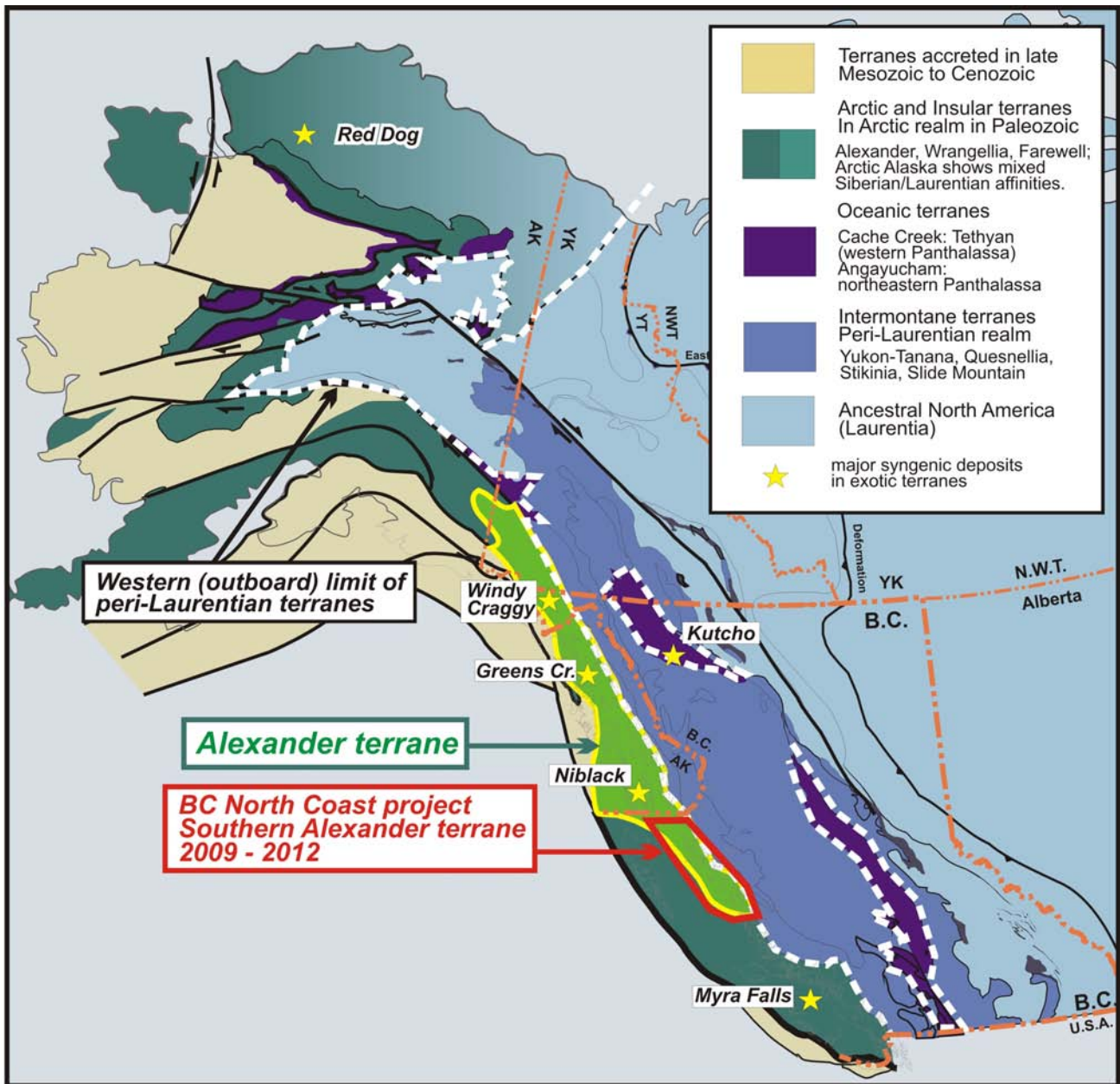


Fig. 1. Location of the Alexander terrane and BC North Coast project 2009-2012.

Pb isotopic data from an Ordovician VMS deposit in the Alexander terrane that support this hypothesis.

The southern Alexander terrane in southeastern Alaska hosts three suites of VMS deposits, Neoproterozoic, Ordovician, and Triassic (Fig. 3; Gehrels, et al., 1983). The Neoproterozoic and Ordovician suites are particularly significant because VMS deposits of this antiquity are unknown elsewhere in the North American Cordillera. The Neoproterozoic deposits, notably the Niblack, are hosted by the Neoproterozoic Wales Group. The Ordovician deposits are in the Moira Sound unit on southern Prince of Wales Island, an informal stratigraphic term introduced by Ayuso et al. (2005) and Slack et al. (2005), which is age-equivalent to, but lithologically

distinct from, the Descon Formation as defined on northwestern Prince of Wales Island by Eberlein and Churkin (1970). Although Gehrels and Saleeby (1987) included Moira Sound unit rocks on southern Prince of Wales Island as part of the Descon Formation, their unique character and role as host of volcanogenic deposits are worthy of distinction as a separate unit.

This paper reports the results of mineral deposit documentation and Pb isotopic sampling and analysis completed as part of a three-year regional geological and metallogenetic study of the Alexander terrane in coastal northwest British Columbia. The project, designed to upgrade previous reconnaissance-level geoscience (see Nelson *et al.* 2010, 2011, 2012a) was part of the

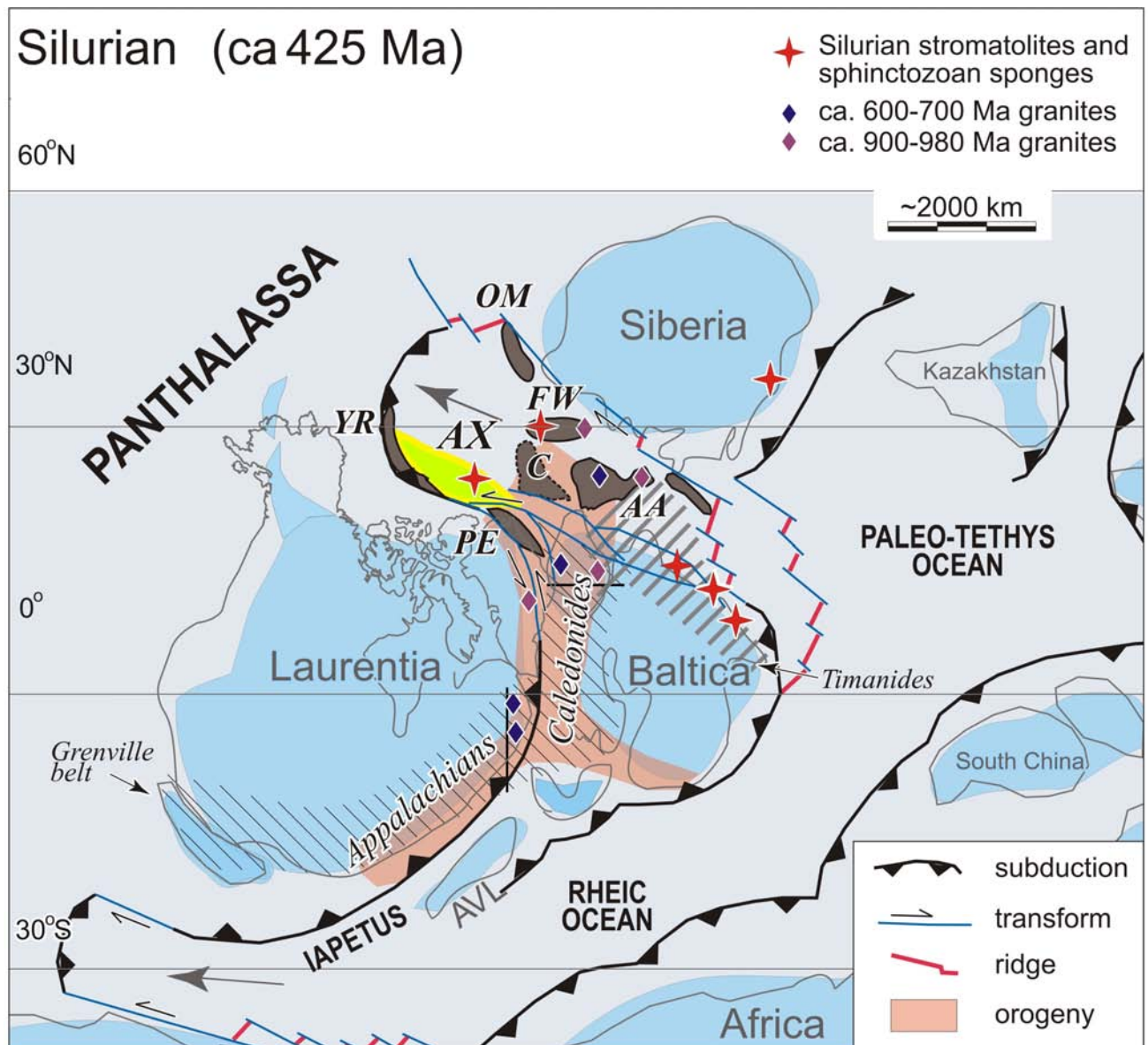


Fig. 2. Inferred paleogeographic position of Alexander terrane in Silurian time (based on Bazard et al., 1995, Colpron and Nelson, 2009, 2011; Nelson et al., 2012a). AX = Alexander terrane; FW = Farewell, YR = Yreka, Northern Sierra, Okanagan, AA = Arctic Alaska-Chukotka; OM = Omolon; P = Pearya. Alexander shown in yellow, other mobile terranes in brown.

GEM-Edges (Cordilleran Multiple Metals) initiative, a collaboration between the Geological Survey of Canada, British Columbia Geological Survey, and Yukon Geological Survey. The BC North Coast component also involved co-research with Brian Mahoney (University of Wisconsin at Eau Claire) and George Gehrels and Mark Pecha (University of Arizona.) A primary goal was to document volcanogenic occurrences and the age and character of their enclosing volcanic sequences, and to correlate them with the much better known deposits on Prince of Wales Island. The only well-described set of VMS-type occurrences in the Alexander terrane of northwestern British Columbia, the Pitt prospect on Pitt Island, was specifically targeted for study.

2. Regional geology and VMS mineralization of the Alexander terrane

The Alexander terrane comprises three distinct tectonostratigraphic entities, the Craig, Admiralty and informal “St. Elias” subterrane (Fig. 3). The Craig subterrane, the most widespread and best documented, has been the subject of many stratigraphic and geochronological studies in southeastern Alaska (Eberlein and Churkin, 1970; Gehrels and Saleeby, 1987; Gehrels and Berg, 1992, 1994). Basal units include primitive arc-related volcanic and lesser sedimentary strata of the Neoproterozoic Wales Group. Host felsic rocks of the Niblack deposit on southern Prince of Wales Island have yielded ca. 565 Ma U-Pb zircon ages (J. Oliver et al., 2011 oral communication). As of March 2011, combined

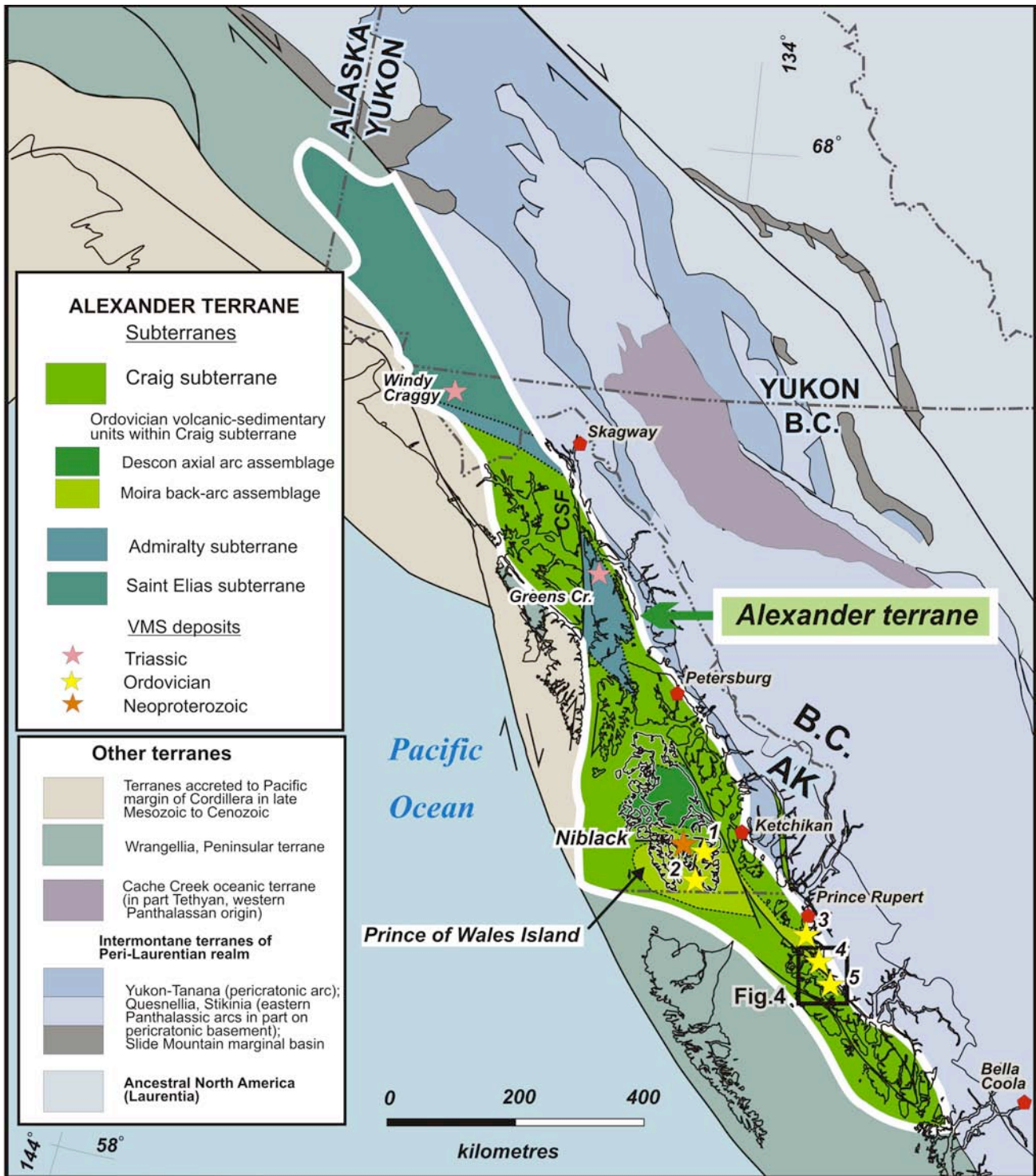


Fig. 3. Regional geology of the Alexander terrane. Craig and Admiralty subterrane from Gehrels and Berg (1994). Saint Elias subterrane is an informally defined and very approximately delimited. Approximate outline of Descon Formation from Gehrels and Berg (1992). Outline of Moira Sound unit on Prince of Wales Island from Ayuso et al. (2005). Ordovician rocks in NW British Columbia, assigned here to the Moira back-arc assemblage, are from mapping and geochronological studies conducted during the present project. POW = Prince of Wales Island. CSF = Chatham Strait fault. Ordovician volcanogenic sulphide occurrences: 1. Moira Copper 2. Barrier Islands 3. Digby Island 4. Kennedy Island 5. Pitt prospect, Pitt Island.

indicated and inferred resources at this deposit were 6.63 Mt at 1.16% Cu, 2.11 g/t Au, 2.28% Zn and 33.89 g/t Ag (J. Oliver et al., 2011 oral communication).

Deformed and metamorphosed Wales Group strata and post-kinematic Neoproterozoic-Cambrian plutons are unconformably overlain by Ordovician volcanic and

sedimentary strata on southern Prince of Wales Island (Fig. 3). Although Gehrels (1992) included these rocks in the Descon Formation, Ayuso et al., (2005) and Slack et al. (2005) redefined them as a separate unit, the Moira Sound unit. Volcanic rocks in the Moira Sound unit are markedly bimodal, and interbedded with deep-water sedimentary strata, including siltstone, mudstone, greywacke, carbonaceous argillite, and minor conglomerate and limestone. This stratigraphy differs markedly from the Descon Formation farther north on Prince of Wales Island, which consists of voluminous intermediate volcanic and volcanoclastic accumulations typical of the central region of an island arc. The Moira Sound unit unconformably overlies the Wales Group (Ayuso et al., 2005), whereas the basement of the Descon Formation is unknown because its base is unexposed. There is evidence for local Devonian tectonism in the shear zone separating the Moira Sound unit and underlying Wales Group on southern Prince of Wales Island from the Descon Formation farther north (S. Karl, unpublished data and personal communication, 2010). It is thus possible that either the Moira Sound unit represents a collapsed back-arc sequence linked to the Descon arc, or a separate and unrelated crustal fragment. In any event, the distribution of known Ordovician VMS deposits (Moira Copper and Barrier Islands, Fig. 3) suggests that the Moira Sound unit is the exploration target of choice, rather than the arc-central Descon Formation proper (S. Karl, written communication, 2009). North of Prince of Wales Island, Silurian and younger clastic and carbonate units blanket the Craig subterrane (Gehrels and Berg, 1992).

The Admiralty subterrane outcrops on Admiralty and Kupreanof islands and the Chilkat Mountains west of Skagway, separated by approximately 180 km of dextral motion across the Chatham Strait fault (Fig. 3; Karl et al., 2010). It includes metamorphic equivalents of some Craig subterrane units, such as Neoproterozoic volcanic and plutonic rocks equivalent to the Wales Group (Karl et al., 2006). Some Paleozoic strata within it represent deep-water facies: graphitic schist of the Precambrian-early Paleozoic Retreat Group; chert, argillite, greywacke, limestone, and basalt of the overlying Ordovician-Devonian Hood Bay Formation; and ribbon chert, argillite, greywacke, and basalt of the Devonian to Early Permian Cannery Formation (Karl et al., 2010). Both Devonian (Forbes et al., 1987) and Permian (Haeussler et al., 1999; Karl et al., 2010) metamorphic ages are recorded within this subterrane. The oldest overlap unit between it and the Craig subterrane is the Permian Pybus Formation (Gehrels and Berg, 1994). The Greens Creek mine on Admiralty Island (Fig. 3) is developed on a Triassic silver-rich polymetallic VMS orebody, which formed in a rift that cut the Alexander terrane along its length (Taylor et al., 2008), after juxtaposition of the Craig and Admiralty subterrane.

The St. Elias subterrane is a pericratonic crustal fragment that contains a > 2000 m thick sequence of

Cambro-Ordovician siliciclastic, carbonate, and mafic volcanic rocks, and Paleozoic carbonate and siliciclastic strata (Mihalynuk et al., 1993). It contrasts strongly with the primitive arc assemblages on Prince of Wales Island. Beranek et al. (2012) suggested that the Cambro-Ordovician basalts represent the peri-continental backarc region corresponding to the Descon arc. The St. Elias subterrane hosts the Triassic Windy Craggy VMS deposit. This very large Cu-Zn-Au-Co deposit formed in the same rift as Greens Creek; their contrasting ore compositions reflect immediate host rocks: mafic at Windy Craggy; felsic calcalkaline at Greens Creek (Taylor et al., 2008).

3. Ordovician VMS mineralization in the Alexander terrane of NW British Columbia

3.1. Setting

A volcano-sedimentary suite with high-level intrusions underlies northeastern Porcher Island and extends southwards to eastern Pitt Island and the mainland coast east of Grenville Channel (Figs. 3, 4). These rocks were assigned to the Alexander terrane by Wheeler and McFeely (1991), but because they failed to yield fossils and only one U-Pb age was available (482 Ma, trondjemite intrusion, Gehrels and Boghossian, 2000), their age and affinity were uncertain. Five new U-Pb age determinations from plutonic, volcanic and volcanoclastic units, ranging from 495 to 472 Ma (J.B. Mahoney, unpublished data, 2012), confirm an Early Ordovician age, coeval with the Descon Formation and Moira Sound unit. The suite most resembles the Moira Sound unit. It includes a variety of lithologic units (shown in detail on Nelson et al., 2010; 2012b, fig. 5). Far northern Porcher Island is underlain by metamorphosed thin-bedded to laminated andesitic to dacitic tuffs, volcanoclastic sandstone and conglomerate, and metre- to decimetre-scale interbeds of tuff, breccia and limestone. Rhyolites and subvolcanic trondjemite-diorite intrusions form a belt along the islands east of Porcher Island. This belt appears to continue southeastwards onto the northeastern shoulder of Pitt Island. Small felsic centres on Kennedy Island host the Kennedy and Dogfish showings. The most eastern exposures of the Moira Sound unit are of mainly mafic metavolcanic rocks and biotite schist. Metamorphic grades range from greenschist on far northern Porcher Island through lower amphibolite on Kennedy Island to upper amphibolite on northeastern Pitt Island and the mainland coast.

3.2. Volcanogenic-style mineralization

Volcanogenic mineralization and associated alteration zones in the area include: 1) the Pitt prospect (103H 066), a 3.5 kilometre-long trend of small polymetallic sulphide bodies on northeastern Pitt Island, classified as a probable VMS-style trend, that was explored, geologically mapped, and drilled in the 1990s (Bradley, 1987; Lo, 1992; Bohme, 1993); 2) zones of pyrite-pyrrhotite (\pm chalcopyrite-sphalerite) stockwork and partial replacement in metarhyolite, (Kennedy or Hard Case and Dogfish) discovered on the shores of

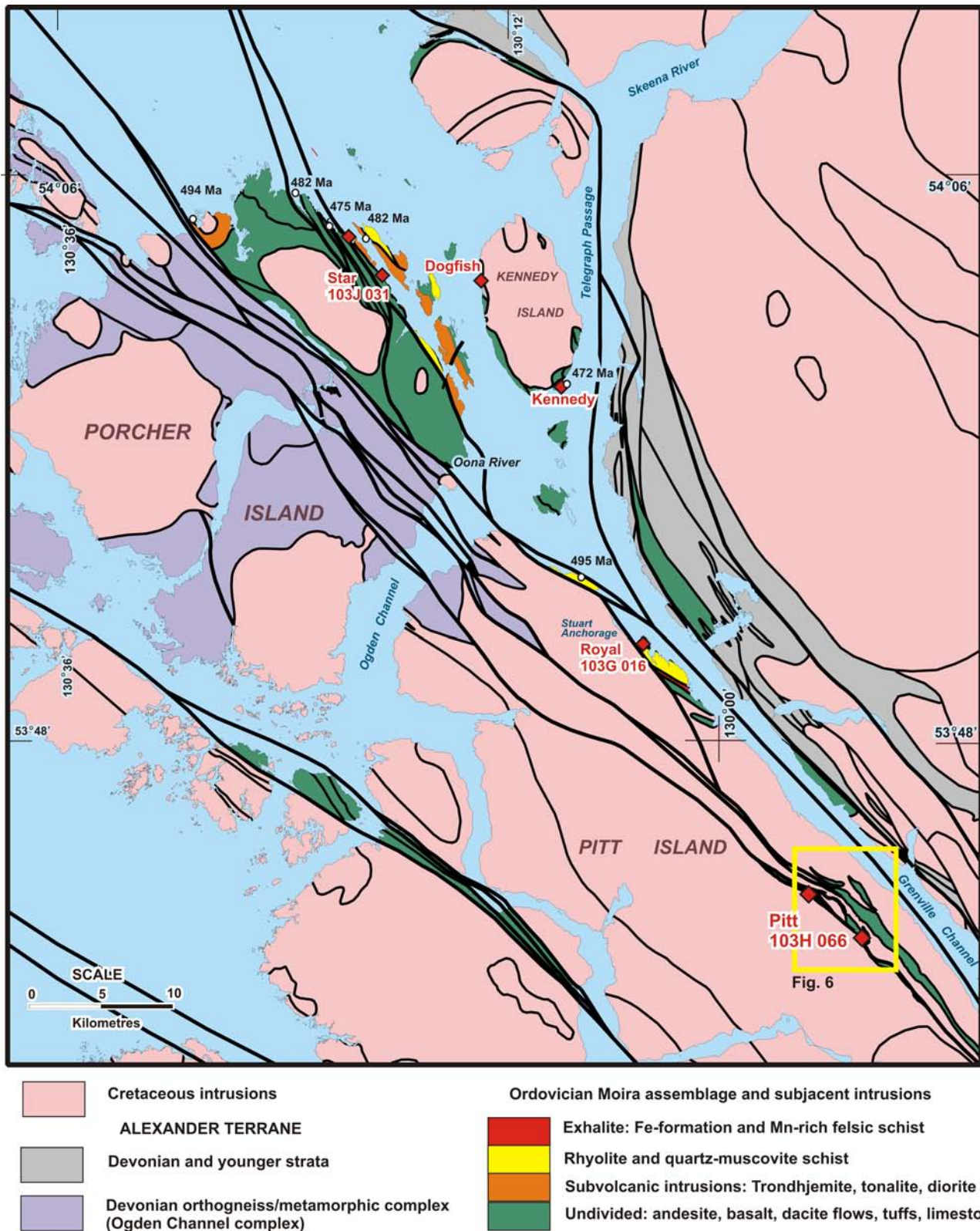


Fig. 4. Generalized geological map of Porcher and Pitt islands, showing Ordovician Moira assemblage exposures, volcanogenic sulphide and related occurrences, and locations of U-Pb ages. All U-Pb data are J.B. Mahoney, unpublished, except for the ca. 482 Ma date on trondhjemite from McMicking Island (Gehrels and Boghossian, 2000).

Kennedy Island in 2011 (Nelson et al., 2012b); and 3) meta-exhalite(?) and magnetite iron formation, including MINFILE localities, 103G 016 Royal and 103J 031 Star (Fig. 3). Because of its extensive exploration history, followed up by our 2011 field investigations and analytical results, the Pitt prospect is discussed in more detail in a following section.

On Kennedy Island, the Kennedy showing (Fig. 4) comprises massive pyrite-pyrrhotite with accessory chalcopyrite and sphalerite and stockwork-like mineralization hosted by a felsic pyroclastic rock, components of which have been replaced by sulphide (Fig. 5a). At the Dogfish showing, mineralization occurs in intensely quartz-sericite-altered volcanic protoliths as: disseminated pyrite and pyrrhotite; massive pyrrhotite, local pyrite, sphalerite, and minor chalcopyrite; and brecciated, sulphide-bearing quartz-sericite schist veined by pyrrhotite and sphalerite (Fig. 5b). Because Kennedy Island is protected as part of the Kennedy Island Conservancy Area, these two new occurrences are not potential exploration targets in themselves. However, they demonstrate the potential for VMS-style mineralization in the Moira Sound unit. The sulphide textures and lithic associations resemble the massive marcasite-pyrite stockwork and replacement in Ordovician felsic breccia (Figs. 5c, d) on the western side of Digby Island (near Prince Rupert, Fig. 3). The Digby Island site yielded a U-Pb zircon age of ca. 472 Ma (Gehrels and Boghossian 2000), identical to that of felsic lapilli tuff at the Kennedy showing.

Stratabound, stratiform magnetite is widely scattered along the northeastern side of Porcher Island, and on the eastern side of Pitt Island near Stuart Anchorage (Fig. 4, including MINFILE localities, 103G 016 Royal and 103J 031 Star). The bodies are continuous over tens to hundreds of metres, enclosed in highly strained meta-tuffs. The Royal occurrence and its southern extension lie immediately above a felsic meta-tuff body. Individual layers vary in thickness from tens of centimetres to a maximum at the Royal showing of several metres, which is interpreted as a thickened fold hinge zone. Most commonly, mineralization consists of pure, fine-grained magnetite with shiny grey hematite partings (Fig. 5e). Magnetite also forms fine laminae and blebs within meta-tuff (Fig. 5f).

Atypical of skarns, calcsilicates are minor; epidote and epidote-garnet accompany the magnetite only in a few cases. Carbonate rocks, common elsewhere in the volcanic sequences, are not in direct association with the magnetite bodies. Hence we argue that the magnetite layers record exhalative processes during volcanism, rather than metamorphic replacement, and that they represent the distal equivalents of a regional system that included more proximal sulphide-rich facies. Schists containing manganoan zoisite and axinite occur within tens of metres of the iron formation in Stuart Anchorage, (Fig. 4). Their unusual compositions and association with felsic metatuffs support an exhalative origin.

3.3. The Pitt prospect: Geology, mineralization and modelling

The Pitt prospect or Pitt/Trinity claim group (MINFILE 103H 066), is a 3.5 km long trend of sulphide showings on northeastern Pitt Island distributed along the ridges near Grenville Channel (Figs. 4, 6). Prospecting near a rusty gossan in Pyrite Creek in 1980 led to the discovery of massive sulphides. The discovery was followed by further exploration and preliminary mapping to determine the geological setting of the polymetallic mineralization (Bradley, 1987). Detailed geological mapping at 1:10 000 scale, prospecting, sampling and airborne geophysical surveys were carried out in 1992 (Bohme, 1993; Lo, 1992). Figure 6 depicts the major units and faults identified in the 1992 mapping, along with new information and interpretations from the present project.

Mineralization at Pitt consists of zones in two NW-trending metasedimentary-metavolcanic inliers within foliated Cretaceous plutons (Fig. 6; Bohme, 1993). Layering is aligned along the regional steeply dipping, northwest-trending foliation. Greenish to brown metapelite and metatuff are the main host rocks. Minor in abundance, but important to modelling the deposit, are rusty, pyritic metarhyolite (Fig. 7a), quartz-muscovite schist and massive quartz-rich schist with relics of pre-metamorphic stockworking (referred to as “quartzite” by Bohme, 1993). The Pyrite Creek and Pitt zones are the most significant of the known showings. Located 3.5 kilometres apart along strike, they coincide with a prominent northwest-trending topographic lineament, which is marked by incised drainage and rusty oxidized gossans. Along the lineament, the supracrustal rocks and Cretaceous plutons display shear, locally mylonitic, fabrics. In both zones, pyrite-rich, semimassive and massive sulphides occur in quartz-muscovite schist interlayered with quartz-rich zones, garnet-quartz-biotite schist, and carbonaceous argillite (Fig. 6). The true thickness of sulphides varies between 0.2 and 1.6 metres (Bohme, 1993). Principal sulphide minerals consist of pyrite, chalcopyrite, sphalerite, pyrrhotite, galena, covellite and, possibly, bornite. Based on values of 1.0-5.5% Ba in assays, barite is suspected. Drill intersections of the Pyrite Creek zone returned between 0.94 and 2.2% Cu, 0.41 to 1.2% Pb, and 1.5 to 4.9% Zn over 2-metre widths.

In 2011, a brief property visit aimed to verify map relationships of Bohme (1993). At the Pyrite Creek showing, sulphides are hosted by decimetre-scale layers of quartzose schist that alternate with laminated garnet biotite schist. Coarse quartz-muscovite schist comprises a half-metre thick, friable weathered layer exposed at creek level in a steep, incised gully. It is composed mainly of muscovite and quartz with disseminated and semimassive millimetre-thick bands of pyrite-chalcopyrite ± sphalerite ± galena. Thus, our field investigations demonstrated that both showings are associated with metamorphosed felsic and/or altered hosts: rusty metarhyolite at the Pitt zone (Fig. 7a), and quartz-muscovite schist at the northern end

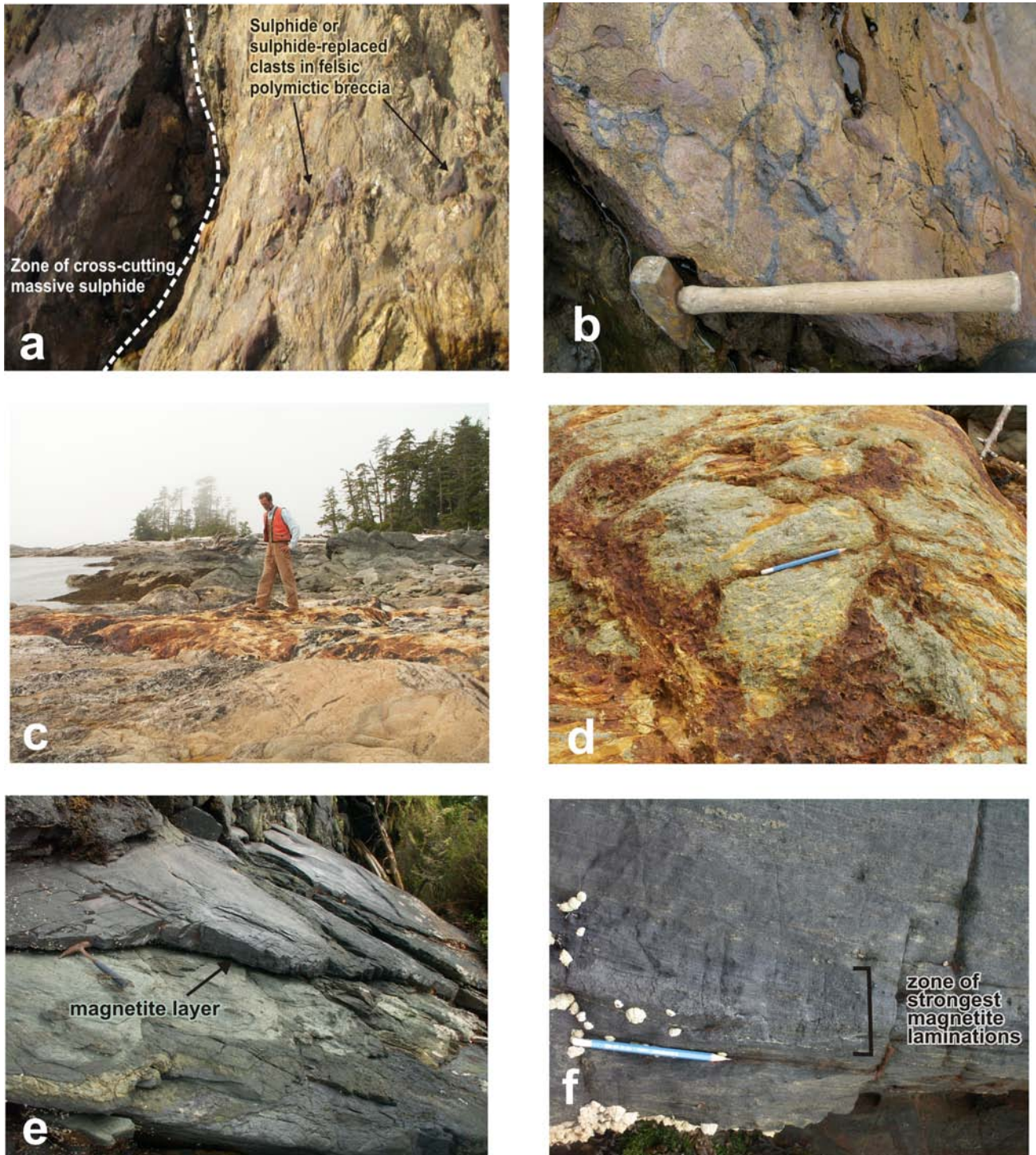


Fig. 5. Mineralization in Ordovician felsic volcanic hosts on Digby and southern Kennedy islands. **a)** Kennedy showing, with crosscutting massive sulphides, also replacing clasts in felsic breccia. **b)** Dogfish showing, displaying brecciated sulphide bearing quartz sericite schist surrounded by pyrrhotite and sphalerite. **c)** Massive marcasite-pyrite gossan in Ordovician metarhyolite, Digby Island; George Gehrels examining the site of ca. 472 Ma U-Pb zircon sample reported in Gehrels and Boghossian (2000). **d)** Digby Island metarhyolite breccia with irregular replacement and fracture-filling sulphides. **e)** Layer of magnetite in thinly laminated Wales Group meta-tuff, northeastern Porcher Island. **f)** Magnetite laminations in siliceous, iron-rich meta-tuff, Stuart Anchorage.

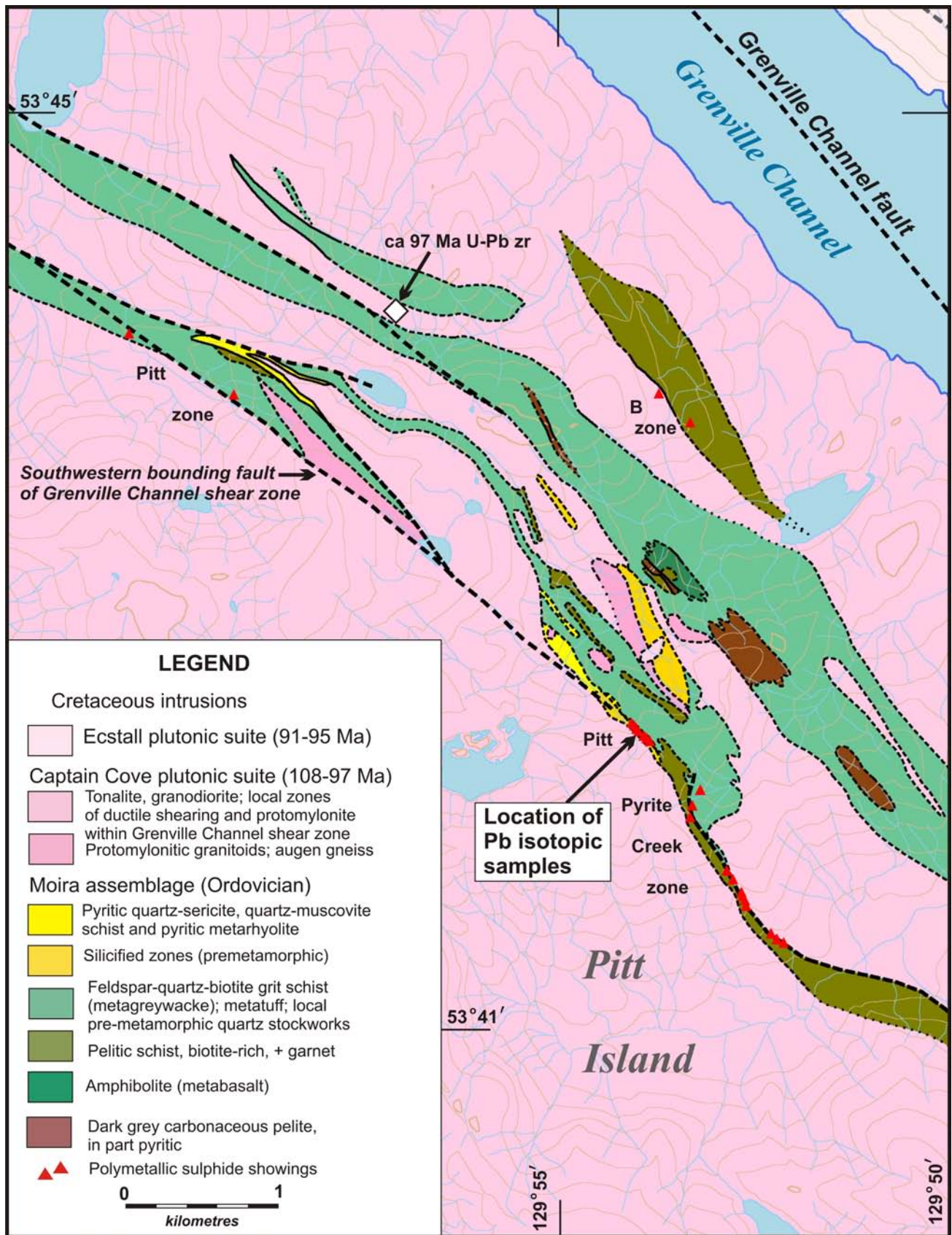


Fig. 6. Detailed geologic map of the Pitt prospect and vicinity. Geology from Bohme (1993) and field observations in 2011. Location of Pb isotopic samples shown (11LDi02-01). U-Pb age, M. Pecha, unpublished data 2011.

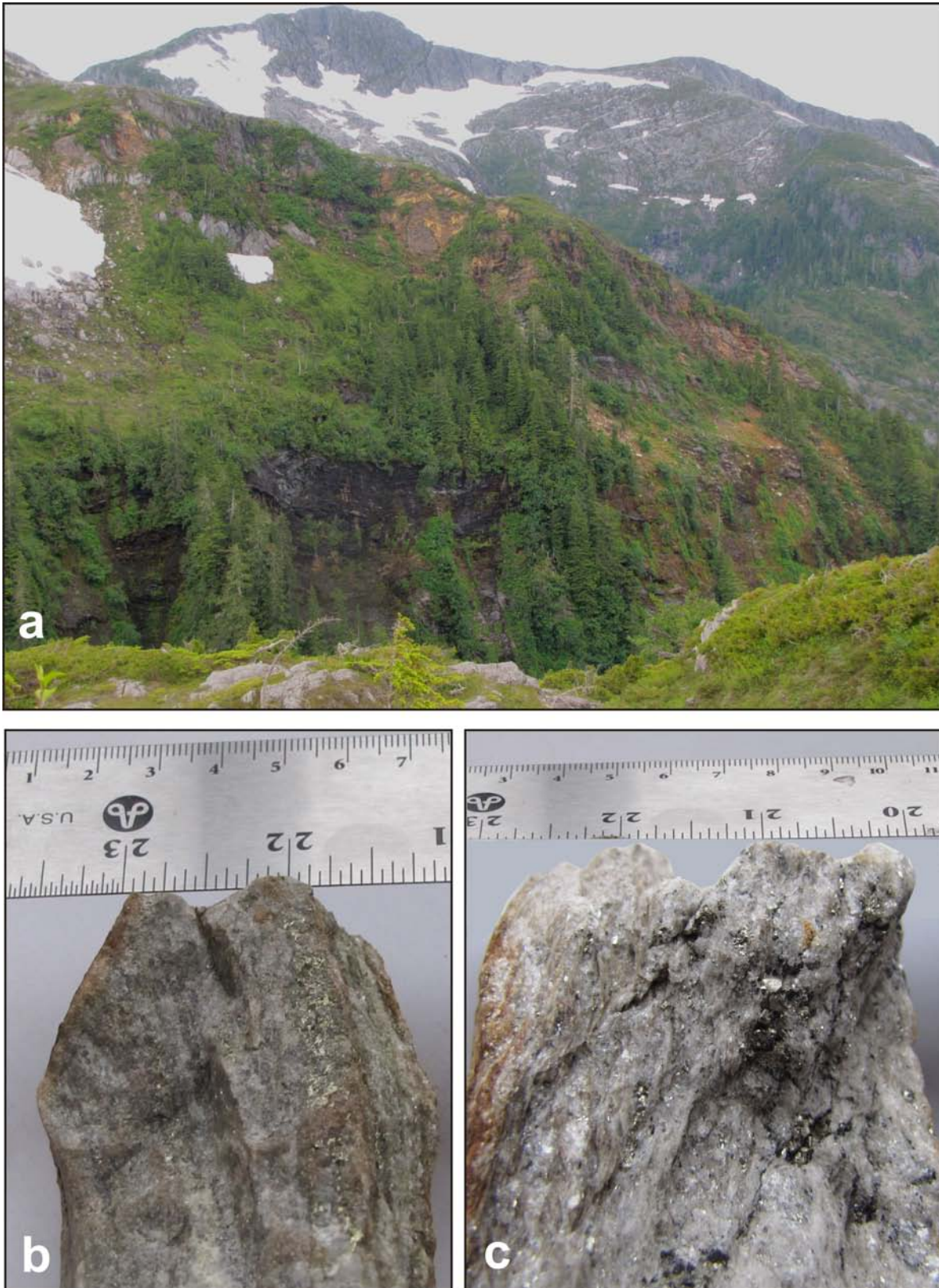


Fig. 7. Mineralization at the Pitt prospect. **a)** Rusty, pyritic quartz sericite schist (metarhyolite) along the Pitt zone lineament. For location of this body see Figure 4. **b)** Close-up of Pb isotopic sample 11LDi02-01a, showing chalcopyrite-rich laminae in quartz-muscovite schist. **c)** Close-up of Pb isotopic sample 11LDi02-01b, showing apparently crosscutting sphalerite-pyrite veinlets in quartz-muscovite schist.

of the Pyrite Creek zone (Figs. 7b, 7c).

However, our work also confirmed the strong structural control on the 3.5 km long trend of mineralization that comprises the main Pyrite Creek and Pitt zones. All of the mineralization, except the B zone (Fig. 6), lies within a major Cretaceous shear zone. Regionally, the host fault forms the most southwesterly strand of the Grenville Channel fault system, a mid-Cretaceous sinistral transpressive ductile shear zone recognized over a 200 km strike length from northern Porcher Island to south of Klemtu (Nelson et al., 2012b). The shear zone is particularly wide and well developed around Grenville Channel. The strand that hosts the Pitt showing displays a crustal-scale strain discontinuity. East of the fault, Cretaceous granitoids as young as 97 Ma (Fig. 6; M. Pecha, unpublished U-Pb data 2012) display pervasive mylonite fabrics, whereas to the southwest, large granitoid bodies of the mid-Cretaceous (108-97 Ma) Captain Cove suite are undeformed.

Field evidence at the Pitt prospect supports two alternative models for its origin. First, the association of layered, apparently stratabound mineralization with metatuffs, pelitic rocks, meta-rhyolites, and metamorphosed quartz-sericite and siliceous alteration assemblages led Bohme (1993) to classify it as volcanogenic. Alternatively, the localization of most mineralization along the trace of a major Cretaceous fault could be taken as support for an epigenetic origin. To address this question, we collected samples of host felsic rocks (quartz-muscovite schist) for U-Pb geochronology, and of stratiform sulphide mineralization for Pb-Pb isotopic analysis. The schist failed to yield zircons. Pb-isotopic analytical results for two sulphide samples are reported below.

4. Pb isotopic analysis of sulphides

Two sulphide-bearing samples were collected from the northern end of the Pyrite Creek zone. Both consist of sulphide laminae and stockworks within coarse-grained quartz-muscovite schist (Figs. 7b, c). Therefore, if this mineralization is part of a volcanogenic system, it is more likely to be “stringer ore” from a feeder zone, rather than bedded massive sulphide. The lack of zircon yield from the host could indicate that it was a metamorphosed altered mafic rock rather than a rhyolite. The sulphide textures are also consistent with an epigenetic origin overprinted by shear. Sample 11LDi02-1a contains centimetre-scale chalcopyrite laminae; 11LDi02-1b contains veinlets of sphalerite and pyrite.

4.1. Analytical procedures

Meaningful Pb isotopic analysis of sulphides requires that the sample be free of silicate grains, particularly those such as micas that contain uranium and thus cause a change in the isotopic ratios after crystallization of the sulphides. Concentrates of 300-500 mg of chalcopyrite and sphalerite were separated by selection of sulphide-rich areas in the sample, followed by crushing, milling,

and concentrating, and finally by hand picking to ensure purity (Overburden Drilling Management Ltd.).

The lead isotopic analyses were performed at Queen's University Facility for Isotope Research. Approximately 5 g of each sample was weighed into a clean Savillex beaker. Savillex beakers without samples, but containing all reagents, were included as procedure blanks to monitor contamination. To each beaker, 5 mL of 50% HNO₃ (distilled HNO₃ and >18.2 MegaOhm H₂O) was added. The closed beakers were heated on a hotplate at 120°C for 24 hours to dissolve the sulphides. Samples were cooled and centrifuged to remove remaining solids. The solutions were then evaporated to dry on a hotplate at 70°C. 2% HNO₃ was added to dissolve the sample and dilute appropriately for measurement. All sample preparation was performed in a class 100 clean lab. Measurement of the lead isotope ratios was by Thermo Finnigan Neptune MC-ICP-MS. All masses (²⁰⁰Hg, ²⁰²Hg, ²⁰³Tl, ²⁰⁴Pb, ²⁰⁵Tl, ²⁰⁶Pb, ²⁰⁷Pb and ²⁰⁸Pb) were measured on Faraday detectors in low resolution. Mercury was measured for correction of the mass 204 signal (²⁰⁴Hg+²⁰⁴Pb). Samples were bracketed with NIST 981 standards during measurement. Tl spikes (²⁰⁵Tl/²⁰³Tl=2.388) were added to each sample, as well as to each standard and each procedure blank, for the purpose of mass bias correction. Sample uptake was 100 microlitres per minute using a ESI PFA nebulizer. All gas flows and lenses were optimized for maximum stability and signal intensity (Table 1).

Table 1. Conditions and specifications for isotopic analysis on Thermo Finnigan Neptune MC-ICP-MS.

RF Power	1250W
Cool gas flow	17 L/min.
Aux gas flow	1 +/- 0.1 L/min.
Sample gas flow	0.9 L/min.
Integration time	4 sec.
Number of integrations	60

4.2. Analytical results and local comparisons

Lead isotopic ratios for the two samples are shown in Table 2. Isotopic ratios for the chalcopyrite are: ²⁰⁶Pb/²⁰⁴Pb, 18.1911; ²⁰⁷Pb/²⁰⁴Pb, 15.5643 and ²⁰⁸Pb/²⁰⁴Pb, 38.1015. For the sphalerite they are: ²⁰⁶Pb/²⁰⁴Pb, 18.1701, ²⁰⁷Pb/²⁰⁴Pb, 15.5660, and ²⁰⁸Pb/²⁰⁴Pb, 38.0893. Radiogenic isotopes are presented in their ratios to common, non-radiogenic ²⁰⁴Pb. The isotopic ratios for the two concentrates are very close, although not quite within analytical error of each other. Their consistency is comparable to that of deposits with notably uniform Pb isotopic compositions such as Pine Point (Cumming et al., 1990), suggesting that lead isotopic homogenization took place in the original hydrothermal system, and that these Pb isotopic values preserve a record of the ore chemistry of the original deposit.

Table 2. Lead isotopic analytical data for sulphide samples from the Pitt showing.

Sample locations and descriptions						
Pitt samples	UTM east	UTM north	Description			
11LDi02-1a	442372	5950488	Chalcopyrite-rich laminae in quartz-muscovite schist			
11LDi02-1b	442372	5950488	Quartz-muscovite schist with sphalerite-pyrite veinlets			
Analytical results						
Sample		$^{206}\text{Pb}/^{204}\text{Pb}$	$^{207}\text{Pb}/^{204}\text{Pb}$	$^{208}\text{Pb}/^{204}\text{Pb}$	$^{207}\text{Pb}/^{206}\text{Pb}$	$^{208}\text{Pb}/^{206}\text{Pb}$
Standards						
NIST NBS 981 correct values		16.937	15.492	36.722	0.91464	2.16810
981A	Mean	16.9317	15.4860	36.6823	0.91461	2.16647
	StdErr (abs)	0.0004	0.0004	0.0009	0.00001	0.00001
981B	Mean	16.9313	15.4861	36.6812	0.91463	2.16647
	StdErr (abs)	0.0004	0.0003	0.0008	0.000005	0.00001
981C	Mean	16.9313	15.4856	36.6808	0.91462	2.16647
	StdErr (abs)	0.0004	0.0004	0.0009	0.00001	0.00001
Pitt samples						
11LDI02-1a chalcopyrite	Mean	18.1911	15.5643	38.1015	0.85560	2.09452
	StdErr (abs)	0.0007	0.0006	0.0015	0.00001	0.00003
11LDi02-16 sphalerite	Mean	18.1701	15.5660	38.0893	0.85668	2.09626
	StdErr (abs)	0.0002	0.0002	0.0006	0.000004	0.00001

Note: Procedure blank measured less than 0.02% of sample signal

Figure 8 is a standard uraniumogenic lead plot of $^{207}\text{Pb}/^{204}\text{Pb}$ vs. $^{206}\text{Pb}/^{204}\text{Pb}$. The Pitt samples plot close to the “orogene” curve of Doe and Zartman (1979) and Zartman and Doe (1981). This theoretical curve depicts mixing between upper crustal and mantle sources such as is common at convergent plate boundaries, for instance in back-arc basins where fluid systems sample both primitive mantle-derived volcanic rocks and continent-derived sediments (Bjørlykke et al., 1993). Modern back-arc seabed sulphide deposits, such as in the Lau Basin (Fouquet and Marcoux, 1995) and central Okinawa trough (Halbach et al., 1997), show such intermediate, mixed signatures due to continent-derived sediments and attenuated continental crust in the source area. Mixing lines can be drawn between values at a given age on all three curves. The Pitt data lie between the 500 and 400 Ma mixing lines, indicating that the Pitt mineralization formed in the Ordovician, coeval with the Moira Sound units dated locally, without subsequent introduction of radiogenic Pb during Cretaceous metamorphism and deformation. Note that, because of the shorter half life of ^{235}U (which decays to ^{207}Pb) compared to ^{238}U (^{206}Pb), in

Phanerozoic reservoirs the $^{206}\text{Pb}/^{204}\text{Pb}$ ratio increases rapidly with decreasing age. For comparison, data for the Late Devonian (ca. 370 Ma) Myra Falls VMS deposit of Wrangellia shows comparatively higher $^{206}\text{Pb}/^{204}\text{Pb}$, consistent with a younger age of mineralization. Furthermore, representative Cretaceous deposits from the Coast belt, the Britannia VMS deposit and gold-polymetallic mesothermal veins at Bralorne and Banks Island, show even higher $^{206}\text{Pb}/^{204}\text{Pb}$, plotting on a very young mixing curve between mantle and orogene values. Two samples from Ordovician deposits on Prince of Wales Island plot near or below the mantle curve but at “future” lead positions (Fig. 8; data from Ayuso et al., 2005). Enriched mantle sources may have contributed to these leads (Ayuso et al., 2005) but because of uncertain modelling, these data are not considered further in this study.

Figure 9 shows the Pitt data relative to Neoproterozoic and Triassic VMS deposits in the Alexander terrane. Also included are Devonian and Mississippian syngenetic deposits of Arctic Alaska and the Devonian Myra Falls deposit of Wrangellia, because

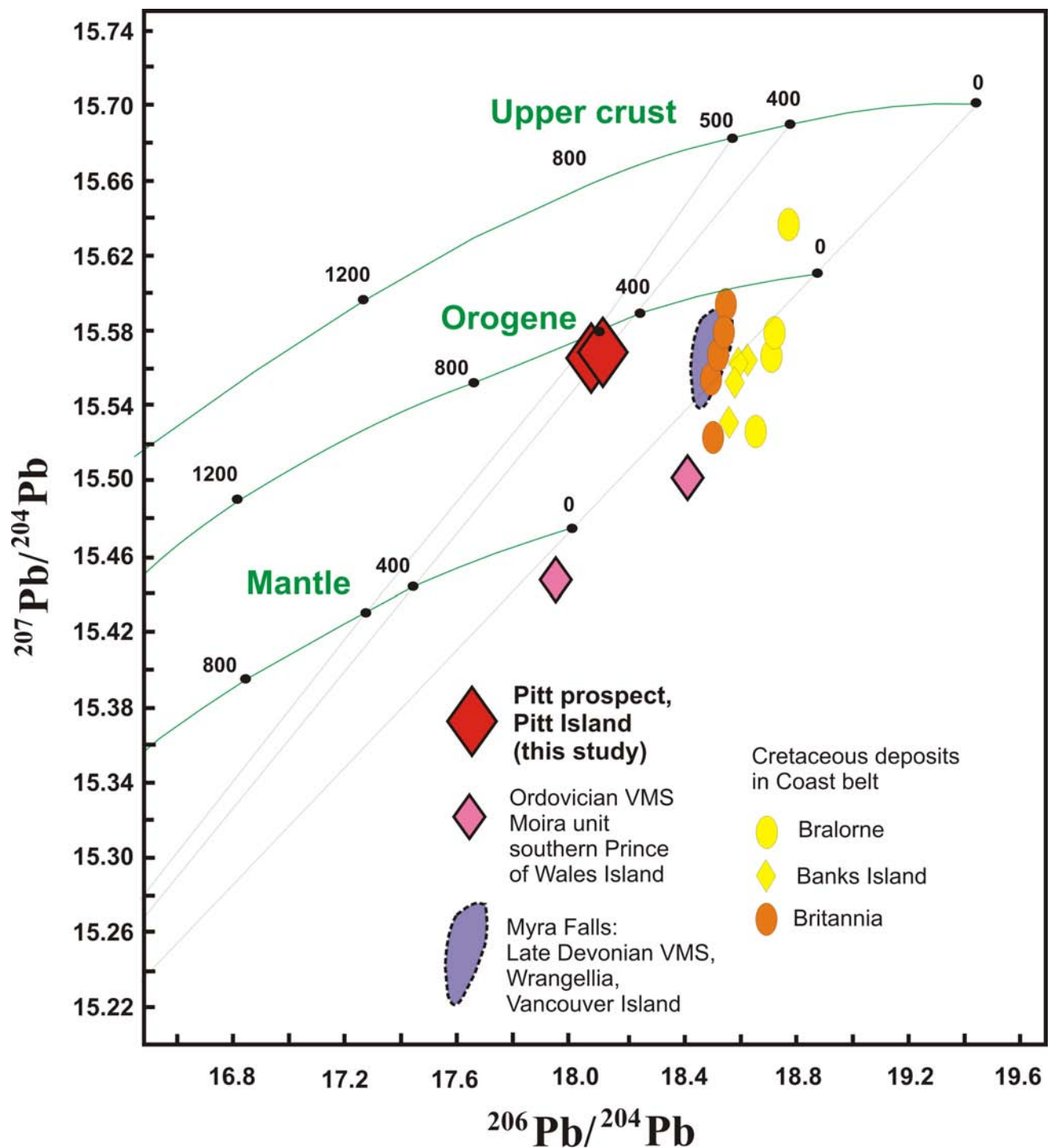


Fig. 8. $^{207}\text{Pb}/^{204}\text{Pb}$ vs. $^{206}\text{Pb}/^{204}\text{Pb}$ plot comparing the Pitt occurrence with the Devonian Myra Falls volcanogenic deposit on Vancouver Island (Wrangellia) and Cretaceous deposits of the Coast belt. Data from Godwin et al. (1988). Also shown are two analyses from the Moira Copper and Barrier Islands Ordovician volcanogenic occurrences in the Alexander terrane on Prince of Wales Island (Ayuso et al., 2005; S. Karl, unpublished data).

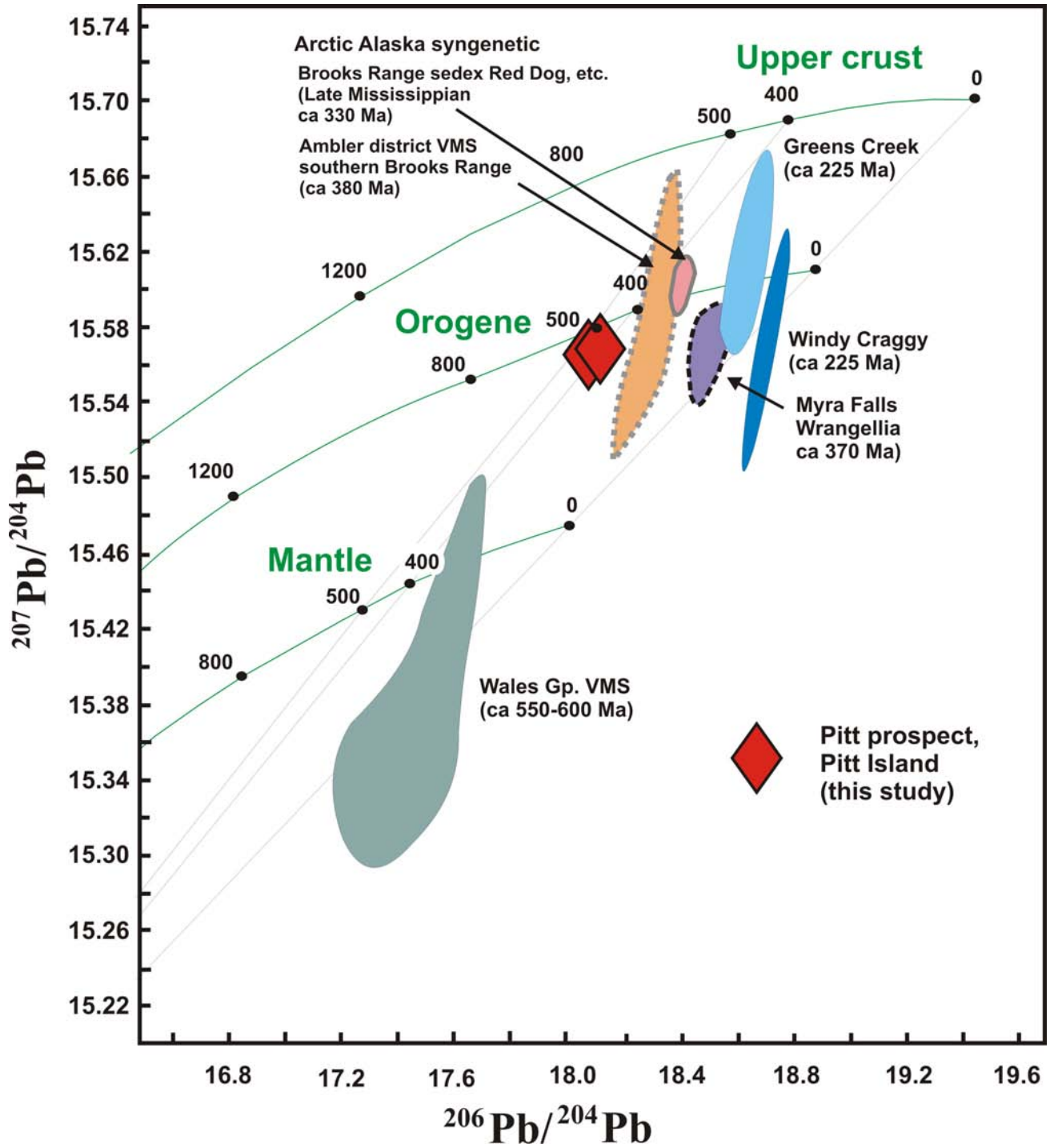


Fig. 9. $^{207}\text{Pb}/^{204}\text{Pb}$ vs. $^{206}\text{Pb}/^{204}\text{Pb}$ plot of Neoproterozoic, Ordovician and Triassic volcanogenic deposits of the Alexander terrane. Except for the Neoproterozoic leads, which exhibit extremely unradiogenic values, all of the deposits plot on the “orogene” (mixed upper crustal and mantle) lead isotopic growth curve (Doe and Zartman, 1979; Zartman and Doe, 1981). Arctic Alaska Devonian and Mississippian leads (Church et al., 1987) and Myra Falls (Godwin et al., 1988) are also shown for comparison.

these terranes are potentially related to the Paleozoic Alexander terrane in paleogeographic position and crustal composition (Gardner et al., 1988; Beranek et al., 2012). The data for the Neoproterozoic Niblack and related deposits are diffuse and generally plot below the mantle curve. Ayuso et al. (2005) considered the possibility of plume-related mantle contributions to the very primitive Wales Group arc. The younger deposits however, all lie on or near the “orogene” curve, more or less in order of decreasing age. Myra Falls lies closer to the mantle curve than Ambler or Red Dog but also at slightly higher $^{206}\text{Pb}/^{204}\text{Pb}$ values, which indicates a slightly different crustal source. Greens Creek shows a greater degree of upper crustal influence than does Windy Craggy, consistent with their evolved vs. primitive volcanic hosts. Overall, the Ordovician through Triassic deposits define an Insular-Arctic terrane growth curve that is roughly equivalent to the worldwide “orogene” curve. The marked departure of this growth trend from the Wales Group population suggests that the Wales Group primitive arc was amalgamated with more evolved crustal elements prior to the Ordovician. The Wales orogeny (Gehrels and Saleeby, 1987), which affected the Wales Group prior to deposition of the Ordovician Descon Formation, resulted from collision of the Wales arc with another, unidentified crustal block. The affinity of that block is uncertain because it is not preserved at surface; however the overall lead growth pattern between Ordovician and Triassic provides indirect evidence that the basement of the Alexander terrane in Paleozoic and Mesozoic time was partly pericratonic.

4.3. The Pitt lead signature and its Caledonian counterparts

In Figure 10, Pitt lead isotopic values are compared to Ordovician VMS deposits from the Paleozoic Caledonian orogen that surrounds the present-day Atlantic ocean, and formed during closing of the Iapetus ocean, precursor to the Atlantic. These deposits originated in arcs and back arcs settings fringing and within the Iapetus ocean (Fig. 11). They are now preserved in allochthons derived from the eastern peri-Laurentian realm, from the borders of Gondwana, and from Baltica in the Scandinavian Caledonides (van Staal, 2007; Bjørlykke et al., 1993). Among them is the Bathurst district of New Brunswick, in which the giant Bathurst No. 12 mine has produced 230 million tonnes of ore (van Staal, 2007).

The Appalachian leads are from a compilation of Newfoundland, New Brunswick and Quebec data by Swinden and Thorpe (1984). They represent terranes on both the peri-Laurentian and peri-Gondwanan sides of the Iapetus ocean (Fig. 11; also see maps and discussion in Swinden and Thorpe 1984, and van Staal, 2007 for modern terrane assignments and tectonic analysis). All of the deposits lie on a single mixing line between mantle and Grenvillian upper crust (Swinden and Thorpe 1984). The “old” (i.e. unevolved) intersection of this line with the model upper crustal lead reservoir of Doe and Zartman is due to the comparatively young age of the

Grenville orogen (ca. 1100 Ma) compared to average cratonic crust (Swinden and Thorpe 1984). The most radiogenic leads are from the Bathurst camp in New Brunswick and from deposits in the Tetagouche-Exploits back-arc basin that separated the Victoria Lake arc from the peri-Gondwanan Ganderia microcontinent in Newfoundland (Fig. 11; van Staal, 2007). In general, Pb in the peri-Laurentian deposits tends to be closer to mantle values. Their hosts are for the most part extremely juvenile arc and back-arc sequences. The Pitt signature nearly centres the Appalachian data, and falls near the least-radiogenic end of the peri-Gondwanan trend. It is nearly identical to that of the Tulks Hill, Burnt Pond, and Tally Pond deposits (Swinden and Thorpe 1984). They lie within the part of the Tetagouche-Exploits back-arc that is closest to the Victoria Lake arc, immediately south of the Red Indian Line, which represents the closed Iapetus ocean (van Staal, 2007).

The Pitt lead signature is also centred within the linear trend of leads from Ordovician VMS deposits in the Upper and Uppermost allochthons of the Norwegian Caledonides (Fig. 11; Bjørlykke et al., 1993). The elongate linear trend for $^{207}\text{Pb}/^{204}\text{Pb}$ vs. $^{206}\text{Pb}/^{204}\text{Pb}$ from these deposits results from their origin in diverse tectonic environments including ensialic back-arc basins with radiogenic lead signatures and marginal basin ophiolitic crust with comparatively primitive, mantle-like lead (Bjørlykke et al., 1993). The Uppermost allochthon is considered to be of peri-Laurentian origin, but the “homeland” of the Upper Allochthon is debated. Although Bjørlykke et al. (1993) interpreted it as entirely of Baltican affinity, some of the nappes within it are of peri-Laurentian origin (Gee, 2005). Lead trends within the Upper and Uppermost allochthons are distinct, with higher $^{207}\text{Pb}/^{206}\text{Pb}$ in the Uppermost Allochthon. Generally lead becomes less radiogenic upwards within the Upper Allochthon: the most mantle-like leads come from the Løkken ophiolite near its structural top. This led Bjørlykke et al. (1993) to model the Upper Allochthon as a collapsed peri-Baltican margin in which the amount and influence of craton-derived sediments lessened away from the continent. They also point out that the anomalously ‘young’ intersection of the Scandinavian trend with the upper crustal curve reflects a concentration of very radiogenic Middle Proterozoic granites in the Baltican shield. The Pitt signature is centred within the Norwegian trend, closest to deposits of the Sulitjelma district, which Bjørlykke et al. (1993) place in a peri-Baltican marginal basin.

A plot of $^{208}\text{Pb}/^{204}\text{Pb}$ vs. $^{206}\text{Pb}/^{204}\text{Pb}$ (Fig. 12) provides a further means to compare the Pitt and Caledonian deposits, as it combines uranium and thorogenic lead. On this diagram, the Pitt data plot at the upper, most thorogenic end of Appalachian trend, nearly coincident with the Bathurst camp. The Pitt signature is more thorogenic than the Norwegian leads from either Baltica or Laurentia, and reflects mixing of lead from primitive mantle and pericratonic sources. By comparison

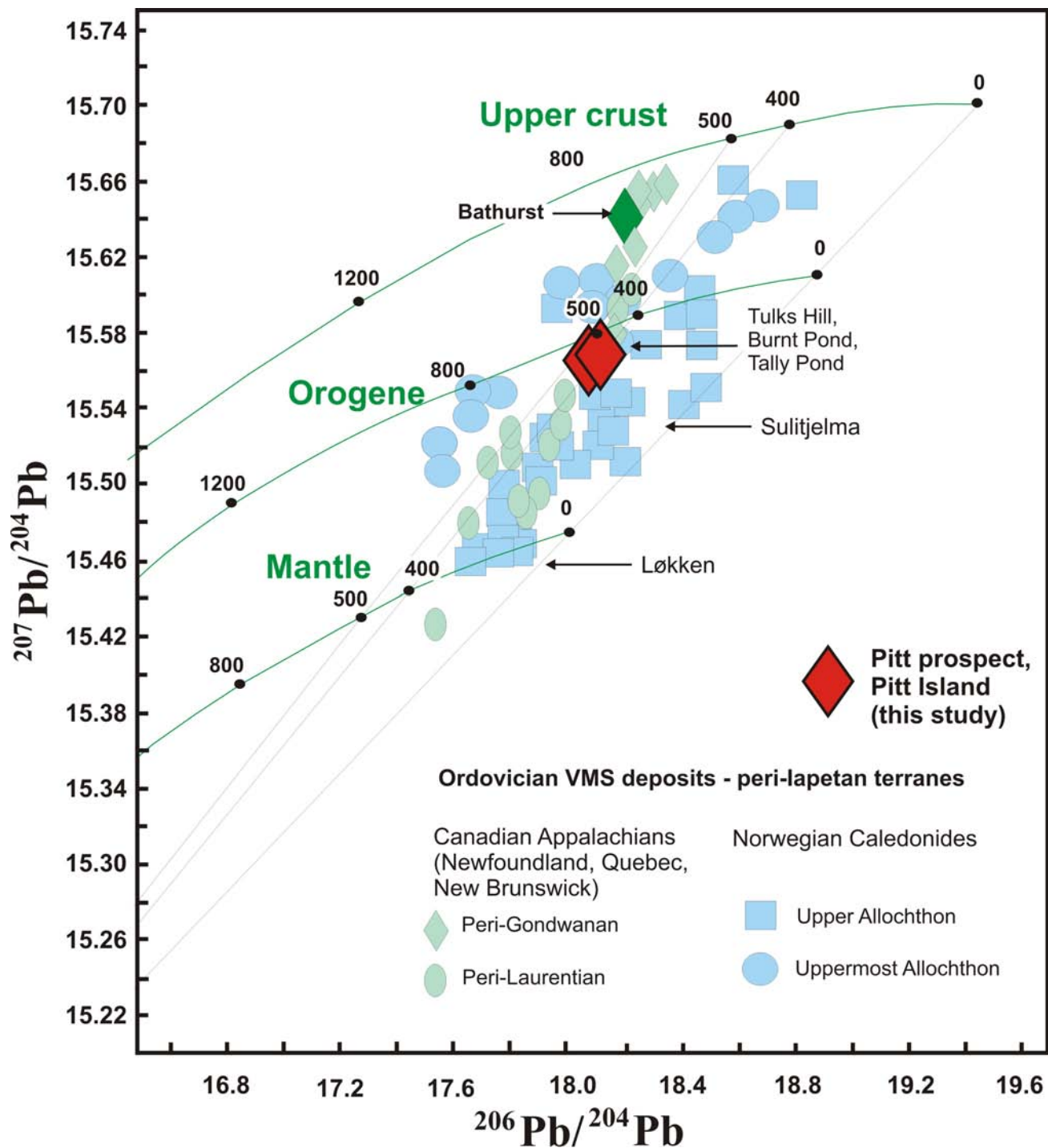


Fig. 10. $^{207}\text{Pb}/^{204}\text{Pb}$ vs. $^{206}\text{Pb}/^{204}\text{Pb}$ plot for Alexander leads vs. Ordovician VMS deposits of the Caledonides. Appalachian deposits from Swinden and Thorpe (1984); Norwegian deposits from Bjørlykke et al. (1993).

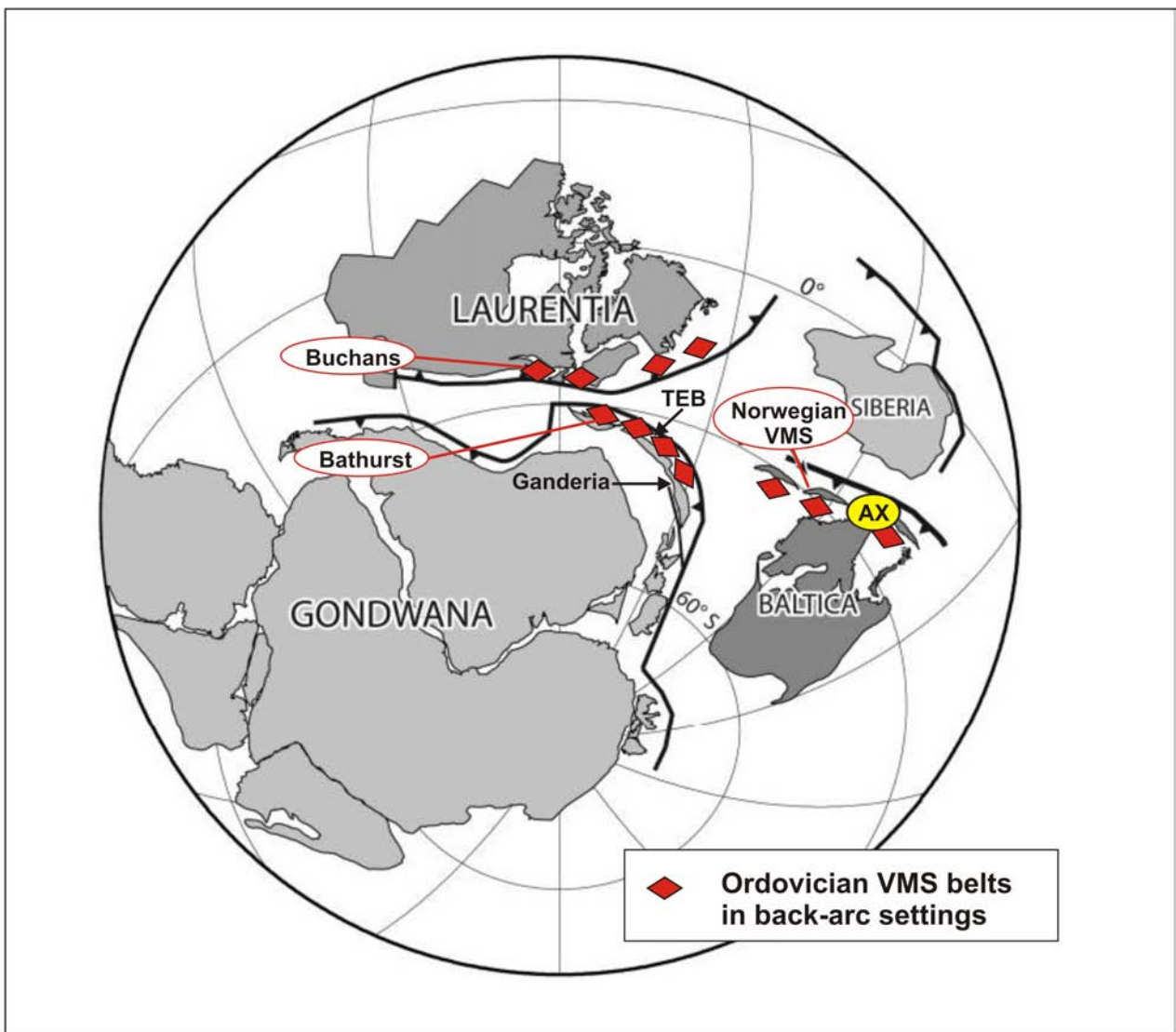


Fig. 11. Suggested paleogeographic position of Alexander terrane in Ordovician time. Global reconstruction from figure 18 of Beranek et al. (2012). Inferred locations of VMS deposits based on van Staal (2007). AX = Alexander terrane; TEB = Tetagouche-Exploits back-arc.

with Swinden and Thorpe’s (1984) analysis of the Appalachian $^{207}\text{Pb}/^{204}\text{Pb}$ vs. $^{206}\text{Pb}/^{204}\text{Pb}$ trend on Figure 10, the most likely pericratonic source would be the Grenville orogen. As Grenvillian basement is found throughout the Caledonides, it does not provide a specific constraint.

However, the lead isotopic signature of the Pitt deposit clearly allies it with Ordovician deposits of pericratonic origin, coinciding with the centres of both Appalachian and Norwegian data sets. Given the other strong evidence that the Alexander terrane was located north of the Scandinavian Caledonides in mid-Paleozoic time (Bazard et al., 1995; Beranek et al., 2012), a case can be built that its Ordovician arc and back-arc assemblages,

and their enclosed VMS deposits, are an “orphaned” fragment of the circum-Iapetan volcanogenic metallogenic belt (Fig. 11).

5. Conclusions

Geological mapping, supported by geochronology, has established that the Ordovician Moira Sound unit, of southern Prince of Wales Island extends as far south as Grenville Channel in northwestern coastal British Columbia. Indicators of volcanogenic potential within this belt include: the polymetallic massive and stringer zone showings at the Pitt prospect (103H 066); sulphide-laced rhyolites on Digby and Kennedy islands; and probable exhalites and magnetite iron formation on northeastern Pitt and Porcher islands. Pb isotopic results from the Pitt

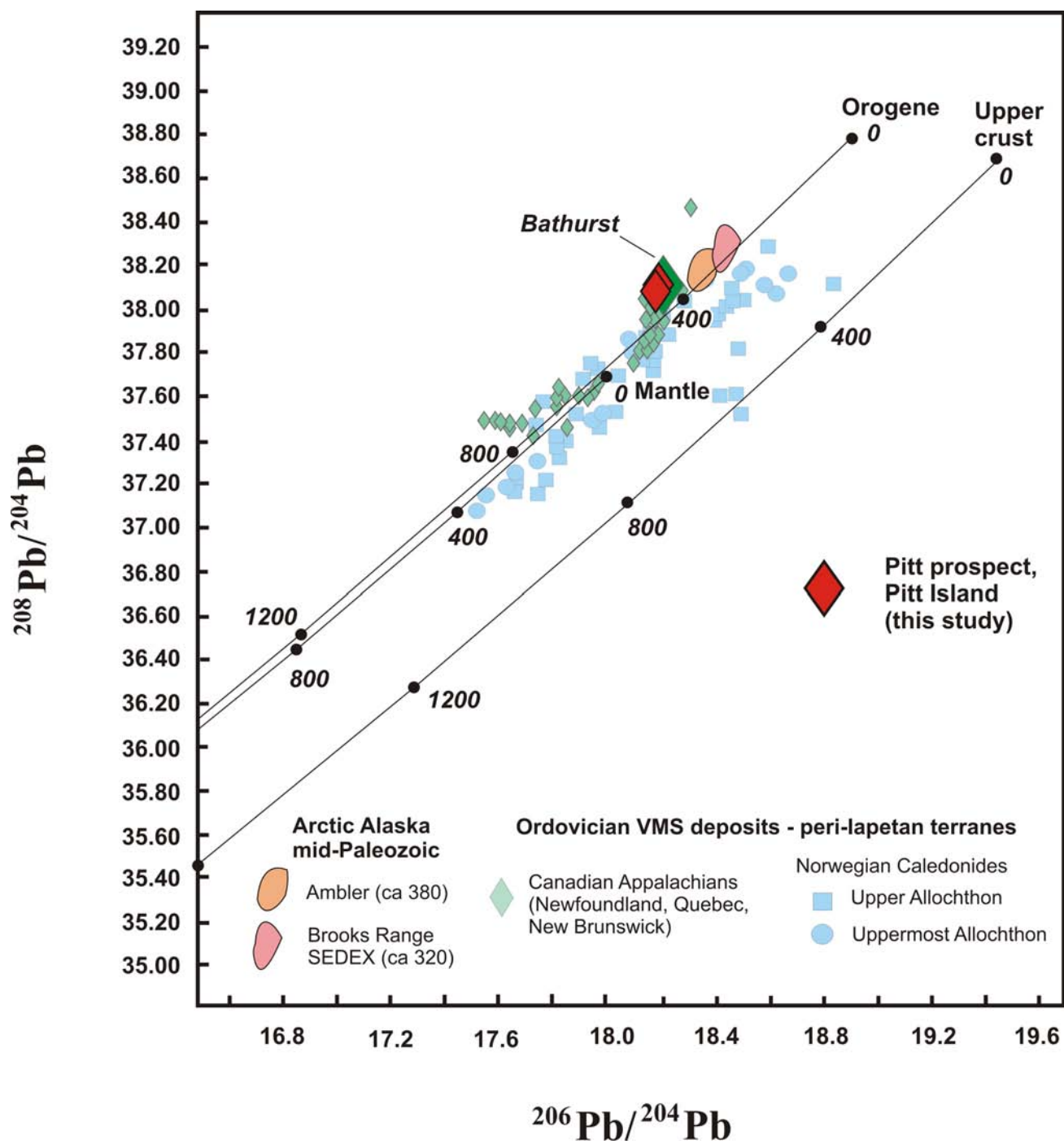


Fig. 12. $^{208}\text{Pb}/^{204}\text{Pb}$ vs. $^{206}\text{Pb}/^{204}\text{Pb}$ for Alexander leads vs. Ordovician VMS deposits of the Caledonides. Appalachian deposits from Swinden and Thorpe (1984) and Stacey and Kramers (1975); Norwegian deposits from Bjørlykke et al. (1993).

prospect confirm that it is Ordovician, syngenetic mineralization, rather than a Cretaceous epigenetic occurrence.

The strong structural control of the Pitt trend, the elongation of the sulphide-rich zone, and stringer-style (as opposed to bedded) mineralization suggest that it was a feeder zone to seabed massive sulphides, likely controlled by pencontemporaneous, basin-bounding faults. The Pitt trend structure was remobilized during the Early Cretaceous to form the southwestern boundary of the Grenville Channel shear zone on Pitt Island. Reactivation of original normal faults into thrusts and/or transcurrent faults is common in syngenetic mineralized systems, and has been observed at tectonised volcanogenic deposits such as Britannia and Tulsequah Chief, as well as SEDEX deposits (Nelson, 1998).

The Pitt Pb isotopic signature lies within the field of Ordovician VMS deposits of eastern Canada and Scandinavia. The Caledonian leads represent a mixing of sources between primitive Ordovician mantle and upper continental crust, most likely Grenvillian. Previously, the southern Alexander terrane was considered entirely primitive and ensimatic (Samson et al., 1989), although recent detrital zircon studies have offered strong evidence for nearby pericratonic crust (Gehrels and Boghossian, 2000; Nelson et al., 2012b; Beranek et al., 2012). The Moira Sound unit was probably deposited in a pericontinental marginal basin similar to modern sites of seafloor sulphide mineralization such as the Lau Basin and the Central Okinawa Trough.

Acknowledgments

Thanks go to Remy Huneault of Overburden Drilling Management Ltd. for the careful handling of the sulphide separates, and to Sarah Rice of ALS Chemex for orchestrating the Pb analytical process. Our understanding of the Alexander terrane has benefitted greatly from teaching and guidance by Sue Karl and Peter Hauessler of the USGS, and George Gehrels of the University of Arizona. Sue Karl's review greatly improved the paper. Larry Aspler is thanked for a thorough early review and thoughtful editing.

References cited

Ayuso, R.A., Karl, S.M., Slack, J.F., Haeussler, P.J., Bittenbender, P.E., Wandless, G.A., and Colvin, A.S., 2005. Oceanic Pb-isotopic sources of Proterozoic and Paleozoic volcanogenic massive sulphide deposits on Prince of Wales Island and vicinity, southeastern Alaska. In: *Studies by the U.S. Geological Survey in Alaska 2005*, US Geological Survey, Professional Paper 1732-E, 1-20.

Bazard, D. R., Butler, R. F., Gehrels, G. E. and Soja, C. M. 1995. Early Devonian paleomagnetic data from the Lower Devonian Karheen Formation suggest Laurentia-Baltica connection for the Alexander terrane. *Geology* 23, 707-710.

Beranek, L.P., van Staal, C.R., Gordee, S.M., McClelland, W.C., Israel, S., and Mihalyuk, M.G., 2012. Tectonic

significance of Upper Cambrian–Middle Ordovician mafic volcanic rocks on the Alexander terrane, Saint Elias Mountains, northwestern Canada. *Journal of Geology* 120, 293-314.

Bjørlykke, A., Vokes, F. M., Birkeland, A., and Thorpe, R. I., 1993. Lead isotope systematics of strata-bound sulfide deposits in the Caledonides of Norway. *Economic Geology* 88, 397-417.

Bohme, D.M., 1993. Geological, geochemical and geophysical report on the Pitt/Trinity claim group; B.C. Ministry of Energy, Mines and Petroleum Resources, Assessment Report 22912, 34 p.

Bradley, W., 1987. Report of exploration on the Trinity Property, BP Resources Canada. B.C. Ministry of Energy Mines and Petroleum Resources, Assessment Report 15674, 57 p.

Church, S.E., Gray, J.E., Delevaux, M.H. and LeHuray, A.P., 1987. Pb-isotopic signatures of Devonian-Mississippian massive sulphide deposits in Alaska and their significance to mineral exploration. In: Elliott, I.L. and Smee, B.W. (Eds.), *GEOEXPO/86, Exploration in the North American Cordillera*. Association of Exploration Geochemists, Rexdale, 132-141.

Cumming, G.L., Kyle, J.R., and Sangster, D.F., 1990. Pine Point: A case history of lead isotope homogeneity in a Mississippi-type district. *Economic Geology* 85, 133-144.

Colpron, M., and Nelson, J.L., 2009. A Paleozoic Northwest Passage: Incursion of Caledonian, Baltican and Siberian terranes into eastern Panthalassa, and the early evolution of the North American Cordillera. In: Cawood, P.A. and Kröner, A. (Eds.), *Earth Accretionary Systems in Space and Time*. Geological Society of London Special Publication 318, 273-307.

Colpron, M., and Nelson, J.L., 2011. A Paleozoic Northwest Passage and the Timanian, Caledonian and Uralian connections of some exotic terranes in the North American Cordillera. In: Spencer, A.M., Embry, A.F., Gautier, D.L., Stoupakova, A.V., and Sørensen, K. (Eds.), *Arctic Petroleum Geology*. Geological Society of London, Memoir 35, 463-484.

Doe, B.R. and Zartman, R.E., 1979. Chapter 2, Plumbotectonics I, the Phanerozoic. In: Barnes, H.L. (Ed.), *Geochemistry of Hydrothermal Ore Deposits*, 2nd edition, Wiley Interscience, New York, NY, 22-70.

Eastoe, C.J., and Gustin, M.M., 1996. Volcanogenic massive sulphide deposits and anoxia in the Phanerozoic oceans. *Ore Deposit Reviews*, 10, 179-197.

Eberlein, G.D., and Churkin, M. Jr., 1970. Paleozoic stratigraphy in the northwest coastal area of Prince of Wales Island, southeastern Alaska: U.S. Geological Survey Bulletin 1284, 67 p., 2 sheets, 1:125 000 scale.

Forbes, R.B., Gilbert, W.G., and Redman, 1987. The Four Winds complex; A newly recognized Paleozoic metamorphic complex in southeastern Alaska. *Geological Society of America Abstracts with Programs*, 19, 378.

Fouquet, Y. and Marcoux, E. 1995. Lead isotope systematics in Pacific hydrothermal sulfide deposits. *Journal of Geophysical Research*, 100, B4, 6025-, doi:10.1029/94JB 02646.

- Fox, J. S., Farquhar, R., Rui, I. and Cook, N., 1988. Genesis of basalt-hosted massive sulphide deposits from the Trondheim and Sulitjelma districts, Norway: Ore lead isotopic considerations. *Mineralium Deposita* 23, 276-285.
- Gardner, M.C., Bergman, S.C., Cushing, G.W., MacKevett, E.M. Jr., Plafker, G., Campbell, R.B., Dodds, C.J., McClelland, W.C., and Mueller, P.A., 1988. Pennsylvanian pluton stitching of Wrangellia and the Alexander terrane, Wrangell Mountains, Alaska. *Geology* 16, 967-971.
- Gehrels, G.E., 2001. Geology of the Chatham Sound region, southeast Alaska and coastal British Columbia. *Canadian Journal of Earth Sciences* 38, 1579-1599.
- Gehrels, G.E., and Berg, H.C., 1992. Geologic map of southeastern Alaska. United States Geological Survey Miscellaneous Investigation Series Map 1-1867, 1:600 000 scale.
- Gehrels, G.E., and Berg, H.C., 1994. Geology of southeastern Alaska. In: *The Geology of Alaska; v. G-1, The Geology of North America*, The Geological Society of America, 451-467.
- Gehrels, G.E., and Boghossian, N.D., 2000. Reconnaissance geology and U-Pb geochronology of the west flank of the Coast Mountains between Bella Coola and Prince Rupert, coastal British Columbia. In: Stowell, H.H. and McClelland, W.C. (Eds.), *Tectonics of the Coast Mountains, Southeastern Alaska and British Columbia*. Geological Society of America, Special Paper 343, 61-76.
- Gehrels, G. E., and Saleeby, J. B., 1987. Geologic framework, tectonic evolution and displacement history of the Alexander terrane. *Tectonics* 6, 151-174.
- Gehrels, G.E., Berg, H.C., and Saleeby, J.B., 1983. Ordovician Silurian volcanogenic massive sulfide deposits on southern Prince of Wales Island and the Barrier Islands, southeastern Alaska. US Geological Survey, Open File Report 83318, 11 p.
- Godwin, C.I., Gabites, J.E., and Andrew, A., 1988. Leadtable: A Galena lead isotope database for the Canadian Cordillera, with a guide to its use by explorationists. British Columbia Ministry of Energy, Mines and Petroleum Resources, British Columbia Geological Survey Paper 1988-4, 187 p. Database available in MS Access: <http://www.empr.gov.bc.ca/Mining/Geoscience/PublicationsCatalogue/Papers/Pages/1988-4.aspx>
- Godwin, C.J., and Sinclair, A.J., 1982. Average lead isotope growth curves for shale-hosted zinc-lead deposits, Canadian Cordillera. *Economic Geology* 77, 675-690.
- Haeussler, P., Karl, S., Mortensen, J.K., Layer, P., and Himmelberg, G., 1999. Permian and mid-Cretaceous deformation of the Alexander terrane on Admiralty and Kupreanof Islands, southeastern Alaska. *Geological Society of America Abstracts with Programs*, 31, A-60.
- Halbach, P., Hansmann, W., Köppel, V. and Pracejus, B., 1997. Whole-rock and sulfide lead-isotope data from the hydrothermal JADE field in the Okinawa back-arc trough. *Mineralium Deposita* 32, 70-78.
- Karl, S., Haeussler, P., Friedman, R.M., Mortensen, J.K., Himmelberg, G.R., and Zumsteg, C.L., 2006. Late Proterozoic ages for rocks on Mount Cheetdeekayu and Admiralty Island, Alexander terrane, southeast Alaska. *Geological Society of America Abstracts with Programs*, 38, 20.
- Karl, S.M., Layer, P.W., Harris, A.G., Haeussler, P.J., and Murchey, B.L., 2010. The Cannery Formation: Devonian to Early Permian arc-marginal deposits within the Alexander terrane, southeastern Alaska. In: *Studies by the U.S. Geological Survey in Alaska 2008-2009*, United States Geological Survey Professional Paper 1776-B, 45 p.
- Lo, B.B.H., 1992. Geophysical report on a helicopter-borne electromagnetic and magnetometer survey at the Pitt/Trinity property, British Columbia, NTS 103H/12. B.C. Ministry of Energy and Mines and Petroleum Resources, Assessment Report 22475, 45 p.
- Mihalynuk, M. G., Smith, M. T., MacIntyre, D. G., and Deschênes, M. 1993. Tashenshini Project part b: Stratigraphic and magmatic setting of mineral occurrences. In: *Geological Fieldwork 1992*, British Columbia Ministry of Energy, Mines and Petroleum Resources, British Columbia Geological Survey Paper 1993-1, 189-228.
- Nelson, J., 1998. The quiet counter-revolution: Structural control of syngenetic deposits. *Geoscience Canada*, 24, 91-98.
- Nelson, J. L., and Colpron, M. 2007. Tectonics and metallogeny of the Canadian and Alaskan Cordillera, 1.8 Ga to present. In: Goodfellow, W.D. (Ed.) *Mineral Deposits of Canada: A Synthesis of Major Deposit Types, District Metallogeny, the Evolution of Geological Provinces, and Exploration Methods*. Mineral Deposit Division, Geological Association of Canada, Special Publication, 5, 755-791.
- Nelson, J.L., Mahoney, J.B., Gehrels, G.E., van Staal, C., and Potter, J.J., 2010. Geology and mineral potential of Porcher Island, northern Grenville Channel and vicinity, northwestern British Columbia. In: *Geological Fieldwork 2009*, British Columbia Ministry of Energy and Mines, British Columbia Geological Survey Paper 2010-1, 19-42.
- Nelson, J.L., Mahoney, J.B., Gehrels, G., Pecha, M., van Staal, C., Diakow, L., Karl, S., and Angen, J., 2012a. The "British Columbia Caledonides": mid-Paleozoic orogeny in the southern Alexander terrane. *Geological Association of Canada Abstracts*, 35, 97-98.
- Nelson, J.L. Diakow, L.J., Mahoney, J.B., van Staal, C., Pecha, M., Angen, J.J., Gehrels, G., and Lau, T., 2012b. North Coast Project: Tectonics and metallogeny of the Alexander terrane, and Cretaceous sinistral shearing of the western Coast belt. In: *Geological Fieldwork 2011*, British Columbia Ministry of Energy, and Mines, British Columbia Geological Survey Paper 2012-1, 157-180.
- Samson, S.D., McClelland, W.C., Patchett, P.J., Gehrels, G.E., and Anderson, R.A., 1989. Evidence from neodymium isotopes for mantle contributions to Phanerozoic crustal genesis in the Canadian Cordillera. *Nature*, 337, 705-709.
- Slack, J.F., Shanks, W.C., Karl, S.M., Gemery, P.A., Bittenbender, P.E. and Ridley, W.I., 2005. Geochemical and sulfur-isotopic signatures of volcanogenic massive sulphide deposits on Prince of Wales Island and vicinity, southeastern Alaska. In: *Studies by the U.S. Geological Survey in Alaska*, U.S. Geological Survey Paper 1732C.

- Soja, C.M., 1994. Significance of Silurian stromatolite-sphinctozoan reefs. *Geology* 22, 355-358.
- Soja, C. M., and Antoshkina, A. I. 1997. Coeval development of Silurian stromatolite reefs in Alaska and the Ural Mountains: Implications for paleogeography of the Alexander terrane, *Geology* 25, 539-542.
- Soja, C.M., and Krutikov, L., 2008. Provenance, depositional setting and tectonic implications of Silurian polymictic conglomerates in Alaska's Alexander terrane. In: Blodgett, R.B. and Stanley, G.D. (Eds.), *The Terrane Puzzle: New Perspectives on Paleontology and Stratigraphy from the North American Cordillera*. Geological Society of America Special Paper 442, 63-75.
- Stacey, J.S., and Kramers, J.D., 1975. Approximation of terrestrial lead isotope evolution by a two-stage model. *Earth and Planetary Science Letters* 26, 207-221.
- Swinden, H.S., and Thorpe, R.I., 1984. Variations in style of volcanism and massive sulfide deposition in Early to Middle Ordovician island-arc sequences of the Newfoundland Central Mobile Belt. *Economic Geology* 79, 1596-1619.
- Taylor, C.D., Premo, W.R., Meier, A.L., and Taggart, J., Jr., 2008. The metallogeny of Late Triassic rifting of the Alexander terrane in southeastern Alaska and northwestern British Columbia. *Economic Geology* 103, 89-115.
- Van Staal, C., 2007. Pre-Carboniferous metallogeny of the Canadian Appalachians. In: Goodfellow, W. D. (ed.), *Mineral Deposits of Canada: A Synthesis of Major Deposit Types, District Metallogeny, the Evolution of Geological Provinces, and Exploration Methods*. Mineral Deposit Division, Geological Association of Canada, Special Publication 5, 793-818.
- Wheeler, J.O., and McFeely, P., 1991. Tectonic assemblage map of the Canadian Cordillera and adjacent parts of the United States of America: Geological Survey of Canada, Map 1712A, scale 1:2 000 000.
- Zartman, R.E., and Doe, B.R., 1981. Plumbotectonics-the model. *Tectonophysics* 75, 135-162.

LA-ICP-MS geochronology of the Greenwood gabbro, Knob Hill complex, southern Okanagan, British Columbia

N.W.D. Massey^{1,a}, J.E. Gabites² and J.K. Mortensen²

¹ British Columbia Geological Survey, Ministry of Energy, Mines and Natural Gas, Victoria, BC, V8W 9N3 (Emeritus Scientist)

² Pacific Centre for Isotopic and Geochemical Research, Department of Earth and Ocean Sciences, University of British Columbia, Vancouver, BC, V6T 1Z4

^a corresponding author: nickmassey@shaw.ca

Recommended citation: Massey, N.W.D., Gabites, J.E. and Mortensen, J.K., 2013. LA-ICP-MS geochronology of the Greenwood gabbro, Knob Hill complex, southern Okanagan, British Columbia. In: Geological Fieldwork 2012, British Columbia Ministry of Energy, Mines and Natural Gas, British Columbia Geological Survey Paper 2013-1, pp. 35-44.

Abstract

The Paleozoic basement of Quesnellia in the southern Okanagan region includes rocks of the Knob Hill complex, an ophiolitic suite of gabbros, serpentinites, basaltic rocks, cherts, and argillites. Near the towns of Rock Creek and Greenwood, the Knob Hill complex is exposed in an east-trending belt of inliers within south-vergent thrust panels. These rocks are considered to record intraoceanic arc to back-arc basin environments, but precise U-Pb zircon ages have been lacking. Using laser ablation inductively coupled plasma mass spectrometry (LA-ICP-MS), four samples of pegmatitic gabbro from the Greenwood gabbro unit of the Knob Hill complex yielded U-Pb zircon ages of: 389.3 ±2.5 Ma; 387.3 ±2.5 Ma; 386.9 ±3.0 Ma; and 380.0 ±2.9 Ma (all errors at the 2σ level). Together with tectonostratigraphic and geochemical data, the new ages indicate that intraoceanic subduction processes represented by the Knob Hill complex began as early as 390-380 Ma, entirely outboard of Laurentia. Combined with sparse paleontologic age determinations, these new ages help reveal a protracted history in the Knob Hill complex, spanning the interval from ~390 to 300 Ma, that is now largely masked by younger structures and cover rocks. With the notable exception of the Trail gneiss complex, exposed about 75 km northeast of Greenwood and with a published U-Pb zircon age of ~372 Ma, potentially equivalent rocks elsewhere in the Okanagan subterrane, such as the Anarchist Group west of Osoyoos, the Old Tom Formation southwest of Penticton, and the Palmer Mountain Greenstone in Washington State, remain undated.

Keywords: Quesnellia, Knob Hill complex, Greenwood gabbro, geochronology, Middle Devonian

1. Introduction

In 2005, the British Columbia Geological Survey initiated the Boundary Project to better characterize the lithological and geochemical variations of Paleozoic successions in the southern Okanagan region along the Canada-USA border (Massey 2006, 2007a, 2007b; Massey and Duffy 2008a, 2008b, 2008c). These successions form part of Quesnellia (Fig. 1), which consists mainly of: a Paleozoic basement of mafic and pelitic rocks; unconformably overlying Triassic and Jurassic volcanic and sedimentary rocks; and crosscutting suites of Triassic, Jurassic, and Eocene granitic intrusions. Ongoing tectonic syntheses (e.g., Nelson and Colpron, 2007; Colpron and Nelson, 2009; 2011) emphasize the distinction between Cordilleran terranes with a western Laurentian heritage and those that are entirely exotic to North America. In contrast to farther north, Paleozoic basement in southern Quesnellia (Okanagan subterrane of Monger, 1977; Peatfield, 1978) may not have been built on Laurentian crust (as interpreted by Thompson et al., 2006), but be entirely exotic (e.g., Simony et al., 2006; Colpron and Nelson, 2009). Essential to such evaluations

are robust geochronological and geochemical data, hitherto lacking from Paleozoic rocks in the southern Okanagan.

Herein we present laser ablation inductively coupled plasma mass spectrometry (LA-ICP-MS) data from zircons in gabbroic rocks of the Knob Hill complex (Fig. 2), a structurally disrupted ophiolitic suite of gabbros, serpentinites, basaltic rocks, cherts, and argillites (Little, 1983; Dostal et al., 2001). In a companion paper (Massey and Dostal, this volume) we present geochemical data from the Knob Hill complex and the Anarchist Group, a likely equivalent exposed in structural panels south and west of the complex. Four samples from outcrops of the Greenwood gabbro (Fig. 2) yielded U-Pb zircon ages of 390-380 Ma. These results, together with geochemical data (Massey and Dostal, this volume), and a juvenile εNd value of +7.2 (Ghosh, 1995) suggest that the Knob Hill complex records Middle to Late Devonian intraoceanic subduction processes outboard of North America. However, coupled with a Late Pennsylvanian to earliest Permian (~300 Ma) determination from radiolarians in a single chert sample (Cordey, in Massey,

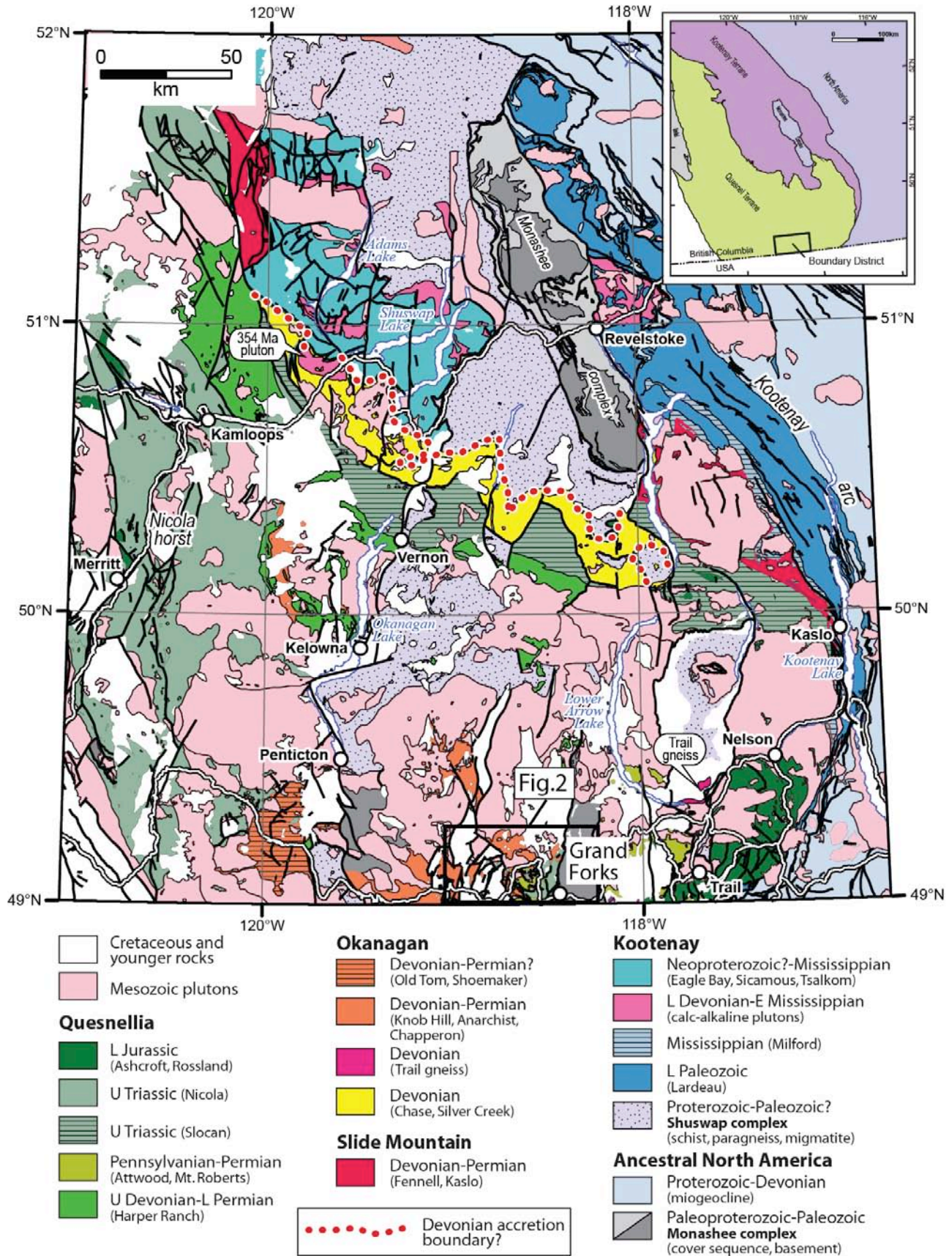


Fig. 1. Regional setting of the Knob Hill complex (after Colpron and Nelson, 2009). Inset, simplified terrane map of southeastern British Columbia (amended from digital geology of Massey et al., 2005).

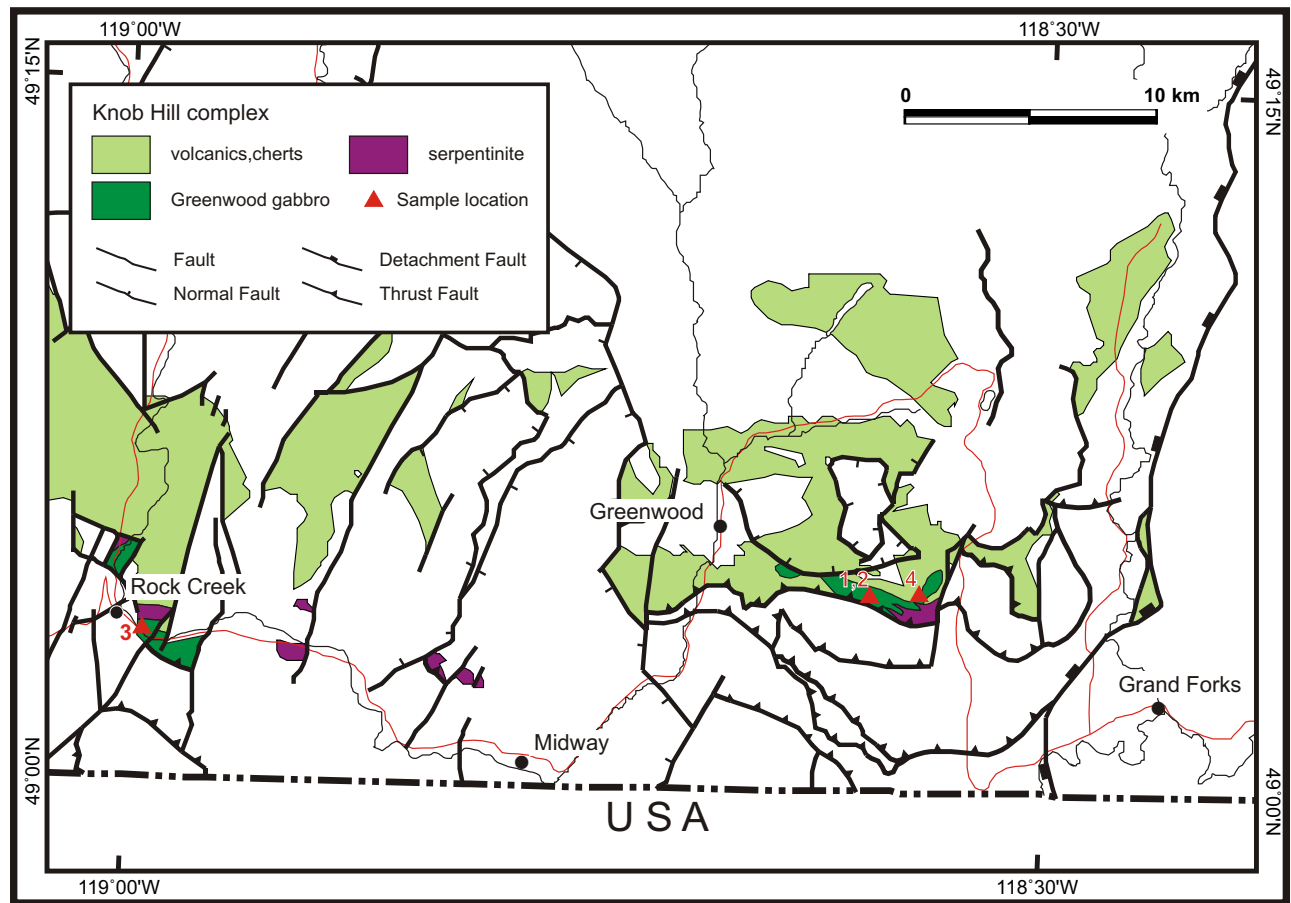


Fig. 2. Distribution of the Knob Hill complex succession; gabbro and serpentinite shown separately. Location of the gabbro sample sites, numbered as in Table 1. Geology amended from the digital geology map of British Columbia (Massey et al., 2005).

2007b), and a Late Devonian (385-375 Ma) determination from conodonts (Orchard, 1993), the U-Pb ages indicate that the geological record of the Knob Hill complex spans 80-90 million years, hinting at multiple, but structurally masked, tectonic environments.

2. Knob Hill complex and Greenwood gabbro

Interpreted stratigraphic arrangement of map units in the Kettle Valley River area north of Rock Creek (Fig. 2) suggests that Knob Hill complex constitutes a disrupted ophiolite (Little, 1983; Fyles, 1990; 1995). Gabbro and serpentinite pass northwards, and probably upwards, into greenstones, mixed greenstones and cherts, and finally into cherts and argillites (Massey, 2007a). Stratigraphic relationships between map units are less clear in the Greenwood area. However, outcrops along the power line adjacent to the Winnipeg Mine, east of Greenwood (location 4, Fig. 2), show well developed chilled margins in medium-grained diabase and microgabbro, suggesting they may be part of a yet to be delineated sheeted dike complex. The stratigraphic thickness of the Knob Hill complex is uncertain and difficult to estimate due to structural disruption. Nonetheless, Little (1983) suggested “a minimum of a few thousands of metres”, and Fyles (1990, 1995) gave an estimate of at least 5 km.

The Greenwood gabbro was informally referred to as the “Old Diorite” by previous authors (e.g., Church, 1986) but renamed the “Greenwood gabbro” by Dostal et al. (2001), the term we use herein. The gabbros are composed of white plagioclase and green to black pyroxenes that have been extensively replaced by hornblende. Chlorite is common on fracture surfaces. The gabbros are characteristically variable and patchy in texture (Fig. 3a). Coarse-grained gabbro phases grade into finer microgabbro or even coarser pegmatitic phases (Fig. 3b), and chilled contacts are notably lacking. This suggests that different phases are co-magmatic and were injected over a short time interval. Light-coloured felsic veins (plagiogranite?) crisscross some outcrops (Fig. 3d). Diabase dikes crosscut the gabbro, but local diabase xenoliths in gabbro imply multiple injection episodes of both. Church (1986) reported a K-Ar whole rock age of 258 ± 10 Ma (Permian) for uraltized gabbro from the Winnipeg Mine. However it is doubtful that this age records the time of crystallization.

3. Geochronology

Four coarse-grained samples from pegmatitic zones in the Greenwood gabbro were collected at three sites for U-Pb zircon geochronology (Fig. 2; Table 1).

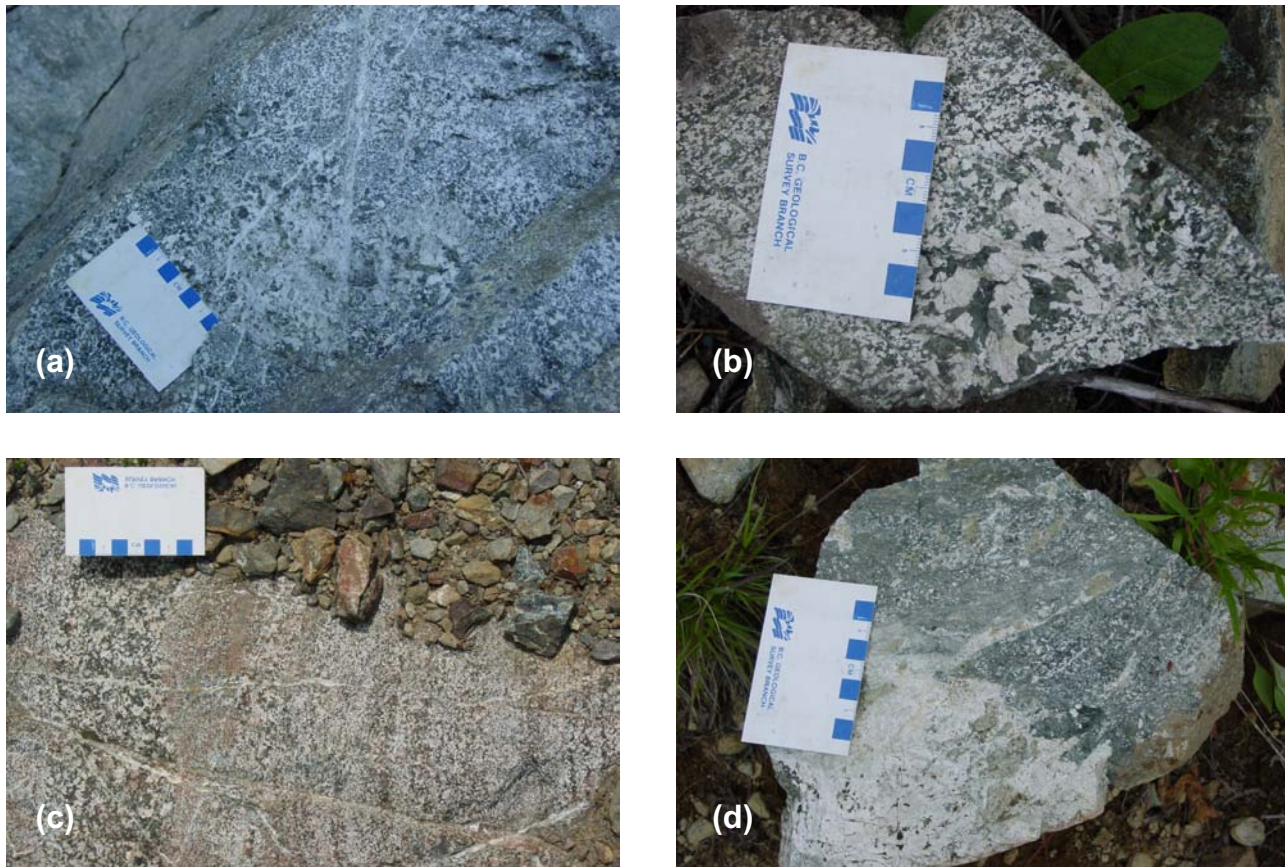


Fig. 3. Greenwood gabbro in outcrop. **a)** Typical varitextured gabbro, with white felsic vein network (05NMA21-02, UTM zone 11, 5436561N, 353922E NAD83). **b)** pegmatitic gabbro (05NMA02-03; UTM zone 11, 5436880N, 385180E NAD83). **c)** compositional and grain size layering (05NMA02-11; UTM zone 11, 5436808N, 385264E NAD83). **d)** plagiogranite dike in varitextured gabbro (05NMA02-11; UTM zone 11, 5436808N, 385264E NAD83).

Table 1. Summary of U-Pb zircon ages from Greenwood pegmatitic gabbro samples, Knob Hill complex. All UTM location data are in zone 11, NAD83. Errors associated with individual ages are listed at the 2σ level (95% confidence interval).

Sample number	Latitude	Longitude	UTM		Area	Age	
	°N	°W	Northing	Easting		Ma	±
05NMAWin	49.071680	118.586500	5436636	384128	Winner Quarry	380.0	2.9
06NMAWinner	49.071680	118.586500	5436636	384128	Winner Quarry	386.9	3.0
06NMA GABB1	49.064603	118.999792	5436564	353924	Rock Creek	389.0	2.9
06NMA04-004	49.074179	118.572028	5436892	385191	Powerline, N of Winnipeg Mine	387.3	2.5

3.1. Analytical methods

Uranium-lead dating of zircons was carried out at the Pacific Centre for Geochemical and Isotopic Research at the University of British Columbia, using laser ablation inductively coupled plasma mass spectrometry (LA-ICP-MS). Instrumentation included a New Wave UP-213 laser ablation system and a ThermoFinnigan Element2 single collector, double-focusing, magnetic sector ICP-MS. Data acquisition and reduction protocols detailed by Tafti et al.

(2009), are summarized below. Zircons were handpicked from the heavy mineral concentrate and mounted in an epoxy puck along with several grains of the Plešovice zircon standard (Sláma et al., 2007), together with an in-house, 197 Ma standard zircon, and brought to a very high polish. High quality portions of each grain (free of alteration, inclusions, or possible inherited cores) were selected for analysis. The surface of the mount was washed for 10 minutes with dilute nitric acid and rinsed in

ultraclean water prior to analysis. Line scans rather than spot analyses were employed in order to minimize elemental fractionation during the analyses. Backgrounds were measured with the laser shutter closed for ten seconds, followed by data collection with the laser firing for approximately 29 seconds. The time-integrated signals were analysed using GLITTER software (Van Achterbergh et al., 2001; Griffin et al., 2008), which automatically subtracts background measurements, propagates all analytical errors, and calculates isotopic ratios and ages. Corrections for mass and elemental fractionation were made by bracketing analyses of unknown grains with replicate analyses of the Plešovice zircon standard. A typical analytical session consisted of four analyses of the standard zircon, followed by four analyses of unknown zircons, two standard analyses, four unknown analyses, etc., and finally four standard analyses. The 197 Ma in-house zircon standard was analysed as an unknown in order to monitor the reproducibility of the age determinations on a run-to-run basis. Final interpretation and plotting of the analytical results used Ludwig's (2003) ISOPLOT software. Interpreted ages are based on a weighted average of the individual calculated $^{206}\text{Pb}/^{238}\text{U}$ ages.

Although zircons typically contain negligible amounts of initial common Pb, it is important to monitor the amount of ^{204}Pb to evaluate the amount of initial common Pb, and/or blank Pb, in the zircons being analyzed. The argon that is used in an ICP-MS plasma commonly contains at least a small amount of Hg, and approximately 7% of natural Hg has a mass of 204. Measured count rates on mass 204 include ^{204}Hg as well as any ^{204}Pb that might be present, and direct measurement of ^{204}Pb in a laser ablation analysis is therefore not possible. Instead, mass 202 is monitored; this corresponds exclusively to ^{202}Hg . The expected count rate for ^{204}Hg present in the analysis can then be calculated from the known isotopic composition of natural Hg, and any remaining counts at mass 204 can be attributed to ^{204}Pb . Using this method it is possible to conclude that there was no measurable ^{204}Pb present in any of the analyses in this study.

3.2. Results

Results of the dating studies are summarized in Table 1 and complete analytical data are presented in Table 2. Laser-ablation ICP-MS analyses of the four samples indicate ages that range between 380 and 390 Ma (Middle to Late Devonian; Fig. 4). The two samples from the Winner quarry (1 and 2 in Table 1, Fig. 2) show a spread of 6.9 Ma. Although this spread is only slightly greater than the 2σ error limits of the age determinations (Table 1), it could signify multiple intrusion events.

4. Discussion

Field tectonostratigraphic (e.g., Little, 1983; Fyles, 1990; 1995; Massey et al., 2010), geochemical (Dostal et al., 2001; Massey and Dostal, this volume), and Nd isotopic (Ghosh, 1995) studies indicate that the basement

to Quesnellia in the southern Okanagan region represents growth of an intraoceanic subduction complex outboard of North America (Colpron and Nelson, 2009). Geochronologic data presented herein document that subduction processes initiated by at least 390-380 Ma. Previously, Little (1983) assigned a Carboniferous to Permian age to the Knob Hill complex, based on a single macro-fossil locality (his locality F7, page 12), about a kilometre east of the Winnipeg Mine (location 4, Fig. 2). However, this same limestone bed yielded conodonts of Late Devonian (Frasnian; 385-375 Ma) age (Orchard, 1993). Determinable radiolarians are rare in the cherts of the Knob Hill Complex, though one sample from the greenstone-chert sequence has yielded a Late Pennsylvanian to earliest Permian (~300 Ma) age (Cordey, in Massey, 2007b). The geochronologic data in the present paper, together with the sparse paleontologic data in Orchard (1993) and Cordey (in Massey, 2007b), suggest that the Knob Hill complex, as a whole, spans an interval of 80 to 90 million years, seemingly excessive for a single, small subduction-related basin (see Woodcock, 2004). This apparent longevity might imply cryptic tectonic processes and environments now masked by structural complexities and cover rocks.

Potential correlatives to the Knob Hill complex outcrop south and west of the Greenwood area, and include: the Anarchist Group (e.g., Massey et al., this volume); the Old Tom Formation (Bostock 1939, 1940) in the Keremeos area, southwest of Penticton; and the Palmer Mountain greenstone in Washington (Rinehart and Fox, 1972). Isotopic ages are currently unavailable for these units, although studies are ongoing in the Keremeos area (Mortensen et al., 2010). Possibly a tectonostratigraphic equivalent to the Knob Hill complex, the Trail gneiss complex (exposed ~75 km northeast of Greenwood) has yielded a U-Pb zircon age of ~372 Ma and positive initial ϵNd values (+4.7 - +5.6), and is thought to represent a Late Devonian intraoceanic arc lacking a North American heritage (Simony et al., 2006).

5. Conclusions

Laser-ablation ICP-MS analyses of zircons from four samples of pegmatitic gabbro from the Knob Hill Complex yield late Middle to early Late Devonian crystallization ages that range between 390 and 380 Ma. Together with field tectonostratigraphy, geochemical data, and Nd isotopic data, these ages indicate that the basement to Quesnellia in the southern Okanagan region may represent intraoceanic arc to back-arc environments developed outboard of, and unrelated to, Laurentia.

Acknowledgments

The senior author is much indebted to Jim Fyles and Neil Church for all their invaluable help and advice during the planning and early stages of this project. The collaboration, support, and ready welcome of the boundary district exploration community were exceptional. The project would not have made progress without the indispensable assistance of Alan Duffy,

Table 2. Laser ablation ICP-MS analytical data for zircons from Greenwood gabbro samples, Knob Hill Complex. Isotopic ratios and calculated ages for each zircon grain are listed with their associated errors at the 1σ level. “Rho” refers to the correlation coefficient between the calculated ratios of ²⁰⁶Pb/²³⁸U and ²⁰⁷Pb/²³⁵U.

Analysis	²⁰⁷ Pb/ ²³⁵ Pb			Isotopic ratios and one sigma errors			²⁰⁶ Pb/ ²³⁸ U			Rho			Calculated ages and one sigma errors			Background-corrected counts per second on individual masses					
	error	207Pb/235Pb	error	207Pb/235U	error	207Pb/235U	error	206Pb/238U	error	206Pb/238U	error	206Pb/238U	207Pb/235U	error	207Pb/235U	error	207Pb/235U	206Pb/238U	error	206Pb/238U	
06NMA-WIN																					
1	0.04927	0.000391	0.41424	0.03499	0.06144	0.00146	0.28	160.6	175.62	351.9	25.12	384.4	8.85	24	48	1524	71	428	6184	161	16823
2	0.04773	0.00291	0.39467	0.026	0.0601	0.00127	0.32	84.8	139.55	337.8	18.93	376.2	7.71	9	39	7407	405	905	11632	837	84344
3	0.05329	0.00231	0.45666	0.02183	0.06178	0.00106	0.36	341.3	94.81	381.9	15.21	386.4	6.43	30	0	4607	257	147	1424	613	60458
4	0.05348	0.00155	0.44939	0.01415	0.06049	0.00073	0.38	349.2	64.38	376.9	9.92	378.6	4.43	1	0	14235	806	1942	21406	1646	166097
5	0.0554	0.00164	0.46544	0.01498	0.06066	0.00075	0.38	428.2	64.2	388	10.38	379.6	4.56	12	0	5183	279	1006	10974	590	60118
6	0.05282	0.00188	0.45125	0.01755	0.06115	0.00086	0.36	321	79.15	378.2	12.28	382.6	5.23	0	0	12242	720	1195	13547	1395	145764
7	0.0578	0.00182	0.49385	0.01709	0.06052	0.0008	0.38	522	67.92	407.5	11.62	378.8	4.86	0	0	5571	304	154	1798	742	73832
8	0.05229	0.00199	0.44292	0.01847	0.06091	0.00091	0.36	298.3	84.6	372.3	13	381.1	5.54	96	0	3034	166	548	6744	362	36536
9	0.05402	0.00266	0.44189	0.02371	0.05939	0.0011	0.35	371.6	106.65	371.6	16.7	371.9	6.68	21	5	5391	283	989	11831	608	62546
10	0.05199	0.00209	0.45027	0.01981	0.06177	0.00096	0.35	284.9	89.3	377.5	13.87	386.4	5.8	0	0	1720	112	253	3513	236	23520
11	0.06491	0.00476	0.46312	0.03674	0.05254	0.00147	0.35	771.6	147.06	386.4	25.5	330.1	9.02	37	5	6215	335	180	2678	826	82793
12	0.05342	0.00205	0.44495	0.01861	0.0609	0.00089	0.36	346.5	84.27	373.7	13.07	378	5.47	21	26	18	0	0	0	0	0
13	0.05209	0.00209	0.45556	0.01867	0.06082	0.00089	0.36	441.2	81.58	381.2	13.02	380.6	5.41	0	10	2260	126	272	4236	275	26828
14	0.0556	0.00333	0.44891	0.02919	0.06115	0.00131	0.33	458.3	128.51	376.5	20.46	382.6	7.97	36	8	1960	107	63	834	290	29885
15	0.05346	0.00249	0.45567	0.02339	0.06189	0.00111	0.35	344.1	101.81	381.2	16.31	387.1	6.73	26	0	4802	285	1122	15579	543	57999
16	0.05961	0.00252	0.52076	0.02424	0.06047	0.001	0.36	589.5	89.02	425.7	16.19	378.5	6.05	8	32	9	0	0	9	0	0
17	0.05978	0.00307	0.49954	0.02807	0.0588	0.00113	0.34	595.2	108.11	411.4	19.01	368.3	6.88	0	0	4729	240	201	2226	657	64995
18	0.05356	0.00547	0.4475	0.04934	0.0654	0.0022	0.31	352.4	215.65	375.5	34.61	408.4	13.32	0	0	11700	619	2524	31939	1304	131945
19	0.05352	0.00222	0.47778	0.02191	0.06546	0.00105	0.35	350.8	90.83	396.5	15.05	408.7	6.38	0	37	6563	364	1591	19405	710	74865
20	0.05818	0.00253	0.51698	0.02587	0.06486	0.00113	0.35	458.7	97.73	423.1	17.32	405.1	6.81	0	43	19898	1082	3731	46076	2283	228141
21	0.05517	0.00219	0.47962	0.02105	0.06466	0.001	0.35	418.8	85.93	397.8	14.45	403.9	6.05	0	1	5472	280	208	2703	724	76085
06NMA-WINNER																					
1	0.05569	0.00086	0.49537	0.00845	0.06612	0.0004	0.35	439.9	33.41	408.6	5.74	412.7	2.41	72	19	16335	911	2673	50483	1908	241811
2	0.06267	0.00094	0.54543	0.00912	0.06117	0.00038	0.37	697	31.62	440.7	6	382.8	2.31	0	19	22241	1398	3024	53463	2668	356308
3	0.05587	0.00063	0.48125	0.00598	0.06181	0.00029	0.38	446.7	24.35	398.9	4.1	386.6	1.75	0	0	30884	1734	3949	68631	3735	490259
4	0.05488	0.00065	0.46901	0.00609	0.06199	0.0003	0.37	407.1	25.88	390.5	4.21	387.7	1.79	42	59	24359	1345	3651	66858	2973	386019
5	0.06161	0.00135	0.51655	0.01249	0.06205	0.00053	0.35	660.4	46.25	422.8	8.36	387.9	3.24	0	0	7527	469	637	8761	940	119649
6	0.05274	0.00162	0.44867	0.01502	0.06187	0.00068	0.33	317.6	68.15	376.3	10.53	387	4.14	199	0	6493	346	450	7679	800	103384
7	0.05504	0.00089	0.46685	0.00836	0.06319	0.00041	0.36	413.6	35.51	389	5.79	395	2.47	0	3	17566	981	2316	41441	2173	274657
8	0.05454	0.00089	0.47409	0.00859	0.06222	0.00041	0.36	393.2	36.13	394	5.92	389.1	2.47	99	0	15942	883	1346	25049	1926	253443
9	0.05798	0.00367	0.53765	0.03736	0.06553	0.00145	0.32	528.5	133.5	436.9	24.67	409.2	8.8	0	0	1558	92	533	10121	177	23613
10	0.05414	0.00068	0.48442	0.00792	0.06506	0.00038	0.36	376.6	32.97	401.1	5.42	406.3	2.31	45	0	17623	975	3425	66727	2080	269267
11	0.05507	0.00141	0.49707	0.01391	0.06563	0.00061	0.33	415.1	55.43	409.7	9.43	409.8	3.69	8	0	5661	319	636	12695	663	85839
12	0.04985	0.00141	0.43372	0.01342	0.06624	0.00063	0.33	188	64.57	365.8	9.51	389.2	3.83	40	0	9934	508	1178	22839	1210	159258
13	0.05424	0.00068	0.45776	0.00629	0.06105	0.00031	0.37	380.8	27.87	382.7	4.38	382	1.91	0	0	36083	2009	6159	13293	4535	590204

Table 2. Continued.

Analysis	²⁰⁶ Pb/ ²⁰⁸ Pb			²⁰⁶ Pb/ ²⁰⁷ Pb			Isotopic ratios and one sigma errors			²⁰⁶ Pb/ ²³⁸ U			Calculated ages and one sigma errors			Background-corrected counts per second on individual masses								
	error	²⁰⁶ Pb/ ²⁰⁸ Pb	error	error	²⁰⁶ Pb/ ²⁰⁷ Pb	error	Rho	error	²⁰⁶ Pb/ ²³⁸ U	error	²⁰⁶ Pb/ ²³⁸ U	error	error	²⁰⁶ Pb/ ²³⁸ U	error	202	204	206	207	208	232	235	238	
06NMA-04																								
1	0.05237	0.00052	0.48046	0.00529	0.06641	0.00028	0.38	301.6	22.44	398.4	3.63	414.5	1.71	0	11	85890	4693	18192	331607	9979	1304681			
2	0.05283	0.00065	0.47561	0.00631	0.06296	0.00031	0.37	363.8	27.06	395.1	4.34	393.6	1.89	0	87	49530	2737	13336	253836	5988	790246			
3	0.05451	0.00083	0.46779	0.00783	0.06184	0.00037	0.36	392	33.71	389.7	5.42	386.8	2.26	12	0	41410	2293	9729	212131	5158	670598			
4	0.05484	0.00093	0.46821	0.00872	0.0612	0.00041	0.36	405.8	37.26	390	6.03	382.9	2.46	26	24	26780	1489	5564	130841	3353	437967			
5	0.05404	0.00086	0.47014	0.00816	0.06283	0.00039	0.36	372.7	35.45	391.3	5.64	392.8	2.35	89	0	59697	3266	17202	310456	7336	950305			
6	0.05448	0.00098	0.46678	0.00918	0.06261	0.00043	0.35	391	39.65	389	6.35	391.5	2.62	0	0	68388	3756	16175	327490	8331	1090759			
7	0.05583	0.00113	0.48553	0.01075	0.06149	0.00047	0.35	445.5	44.08	401.9	7.35	384.7	2.87	52	5	42643	2395	9630	178415	5239	691880			
8	0.054	0.00115	0.46076	0.01068	0.06101	0.00049	0.35	371	47.12	384.8	7.43	381.8	2.97	65	37	40402	2193	8775	179579	5057	660405			
9	0.05386	0.00131	0.4726	0.01249	0.06297	0.00057	0.34	365.2	53.78	393	8.61	393.6	3.45	0	36	67645	3652	22585	490258	8222	1069492			
10	0.05429	0.00142	0.46334	0.01317	0.06149	0.0006	0.34	382.9	57.42	386.6	9.14	384.7	3.62	79	0	34207	1861	8364	171801	4272	553561			
11	0.05488	0.00147	0.45077	0.01316	0.0594	0.00059	0.34	407.1	58.25	377.8	9.21	372	3.6	13	0	39429	2167	10651	211389	5113	660354			
12	0.05426	0.00161	0.46775	0.01506	0.06226	0.00068	0.34	381.6	65.13	389.6	10.42	389.4	4.13	93	8	60750	3302	14496	298368	7493	969625			
13	0.0546	0.00166	0.47619	0.01569	0.06241	0.0007	0.34	395.9	65.99	395.5	10.79	390.3	4.23	64	0	123410	6753	35051	749211	15037	1964437			
14	0.0556	0.0018	0.48058	0.01691	0.06299	0.00075	0.34	436	70.52	398.5	11.6	393.8	4.56	52	10	33239	1852	7309	160494	4083	524058			
06NMA-07-GABRO																								
1	0.05429	0.00069	0.472	0.00664	0.06311	0.00033	0.37	383	28.43	392.6	4.58	394.5	2.02	21	0	52439	2931	4799	87599	6423	832871			
2	0.05274	0.00076	0.4547	0.00725	0.06297	0.00037	0.37	317.7	32.41	380.6	5.06	393.7	2.23	0	23	38950	2116	5964	128424	4814	620453			
3	0.05316	0.00079	0.45711	0.00747	0.06255	0.00038	0.37	335.8	33.03	382.2	5.2	391.1	2.28	31	0	63662	3488	13504	280186	7896	1021707			
4	0.05384	0.00066	0.45419	0.00617	0.06193	0.00032	0.38	364.3	27.61	380.2	4.31	387.4	1.93	57	0	100129	5558	23513	461525	12666	1623941			
5	0.05322	0.00067	0.45116	0.00624	0.0615	0.00032	0.38	338	28.01	378.1	4.36	384.8	1.95	65	0	117129	6429	12961	283545	14769	1916427			
6	0.05245	0.00075	0.44109	0.00697	0.06109	0.00036	0.37	304.9	32.25	371	4.91	382.3	2.17	49	64	59699	3230	13190	284831	7592	983918			
7	0.05257	0.00077	0.43737	0.00703	0.06088	0.00036	0.37	310.5	32.76	368.4	4.97	381	2.2	28	0	81459	4418	14458	292523	10478	1347842			
8	0.05211	0.00077	0.45111	0.00668	0.06273	0.00035	0.38	289.8	30.27	378.1	4.67	392.2	2.11	60	0	106479	5723	24087	475388	13167	1710991			
9	0.05372	0.00075	0.45086	0.00699	0.06141	0.00036	0.38	359.1	31.4	377.9	4.89	384.2	2.16	39	55	292619	16207	89701	1871480	37376	4809285			
10	0.05287	0.00081	0.44831	0.00759	0.06185	0.00039	0.37	323.2	34.31	376.1	5.32	386.8	2.35	3057	709	62066	3382	10937	214644	7850	1013354			
11	0.05317	0.00094	0.46823	0.00916	0.06404	0.00045	0.36	336.1	39.37	390	6.33	400.2	2.75	121	402	35022	1918	3328	61189	4267	552418			
12	0.0533	0.00104	0.46245	0.00998	0.06195	0.00048	0.36	341.7	43.56	386	6.93	387.5	2.9	0	17	18721	1027	2068	42868	2316	305382			
13	0.05335	0.00088	0.45996	0.00843	0.0628	0.00042	0.36	345.6	36.91	384.2	5.86	392.6	2.56	12185	2816	95002	5212	10636	208574	11836	1530123			
14	0.05286	0.00087	0.49433	0.0072	0.06393	0.00036	0.37	322.7	36.97	375.5	5.24	338.6	2.21	145	44	298428	16214	136799	3057814	42984	5599116			
15	0.0538	0.00094	0.44319	0.00854	0.06025	0.00042	0.36	362.5	38.92	372.5	6.01	377.2	2.58	0	20	85498	4724	7173	145024	11154	1436021			
16	0.05251	0.00095	0.4426	0.00885	0.06181	0.00045	0.36	307.6	40.56	372.1	6.23	386.6	2.72	10	0	99791	5378	12001	233858	12726	1634128			
17	0.05317	0.00099	0.44229	0.00911	0.06051	0.00045	0.36	336	41.47	371.9	6.42	378.7	2.75	361	91	321351	17491	53671	1193626	41544	5378413			
18	0.05306	0.00108	0.45078	0.01015	0.06091	0.00049	0.36	331.4	45.31	377.8	7.1	381.2	3	0	41	52743	2862	9168	173499	6677	877070			
19	0.05303	0.00106	0.45832	0.01013	0.06279	0.0005	0.36	330	44.5	383.1	7.06	392.6	3.03	0	2	95620	5180	24007	516676	11900	1542538			
20	0.05271	0.00115	0.46977	0.00991	0.06552	0.00048	0.36	316.4	48.89	348.7	7.14	348.3	2.94	926	264	99107	5331	34396	716843	13713	1808201			
21	0.05406	0.00118	0.46221	0.0112	0.06185	0.00053	0.35	373.2	48.45	385.8	7.78	386.8	3.24	135	24	189771	10416	30422	658526	23871	3108569			
22	0.05346	0.0012	0.44281	0.01099	0.06132	0.00054	0.35	348.3	49.93	372.2	7.73	383.6	3.29	324	105	491987	26670	123955	2287381	63884	8127772			
24	0.05409	0.00124	0.46443	0.01183	0.06156	0.00056	0.36	374.7	50.87	387.3	8.2	385.1	3.38	209	21	280481	15361	72927	1390259	35130	4615175			

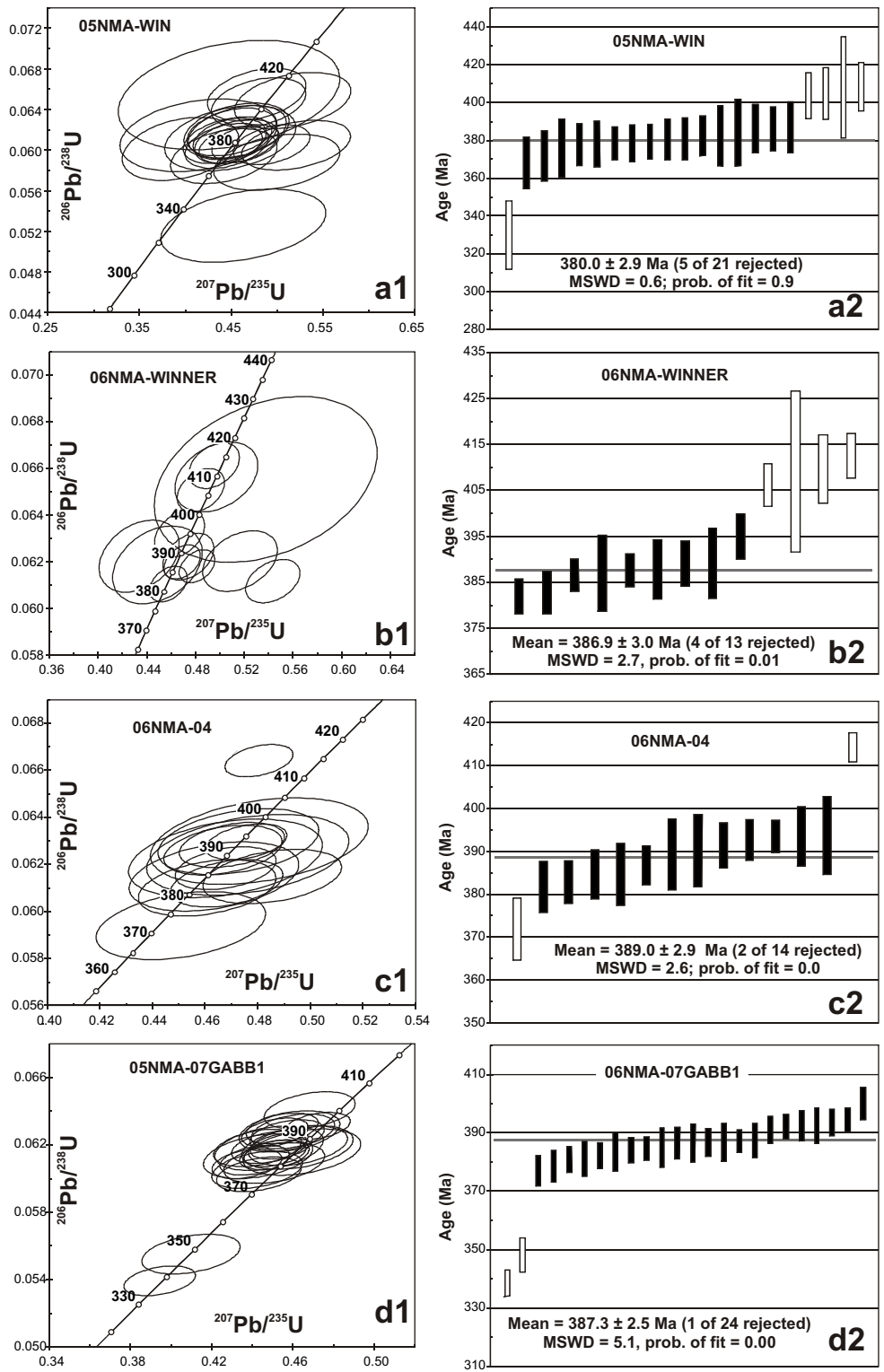


Fig. 4. LA-ICP-MS zircon age determinations for Greenwood gabbro samples, Knob Hill complex. Results are shown as both conventional concordia diagrams and as plots of the weighted average of calculated $^{206}\text{Pb}/^{238}\text{U}$ ages. **a)** and **b)** separate samples from the Winner Mine, **c)** Rock Creek; **d)** Powerline, north of Winnipeg Mine. See Table 1 and Fig. 2 for locations. Error ellipses and bars for individual analyses, and for the final weighted average ages, are shown at a 2σ level (95% confidence interval). Analyses that were included in the weighted average age are shown as filled bars and those that were rejected are shown as open bars. Rejected analyses are interpreted to represent either older xenocrystic zircon grains, or grains with significant amounts of post-crystallization Pb-loss.

Kevin Paterson, Bev Quist, Eric Westberg, Ashley Dittmar, and Sean Mullan during fieldwork and in the office. Larry Aspler provided an insightful review of an earlier version of this manuscript, and JoAnne Nelson contributed a thorough final critical review.

References cited

- Bostock, H.S., 1939. Geology, Keremeos; Geological Survey of Canada, Map 341A, scale 1:63 360.
- Bostock, H.S., 1940. Geology, Olalla; Geological Survey of Canada, Map 628A, scale 1:63 360.
- Church, B.N., 1992. The Lexington porphyry, Greenwood Mining Camp, southern British Columbia: geochronology (82E/2E). In: Geological Fieldwork 1991, British Columbia Ministry of Energy and Mines, British Columbia Geological Survey Paper 1992-1, pp. 295-297.
- Colpron, M. and Nelson, J.L., 2009. A Palaeozoic Northwest Passage: incursion of Caledonian, Baltican and Siberian terranes into eastern Panthalassa, and the early evolution of the North American Cordillera. In: Cawood, P.A., and Kroner, A. (Eds.), *Earth Accretionary Systems in Space and Time*. Geological Society of London Special Publication, 318, 273-307.
- Colpron, M. and Nelson, J.L., 2011. A Palaeozoic NW Passage and the Timanian, Caledonian and Uralian connections of some exotic terranes in the North American Cordillera. In: Spencer, A.M., Embry, A.F., Gautier, D.L., Stoupakova, A.V., and Sorensen, K., (Eds.) *Arctic Petroleum Geology*. Geological Society of London Memoir 35, 463-484.
- Dostal, J., Church, B.N., and Høy, T., 2001. Geological and geochemical evidence for variable magmatism and tectonics in the southern Canadian Cordillera: Paleozoic to Jurassic suites, Greenwood, southern British Columbia. *Canadian Journal of Earth Sciences*, 38, 75-90.
- Fyles, J.T., 1990. Geology of the Greenwood – Grand Forks area, British Columbia, NTS 82E/1,2. British Columbia Ministry of Energy and Mines, British Columbia Geological Survey, Open File 1990-25, 61 p.
- Fyles, J.T., 1995. Day 3 (Morning): Knob Hill Group, Attwood Group and Brooklyn Formation. In *Victoria '95, Field Trip Guidebook B2*, Geological Association of Canada-Mineralogical Association of Canada, 1995 Annual Meeting, Victoria, B.C., 40-49.
- Ghosh, D. K., 1995. U–Pb geochronology of Jurassic to early Tertiary granitic intrusives from the Nelson–Castlegar area, southeastern British Columbia. *Canadian Journal of Earth Sciences*, 32, 1668-1680.
- Griffin, W.L., Powell, W.J., Pearson, N.J, and O'Reilly, S.Y., 2008. Glitter: Data reduction software for laser ablation ICP-MS. In: Sylvester, P.J. (Ed.), *Laser Ablation ICP-MS in the Earth Sciences: Current Practices and Outstanding Issues*, Mineralogical Association of Canada Short Course 40, Vancouver, B.C., 308-311.
- Little, H.W., 1983. Geology of the Greenwood Map-area, British Columbia. Geological Survey of Canada Paper 79-29, 37 p.
- Ludwig, K.R., 2003. Isoplot 3.09 - A geochronological toolkit for Microsoft Excel: Berkeley Geochronology Center, Special Publication No. 4.
- Massey, N.W.D., 2006. Boundary Project: reassessment of Paleozoic rock units of the Greenwood area (NTS 82E/02), southern British Columbia. In: *Geological Fieldwork 2005*, British Columbia Ministry of Energy and Mines, British Columbia Geological Survey Paper 2006-1 and Geoscience BC, Report 2006-1, 99-107.
- Massey, N.W.D., 2007a. Geology and mineral deposits of the Rock Creek area, British Columbia (82E/02W; 82E/03E). British Columbia Ministry of Energy and Mines, British Columbia Geological Survey Open File 2007-7, scale 1:25 000.
- Massey, N.W.D., 2007b. Boundary Project: Rock Creek area (82E/02W; 82E/03E). In: *Geological Fieldwork 2006*, British Columbia Ministry of Energy and Mines, British Columbia Geological Survey Paper 2007-1 and Geoscience BC, Report 2007-1, 117-128.
- Massey, N.W.D., and Dostal, J., 2013. Geochemistry of metabasalts from the Knob Hill complex and Anarchist Group in the Paleozoic basement to southern Quesnellia. In: *Geological Fieldwork 2012*, British Columbia Ministry of Energy, Mines, and Natural Gas, British Columbia Geological Survey Paper 2013-1 (this volume).
- Massey, N.W.D., and Duffy, A., 2008a. Boundary Project: McKinney Creek (82E/03) and Beavertell (82E/06E, 82E/07W, 82E/10W and 82E/11W) areas. In: *Geological Fieldwork 2007*, British Columbia Ministry of Energy and Mines, British Columbia Geological Survey Paper 2008-1, 87-102.
- Massey, N.W.D., and Duffy, A., 2008b. Geology and mineral deposits of the area east of Beavertell, British Columbia (parts of NTS 082E/6E; 082E/07W; 082E/10W; 082E/11E). British Columbia Ministry of Energy and Mines, British Columbia Geological Survey Open File 2008-9, scale 1:25 000.
- Massey, N.W.D., and Duffy, A., 2008c. Geology and mineral deposits of the McKinney Creek area, British Columbia (parts of NTS 082E/3). British Columbia Ministry of Energy and Mines, British Columbia Geological Survey Open File 2008-10, scale 1:20 000.
- Monger, J.W.H., 1977. Upper Paleozoic rocks of the western Canadian Cordillera and their bearing on Cordilleran evolution. *Canadian Journal of Earth Sciences*, 14, 1832-1859.
- Mortensen, J.K., Lucas, K., Monger, J.W.H. and Cordey, F., 2011. Geological investigations of the basement of the Quesnel terrane in southern British Columbia (NTS 082E, F, L, 092H, I): Progress Report. In: Geoscience BC, Summary of Activities 2010, Report 2011-1, 133-142.
- Nelson, J., and Colpron, M., 2007. Tectonics and metallogeny of the British Columbia, Yukon and Alaskan Cordillera, 1.9 Ga to the present. In: Goodfellow, W.D., (Ed.) *Mineral Deposits of Canada: A Synthesis of Major Deposit-Types, District Metallogeny, the Evolution of Geological Provinces, and Exploration Methods*. Geological Association of Canada, Mineral Deposits Division, Special Publication 5, 755-791.
- Orchard, M.J., 1993. Report on conodonts and other microfossils, Penticton (82E). Geological Survey of Canada, Report Number Open File 1993-19.
- Peatfield, G.R., 1978. Geologic history and metallogeny of the 'Boundary District', southern British Columbia and northern Washington. Unpublished Ph.D. thesis, Queen's University, 462 p.

- Rinehart, C.D., and Fox, K.F., Jr., 1972). Geology and mineral deposits of the Loomis Quadrangle, Okanogan County, Washington. Washington Division of Mines and Geology Bulletin 64, 124 p.
- Simony, P.S., Sevigny, J.H., Mortensen, J.K., and Roback, R.C., 2006. Age and origin of the Trail Gneiss Complex: Basement to Quesnel terrane near Trail, southeastern British Columbia. In: Colpron, M., and Nelson, J.L. (Eds.), Paleozoic evolution and metallogeny of pericratonic terranes at the ancient Pacific margin of North America, Canadian and Alaskan Cordillera. Geological Association of Canada, Special Paper, 45, 505-515.
- Sláma, J., Košler, J., Condon, D.J., Crowley, J.L., Gerdes, A., Hanchar, J.M., Horstwood, M.S.A., Morris, G.A., Nasdala, L., Norberg, N., Schaltegger, U., Xchoene, B., Tubrett, M.N. and Whitehouse, M.J., 2007. Plešovice zircon — A new natural reference material for U–Pb and Hf isotopic microanalysis. *Chemical Geology*, 249, 1-35.
- Tafti, R., Mortensen, J.K., Lang, J.R., Rebagliati, M., and Oliver, J., 2009. Jurassic U-Pb and Re-Os ages for the newly discovered Xietongmen Cu-Au porphyry district, Tibet, PRC: Implications for metallogenic epochs in the southern Gangdese belt. *Economic Geology*, 104, 127-136.
- Thompson, R. I., Glombick, P., Erdmer, P., Heaman, L.M., Lemieux, Y., and Daughtry, K. L., 2006. Evolution of the ancestral Pacific margin, southern Canadian Cordillera: Insights from new geologic maps. In: Colpron, M., and Nelson, J.L. (Eds.), Paleozoic evolution and metallogeny of pericratonic terranes at the ancient Pacific margin of North America, Canadian and Alaskan Cordillera. Geological Association of Canada, Special Paper, 45, pp. 433-482.
- Van Achterbergh, E., Ryan, C.G., Jackson, S.E., and Griffin, W.L., 2001. Data reduction software for LA-ICP-MS: appendix. In: Sylvester, P.J. (Ed.), *Laser Ablation –ICP-Mass Spectrometry in the Earth Sciences: Principles and Applications*. Mineralogical Association of Canada Short Course 29, Ottawa, Ontario, Canada, 239-243.
- Woodcock, N.H., 2004. Life span and fate of sedimentary basins. *Geology*, 32, 685-688.

Geochemistry of metabasalts from the Knob Hill complex and Anarchist Group in the Paleozoic basement to southern Quesnellia

N.W.D. Massey^{1,a} and J. Dostal²

¹ British Columbia Geological Survey, Ministry of Energy, Mines and Natural Gas, Victoria, BC, V8W 9N3 (Emeritus Scientist)

² Department of Geology, St. Mary's University, Halifax, NS B3H 3C3

^a corresponding author: nickmassey@shaw.ca

Recommended citation: Massey, N.W.D. and Dostal, J., 2013. Geochemistry of metabasalts from the Knob Hill complex and Anarchist Group in the Paleozoic basement to southern Quesnellia. In: Geological Fieldwork 2012, British Columbia Ministry of Energy, Mines and Natural Gas, British Columbia Geological Survey Paper 2013-1, pp. 45-52.

Abstract

The Knob Hill complex and Anarchist Group constitute part of the Paleozoic basement to southern Quesnellia. These units occupy adjacent northward dipping, south-vergent thrust sheets extending along the Canada-Washington State border. Metabasalts in both units are tholeiitic to transitional or alkalic, comprising three magma types. The ophiolitic Knob Hill complex contains rocks of predominantly island arc affinity (IAT), with local MORB and E-MORB varieties. They probably formed by subduction-related rifting processes, but the precise setting remains unclear. The Anarchist Group metabasalts display predominantly within-plate E-MORB geochemical traits; local IAT and MORB signatures are indistinguishable from those in the Knob Hill Complex. The basalt geochemistry suggests that the two units share a magmatic history and may have once been contiguous, with the Anarchist Group having formed off axis relative to spreading represented by the Knob Hill complex.

Keywords: Quesnellia, Okanagan subterrane, Knob Hill complex, Anarchist Group, basalt geochemistry, supra-subduction zone basin

1. Introduction

Various Paleozoic mafic volcanic and pelitic successions form basement to the Quesnel terrane in the southern Okanagan along the Canada-USA border (Figs. 1, 2). Depending on geographic locale, different workers have assigned different names to these successions. They are called: the Knob Hill complex and Attwood Formation in the Greenwood area; the Anarchist Group in the Osoyoos-Rock Creek and Beavercreek areas; and the Kobau Group and Apex Mountain Complex in the area between Oliver and Keremeos (Fig. 2). The terms 'Kobau' and 'Anarchist' have also been used in Washington State, though not always for directly correlatable rock packages. Most of these packages have been included in the Okanagan subterrane (Monger, 1977; Peatfield, 1978).

The multiplicity of lithostratigraphic terms is likely an artifact of different geologists mapping in different areas. Recent mapping has revised some stratigraphic designations, recognizing that the successions define an east-trending belt, with individual units separated by northward-dipping, south-vergent thrust sheets (Fig. 2; Fyles, 1990; Massey, 2007; Massey and Duffy, 2008). Nonetheless, relationships between structurally separated units remain unclear. Tertiary extensional faults have disrupted and modified the thrusts, which limits correlating units by lateral tracing. With the exception of ~390-380 Ma ages from the Knob Hill complex (Massey et al., this volume), reliable U-Pb zircon data are lacking for the Paleozoic successions. In an effort to address

correlation questions, herein we present geochemical data from mafic rocks in the Knob Hill complex and the Anarchist Group. We also use these data to test field-based models that regard these successions as recording Devonian intraoceanic subduction processes.

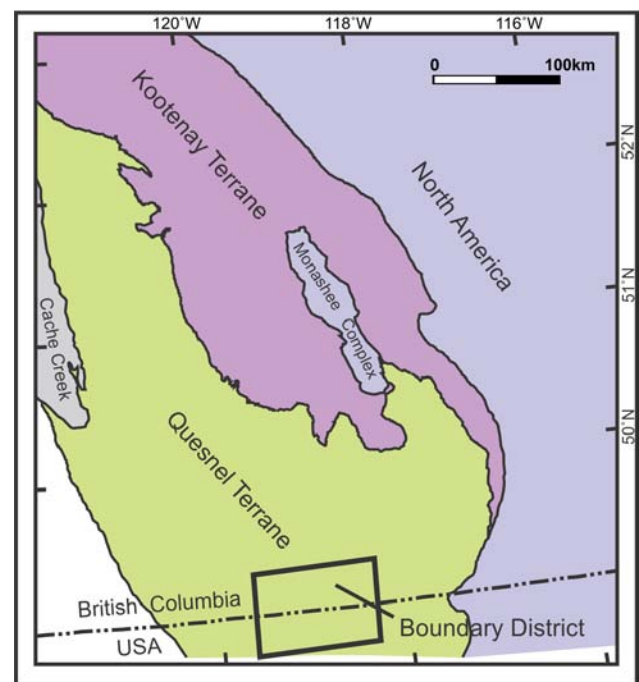


Fig. 1. Simplified terrane map of southeastern British Columbia (amended from digital geology of Massey et al., 2005). Location of the Boundary District shown by rectangle.

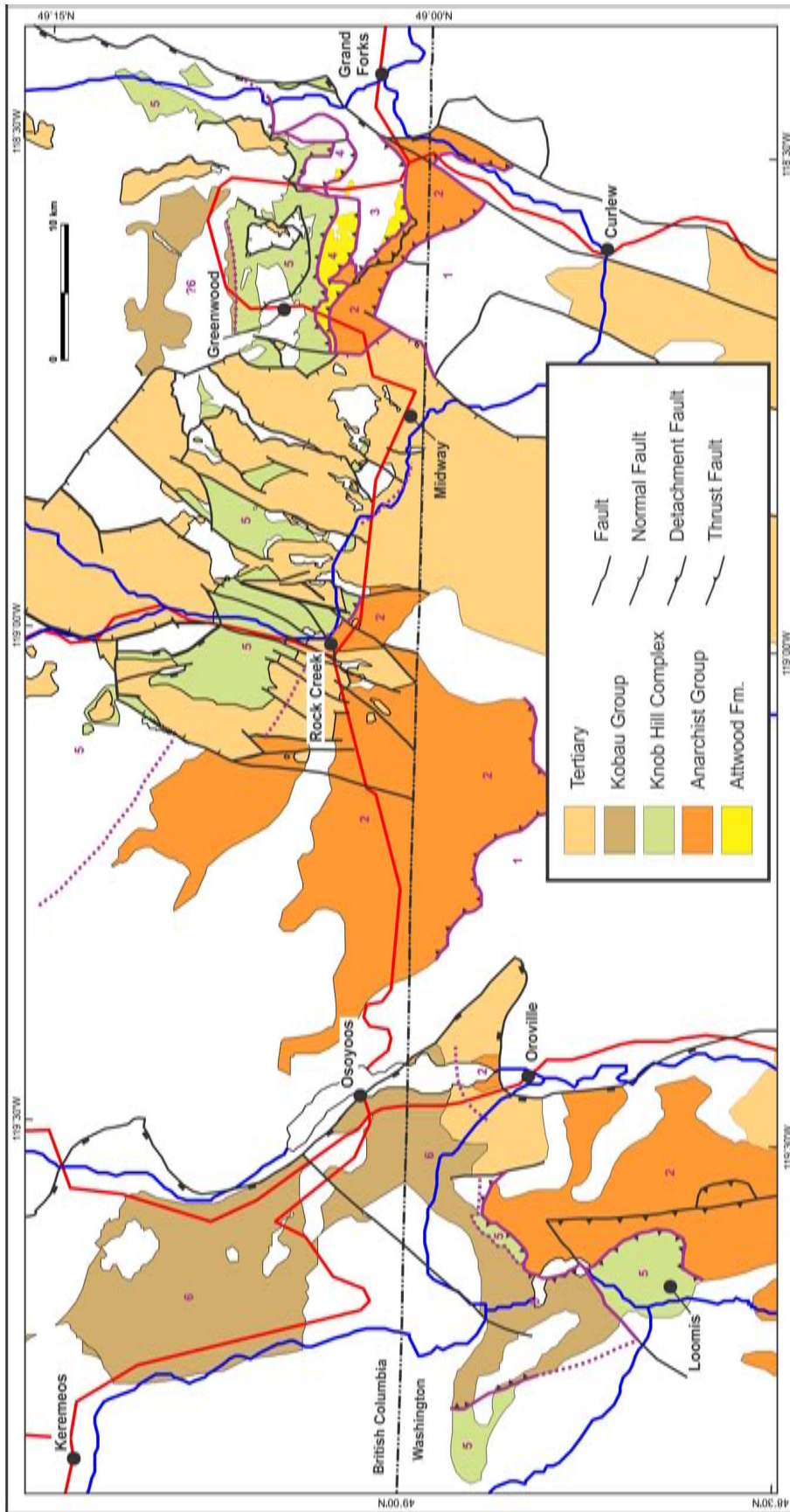


Fig. 2. Distribution of Paleozoic Quesnellian rock suites in the southern Okanagan region and adjacent Washington State, amended from digital geology maps of British Columbia (Massey et al., 2005) and from geological maps of Washington State (Ludington et al., 2005; Cheney et al., 1994). Purple lines and numbers identify the east-west trending thrust sheet packages.

2. Paleozoic successions

2.1. Knob Hill complex

Interpreted stratigraphic arrangement of map units in the Kettle River valley area north of Rock Creek suggest that Knob Hill complex constitutes a disrupted ophiolite (Little, 1983; Dostal et al., 2001; Massey, 2006). Gabbro and serpentinite pass northwards, and probably upwards, into greenstones, mixed greenstones and cherts, and finally into cherts and argillites (Massey, 2007a). This pattern is repeated on the west side of the valley in the Johnstone Creek area (Fig. 2), although disrupted by north-northeast trending Tertiary faults. Stratigraphic relationships between map units are less clear in the Greenwood area. However, outcrops along the power line adjacent to the Winnipeg Mine, east of Greenwood, show well developed chilled margins in medium-grained diabase and microgabbro, suggesting they may be part of a yet-to-be delineated sheeted dike complex. The stratigraphic thickness of the Knob Hill complex is uncertain and difficult to estimate due to structural disruption. Nonetheless, Little (1983) suggested “a minimum of a few thousands of metres”, and Fyles (1990, 1995) gave an estimate of at least 5 km.

U-Pb zircon (Massey et al., this volume) and biostratigraphic data (Orchard, 1993) show that the complex originated from Middle to Late Devonian (380-390 Ma); biostratigraphic data from a chert bed in the mixed greenstone-chert succession (Cordey in Massey, 2007) indicate that it continued to evolve into the Late Pennsylvanian or Early Permian (290-295 Ma.). This 80 to 100 million year time span seems excessive for a single ophiolite as small as the Knob Hill Complex (see Woodcock, 2004). It suggests a complex tectonostratigraphy, probably involving more than one extensional event, and cryptic stratigraphic or structural breaks in the sequence.

2.1.1. Serpentinite and gabbro

Serpentinite is typically black to bright green. It is commonly phyllitic to schistose but locally contains coherent serpentinite lozenges in a foliated matrix. Cores of relict pyroxenite occur, though rarely. Listwanite is exposed in outcrops along Highway 33. This carbonate-rich rock is pale buff on fresh surfaces but typically bright orange on weathered surfaces.

Gabbro is composed of white plagioclase and green to black pyroxenes extensively replaced by hornblende. Chlorite is common on fractures and in shears. The gabbros are generally coarse grained and massive but can show a characteristic variable and patchy texture, with coarse-grained gabbro phases grading into finer microgabbro or even coarser pegmatitic phases.

2.1.2. Greenstone

Greenstones are mostly massive basaltic flows. They are medium grey to green and, although typically aphyric, contain rare feldspar, pyroxene and magnetite phenocrysts. Chlorite, epidote, calcite, and quartz are

common alteration minerals in veins, fractures, and within the rock. Pillow structures are rare. Minor breccia, agglomerate, tuff, and chlorite schist are interlayered with the flows, as are chert, cherty argillite, and rare grey limestone beds. In some areas, the abundance of chert beds defines a mixed greenstone-chert unit transitional to the overlying chert-argillite unit.

Medium-grained diabase to micro-gabbro bodies also occur within the greenstone unit. Although typically massive, outcrops along the power line adjacent to the Winnipeg Mine, east of Greenwood, show well developed chilled margins which suggest they are part of an unmapped sheeted dike complex. Diabase dikes preserve screens of gabbro, and diabasic xenoliths occur within the gabbro itself. These complex crosscutting relationships are typical of ophiolitic complexes.

2.1.3. Chert-Argillite Unit

Fine-grained sedimentary rocks are predominant in the Knob Hill complex and consist mainly of grey to white cherts that are interbedded with grey to black argillites, black siliceous argillites, and local chert breccia. Cherts are highly fractured and jointed, tend to be massive to thickly bedded, and only rarely show ribbon structures. Recrystallization of the cherts has produced a fine- to medium-grained saccharoidal texture and limited preservation of radiolaria. Chert breccias contain angular to subrounded clasts of chert and cherty tuff in a siliceous matrix.

2.2. Anarchist Group

Based on predominant rock type, the Anarchist Group can be subdivided into a metasedimentary unit and a metavolcanic unit in the Greenwood-Rock Creek area (Massey and Duffy, 2008). The stratigraphic relationship between the two units is uncertain, and isotopic and paleontological age determinations are unavailable. Rubidium-strontium geochronology in the Osoyoos area only records Tertiary metamorphic ages (Ryan, 1973). Broad similarities between the Anarchist Group and the upper parts of the Knob Hill Complex suggest that the two, now structurally disrupted, were originally continuous.

2.2.1. Metasedimentary unit

The metasedimentary unit consists mainly of chert, argillaceous chert, and meta-argillite with minor metabasalt and limestone. The cherts are recrystallized, displaying a fine to-medium grained, sugary texture, and are typically white to pale grey or darker blue grey. Beds are usually 1 to 2 metres thick, but some are up to 10 metres. Some beds are massive, others show dark and light layering; ribbon bedding is rarely preserved.

Phyllitic to schistose argillaceous metasedimentary rocks are darker, with fine grained black chlorite or biotite schist layers interbedded with lighter quartz-rich layers. Epidote laminae and bands suggest fine grained tuffaceous interbeds. Some less siliceous meta-argillites are carbonaceous. Minor fine- to medium-grained,

recrystallized limestones form beds 2 cm to 10 m thick.

2.2.2. Metavolcanic unit

The metavolcanic unit comprises greenstone flows with minor breccias, tuffs, and metasedimentary rocks. The flows are massive and medium to dark grey or black. They are fine grained and generally aphyric, though rare feldspar and pyroxene crystals are seen. Chlorite \pm epidote alteration is common, along with veining of quartz=chlorite=calcite. Chlorite and brown to black oxides are present on fractures. Tuffaceous interbeds are altered to green quartz-chlorite=sericite schists with epidote pods and laminae.

3. Geochemistry

A suite of metabasalts from the Knob Hill Complex and Anarchist Group were analyzed for whole-rock major, minor, and trace elements. Major elements and Rb, Sr, Ba, Y, Zr, Nb, V, Ni and Cr were determined by XRF (majors on fused disc, traces on pressed powder pellet) by St Mary's University or Teck (Global Discovery) Labs. REEs, Th, Ta, Hf were determined by peroxide fusion-ICPMS by Memorial University of Newfoundland. Full analyses, including details of duplicate analyses, are tabulated in Massey and Dostal (2013).

3.1. Knob Hill complex

Interpretation of these new data and previously published (Dostal et al., 2001) data from the Greenwood area suggests three distinct suites in the Knob Hill Complex: a) typical ocean basalt (MORB); b) enriched MORB; and c) island-arc tholeiite (IAT). Although subjected to alteration, which affected the alkalis and, to some extent, silica, most samples display a subalkaline, tholeiitic character, though the E-MORB suite is transitional to alkalic (Figs. 3a, b). Most of the samples are basalts, though some are basaltic andesites and andesites. Petrotectonic discrimination plots using the immobile high-field strength elements help to distinguish the three magma types (Figs. 3c-f).

Chondrite-normalized REE patterns further support the discrimination of the three suites (Fig. 4). The IAT samples have a LREE depleted pattern, whereas the MORB samples show a flat pattern and the E-MORBs have LREE enriched patterns.

Spatial or stratigraphic control on the occurrence of the three suites is equivocal. The IAT suite, found throughout most of the section, is predominant. In the Rock Creek – Kettle Valley area, the MORB suite is restricted to horizons higher, and younger, in the basalt package and in the mixed greenstone-chert unit. Relations in the Greenwood area are, however, less clear. E-MORB samples appear to lack a stratigraphic control, and are intermixed with both IATs and MORBs.

3.2. Anarchist Group

Metabasalts from the Anarchist Group show strong similarities with samples from the Knob Hill Complex. They are predominantly basalts, with minor basaltic andesite to andesite, and generally classify as subalkaline,

tholeiitic to transitional (Figs. 5a, b). They also show a division into three distinct suites, directly comparable to those in the Knob Hill complex (Figs. 5c-f). However, the E-MORB samples are predominant in the Anarchist Group, and the IAT and N-MORB samples are less common.

The immobile high-field strength elements and REES help to distinguish and characterize the three groups (Figs. 5c-f, 6a-c). REE patterns are comparable to those in the Knob Hill Complex suites, except for the IAT samples which, though lower in overall REE content, have less LREE-depleted patterns (Fig. 6c).

4. Discussion

The ophiolitic field character of the Knob Hill complex has long suggested an oceanic origin (Little, 1983; Dostal et al., 2001; Massey, 2006). Rather than a mid-ocean ridge setting however, the mixed IAT, MORB, and E-MORB geochemistry likely represents intraoceanic subduction processes, although the precise setting (back arc? fore arc?) remains unclear. The 80 to 90 million year time span indicated by U-Pb zircon and paleontologic data (Massey et al., this volume) indicates a complex history that may have included more than one arc rifting event now hidden by cryptic stratigraphic breaks in the voluminous basaltic sequence.

The basalt geochemistry also offers evidence for a shared magmatic history between the Anarchist Group and at least the upper part the Knob Hill complex. However, the predominance of E-MORB samples and the relative abundance of argillites in the Anarchist Group, may point to its formation more off axis relative to active spreading represented by the Knob Hill complex.

The Old Tom and Shoemaker assemblages in the Keremeos area are lithologically similar to the Knob Hill complex, and Mortensen et al. (2011a, b) have reported similar geochemical data, including IAT, MORB and E-MORB types, consistent with correlation between these units. West of the Okanagan Fault, the Palmer Mountain greenstone in Washington comprises mafic flows and pyroclastic rocks with varitextured gabbro and serpentinite (Rinehart and Fox, 1972) that can be correlated with the Knob Hill complex. As in British Columbia, these rocks are thrust over "Anarchist Group" (which in the Loomis area appears to include significant Triassic Brooklyn Formation) and are structurally overlain by metamorphic rocks of the Kobau Group (Cheney et al., 1994). Two samples from possible Kobau Group greenstones in the Mount Roderick Dhu area yield IAT chemistry (Massey and Dostal, 2013). However, a larger suite of samples from the Kobau Group of the Keremeos area (Mortensen et al., 2011a, b) displays predominantly E-MORB or OIB-types with minor MORB, similar to the Anarchist Group. Because the Kobau and Anarchist groups occupy different thrust slices, with the Knob Hill Complex and equivalents intervening (Fig. 2), it remains unclear if these two units represent the same lithologic package structurally

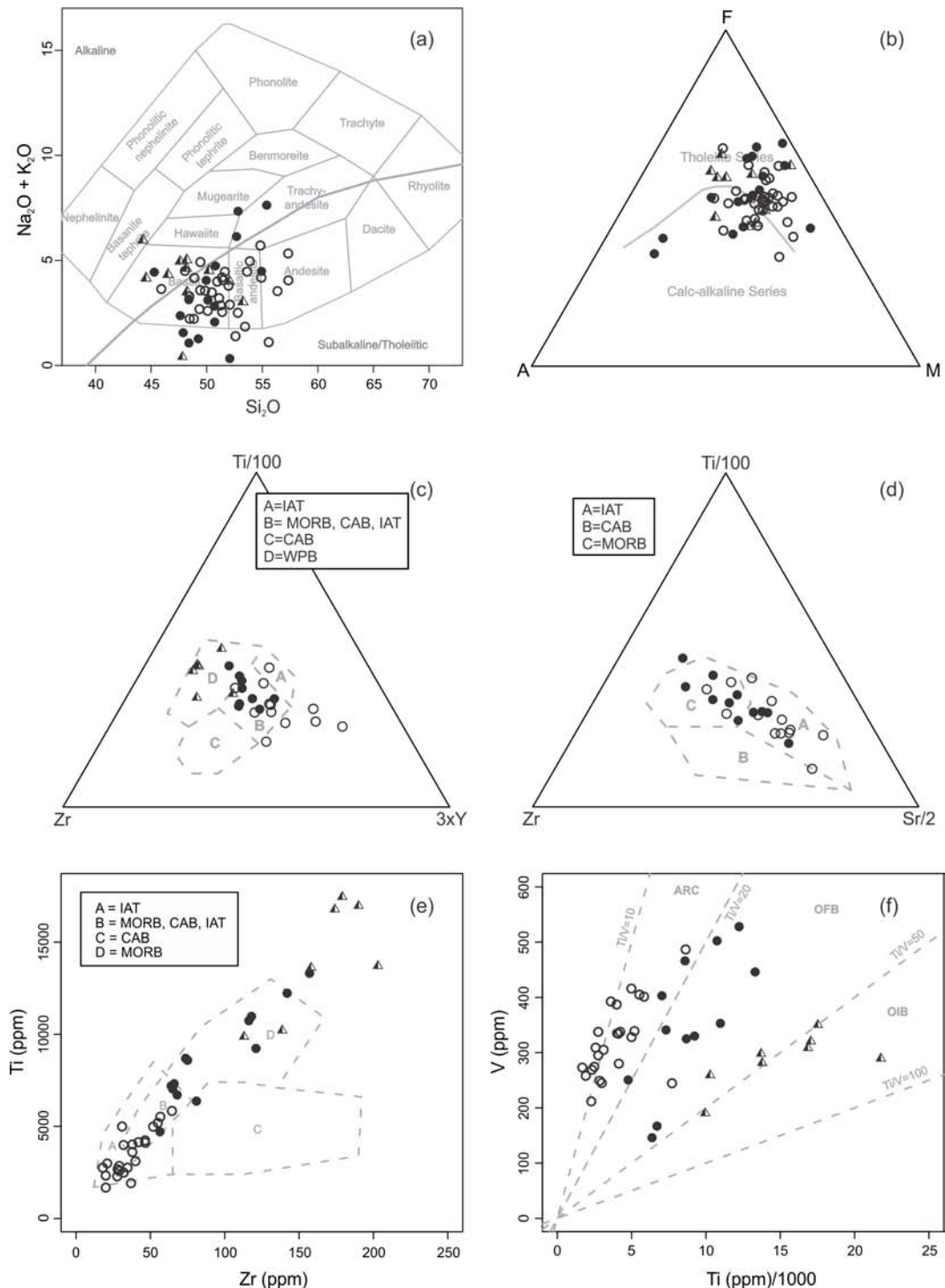


Fig. 3. Geochemical discrimination diagrams for Knob Hill complex metabasalts. Filled circles: MORB suite samples; half filled triangles: E-MORB suite; open circles: IAT suite. **a)** Total alkali vs. SiO_2 (anhydrous weight %) diagram. Classification fields and nomenclature after Cox et al. (1979). The alkaline-subalkaline dividing line after Irvine and Baragar (1971). **b)** AFM diagram after Irvine and Baragar (1971), A = $\text{Na}_2\text{O} + \text{K}_2\text{O}$; F = $\text{FeO}_{\text{total}}$; M = MgO. **c)** Ti-Zr-Y discriminant triangle diagram; petrotectonic fields after Pearce and Cann (1973). IAT: island arc tholeiites; MORB: mid-ocean ridge basalts, CAB: calcalkaline basalts, WPB: within-plate basalts. Only basaltic samples with $12 < \text{CaO} + \text{MgO} < 20$ are shown. **d)** Ti-Zr-Sr discriminant triangle diagram; petrotectonic fields after Pearce and Cann (1973). IAT: island arc tholeiites; MORB: mid-ocean ridge basalts, CAB: calcalkaline basalts, WPB: within-plate basalts. Only basaltic samples with $12 < \text{CaO} + \text{MgO} < 20$ are shown. E-MORB samples are not plotted as this diagram is not designed to discriminate such within-plate basalts. **e)** Ti-Zr discriminant diagram; petrotectonic fields after Pearce and Cann (1973). IAT: island arc tholeiites, MORB: mid-ocean ridge basalts, CAB: calcalkaline basalts. Only basaltic samples with $12 < \text{CaO} + \text{MgO} < 20$ are shown. **f)** Ti-V discriminant diagram; petrotectonic fields after Shervais (1982). ARC: island arc tholeiites, OFB: ocean floor basalts, OIB: ocean island basalts and alkalic basalts.

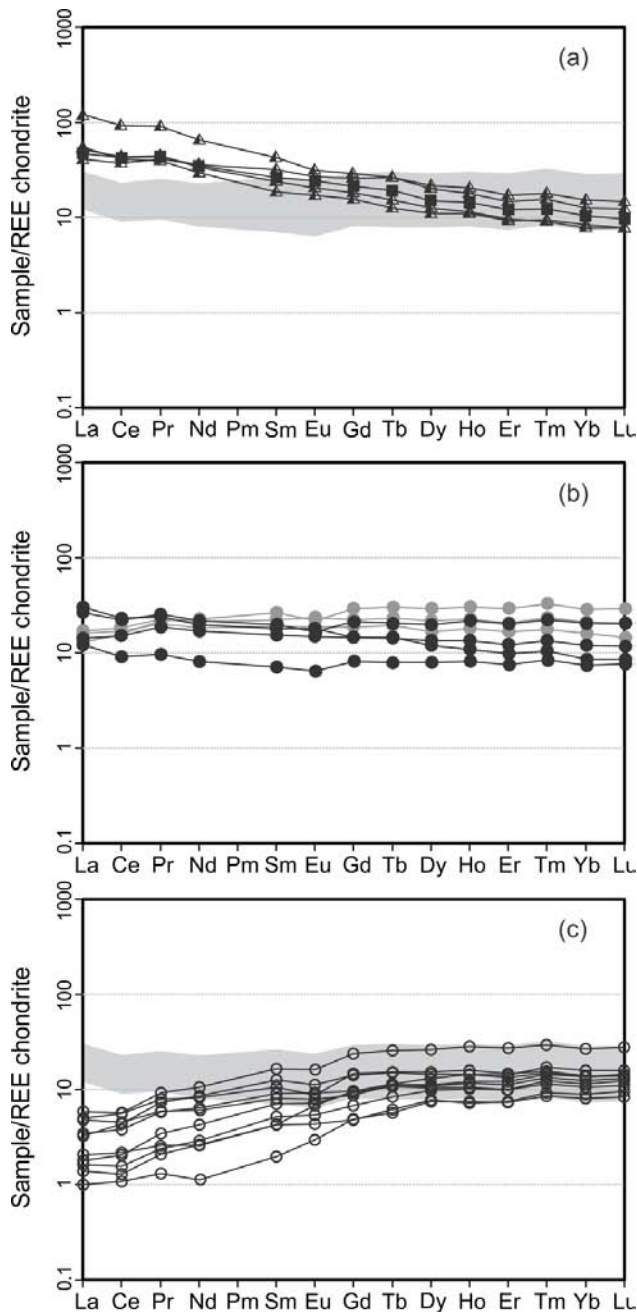


Fig. 4. Rare earth element abundances for Knob Hill Complex metabasalts; analyses normalized to chondrite (after Nakamura, 1974). **a)** E-MORB samples, including one sample (solid squares) from Dostal et al. (2001). Grey shaded field includes all MORB samples in b), shown for comparison. **b)** MORB samples, including three samples (filled grey circles) from Dostal et al. (2001). **c)** IAT samples. Grey shaded field includes all MORB samples in b), shown for comparison.

repeated or represent opposite sides of a basin centred by the Knob Hill complex that is now closed and telescoped.

Acknowledgments

We are much indebted to the late Jim Fyles and Neil Church for all their invaluable help and advice at all

stages of this project. The collaboration, support and ready welcome of the Boundary District exploration community were exceptional. The project would not have made progress without the indispensable assistance of Ashley Dittmar, Alan Duffy, Sean Mullan, Kevin Paterson, Bev Quist and Eric Westberg during fieldwork and in the office. Larry Aspler provided a thorough review of an earlier version of this manuscript, contributing many significant improvements. We thank JoAnne Nelson for a thorough critical review.

References cited

- Cheney, E.S., Rasmussen, M.G. and Miller, M.G., 1994. Major faults, stratigraphy, and identity of Quesnellia in Washington and adjacent British Columbia. Washington Division of Geology and Earth Resources, Bulletin 80, 49-71.
- Cox, K.G., Bell, J.D., and Pankhurst, R.J., 1979. The interpretation of igneous rocks. George, Allen and Unwin, London.
- Fyles, J.T., 1990. Geology of the Greenwood – Grand Forks area, British Columbia, NTS 82E/1,2. British Columbia Ministry of Energy, Mines and Petroleum Resources, British Columbia Geological Survey, Open File 1990-25, 61 p.
- Fyles, J.T., 1995. Day 3 (Morning): Knob Hill Group, Attwood Group and Brooklyn Formation. In Victoria '95, Field Trip Guidebook B2, Geological Association of Canada-Mineralogical Association of Canada, 1995 Annual Meeting, Victoria, B.C., 40-49.
- Irvine, T.N., and Baragar, W.R.A., 1971. A guide to the chemical classification of the common volcanic rocks. Canadian Journal of Earth Sciences, 8, 523-548.
- Little, H.W., 1983. Geology of the Greenwood Map-area, British Columbia. Geological Survey of Canada, Paper 79-29, 37 p.
- Ludington, S., Moring, B.C., Miller, R.J., Stone, P.A., Bookstrom, A.A., Bedford, D.R., Evans, J.G., Haxel, G.A., Nutt, C.J., Flynn, K.S., and Hopkins, M.J., 2005. Preliminary integrated geological map databases for the United States – western states: California, Nevada, Arizona, Washington, Oregon, Idaho, and Utah. United States Geological Survey, Open File Report 2005-1305.
- Massey, N.W.D., 2006. Boundary Project: reassessment of Paleozoic rock units of the Greenwood area (NTS 82E/02), southern British Columbia. In: Geological Fieldwork 2005, British Columbia Ministry of Energy, Mines, and Petroleum Resources, British Columbia Geological Survey Paper 2006-1 and Geoscience BC, Report 2006-1, 99-107.
- Massey, N.W.D., 2007. Boundary Project: Rock Creek area (82E/02W; 82E/03E). In: Geological Fieldwork 2006, British Columbia Ministry of Energy, Mines and Petroleum Resources, British Columbia Geological Survey Paper 2007-1 and Geoscience BC, Report 2007-1, 117-128.
- Massey, N.W.D., and Dostal, J., 2013. Boundary Project: Geochemistry of metabasalts from the Knob Hill Complex and Anarchist Group: Report, data tables and ancillary diagrams. British Columbia Ministry of Energy, Mines and Natural Gas, British Columbia Geological Survey GeoFile 2013-01.

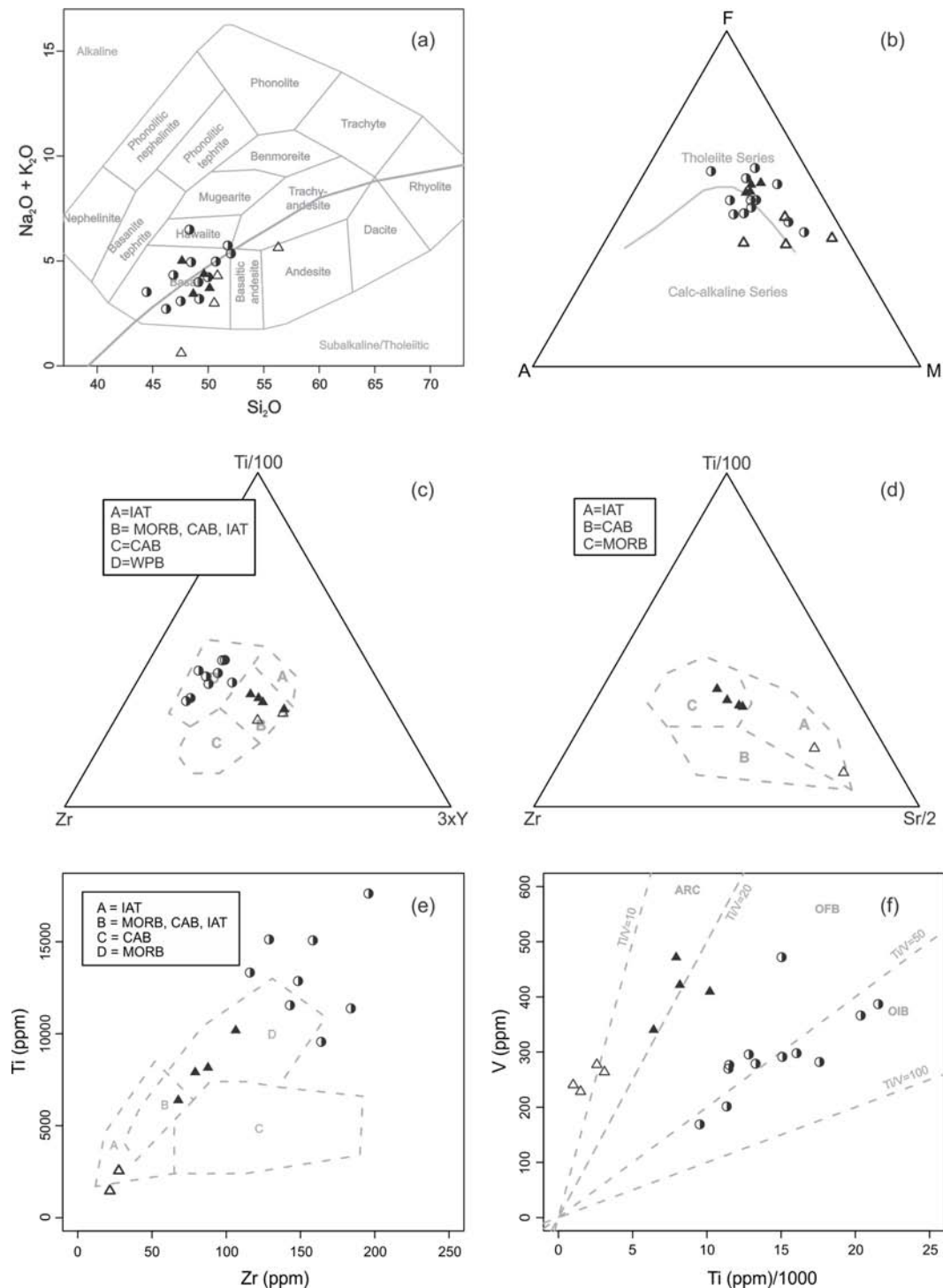


Fig. 5. Geochemical discrimination diagrams for Anarchist Group metabasalts. Filled triangle: MORB suite samples; half filled circles: E-MORB suite; open triangles: IAT suite. **a)** Total alkali vs. Si_2O (anhydrous weight %) diagram. Classification fields and nomenclature after Cox et al. (1979). The alkaline-subalkaline dividing line after Irvine and Baragar (1971). **b)** AFM diagram after Irvine and Baragar (1971). A = $\text{Na}_2\text{O} + \text{K}_2\text{O}$; F = $\text{FeO}_{\text{total}}$; M = MgO. **c)** Ti-Zr-Y discriminant triangle diagram; petrotectonic fields after Pearce and Cann (1973). IAT: island arc tholeiites; MORB: mid-ocean ridge basalts, CAB: calcalkaline basalts, WPB: within-plate basalts. Only basaltic samples with $12 < \text{CaO} + \text{MgO} < 20$ are shown. **d)** Ti-Zr-Sr discriminant triangle diagram; petrotectonic fields after Pearce and Cann (1973). IAT: island arc tholeiites; MORB: mid-ocean ridge basalts, CAB: calcalkaline basalts, WPB: within-plate basalts. Only basaltic samples with $12 < \text{CaO} + \text{MgO} < 20$ are shown. E-MORB samples are not plotted as this diagram is not designed to discriminate such within-plate basalts. **e)** Ti-Zr discriminant diagram; petrotectonic fields after Pearce and Cann (1973). IAT: island arc tholeiites, MORB: mid-ocean ridge basalts, CAB: calcalkaline basalts. Only basaltic samples with $12 < \text{CaO} + \text{MgO} < 20$ are shown. **f)** Ti-V discriminant diagram; petrotectonic fields after Shervais (1982). ARC: island arc tholeiites, OFB: ocean floor basalts, OIB: ocean island basalts and alkalic basalts.

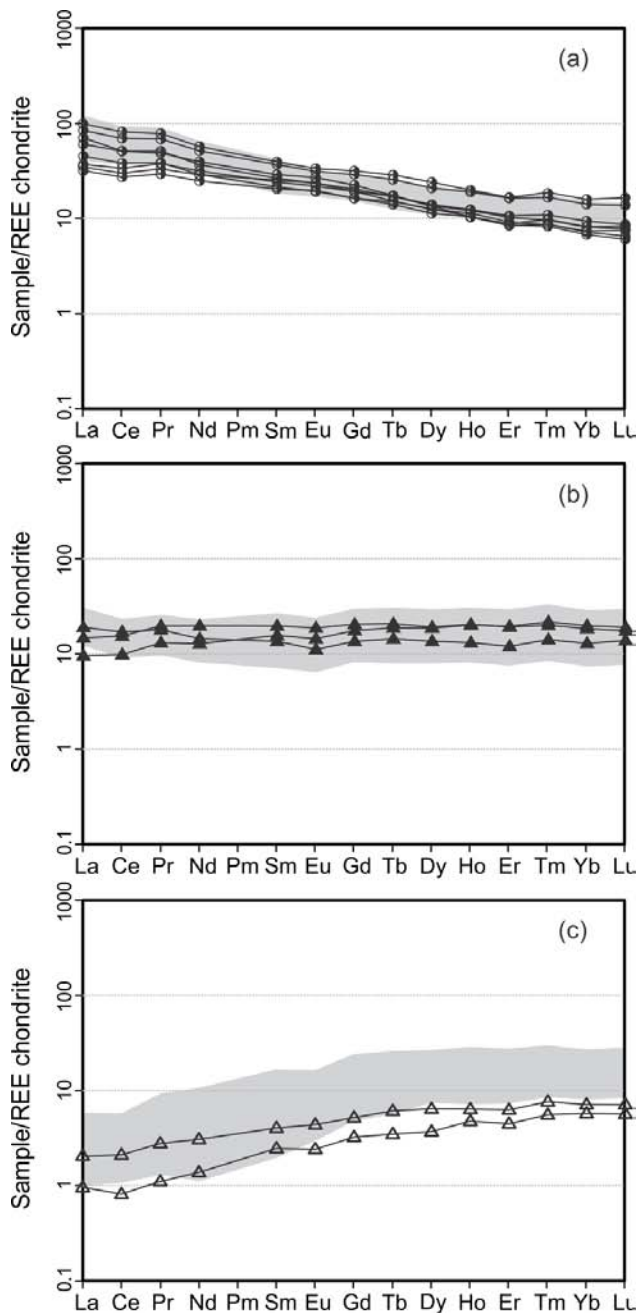


Fig. 6. Rare earth element abundances for Anarchist Group metabasalts; analyses normalized to chondrite (after Nakamura, 1974). **a)** E-MORB samples. Grey-shaded field includes all Knob Hill Complex E-MORB samples (Fig. 4a) shown for comparison; **b)** MORB samples. Grey-shaded field includes all Knob Hill Complex MORB samples (Fig. 4b) shown for comparison; **c)** IAT samples. Grey-shaded field includes all Knob Hill Complex IAT samples (Fig. 4c) shown for comparison.

Massey, N.W.D. and Duffy, A., 2008. Boundary Project: McKinney Creek (82E/03) and Beaverdell (82E/06E, 82E/07W, 82E/10W and 82E/11W) areas. In: Geological Fieldwork 2007, British Columbia Ministry of Energy, Mines and Petroleum Resources, British Columbia Geological Survey Paper 2008-1, 87-102.

Massey, N.W.D., Gabites, J.E., and Mortensen, J.K., 2013. LA-ICP-MS geochronology of the Greenwood gabbro, Knob Hill complex, southern Okanagan, British Columbia. In: Geological Fieldwork 2012, British Columbia Ministry of Energy, Mines, and Natural Gas, British Columbia Geological Survey Paper 2013-1 (this volume).

Massey, N.W.D., MacIntyre, D.G., Desjardins, P.J., and Cooney, R.T., 2005. Digital geology map of British Columbia. British Columbia Ministry of Energy, Mines and Petroleum Resources, British Columbia Geological Survey Open File 2005-2, DVD.

Monger, J.W.H., 1977. Upper Paleozoic rocks of the western Canadian Cordillera and their bearing on Cordilleran evolution. *Canadian Journal of Earth Sciences*, 14, 1832-1859.

Mortensen J.K., Lucas, K.A., Monger, J.W.H. and Cordey, F. (2011a). Geological Investigations of the Basement of Quesnellia in southern British Columbia: Progress Report; Poster, Mineral Exploration Roundup 2011, available for download at <http://www.geosciencebc.com/s/Posters.asp>.

Mortensen, J.K., Lucas, K., Monger, J.W.H. and Cordey, F., 2011b. Geological investigations of the basement of the Quesnel terrane in southern British Columbia (NTS 082E, F, L, 092H, I): Progress Report. In: Geoscience BC, Summary of Activities 2010, Report 2011-1, 133-142.

Nakamura, N., 1974. Determination of REE, Ba, Fe, Mg, Na and K in carbonaceous and ordinary chondrites. *Geochimica et Cosmochimica Acta*, 38, 757-775.

Orchard, M.J., 1993. Report on conodonts and other microfossils, Penticton (82E). Geological Survey of Canada Report Number Open File 1993-19.

Pearce, J.A., and Cann, J.R., 1973. Tectonic setting of basic volcanic rocks determined using trace element analyses. *Earth and Planetary Science Letters*, 19, 290-300.

Peatfield, G.R., 1978. Geologic history and metallogeny of the 'Boundary District', southern British Columbia and northern Washington. Unpublished Ph.D. thesis, Queen's University, 462 p.

Rinehart, C.D., and Fox, K.F., Jr., 1972). Geology and mineral deposits of the Loomis Quadrangle, Okanogan County, Washington. Washington Division of Mines and Geology Bulletin 64, 124 p.

Ryan, B.D., 1973. Structural geology and Rb-Sr geochronology of the Anarchist Mountain area, southcentral British Columbia Unpublished Ph.D. thesis, University of British Columbia, 256 p.

Shervais, J.W., 1982. Ti-V plots and the petrogenesis of modern and ophiolitic lavas. *Earth and Planetary Science Letters*, 59, 101-118.

Woodcock, N.H., 2004. Life span and fate of sedimentary basins. *Geology*, 32, 685-688.

The Wineglass assemblage, lower Chilcotin River, south-central British Columbia: Late Permian volcanic and plutonic rocks that correlate with the Kutcho assemblage of northern British Columbia

Paul Schiarizza^{1,a}

¹ British Columbia Geological Survey, Ministry of Energy, Mines and Natural Gas, Victoria, BC, V8W 9N3

^a corresponding author: Paul.Schiarizza@gov.bc.ca

Recommended citation: Schiarizza, P., 2013. The Wineglass assemblage, lower Chilcotin River, south-central British Columbia: Late Permian volcanic and plutonic rocks that correlate with the Kutcho assemblage of northern British Columbia. In: Geological Fieldwork 2012, British Columbia Ministry of Energy, Mines and Natural Gas, British Columbia Geological Survey Paper 2013-1, pp. 53-70.

Abstract

Late Permian volcanic and plutonic rocks that were identified along the lower Chilcotin River by Read (1993) were examined to evaluate a possible correlation with the Kutcho assemblage of northern British Columbia, host to the Kutcho Creek volcanogenic massive sulphide deposit. These rocks, herein named the Wineglass assemblage, include a lower volcanic unit of mainly basalt, an upper volcanic unit that includes rhyolite, basalt, and felsic volcanoclastic rocks, and an intrusive body of tonalite, quartz diorite, and granodiorite, referred to as the Wineglass pluton. The Wineglass assemblage is correlated with the Kutcho assemblage on the basis of its striking lithologic similarity, overlapping U-Pb zircon ages, similar unconformable relationship with an overlying Triassic-Jurassic sedimentary sequence, and similar relationship to structurally overlying Cache Creek Complex. Clastic sedimentary rocks that unconformably overlie the Wineglass assemblage are part of the predominantly Late Triassic-Middle Jurassic Cadwallader arc terrane. Expanding the definition of Cadwallader terrane to include the Wineglass assemblage and correlatives makes for a compelling correlation with Wallowa terrane, in the Blue Mountains region of northeastern Oregon and west-central Idaho.

Keywords: Late Permian Wineglass assemblage, rhyolite, basalt, tonalite, Kutcho assemblage, Sitlika assemblage, Cache Creek terrane, Cadwallader terrane, Tyaughton Formation, Ladner Group, Hurley Formation, Wallowa terrane

1. Introduction

Read (1992, 1993) identified Late Permian bimodal volcanic and intrusive rocks along the lower reaches of the Chilcotin River southwest of Williams Lake (Fig. 1). He mapped these, together with unconformably overlying Lower Jurassic clastic rocks, as a structural window, which he referred to as the Wineglass slice, beneath the Cache Creek Complex. Read et al. (1995) included rocks of the Wineglass slice in the Cadwallader terrane, which is also represented by Upper Triassic limestone and clastic sedimentary rocks, preserved in adjacent fault slices to the west and north.

The Kutcho assemblage of northern British Columbia, host to the Kutcho Creek volcanogenic massive sulphide deposit, comprises a heterogeneous package of schists derived from felsic and mafic volcanic and volcanoclastic rocks and associated felsic and mafic intrusions (Fig. 1; Schiarizza, 2012a). The Kutcho assemblage was thought to be Late Triassic at the time of Read's (1992, 1993) work near the Chilcotin River (Thorstad and Gabrielse, 1986), but subsequent studies have shown that it is Late Permian to Middle Triassic (Childe and Thompson, 1997; Schiarizza 2012a, b). Similar Late Permian to Middle Triassic ages have been obtained from the correlative Sitlika assemblage in central

British Columbia (Fig. 1), also subsequent to Read's work in the Chilcotin River area (Childe and Schiarizza, 1997; M. Villeneuve, in Struik et al., 2007).

The lithologic descriptions of the Late Permian rocks of the Wineglass slice provided by Read (1992, 1993), together with their similar spatial relationship to Cache Creek terrane (Fig. 1), suggest possible correlation with Permo-Triassic rocks of the Kutcho and Sitlika assemblages. Field studies in 2012 support the hypothesis that the Late Permian rocks of the Wineglass slice, herein assigned to the Wineglass assemblage, correlate with the Kutcho and Sitlika assemblages, and that the overlying Mesozoic rocks correlate with the Tyaughton Formation and Ladner Group of Cadwallader terrane.

2. Geological setting of the Wineglass slice

The area studied is on the Fraser Plateau, just west of the Fraser River, within the traditional territories of the Northern Secwepemc te Qelmuw and Tsilhqot'in First Nations. A good gravel road that branches southward from Highway 20 at Riske Creek crosses the Chilcotin River at Farwell Canyon, and continues south to Gang Ranch. Secondary roads that branch southeast from this road, south of the Chilcotin River, provide easy access to the parts of the Wineglass slice that were examined.

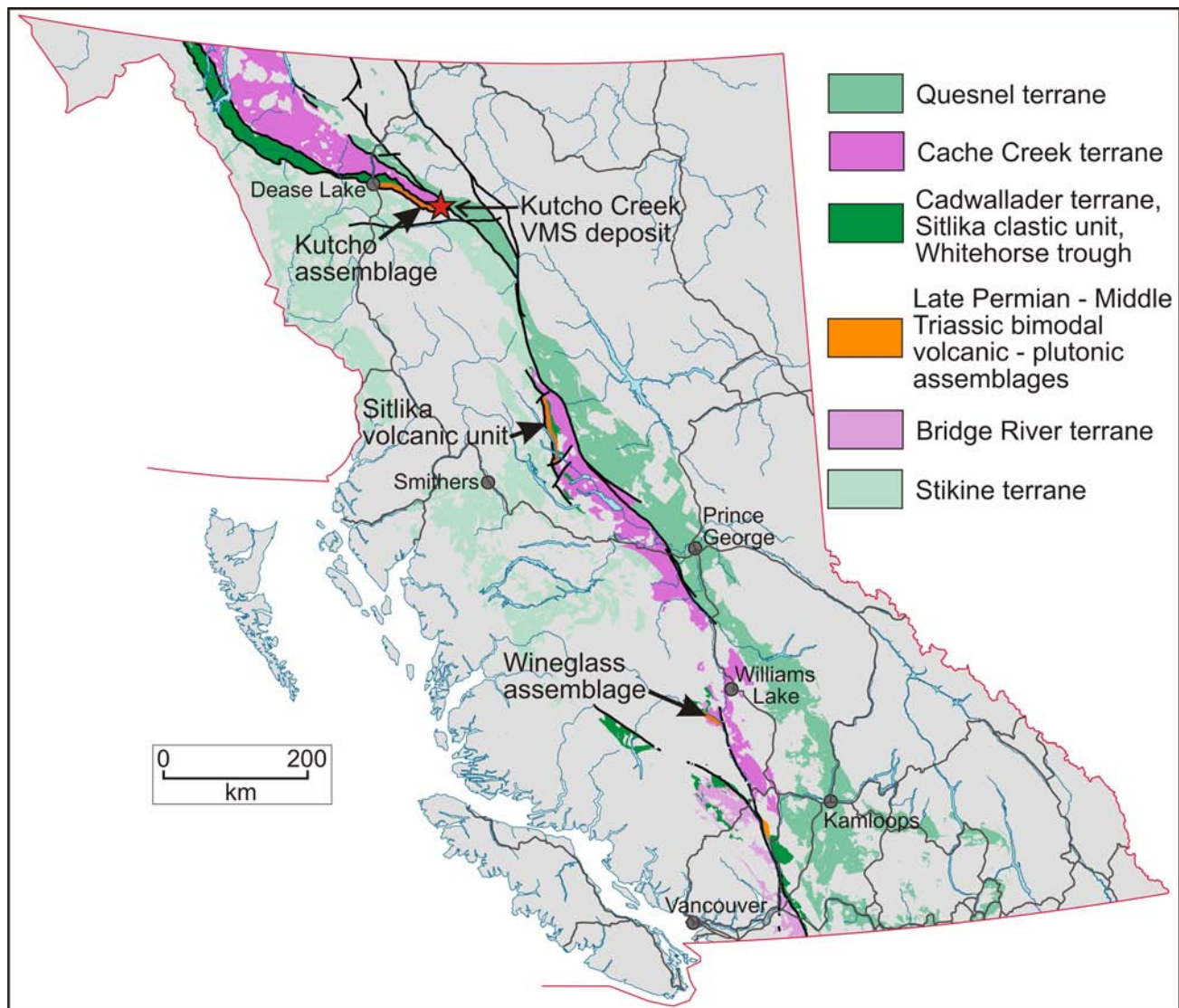


Fig. 1. Map of British Columbia showing the distribution of selected terranes and the Kutcho, Sitlika and Wineglass assemblages.

In the lower Chilcotin River area (Fig. 2), Late Paleozoic and Mesozoic rocks are assigned to three main packages, separated from one another by thrust faults that are commonly marked by units of serpentinite melange. These packages are: Cache Creek terrane, Cadwallader terrane, and Thaddeus assemblage. Younger rocks include plugs of Jura-Cretaceous diorite and quartz diorite that cut Cache Creek rocks in the southern part of the area, Eocene volcanic and sedimentary rocks that overlap thrust faults but are cut by younger north-trending faults, and flat-lying basalt and related sedimentary rocks of the Miocene-Pleistocene Chilcotin Group.

Cache Creek terrane, represented by rocks of the Cache Creek Complex, underlies much of the lower Chilcotin River area. The complex is subdivided into three composite units: one consisting of mainly chert, siliceous phyllite, and limestone; another of predominantly basalt (commonly structurally and/or stratigraphically interleaved with limestone); and a third siliciclastic sedimentary package of mainly siltstone and

sandstone. A large diorite body is also included in the Cache Creek Complex because it locally shows intrusive contacts with mafic volcanic rocks of the complex (Read, 1992), but is apparently faulted against other units in the area. Temporal constraints come mainly from the chert-siliceous phyllite-limestone unit, which has yielded radiolarians of Early Permian, Middle Triassic and Late Triassic age (Cordey and Read, 1992).

Cadwallader terrane is exposed in two fault panels in the northwestern part of the area (Fig. 2). These panels include Upper Triassic limestone and associated conglomerate and sandstone of the Hurley Formation (Cadwallader Group; Rusmore and Woodsworth, 1991), and Jurassic sandstone and conglomerate included in the Ladner Group (Read, 1992; Read et al., 1995). It is also represented by rocks of the Wineglass slice, which are exposed in a structural window, 22 km long and up to 6.5 km wide, beneath Cache Creek terrane on the southwest side of the Chilcotin River. The youngest rocks in this window comprise Upper Triassic(?) and Lower Jurassic

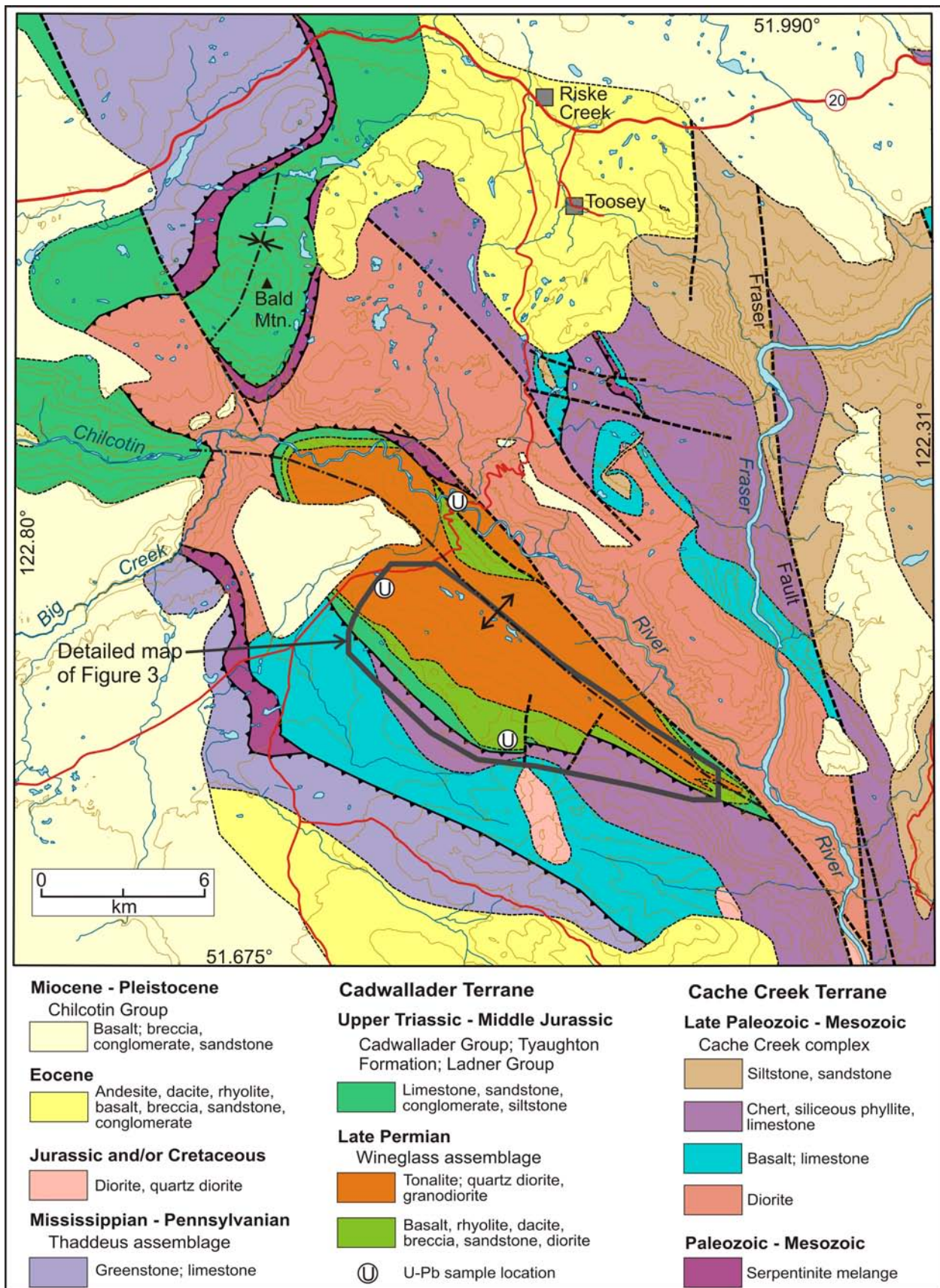


Fig. 2. Geological map of the lower Chilcotin River area, after Tipper (1978), Read (1993), and Mihalyuk and Harker (2007).

siliciclastic rocks correlated with the Tyaughton Formation and Ladner Group, prominent components of Cadwallader terrane elsewhere in the region. The predominant rocks within the window, however, are Late Permian volcanic and plutonic rocks of the Wineglass assemblage, which are unconformably overlain by the Mesozoic rocks. Following Read et al. (1995), this volcano-plutonic suite is included in Cadwallader terrane because of its position beneath the sub-Mesozoic unconformity.

The Thaddeus assemblage comprises massive greenstone that encloses limestone lenses with Mississippian and Pennsylvanian conodonts (Read, 1993). These rocks are thrust above Cache Creek terrane in the southern part of the lower Chilcotin River area, and above Cadwallader terrane in the northwestern part of the area (Fig. 2). Read (1993) noted that Thaddeus rocks are older than any known components of southern Cache Creek terrane, but are similar in age to the oldest known cherts from Bridge River terrane (Cordey and Schiarizza, 1993). However, Read et al. (1995) included the Thaddeus assemblage (Thaddeus slice) in the Pioneer Formation of Cadwallader terrane rather than correlating with either of these terranes. The Thaddeus assemblage was not examined during the present study, and no correlation is attempted herein.

Prominent structures in the lower Chilcotin River area include post-Early Jurassic thrust faults, folds that deform some thrust faults, and north- to northwest-striking faults related to the Eocene and younger Fraser fault system (Read, 1992, 1993). The thrust faults, typically defining the contacts between Cache Creek terrane, Cadwallader terrane, and Thaddeus assemblage, are commonly marked by zones of serpentinite melange. Read (1992, 1993) inferred that thrust movement was to the northeast, based in part on asymmetric folds in serpentinite melange at the south end of the Bald Mountain slice. However, the folded thrust that separates Cache Creek terrane from the Wineglass slice might be westerly directed, because Cache Creek terrane typically occurs to the east of Cadwallader terrane, and to the east of Wineglass correlatives in central and northern British Columbia. Thrust systems that might correlate with those in the lower Chilcotin River area include Jurassic imbrications of Cache Creek terrane and Sitlika assemblage in central British Columbia (Struik et al., 2001), and Cretaceous structures that imbricate Cadwallader terrane and associated rocks in southern British Columbia (Schiarizza et al., 1997). These systems include an older, predominant set of westerly-directed structures and a younger set of easterly-directed structures.

3. Geology of the southern part of the Wineglass slice

The southern part of the Wineglass slice was mapped to evaluate the possible correlation between the Kutcho and Wineglass assemblages (Figs. 3, 4). The area encompasses a large part of the Late Permian Wineglass

pluton, as well as the thickest section of Late Permian volcanic rocks exposed within the slice, including locations where the pluton and volcanic rocks were dated. The map area also includes a substantial section of the overlying Mesozoic rocks, including the fossil locality that yielded an Early Jurassic ammonite.

3.1. Wineglass assemblage

The Wineglass assemblage comprises two major components: a volcanic succession and a tonalitic intrusive body referred to here as the Wineglass pluton. The volcanic succession is divided into two main units (Wv1 and Wv2). Unit Wv1 consists mainly of basalt, whereas unit Wv2 comprises a more heterogeneous package that includes rhyolite, basalt, and fine- to coarse-grained volcanoclastic rocks. Unit Wv2 is inferred to overlie unit Wv1 because the former is unconformably overlain by younger rocks of the Tyaughton Formation, although no independent younging indicators were observed in the volcanic succession. A third unit, Wva, comprises volcanic(?) rocks in the eastern part of the area which, because of poor exposure and intense alteration, could not be confidently assigned to either Wv1 or Wv2.

The Wineglass assemblage is assigned a Late Permian age on the basis of U-Pb zircon ages reported by Friedman and van der Heyden (1992) and Read (1993). Two ages reported by Read (1993) are from the current study area: 259 ± 2 Ma on dacite of unit Wv2, and 254 ± 1.2 Ma on leuco-quartz monzonite of the Wineglass pluton. Friedman and van der Heyden (1992) obtained a date of 258 ± 5 Ma on quartz monzodiorite of the Wineglass pluton to the north of the current study area, at the bridge over the Chilcotin River (Fig. 2). A sample of rhyolite that was collected from unit Wv2 during the 2012 field season has been submitted to the geochronology laboratory at the University of British Columbia for U-Pb zircon geochronology.

3.1.1. Unit Wv1

Unit Wv1 consists mainly of basalt and weakly foliated chloritic schist, but also includes narrow units of felsic volcanic rock, as well as small bodies of diorite and tonalite. It is cut by tonalitic intrusive rocks of the Wineglass pluton to the north, and is in contact with (apparently overlain by) volcanic and volcanoclastic rocks of unit Wv2 to the south. The latter unit pinches out to the west, apparently due to erosion beneath the unconformity at the base of the Tyaughton Formation, such that unit Wv1 is directly overlain by the Tyaughton formation near the western boundary of the map area.

The predominant rock type of unit Wv1 is medium to dark green, greenish brown-weathered, fine-grained basalt that commonly contains 5-15% clinopyroxene and/or plagioclase phenocrysts, 1-2 mm in size. Patches, veins, and fracture-coatings of epidote \pm calcite are ubiquitous, but vary from a minor to a very major component of any given exposure (Fig. 5). Secondary chlorite is also a highly variable component, and where abundant it typically displays a preferred orientation that

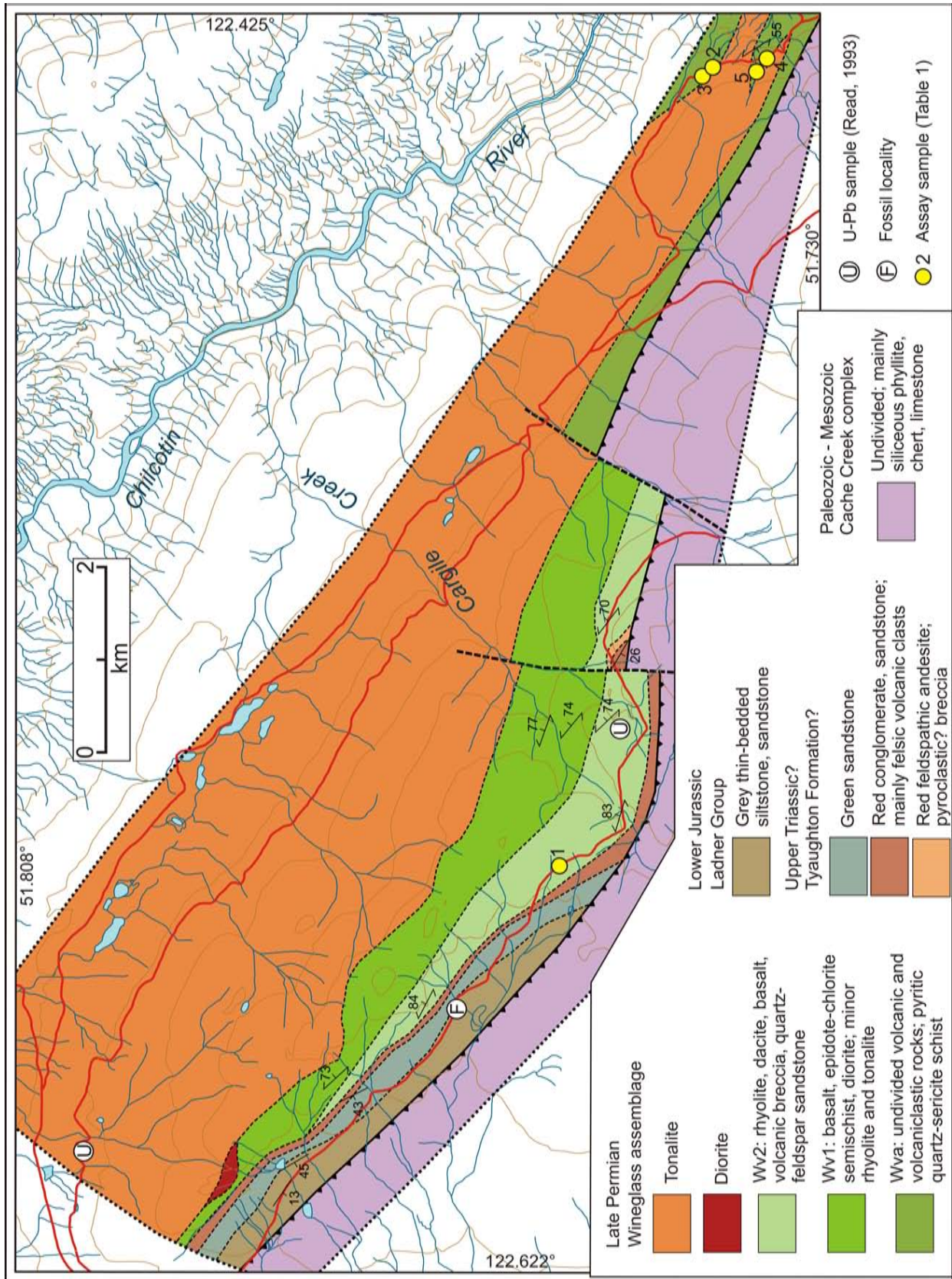


Fig. 3. Geology of the southern part of the Wineglass slice, based on 2012 fieldwork.

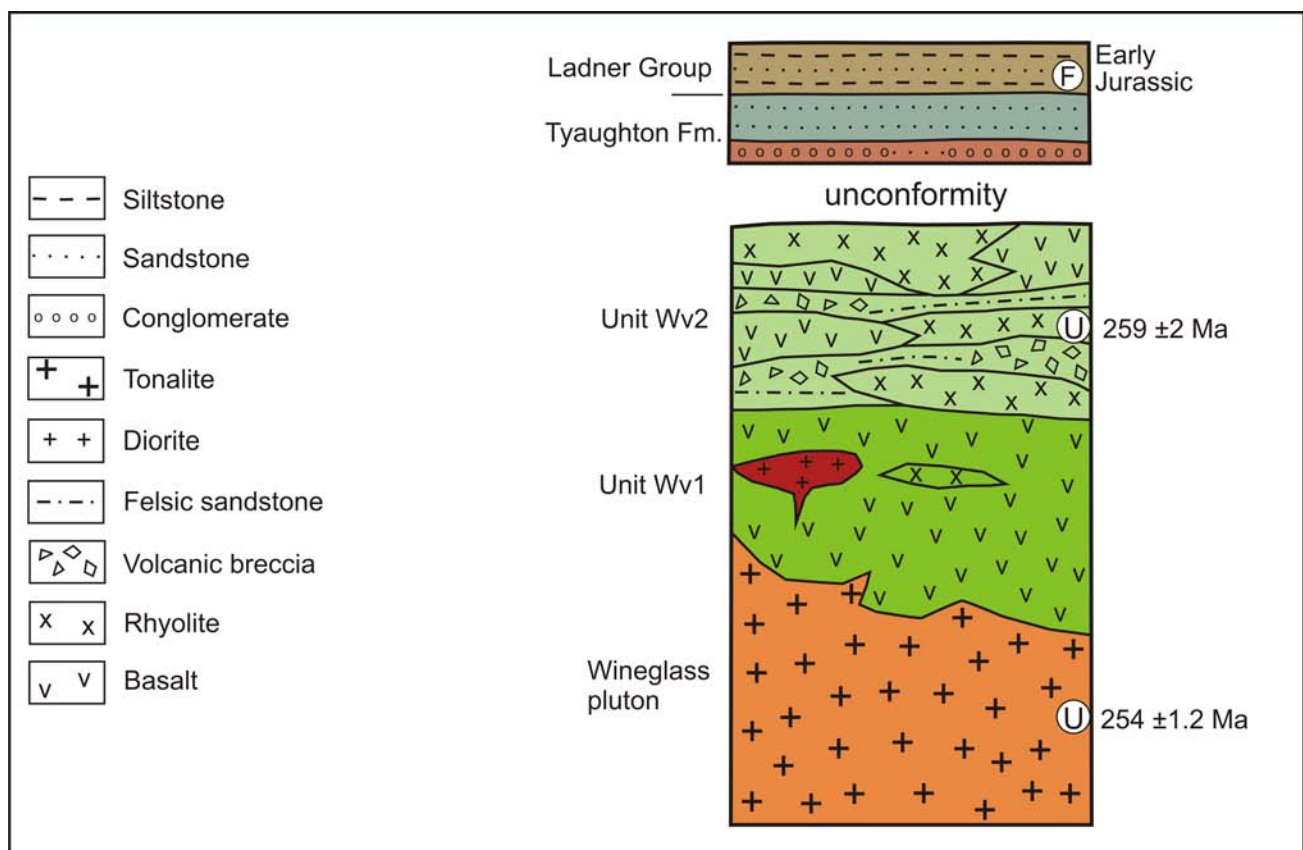


Fig. 4. Schematic stratigraphy of the Wineglass assemblage and overlying sedimentary rocks of the Tyaughton Formation and Ladner Group in the southern part of the Wineglass slice. Early Jurassic fossil determination reported in Hickson (1990); U-Pb zircon ages from Read (1993).

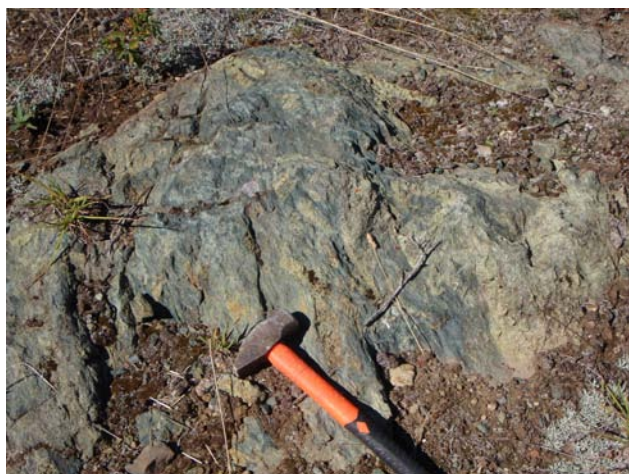


Fig. 5. Epidote-altered chloritic basalt, Wineglass assemblage, unit Wv1.

imparts a weak foliation to the rock. Thin sections show relatively fresh clinopyroxene and/or plagioclase phenocrysts set in a groundmass of variably saussuritized plagioclase, locally aligned in a trachytic texture, that is intergrown with secondary epidote-chlorite±actinolite.

Felsic volcanic rocks are uncommon in unit Wv1. They form 1-10 m wide tabular bodies within basalt, that may constitute dikes, sills, and flows. The felsic rocks are typically pale to medium grey or green, and display a very fine-grained to aphanitic quartzose groundmass, locally with faint flow laminae, containing small phenocrysts of plagioclase and/or quartz.

Diorite was noted at several localities within unit Wv1, and forms a small mappable body near the western boundary of the map area. Diorite exposures typically display strong epidote alteration, and are characterized by a fine- to medium-grained, equigranular, isotropic intergrowth of plagioclase and altered mafic grains. Small intrusive bodies of fine- to medium-grained, equigranular tonalite and quartz diorite, compositionally similar to the Wineglass pluton, are also present at scattered localities within unit Wv1.

3.1.2. Unit Wv2

Unit Wv2 is a heterogeneous succession that includes rhyolite, basalt, fragmental volcanoclastic rocks containing felsic and/or mafic volcanic clasts, and finer volcanoclastic rocks containing granules and sand-size grains of feldspar and quartz. It forms a panel that crops

out south of, presumably stratigraphically above, unit Wv1. It is unconformably overlain by the Tyaughton Formation along most of its length, but locally may be in direct contact, across an inferred thrust fault, with siliceous phyllite and chert of the Cache Creek Complex (Fig. 3).

Coherent rhyolite units are typically pale grey to green, locally with a purplish to medium green mottle. They commonly include 10-25% phenocrysts of glassy quartz and white feldspar (1-4 mm) within an aphanitic to very fine-grained quartzofeldspathic groundmass (Fig. 6). Secondary sericite is common locally, and contributes to a weak foliation. Vague fragmental textures observed within some units may reflect autobrecciation.

Basalt units are typically medium to dark green, fine-grained, variably epidote-calcite-chlorite-altered schists, locally with small plagioclase and/or pyroxene phenocrysts, that resemble basalts from unit Wv1. However, pillow structures, not recognized in unit Wv1, occur locally in the upper part of unit Wv2 in the central part of the map area. Pillows typically display amygdaloidal cores (amygdules of chlorite and calcite), pervasive epidote alteration, and purplish hematite-altered rinds (Fig. 7).

Volcaniclastic rocks in unit Wv2 include both mafic and felsic varieties. Mafic varieties include medium to dark green, weakly to moderately foliated chloritic schists that contain fragments (<1-3 cm) of pale grey to green felsic volcanic rock and dark green mafic volcanic rock, locally accompanied by smaller mineral grains of plagioclase \pm pyroxene (Fig. 8). Felsic varieties are pale grey to green, weakly foliated chlorite-sericite semischists that contain only felsic volcanic fragments, accompanied by grains of feldspar \pm quartz. Finer grained felsic volcaniclastic rocks contain quartz, feldspar, and small lithic fragments in a matrix of weakly foliated chlorite, sericite, and fine quartzofeldspathic material (Fig. 9). Most of the volcaniclastic rocks of unit Wv2, are thought to have been deposited by epiclastic processes (e.g., Fig. 9).



Fig. 6. Quartz-plagioclase-phyric rhyolite, Wineglass assemblage, unit Wv2.



Fig. 7. Pillow from a pillowed basalt unit, Wineglass assemblage, unit Wv2.



Fig. 8. Fragmental rock with felsic and mafic volcanic clasts, Wineglass assemblage, unit Wv2.



Fig. 9. Well sorted, framework-intact volcaniclastic granulestone with subrounded fragments, Wineglass assemblage, unit Wv2.

3.1.3. Unit Wva

Rocks assigned to unit Wva are exposed only near the eastern edge of the map area, where they comprise highly-altered gossanous rocks that interfinger with less-altered tonalite of the Wineglass pluton. Most of the rocks included in unit Wva are pyrite-sericite-quartz semischists, locally with scattered relict grains of quartz and feldspar, which were probably derived from felsic volcanic or intrusive rocks. One exposure on the north side of the belt is a weakly pyritic, fine-grained chlorite-altered rock, with faint ghosts of relict feldspar, which may have been derived from a mafic volcanic rock.

3.1.4. Wineglass pluton

The Wineglass pluton forms most of the northern half of the study area. It is commonly represented by relatively resistant, light grey-weathered, blocky outcrops. The predominant rock type is a light greenish grey, medium- to coarse-grained, equigranular hornblende-biotite tonalite, locally grading to granodiorite or quartz diorite (Fig. 10). Mafic minerals commonly form 10-20% of the rock, with chloritized hornblende predominating over biotite. At one locality, the tonalite contains screens of an older phase, comprising fine grained, chlorite-epidote-altered hornblende diorite. Dikes of aplite and medium-grained leucotonalite cut the tonalite in several places. Contacts between tonalite and basalt were locally observed in the western part of the map area, confirming that the Wineglass pluton intrudes unit Wv1.

3.2. Sedimentary rocks overlying the Wineglass assemblage

A succession of southwest-dipping Mesozoic sedimentary rocks occurs above the Wineglass assemblage in the southwestern part of the map area (Fig. 3). These rocks were first discussed by Hickson (1990) who collected Early Jurassic (Toarcian) fossils from black shale, and suggested that they might belong to Cadwallader terrane. Read (1993) recognized felsic clasts in the basal part of the succession and suggested that it rested unconformably above the Permian rocks of the Wineglass assemblage. Here, the succession is subdivided



Fig. 10. Tonalite, south margin of the Wineglass pluton.

into several mappable units, which are correlated with stratigraphic units of Cadwallader terrane, consistent with the interpretations of Hickson (1990) and Read et al. (1995). Lower units are tentatively assigned to the Upper Triassic Tyaughton Formation, based on similarities to Tyaughton exposures northwest of Bralorne (Umhoefer, 1990; Schiarizza et al., 1997) and east of Tatlayoko Lake (Schiarizza and Riddell, 1997; Schiarizza et al., 2002). The upper unit, which includes the Early Jurassic fossil locality, is included in the Lower to Middle Jurassic Ladner Group, following Read et al. (1995), as this group can reasonably be used to encompass the various formal and informal Lower to Middle Jurassic clastic units that have been included in Cadwallader terrane (Umhoefer, 1990; Schiarizza et al., 1997; Schiarizza et al., 2002).

3.2.1. Tyaughton Formation

Rocks tentatively assigned to the Tyaughton Formation include two main components: a basal red conglomerate unit and an overlying unit of massive green sandstone. A third unit comprises red volcanic rocks, which occur within or below the red conglomerate unit in a set of small, poor exposures at one locality in the south-central part of the map area (Fig. 3).

The basal unit of the Tyaughton Formation consists mainly of red, locally green or mottled red/green, pebble conglomerate. Angular to subrounded clasts (generally 0.5-3 cm but up to 8 cm) are enclosed by a sand matrix of quartz, feldspar, and lithic grains (Fig. 11). The predominant clast types are pale grey, greenish-grey, beige or purple aphanitic felsic volcanic rocks, locally with small quartz and/or feldspar phenocrysts. Other clast types include light grey, fine- to medium-grained tonalite, medium to dark green mafic volcanic rock, grey or green chert, and grey-green microdiorite. The conglomerate defines poorly stratified layers up to several metres thick and thin to medium beds intercalated with gritty sandstone (Fig. 12). Local thinly bedded intervals of finer-grained rock include: red or green, medium- to fine-grained sandstone; red siltstone; and dark red mudstone.

The upper unit of the Tyaughton Formation consists of massive, blue-green to olive-green sandstone, which



Fig. 11. Conglomerate, basal Tyaughton Formation.



Fig. 12. Interlayered conglomerate and parallel-stratified sandstone, lower Tyaughton Formation.

typically weathers to a greenish brown or rusty-brown colour. The sandstone is well indurated, medium to coarse grained, and composed mainly of feldspar, grey and green lithic grains, and quartz.

Red-coloured volcanic rocks tentatively included in the Tyaughton Formation occur as a single set of poor outcrops that underlie red conglomerate in the south-central part of the map area (Fig. 3). Volcanic rocks are absent in the type area of the Tyaughton Formation north of Bralorne (Umhoefer, 1990), but rare feldspathic tuffs are in the formation near Tatlayoko Lake (Schiarizza and Riddell, 1997). The volcanic rocks in the current map area include a fragmental unit directly beneath the conglomerate, and amygdaloidal andesite exposed a short distance to the northeast. The fragmental unit contains flattened intermediate volcanic clasts, up to 1.5 cm in longest dimension, in a weakly foliated matrix of similar composition. The andesite consists of small plagioclase phenocrysts and amygdules of chalcedonic quartz, in a very fine-grained groundmass with predominantly plagioclase laths, in part aligned in a trachytic texture.

3.2.2. Ladner Group

The Ladner Group, represented by only a few scattered exposures, consists of rusty-weathered, medium to dark grey, thinly bedded, variably calcareous, siltstone and fine- to medium-grained sandstone (Fig. 13). A fossil ammonite was collected from one exposure (Fig. 3), presumably the same location that yielded the Early Jurassic (Toarcian) fossil collection reported by Hickson (1990).

3.3. Cache Creek Complex

The Cache Creek Complex crops out at a few scattered localities near the southern margin of the map area (Fig. 3). Exposures in the southeast consist mainly of green to grey siliceous argillite containing thin contorted lenses of chert. A single exposure near the western margin of the map area comprises light grey-weathered, weakly foliated limestone. Contact relationships between the Cache Creek rocks and those of the adjacent Wineglass



Fig. 13. Thinly bedded siltstone and sandstone, Ladner Group.

slice were not observed; the south-dipping thrust contact shown on Figure 3 is based on the interpretation of Read (1992, 1993).

3.4. Structure

Mesozoic sedimentary rocks of the Tyaughton Formation and Ladner Group form a right-way-up panel that dips at moderate angles to the southwest. Underlying volcanic rocks of the Wineglass assemblage are thought to young southwest also, but the orientation of layering is unknown; the few internal contacts observed, typically rhyolite against basalt, generally strike northwest and dip steeply, but might represent dikes rather than bedding orientations. A poor to moderately developed cleavage occurs sporadically within both the Wineglass assemblage and the overlying Mesozoic sedimentary rocks, and displays a fairly uniform orientation, with steep dips to the northeast. The only mesoscopic folds observed comprise a set of complex southwest-plunging folds with gently dipping axial surfaces that deform thin-bedded sedimentary rocks of the Ladner Group. These folds seem to predate the poorly developed cleavage, and it is suspected that they are soft-sediment structures.

According to the interpretation of Read (1992, 1993), the 2012 map area comprises the southwest limb of an anticline that is cored by the Wineglass slice, resulting in its exposure as a window beneath the Cache Creek Complex. The sparse structural observations outlined above are consistent with this interpretation.

3.5. Alteration and mineralization

An extensive zone of predominantly pyrite-sericite-quartz alteration, at least 600 m wide, encompasses the Farwell pluton and adjacent rocks assigned to unit Wva near the eastern boundary of the map area (Fig. 14). This zone has received some attention from exploration geologists (Morton, 1984; Benvenuto and Bailey, 1990) who have thus far failed to locate any base or precious metal occurrences. The alteration zone was mentioned by Read (1992), who noted that similar alteration occurs in the northwestern part of the Wineglass assemblage, along the Chilcotin River, 4.8 km downstream from the mouth of Big Creek (Fig. 2).



Fig. 14. Pyrite-sericite-quartz-altered rocks of the Wineglass assemblage, east end of 2012 map area.

The alteration zone at the east end of the map area consists of variably schistose pyrite-sericite-quartz-altered rocks interspersed with bodies of variably silicified \pm sericite \pm chlorite \pm pyrite-altered tonalite. The schistosity dips at moderate angles to the southwest, as do a set of green microdiorite dikes that postdate the alteration. The altered rocks locally contain relict grains of feldspar and quartz, indicating a felsic volcanic or plutonic protolith, although one exposure at the north end of the belt consists of weakly pyritic chlorite-altered rock that may have been derived from basalt. Four grab samples collected from altered rocks within this zone yielded only background base and precious metal values (locations 2-5, Fig. 3, Table 1).

Weak to moderate pyrite alteration occurs in both rhyolite and basalt of unit Wv2 in and around the upper reaches of Cargile Creek, where old pits and trenches attest to past exploration. A sample of rusty pyritic rock, apparently in basalt, collected from one of these pits contained anomalous concentrations of zinc and lead (location 1, Fig. 3, Table 1).

4. Discussion

4.1. Correlation of the Wineglass, Sitlika and Kutcho assemblages

The Wineglass assemblage is correlated with the Kutcho assemblage and the volcanic unit of the Sitlika

assemblage on the basis of a remarkable similarity in lithologic components, overlapping ages, similar structural relationships to Cache Creek terrane, and similar unconformable relationships with overlying Upper Triassic-Jurassic sedimentary rocks.

The Wineglass assemblage includes three major units, all of which have lithologic counterparts in the Kutcho and Sitlika assemblages. Mafic volcanic rocks of unit Wv1 are very similar to unit KS3 of the Kutcho assemblage (Schiarizza, 2012a) and to mafic volcanic rocks of the Sitlika volcanic unit exposed near Diver Lake (Schiarizza and Payie, 1997; Schiarizza and Massey, 2010). In all cases, basalt is predominant, but is intercalated with narrow units of felsic volcanic or volcanoclastic rock, and includes small bodies of diorite. Unit Wv2 resembles unit KC of the Kutcho assemblage (Schiarizza, 2011, 2012a), which overlies mafic volcanics of unit KS3, and includes coherent rhyolite, metabasalt, and volcanoclastic rocks containing felsic volcanic clasts and granules of quartz and feldspar. A similar heterogeneous package of mafic and felsic volcanic and volcanoclastic rocks forms the upper part of the Sitlika volcanic unit in the area between Mt. Olson and Mt. Bodine (Schiarizza and Payie, 1997; Schiarizza and Massey, 2010). Tonalitic intrusive rocks, similar to the Wineglass pluton, form two mappable stocks in the Sitlika volcanic unit (Schiarizza and Massey, 2010), and several mappable bodies within the Kutcho assemblage, including one sill-like pluton more than 12 km long (Schiarizza, 2012a, b).

U-Pb zircon crystallization ages for the Kutcho, Sitlika and Wineglass assemblages are summarized in Figure 15. The few ages for the Wineglass assemblage are older than many Kutcho and Sitlika determinations, but overlap with the oldest ages from both assemblages.

Correlation of the Kutcho assemblage, the volcanic unit of the Sitlika assemblage and the Wineglass assemblage is corroborated by a virtually identical stratigraphic and structural context. All three are unconformably overlain by Mesozoic sedimentary successions that include a lower conglomerate unit containing felsic volcanic and plutonic clasts probably derived from underlying rocks, and upper stratigraphic levels with predominantly siltstone and sandstone of known or suspected Lower-Middle Jurassic age

Table 1. Selected elements from analyses of altered rock. See Fig. 3 for locations. UTM coordinates are zone 10, North American Datum 1983.

Map Ref.	Sample	Easting	Northing	Rock Type	Mo	Cu	Pb	Zn	Ag	As	Au	Sb	Ba	W	Hg
					PPM	PPM	PPM	PPM	PPM	PPM	PPM	PPM	PPM	PPM	PPM
1	12PSC-28	530473	5733911	altered pyritic rock	0.5	47.1	29.1	237	<0.1	10	<0.5	0.2	22	<0.1	0.06
2	12PSC-84	539121	5732330	quartz-pyrite-sericite-altered rock	0.1	53.1	10.9	106	0.2	1.7	0.7	0.4	11	<0.1	<0.01
3	12PSC-85	539018	5732427	fractured green gossanous rock	0.5	3.8	7.4	130	<0.1	0.7	1.2	<0.1	8	<0.1	<0.01
4	12PSC-87	539205	5731724	pale green pyritic siliceous rock	0.2	65.9	2.3	61	<0.1	<0.5	<0.5	<0.1	4	<0.1	<0.01
5	12PSC-89	539090	5731847	pale green pyrite-altered rock	0.4	35.5	8	66	0.1	1.4	2.2	<0.1	21	<0.1	<0.01

Samples analysed at ACME Analytical Laboratories Ltd., Vancouver BC, by ICP-MS following digestion of a 15 g sample split in hot Aqua Regia

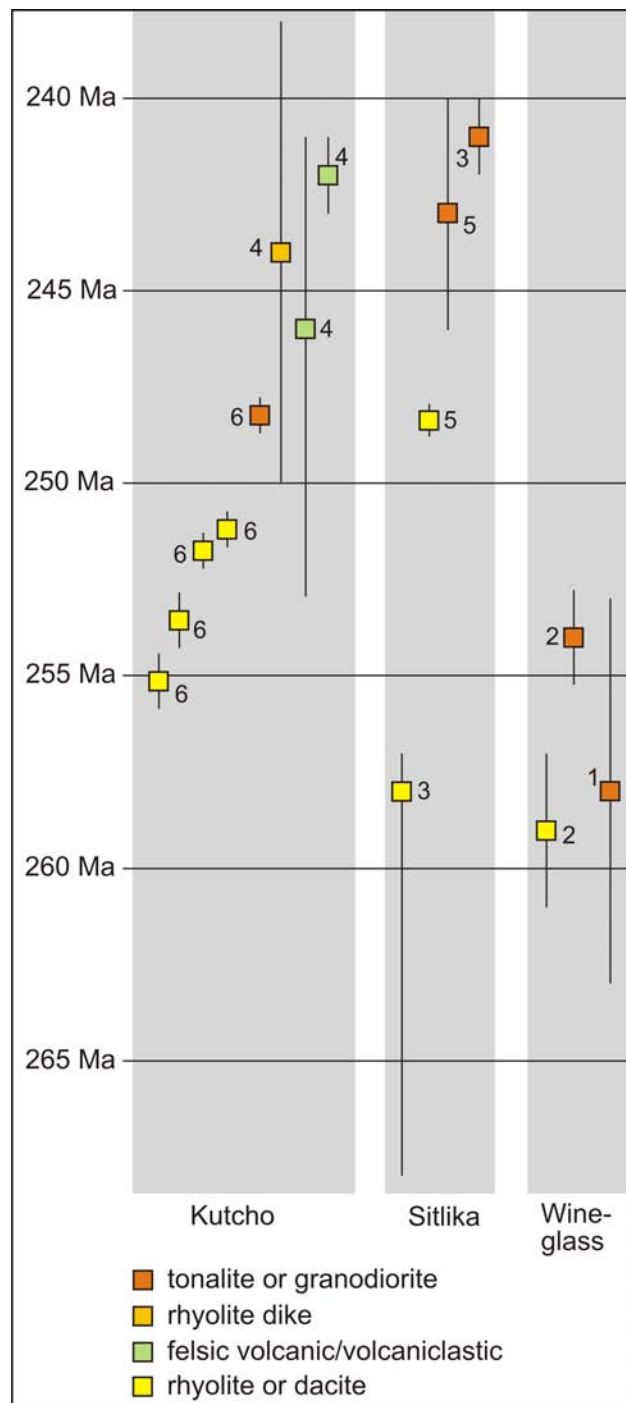


Fig. 15. Summary of U-Pb zircon ages for the Kutcho, Sitlika and Wineglass assemblages. Sources of information: 1) Friedman and van der Heyden, 1992; 2) Read, 1993; 3) Childe and Schiarizza, 1997; 4) Childe and Thompson, 1997; 5) M. Villeneuve in Struik et al., 2007; 6) R. Friedman in Schiarizza, 2012b.

(Schiarizza, 2012a; Schiarizza and Payie, 1997; Read, 1993; this study). In addition, all three Permo-Triassic packages, together with the unconformably overlying Mesozoic sedimentary rocks, are structurally beneath rocks of the Cache Creek Complex, along or near the western margin of Cache Creek terrane (Fig. 1).

The Mesozoic sedimentary rocks that overlie the Kutcho assemblage include discontinuous conglomerate and limestone units of suspected Upper Triassic age, and an extensive package of Lower to Middle Jurassic sandstones and siltstones assigned to the Inklin Formation (Schiarizza, 2012a). The Inklin Formation is the main component of the Whitehorse trough, a sedimentary basin that received detritus mainly from Stikine terrane (Fig. 1; Johannson et al., 1997; English et al., 2005). Similar sedimentary units that overlie the Sitlika volcanic unit are assigned to the clastic sedimentary unit of the Sitlika assemblage (Schiarizza and Payie, 1997; Schiarizza and Massey, 2010) and are probably an offset counterpart of the Whitehorse trough (Fig. 1). In contrast, the very similar Mesozoic rocks that overlie the Wineglass assemblage are included in Cadwallader terrane (Read et al., 1995; this study). This suggests that Cadwallader terrane has paleogeographic links to the Whitehorse trough and Stikine terrane, although addressing these connections is beyond the scope of this paper.

4.2. An expanded definition of Cadwallader terrane

Rusmore et al. (1988) interpreted Cadwallader terrane as a Late Triassic volcanic arc with a Late Triassic to Middle Jurassic fringing sedimentary apron (represented by the Cadwallader Group and the Tyaughton and Last Creek formations in the southern Chilcotin Ranges near Bralorne). Subsequent studies, the results of which are summarized in Figures 16 and 17, have expanded the known distribution of Cadwallader rocks, identified a major plutonic component to the Triassic arc system, included Lower and Middle Jurassic rocks formerly assigned to Methow terrane, and demonstrated that the Mesozoic rocks of Cadwallader terrane are underlain by an older, Late Permian arc system.

The type areas of the Cadwallader Group, the Tyaughton Formation, and the Last Creek Formation are in a large fault-bounded panel north-northwest of Bralorne (Fig. 16). The Cadwallader Group comprises Upper Triassic clastic sedimentary rocks and local limestone of the Hurley Formation and underlying arc basalt of the Pioneer Formation (Rusmore, 1987). The Tyaughton Formation consists of Upper Triassic shallow-marine and nonmarine clastic rocks and limestone that are in fault contact with the Cadwallader Group, and the Last Creek Formation is a transgressive sequence of Lower to Middle Jurassic siliciclastic rocks that overlies the Tyaughton Group disconformably (Umhoefer, 1990). The Cadwallader Group also crops out in numerous fault-bounded slivers southeast of its type area, where it is structurally interleaved with chert, basalt and related rocks of the oceanic Bridge River terrane along complex systems of thrust and strike-slip faults of Cretaceous and Tertiary age (Schiarizza et al., 1997). The Cadwallader rocks within these fault slices are almost invariably accompanied by fault panels of Early Permian diorite, basalt, and serpentinized ultramafite, including the Bralorne diorite which hosts mesothermal gold-quartz

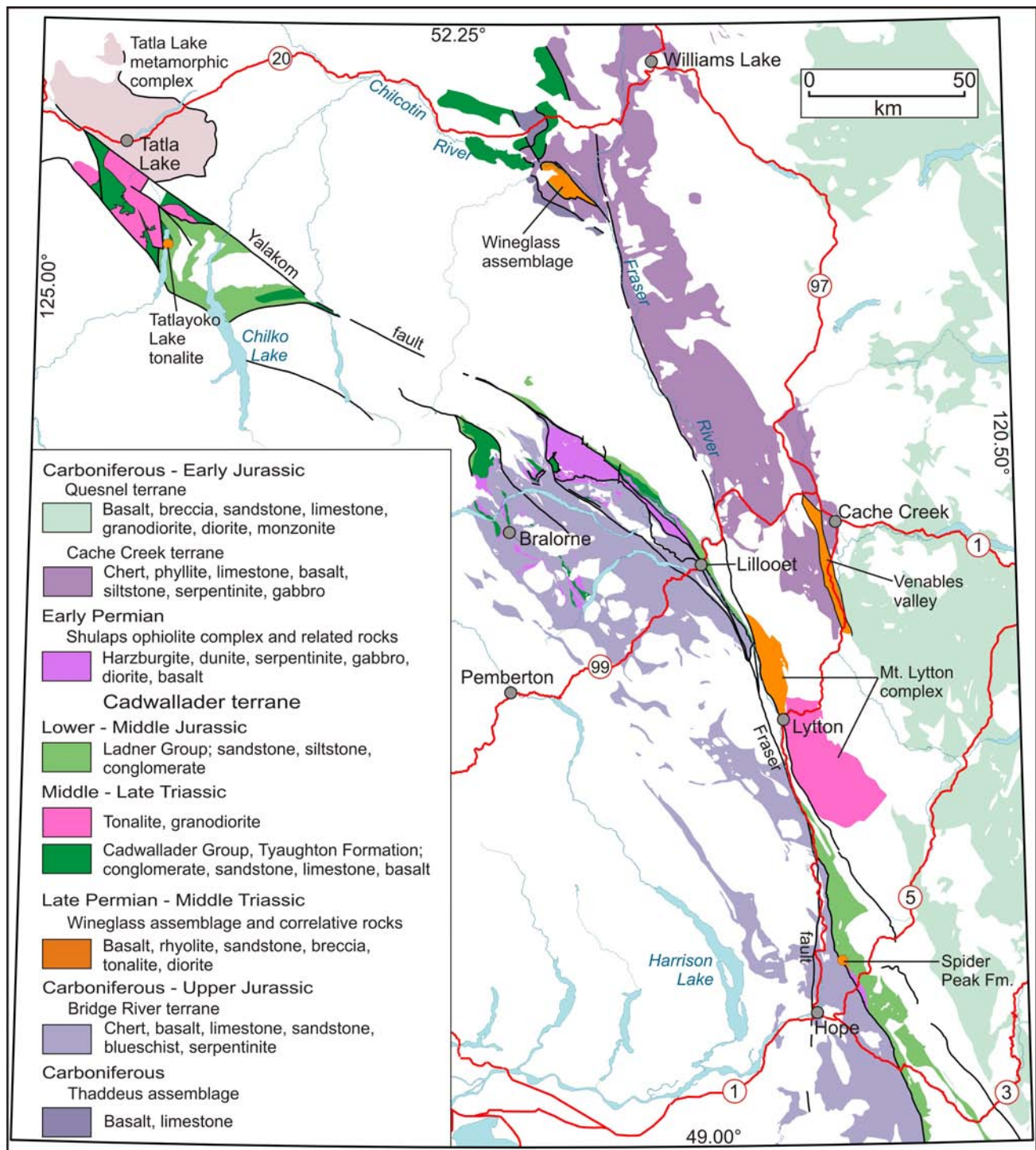


Fig. 16. Map of part of southern British Columbia highlighting Cadwallader terrane and adjacent Paleozoic to mid-Mesozoic terranes. Modified from Massey et al. (2005). Uncoloured areas are mainly younger rocks, including Upper Jurassic and Cretaceous siliciclastic rocks of the Tyaughton-Methow basin, which overlap Cadwallader and Bridge River terranes (see Fig. 17).

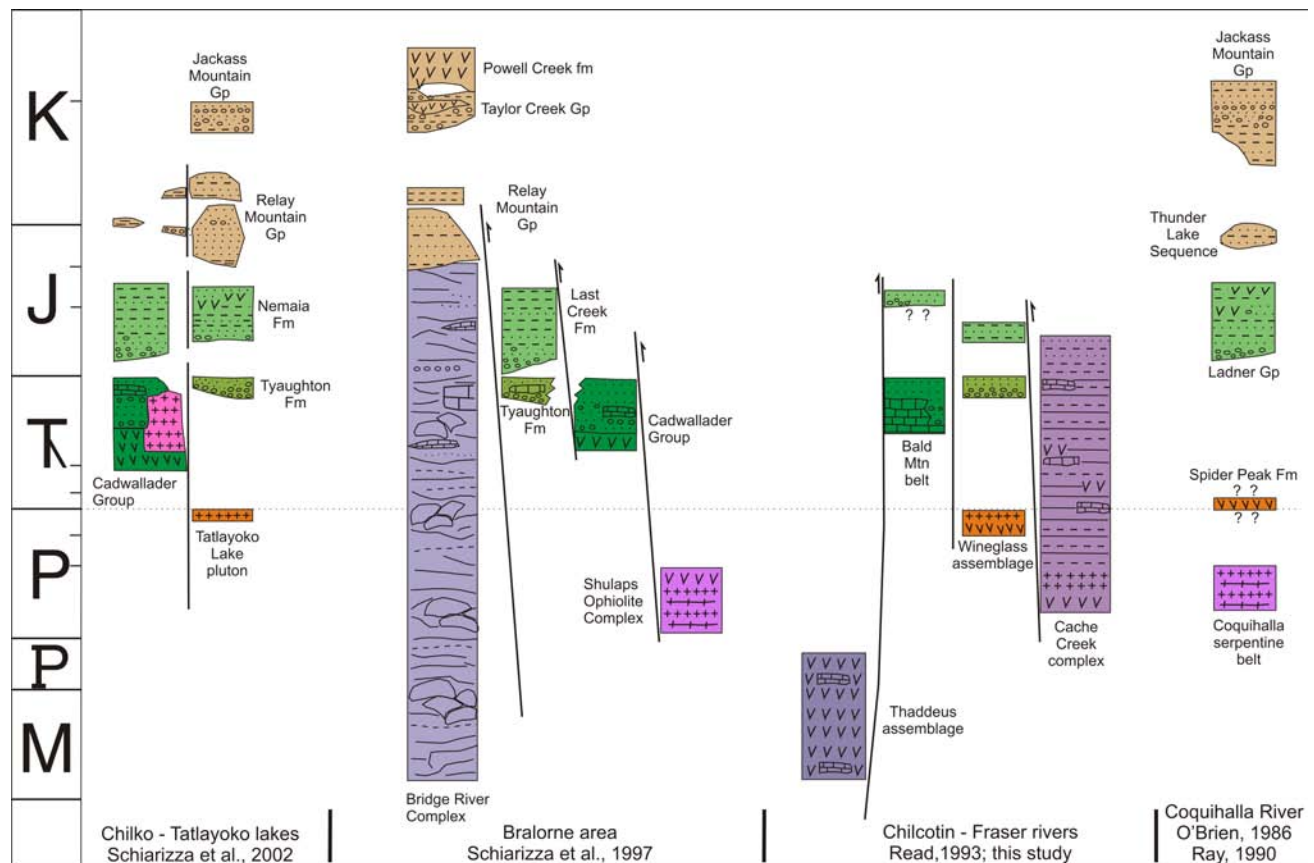


Fig. 17. Schematic stratigraphic sections for Cadwallader terrane and associated units. Upper Triassic and Lower to Middle Jurassic rocks of Cadwallader terrane shown in shades of green; Late Triassic plutons of Cadwallader terrane are magenta; Permo-Triassic rocks of Cadwallader terrane are orange. Pale brown colour denotes Upper Jurassic and Cretaceous rocks of the Tyaughton-Methow basin.

veins at the Bralorne and Pioneer mines. These panels of ultramafic-mafic rock may be related to the Shulaps ophiolite complex, which lies structurally above the Cadwallader Group northeast of Bralorne (Fig. 16).

The Cadwallader Group, Tyaughton Formation, and overlying Lower to Middle Jurassic rocks (Nemaia Formation of Schiarizza et al., 2002) are also exposed over a broad area near Chilko and Tatlayoko lakes (Fig. 16). These exposures are bounded to the northeast by the Yalakom fault, along which they were translated about 115 km to the northwest in early Tertiary time (Riddell et al., 1993; Umhoefer and Schiarizza, 1996). Cadwallader terrane in this area also includes several large plutons consisting of Late Triassic tonalite, granodiorite, and diorite, with crystallization ages ranging from 231 to 207 Ma (Friedman and Schiarizza, 1999; Schiarizza et al., 2002).

The Lower and Middle Jurassic rocks of Cadwallader terrane in the Chilko Lake – Tatlayoko Lake area were referred to as the Huckleberry formation by Schiarizza and Riddell (1997) and the Nemaia Formation by Schiarizza et al. (2002). These rocks are generally similar to the Last Creek Formation, but include some intermediate to mafic volcanic and volcaniclastic rocks in

the Middle Jurassic part of the section (Schiarizza and Riddell, 1997). The Nemaia Formation, together with overlying Jura-Cretaceous sedimentary rocks of the Tyaughton-Methow basin (Relay Mountain and Jackass Mountain groups), can be traced southeastward, with significant dextral offsets along the Yalakom and Fraser faults, into identical rocks of the Lower to Middle Jurassic Ladner Group, which forms a linear belt extending from south of Lytton to the international boundary (Fig. 16; O'Brien, 1986; Mahoney, 1992, 1993; Schiarizza and Riddell, 1997; Schiarizza et al., 1997). The Ladner Group was previously assigned to the basal part of the Methow trough (O'Brien, 1986) or Methow terrane (Wheeler et al., 1991), but is here included in Cadwallader terrane, as suggested by Schiarizza and Riddell (1997), based on its correlation with the Nemaia Formation. Overlying Upper Jurassic and Cretaceous siliciclastic sedimentary rocks are included in the Tyaughton-Methow basin, which overlaps Cadwallader and Bridge River terranes (Umhoefer et al., 2002).

The Wineglass assemblage, first included in Cadwallader terrane by Read et al. (1995), is a Late Permian component of the terrane that has not been widely recognized. It is included in Cadwallader terrane because it rests stratigraphically beneath Mesozoic rocks

that are correlated with the Tyaughton Formation and Ladner Group. Corroboration of a stratigraphic relationship between Triassic rocks of Cadwallader terrane and an older, Late Permian arc assemblage comes from the large belt of Cadwallader terrane rocks in the Chilko Lake – Tatla Lake area. Within this belt, an altered tonalite pluton exposed on the east shore of Tatlayoko Lake is nonconformably overlain (contact exposed and described by Schiarizza et al., 1995) by fossiliferous Upper Triassic rocks of the Tyaughton Formation, which in turn are apparently overlain (contact not exposed) by Lower Jurassic rocks of the Nemaia Formation (Tipper, 1969; Schiarizza et al., 2002). The tonalite body beneath the unconformity has yielded a U-Pb zircon age of 253.8 ± 1.4 Ma (Friedman and Schiarizza, 1999; Schiarizza et al., 2002), virtually identical to the age for the Wineglass pluton reported by Read (1993).

In summary, Cadwallader terrane, as used in this report, includes a Late Permian volcanic-plutonic arc complex, and an overlying Late Triassic to Middle Jurassic arc complex and related arc-derived sedimentary sequence. The Late Permian component is best represented by the Wineglass assemblage. The Mesozoic component includes the traditional units of Cadwallader terrane (Cadwallader Group, Tyaughton Formation, Last Creek Formation), Late Triassic plutons mapped around Tatlayoko Lake, and Lower to Middle Jurassic rocks previously included in Methow terrane (Ladner Group).

4.3. Other possible Kutcho-Sitlika-Wineglass correlatives in southern British Columbia

The Wineglass assemblage, and the Late Permian tonalite body that underlies the Tyaughton Formation along Tatlayoko Lake, show that Kutcho-correlative rocks are basement to Triassic-Jurassic rocks of Cadwallader terrane. Three additional occurrences of Late Permian or Early-Middle Triassic rocks that might correlate with the Kutcho-Wineglass assemblage are briefly described here. At least two of these are reasonably included in Cadwallader terrane.

4.3.1. Mount Lytton complex

The Mount Lytton complex is a belt of mainly plutonic rocks, 70 km long and up to 20 km wide, that is exposed on the east side of the Fraser River near the town of Lytton (Fig. 16). It includes granodioritic to dioritic plutonic rocks, as well as screens of layered quartzofeldspathic rock and amphibolite and, in the southern part of the complex, screens of carbonate (Monger and McMillan, 1989; Monger, 1989). External contacts are mainly faults, but locally the complex is unconformably overlain by mid-Cretaceous volcanic rocks of the Spences Bridge Group, or intruded by Jura-Cretaceous rocks of the Eagle Plutonic complex. Tonalite from the northern part of the complex yielded a U-Pb zircon age of 250 ± 5 Ma (Friedman and van der Heyden, 1992), quartzofeldspathic gneiss farther south was assigned a U-Pb zircon age of 225 ± 5 Ma (Parrish and Monger, 1992), and granodiorite from the east-central

margin of the complex yielded a U-Pb zircon age of 212 ± 1 Ma (Parrish and Monger, 1992). The Late Permian age from the northern part of the Mount Lytton complex prompted Friedman and van der Heyden (1992) to speculate that it correlated with the Wineglass pluton. The Late Triassic ages presented by Parrish and Monger (1992) are within the range (231-207 Ma) obtained from plutonic rocks of Cadwallader terrane near Tatlayoko Lake (Friedman and Schiarizza, 1999; Schiarizza et al., 2002). It may be that the Mount Lytton complex is an uplifted belt exposing relatively deep levels of Cadwallader terrane, including plutonic rocks related to both the Late Permian and Late Triassic arc systems.

4.3.2. Spider Peak Formation

The Spider Peak Formation is a basalt unit that crops out locally in the Coquihalla River area, northeast of Hope (Figs. 16, 17). The base of the unit is a system of faults, related to the Hozameen fault system, and the upper contact is an unconformity with overlying Lower to Middle Jurassic rocks of the Ladner Group (O'Brien, 1986; Monger, 1989; Ray, 1990). The Spider Peak Formation consists of mainly low-potassium tholeiitic basalts, but also includes gabbro and minor amounts of tuff, argillite, volcanic sandstone, and tuffaceous conglomerate that contains quartz grains and felsic volcanic fragments (Ray, 1990). The formation is undated, but Ray (1990) noted that angular chert fragments in conglomerate directly above the unconformity, with conodonts of probable Early Triassic age, might have been derived from interpillow chert breccias of the Spider Peak Formation. Although an Early Triassic age is unproven, the presence of quartz and felsic volcanic-bearing clastic rocks within the basalt, and the unconformable relationship with overlying Ladner Group, invite speculation that the Spider Peak Formation might be related to the Kutcho-Wineglass assemblage.

4.3.3. Venables Valley belt

The Venables Valley belt is a narrow fault-bounded panel of felsic to mafic volcanic and volcanoclastic rocks and associated tonalitic and dioritic intrusions, that is exposed west and south of the town of Cache Creek (Fig. 16). These rocks were assigned mainly to the western belt of the Upper Triassic Nicola Group (Quesnel terrane) by Grette (1978), Ladd (1978) and Monger and McMillan (1989). However, the belt was later correlated with the Kutcho and Sitlika assemblages on the basis of comparable low-potassium tholeiitic geochemistry, primitive Nd isotopic signatures, and an Early to Middle Triassic U-Pb zircon age of 242 ± 2 Ma on a tonalite intrusion (Childe et al., 1997, 1998). This correlation is compelling, but the structural position of the belt, near the eastern edge of Cache Creek terrane, is difficult to reconcile with the structural position of the Kutcho, Sitlika and Wineglass assemblages, which are structurally beneath the western edge of Cache Creek terrane.

4.4. Correlation of Cadwallader and Wallowa terranes

Paleozoic-Mesozoic rocks in the Blue Mountains region of northeastern Oregon and west-central Idaho comprise an inlier that is isolated from terranes to the north and southwest by younger cover, including the Columbia River basalts. These rocks are assigned to three major terranes: Olds Ferry, Baker and Wallowa (Fig. 18). There seems to be general agreement that Olds Ferry and Baker terranes correlate with Quesnel and Cache Creek terranes, respectively, of the Canadian Cordillera (Mortimer, 1986; Monger and Nokleberg, 1996). Correlations for Wallowa terrane are more controversial. It is most commonly correlated with either Wrangellia (Jones et al., 1977; Wernicke and Klepacki, 1988; Kurz et al., 2012) or Stikine terrane (Mortimer, 1986), but has also been correlated with Cadwallader terrane (Umhoefer, 1990; Monger and Nokleberg, 1996).

Wallowa terrane consists of two main components: a Permian submarine intra-oceanic arc complex, and a younger Late Triassic-Middle Jurassic assemblage of arc volcanic and plutonic rocks and arc-related sedimentary rocks (Follo, 1992, 1994; Kays et al., 2006; Kurz et al., 2012). The older component of the terrane has yielded U-Pb crystallization ages on plutonic rocks that overlap those of the Kutcho-Sitlika-Wineglass assemblages (Walker, 1995; Kurz et al., 2012), and hosts Cu-Zn-Ag massive sulphide prospects that resemble the Kutcho Creek deposit of northern British Columbia (Fifarek, 1994).

Previous correlations between Cadwallader and Wallowa terranes (Umhoefer, 1990; Monger and Nokleberg, 1996) have been based on a marked similarity of the Mesozoic rocks in the two terranes, including Middle to Upper Triassic predominantly mafic arc volcanic rocks, Late Triassic arc plutonic rocks, Upper Triassic limestone and arc-derived siliciclastic sedimentary rocks, and Lower to Middle Jurassic siliciclastic sedimentary rocks (Rusmore, 1987; Umhoefer, 1990; Schiarizza et al., 2002; Follo, 1992, 1994; Kays et al., 2006; Kurz et al., 2012). The expanded definition of Cadwallader terrane presented herein strengthens this correlation by including a Late Permian-Early Triassic intra-oceanic arc assemblage, which is markedly similar to the Permian rocks of Wallowa terrane. This correlation is consistent with the spatial relationship of Cadwallader and Wallowa terranes to Cache Creek-Baker and Quesnel-Olds Ferry terranes (Fig. 18), particularly when it is noted that terranes of the Blue Mountains region attain a more north-south orientation when 65° or more post-Early Cretaceous clockwise rotation is restored (Kay et al., 2006; Wilson and Cox, 1980).

5. Conclusions

In the lower Chilcotin River area, the Wineglass assemblage (new name) and unconformably overlying sedimentary rocks are exposed in a structural window enclosed by overthrust rocks of Cache Creek terrane. The

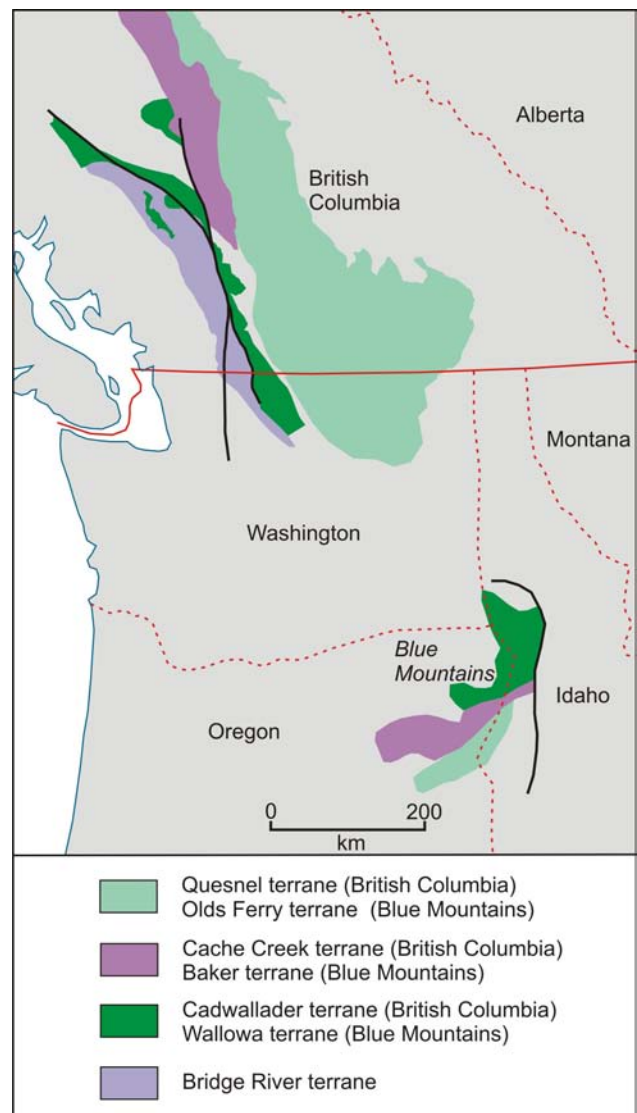


Fig. 18. Map of southern British Columbia and the adjacent United States, showing the distribution of Cadwallader, Wallowa and associated terranes.

Wineglass assemblage comprises Late Permian volcanic rocks cut by a Late Permian tonalitic pluton. The volcanic rocks are subdivided into a lower unit of predominantly basalt, and an upper unit of rhyolite, basalt, and volcaniclastic rocks. The Wineglass assemblage is unconformably overlain by Upper Triassic(?) and Lower Jurassic siliciclastic rocks that are correlated with the Tyaughton Formation and Ladner Group of Cadwallader terrane.

The Wineglass assemblage is correlated with the Kutcho assemblage of northern British Columbia, and its offset counterpart, the Sitlika volcanic unit, of central British Columbia. The correlation is based on a striking similarity of all lithologic components, overlapping U-Pb zircon ages, similar unconformable relationships with overlying Triassic-Jurassic sedimentary successions, and similar structural relationships to overthrust Cache Creek terrane.

The unconformable stratigraphic relationship between the Wineglass assemblage and Mesozoic clastic sedimentary rocks of Cadwallader terrane indicates that the Late Permian rocks of the Wineglass assemblage are part of Cadwallader terrane, as suggested by Read et al. (1995). Late Permian tonalite that nonconformably underlies Upper Triassic and Lower Jurassic rocks of Cadwallader terrane along Tatlayoko Lake (Schiarizza et al., 2002) confirms this relationship, and suggests that this older component of Cadwallader terrane may be widespread. Late Permian granitic rocks documented within the northern part of the Mt. Lytton complex may also correlate with plutonic rocks of the Wineglass assemblage, as suggested by Friedman and van der Heyden (1992), and Late Triassic granodiorite that forms part of the Mt. Lytton complex may correlate with Late Triassic plutons that form a prominent component of Cadwallader terrane near Tatlayoko Lake.

Upper Triassic and Jurassic rocks of Cadwallader terrane are similar to age-equivalent rocks of Wallowa terrane, exposed in the Blue Mountains area of eastern Oregon and adjacent Idaho and Washington states (Umhoefer, 1990; Monger and Nokleberg, 1996), although Wallowa terrane has more commonly been correlated with either Wrangellia or Stikine terranes. Wallowa terrane includes both a Late Triassic – Early Jurassic arc sequence, and a Permian arc sequence of bimodal volcanic and associated plutonic rocks. The Wineglass assemblage shows a strong resemblance to the Permian component of Wallowa terrane, and expanding the definition of Cadwallader terrane to include the Wineglass assemblage and correlatives strengthens the case for a Cadwallader – Wallowa correlation.

Acknowledgments

I thank Robin Chu for his capable assistance and good company during fieldwork. Peter Read established the basic geology of the lower Chilcotin River area, and recognized many of the implications discussed in this report. I thank Jim Monger for many discussions, spanning more than two decades, and in particular for pointing out the similarities between Cadwallader and Wallowa terranes. Lawrence Aspler and Jim Logan reviewed the paper and offered suggestions that improved it.

References cited

- Benvenuto, G., and Bailey, D.G., 1990. Geochemical rock sampling of gossanous intrusives on the Too Good 2 Be True claims, Chilcotin River area, British Columbia. British Columbia Ministry of Energy, Mines and Petroleum Resources, British Columbia Geological Survey Assessment Report 19847, 22 p.
- Childe, F.C., and Schiarizza, P., 1997. U-Pb geochronology, geochemistry and Nd isotopic systematics of the Sitlika assemblage, central British Columbia. In: Geological Fieldwork 1996, British Columbia Ministry of Energy, Mines and Petroleum Resources, British Columbia Geological Survey Paper 1997-1, pp. 69-77.
- Childe, F.C., and Thompson, J.F.H., 1997. Geological setting, U-Pb geochronology, and radiogenic isotopic characteristics of the Permo-Triassic Kutcho assemblage, north-central British Columbia. Canadian Journal of Earth Sciences, 34, 1310-1324.
- Childe, F.C., Friedman, R.M., Mortensen, J.K., and Thompson, J.F.H., 1997. Evidence for Early Triassic felsic magmatism in the Ashcroft (921) map area, British Columbia. In: Geological Fieldwork 1996, British Columbia Ministry of Employment and Investment, British Columbia Geological Survey Paper 1997-1, pp. 117-123.
- Childe, F.C., Thompson, J.F.H., Mortensen, J.K., Friedman, R.M., Schiarizza, P., Bellefontaine, K., and Marr, J.M., 1998. Primitive Permo-Triassic volcanism in the Canadian Cordillera: Tectonic and metallogenic implications. Economic Geology, 93, 224-231.
- Cordey, F., and Read, P.B., 1992. Permian and Triassic radiolarian ages from the Cache Creek Complex, Dog Creek and Alkali Lake areas, southwestern British Columbia. In: Current Research, Part E, Geological Survey of Canada Paper 92-1E, pp. 41-51.
- Cordey, F., and Schiarizza, P., 1993. Long-lived Panthalassic remnant: The Bridge River accretionary complex, Canadian Cordillera. Geology, 21, 263-266.
- English, J.M., Johannson, G.G., Johnston, S.T., Mihalynuk, M.G., Fowler, M., and Wight, K.L., 2005. Structure, stratigraphy and petroleum resource potential of the central Whitehorse Trough, northern Canadian Cordillera. Bulletin of Canadian Petroleum Geology, 53, 130-153.
- Fifarek, R.H., Juhas, A.P., and Field, C.W., 1994. Geology, mineralization, and alteration of the Red Ledge volcanogenic massive sulphide deposit, western Idaho. In: Vallier, T.L., Brooks, H.C. (Eds.), Geology of the Blue Mountains Region of Oregon, Idaho and Washington: Stratigraphy, Physiography, and Mineral Resources of the Blue Mountains Region, U.S. Geological Survey Professional Paper 1439, pp. 113-150.
- Follo, M.F., 1992. Conglomerates as clues to the sedimentary and tectonic evolution of a suspect terrane: Wallowa Mountains, Oregon. Geological Society of America Bulletin, 104, 1561-1576.
- Follo, M.F., 1994. Sedimentology and stratigraphy of the Martin Bridge limestone and Hurwal Formation (Upper Triassic to Lower Jurassic) from the Wallowa terrane, Oregon. In: Vallier, T.L., Brooks, H.C. (Eds.), Geology of the Blue Mountains Region of Oregon, Idaho and Washington: Stratigraphy, Physiography, and Mineral Resources of the Blue Mountains Region, U.S. Geological Survey Professional Paper 1439, pp. 1-27.
- Friedman, R.M., and Schiarizza, P., 1999. Permian and Triassic intrusions and volcanics in southwestern British Columbia: Implications for tectonic setting and terrane correlations. Geological Society of America, Cordilleran Section, Abstracts with Programs, 31 (6), A-55.
- Friedman, R.M., and van der Heyden, P., 1992. Late Permian U-Pb dates for the Farwell and northern Mt. Lytton plutonic bodies, Intermontane Belt, British Columbia. In: Current Research, Part A, Geological Survey of Canada Paper 92-1A, pp. 137-144.

- Grette, J.F., 1978. Cache Creek and Nicola groups near Ashcroft, British Columbia. M.Sc. thesis, The University of British Columbia, 88 p.
- Hickson, C.J., 1990. A new Frontier Geoscience Project: Chilcotin-Nechako region, central British Columbia. In: Current Research, Part F, Geological Survey of Canada Paper 90-1F, 115-120.
- Johansson, G.G., Smith, P.L., and Gordey, S.P., 1997. Early Jurassic evolution of the northern Stikinian arc: evidence from the Laberge Group, northwestern British Columbia. *Canadian Journal of Earth Sciences*, 34, 1030-1057.
- Jones, D.L., Silberling, N.J., and Hillhouse, J., 1977. Wrangellia – A displaced terrane in northwestern North America. *Canadian Journal of Earth Sciences*, 14, 2565-2577.
- Kays, M.A., Stimac, J.P., and Goebel, P.M., 2006. Permian-Jurassic growth and amalgamation of the Wallowa composite terrane, northeastern Oregon. In: Snoko, A.W., Barnes, C.G. (Eds.), *Geological Studies in the Klamath Mountains Province, California and Oregon: A Volume in Honor of William P. Irwin*, Geological Society of America Special Paper 410, pp. 465-494.
- Kurz, G.A., Schmitz, M.D., Northrup, C.J., and Vallier, T.L., 2012. U-Pb geochronology and geochemistry of intrusive rocks from the Cougar Creek Complex, Wallowa arc terrane, Blue Mountains Province, Oregon-Idaho. *Geological Society of America Bulletin*, 124, 578-595.
- Ladd, J.H., 1978. Cache Creek – Nicola contact, Ashcroft area (92I/11W). In: *Geological Fieldwork 1977*, British Columbia Ministry of Mines and Petroleum Resources, British Columbia Geological Survey Paper 1978-1, pp. 89-95.
- Mahoney, J.B., 1992. Middle Jurassic stratigraphy of the Lillooet area, south-central British Columbia. In: Current Research, Part A, Geological Survey of Canada Paper 92-1A, 243-248.
- Mahoney, J.B., 1993. Facies reconstructions in the Lower to Middle Jurassic Ladner Group, southern British Columbia. In: Current Research, Part A, Geological Survey of Canada Paper 93-1A, pp. 173-182.
- Massey, N.W.D., MacIntyre, D.G., Desjardins, P.J., and Cooney, R.T., 2005. Digital geology map of British Columbia: whole province. British Columbia Ministry of Energy, Mines and Petroleum Resources, British Columbia Geological Survey GeoFile 2005-1.
- Mihalynuk, M.G., and Harker, L.L., 2007. Riske Creek Geology (92O/16W). British Columbia Ministry of Energy, Mines and Petroleum Resources, British Columbia Geological Survey Open File 2007-6; scale 1:50 000.
- Monger, J.W.H., 1989. Geology, Hope, British Columbia (92H). Geological Survey of Canada, Map 41-1989, sheet 1; scale 1:250 000.
- Monger, J.W.H., and McMillan, W.J., 1989. Geology, Ashcroft, British Columbia (92I). Geological Survey of Canada, Map 42-1989, sheet 1; scale 1:250 000.
- Monger, J.W.H., and Nokleberg, W.J., 1996. Evolution of the northern North American Cordillera: generation, fragmentation, displacement and accretion of successive North American plate-margin arcs. In: Coyner, A.R., Fahey, P.L. (Eds.), *Geology and Ore Deposits of the American Cordillera*, Geological Society of Nevada Symposium Proceedings, V III, pp. 1133-1152.
- Mortimer, N., 1986. Late Triassic arc-related potassic igneous rocks in the North American Cordillera. *Geology*, 14, 1035-1038.
- Morton, J.W., 1984. A geochemical soil survey and accompanying electromagnetic survey, Dry Farm, Dry Farm 2, D.F. 1 claims. British Columbia Ministry of Energy, Mines and Petroleum Resources, British Columbia Geological Survey Assessment Report 12350, 37 p.
- O'Brien, J., 1986. Jurassic stratigraphy of the Methow Trough, southwestern British Columbia. In: Current Research, Part B, Geological Survey of Canada Paper 86-1B, pp. 749-756.
- Parrish, R.R., and Monger, J.W.H., 1992. New U-Pb dates from southwestern British Columbia. In: *Radiogenic Age and Isotopic Studies; Report 5*, Geological Survey of Canada Paper 91-2, 87-107.
- Ray, G.E., 1990. The geology and mineralization of the Coquihalla gold belt and Hozameen fault system, southwestern British Columbia. British Columbia Ministry of Energy, Mines and Petroleum Resources, British Columbia Geological Survey Bulletin 79, 97 p.
- Read, P.B., 1992. Geology of parts of Riske Creek and Alkali Lake areas, British Columbia. In Current Research, Part A, Geological Survey of Canada Paper 92-1A, pp. 105-112.
- Read, P.B., 1993. Geology of northeast Taseko Lakes map area, southwestern British Columbia. In: Current Research, Part A, Geological Survey of Canada Paper 93-1A, pp. 159-166.
- Read, P.B., Cordey, F., and Orchard, M.J., 1995. Stratigraphy and relationship of the Cache Creek and Cadwallader terranes, south-central B.C. Geological Association of Canada/Mineralogical Association of Canada, Annual Meeting, Victoria, 1995, Program and Abstracts, A-88.
- Riddell, J., Schiarizza, P., Gaba, R.G., Caira, N., and Findlay, A., 1993. Geology and mineral occurrences of the Mount Tatlow map area (92O/5, 6, and 12). In: *Geological Fieldwork 1992*, British Columbia Ministry of Energy, Mines and Petroleum Resources, British Columbia Geological Survey Paper 1993-1, pp. 37-52.
- Rusmore, M.E., 1987. Geology of the Cadwallader Group and the Intermontane-Insular superterrane boundary, southwestern British Columbia. *Canadian Journal of Earth Sciences*, 24, 2279-2291.
- Rusmore, M.E., and Woodsworth, G.J., 1991. Distribution and tectonic significance of Upper Triassic terranes in the eastern Coast Mountains and adjacent Intermontane Belt, British Columbia. *Canadian Journal of Earth Sciences*, 28, 532-541.
- Rusmore, M.E., Potter, C.J., and Umhoefer, P.J., 1988. Middle Jurassic terrane accretion along the western edge of the Intermontane superterrane, southwestern British Columbia. *Geology*, 16, 891-894.
- Schiarizza, P., 2011. Geology of the Kutcho assemblage between Kutcho Creek and the Tucho River, northern British Columbia (NTS 104I/01). In: *Geological Fieldwork 2010*, British Columbia Ministry of Energy and Mines, British Columbia Geological Survey Paper 2011-1, 99-117.
- Schiarizza, P., 2012a. Geology of the Kutcho assemblage between the Kehlechoa and Tucho rivers, northern British Columbia (NTS 104I/01, 02). In: *Geological*

- Fieldwork 2011, British Columbia Ministry of Energy and Mines, British Columbia Geological Survey Paper 2012-1, pp. 75-98.
- Schiarizza, P., 2012b. Bedrock geology of the upper Kutcho Creek area, parts of NTS 104I/01, 02. British Columbia Ministry of Energy and Mines, British Columbia Geological Survey Open File 2012-08, and Geological Survey of Canada, Open File 7234; scale 1:40 000.
- Schiarizza, P., and Massey, N.W.D., 2010. Geochemistry of volcanic and plutonic rocks of the Sitlika assemblage, Takla Lake area, central British Columbia (NTS 093N/04, 05, 12, 13). In: Geological Fieldwork 2009, British Columbia Ministry of Energy, Mines and Petroleum Resources, British Columbia Geological Survey Paper 2010-1, pp. 55-67.
- Schiarizza, P., and Payie, G., 1997. Geology of the Sitlika assemblage in the Kenny Creek - Mount Olson area (93N/12, 13), central British Columbia. In: Geological Fieldwork 1996, British Columbia Ministry of Employment and Investment, British Columbia Geological Survey Paper 1997-1, pp. 79-100.
- Schiarizza, P., and Riddell, J., 1997. Geology of the Tatlayoko Lake - Beece Creek Area (92N/8, 9, 10; 92O/5, 6, 12). In: Diakow, L.J., Newell, J.M. (Eds.), Interior Plateau Geoscience Project: Summary of geological, geochemical and geophysical studies, British Columbia Ministry of Employment and Investment, British Columbia Geological Survey Paper 1997-2, pp. 63-101.
- Schiarizza, P., Melville, D.M., Riddell, J., Jennings, B.K., Umhoefer, P.J., and Robinson, M.J., 1995. Geology and mineral occurrences of the Tatlayoko Lake map area (92N/8, 9 and 10). In: Geological Fieldwork 1994, British Columbia Ministry of Energy, Mines and Petroleum Resources, British Columbia Geological Survey Paper 1995-1, pp. 297-320.
- Schiarizza, P., Gaba, R.G., Glover, J.K., Garver, J.I., and Umhoefer, P.J., 1997. Geology and mineral occurrences of the Taseko - Bridge River area. British Columbia Ministry of Employment and Investment, British Columbia Geological Survey Bulletin 100, 291 p.
- Schiarizza, P., Riddell, J., Gaba, R.G., Melville, D.M., Umhoefer, P.J., Robinson, M.J., Jennings, B.K., and Hick, D., 2002. Geology of the Beece Creek - Niut Mountain area, British Columbia (NTS 92N/8, 9, 10; 92O/5, 6, 12). British Columbia Ministry of Energy and Mines, British Columbia Geological Survey Geoscience Map 2002-3; scale 1:100 000.
- Struik, L.C., Schiarizza, P., Orchard, M.J., Cordey, F., Sano, H., MacIntyre, D.G., Lapierre, H., and Tardy, M., 2001. Imbricate architecture of the upper Paleozoic to Jurassic oceanic Cache Creek Terrane, central British Columbia. *Canadian Journal of Earth Sciences*, 38, 495-514.
- Struik, L.C., MacIntyre, D.G., and Williams, S.P., 2007. Nechako NATMAP project: a digital suite of geoscience information for central British Columbia (NTS map sheets 093N, 093K, 093F, 093G/W, 093L/9, 16, and 093M/1, 2, 7, 8). British Columbia Ministry of Energy, Mines and Petroleum Resources, British Columbia Geological Survey Open File 2007-10, and Geological Survey of Canada Open File 5623.
- Tipper, H.W., 1969. Mesozoic and Cenozoic geology of the northeastern part of Mount Waddington map area (92N), Coast district, British Columbia. Geological Survey of Canada Paper 68-33.
- Tipper, H.W., 1978. Taseko Lakes (92O) map area. Geological Survey of Canada Open File 534; scale 1:125 000.
- Thorstad, L.E., and Gabrielse, H., 1986. The Upper Triassic Kutcho Formation, Cassiar Mountains, north-central British Columbia. Geological Survey of Canada Paper 86-16, 53 p.
- Umhoefer, P.J. (1990): Stratigraphy and tectonic setting of the upper part of the Cadwallader terrane, southwestern British Columbia. *Canadian Journal of Earth Sciences*, 27, 702-711.
- Umhoefer, P.J., and Schiarizza, P., 1996. Latest Cretaceous to Early Tertiary dextral strike-slip faulting on the southeastern Yalakom fault system, southeastern Coast Belt, British Columbia. *Geological Society of America Bulletin*, 108, 768-785.
- Umhoefer, P.J., Schiarizza, P., and Robinson, M., 2002. Relay Mountain Group, Tyaughton-Methow basin, southwest British Columbia: a major Middle Jurassic to Early Cretaceous terrane overlap assemblage. *Canadian Journal of Earth Sciences*, 39, 1143-1167.
- Walker, N.W., 1995. Tectonic implications of U-Pb zircon ages of the Canyon Mountain Complex, Sparta Complex, and related metaplutonic rocks of the Baker terrane, northeastern Oregon. In: Vallier, T.L., Brooks, H.C. (Eds.), *Geology of the Blue Mountains Region of Oregon, Idaho and Washington: Petrology and Tectonic Evolution of pre-Tertiary rocks of the Blue Mountains Region*, U.S. Geological Survey Professional Paper 1438, pp. 247-269.
- Wernicke, B., and Klepacki, D.W., 1988. Escape hypothesis for the Stikine block. *Geology*, 16, 461-464.
- Wheeler, J.O., Brookfield, A.J., Gabrielse, H., Monger, J.W.H., Tipper, H.W., and Woodsworth, G.J., 1991. Terrane map of the Canadian Cordillera. Geological Survey of Canada Map 1713A; scale 1:2 000 000.
- Wilson, D., and Cox, A., 1980. Paleomagnetic evidence for tectonic rotation of Jurassic plutons in the Blue Mountains, eastern Oregon. *Journal of Geophysical Research*, 85, 3681-3689.

Bonaparte gold: another 195 Ma porphyry Au-Cu deposit in southern British Columbia?

James M. Logan^{1,a} and Mitchell G. Mihalynuk¹

¹ British Columbia Geological Survey, Ministry of Energy, Mines and Natural Gas, Victoria, BC, V8W 9N3

^a corresponding author: Jim.Logan@gov.bc.ca

Recommended citation: Logan, J.M and Mihalynuk, M.G., 2013. Bonaparte gold: another 195 Ma porphyry Au-Cu deposit in southern British Columbia? In: Geological Fieldwork 2012, British Columbia Ministry of Energy, Mines and Natural Gas, British Columbia Geological Survey Paper 2013-1, pp. 71-80.

Abstract

An erosional window in the Miocene Chilcotin Group basalt blanket exposes deformed Early Jurassic (?) porphyritic quartz diorite and monzodiorite on the Bonaparte Plateau, 38 km north of Kamloops. These plutonic rocks host Au-Cu quartz veins and reported W-Mo quartz stockworks at the Bonaparte mine. Intrusion and mineralization appear to have coincided temporally and spatially with motion along a greenschist-grade, north-trending reverse (east-side-up) shear zone. Shear strain, characterized by mylonitic fabrics, a prominent down-dip lineation, and local kinematic indicators (sigma and delta porphyroclasts, displaced broken grains) culminated with a later phase of extensive hydrothermal quartz and quartz-carbonate veins, and stockworks. Auriferous veins form at least eight separate, metre to cm-wide, north-trending zones. Two bulk samples (3700 tonnes in 1994 and 364 tonnes in 2009) of mineralized quartz veins from the Bonaparte have produced ~103 kg of gold or 25.58 g/t Au from the total 4064 tonnes shipped. Biotite, sericite- and carbonate-alteration of the intrusions adjacent to the vein structures is accompanied by disseminated pyrite, chalcopyrite and arsenopyrite ± molybdenite, and gold mineralization. Historically, exploration at Bonaparte has focussed on quartz vein networks. Yet the Bonaparte intrusions align with a north-trending belt of Early Jurassic porphyry deposits in the Takomane-Wildhorse magmatic belt, some of which have similar metal and alteration assemblages. We speculate that the Bonaparte deposit represents an upper level of a buried porphyry system.

Keywords: Calcalkaline diorite porphyries, gold quartz veins, chalcopyrite, quartz stockwork, potassic, synkinematic alteration and mineralization

1. Introduction

The eastward migration of Mesozoic arc magmatism in southern Quesnellia (Fig. 1) led to the growth of three temporally distinct, north-trending, plutonic belts (from west to east): Late Triassic; Late Triassic-Early Jurassic; and Early Jurassic (Fig. 2). Three porphyry copper mineralization events are directly linked to each of these calcalkaline-alkaline magmatic episodes. The youngest, easternmost train of granodiorite plutons (Wildhorse-Takomkane suite) defines a 375 km long arcuate belt that is prospective for Cu-Mo±Au mineralization (Logan et al., 2011) and hosts porphyry copper-molybdenum-gold deposits such as the past producing Brenda mine (Cu-Mo) and the recently discovered Woodjam prospect (Cu-Mo, Au). In the central part of this belt, ~38 km northeast of Kamloops and between the Brenda and Woodjam deposits (Fig. 2), is the Bonaparte Au property of WestKam Resources (Fig. 3; MINFILE 092P 050).

Reported mineralization at Bonaparte includes intrusion-hosted Au-Cu quartz veins and W-Mo quartz stockworks. This mineralization is in a dioritic intrusive complex near contacts with hornfelsed and skarned sedimentary rocks of the Paleozoic Harper Ranch Group (Peatfield, 1986; Durfeld, 1980). Although the age of plutonism is unknown, the Bonaparte intrusive complex is assumed to be Early Jurassic, based on its position in the



Fig. 1. Location of the Bonaparte gold property (red), shown straddling the NTS boundary between 92I and 92P map sheets (black), near the eastern edge of Quesnel terrane shown as a transparent green overlay on the coloured topographic map of British Columbia.

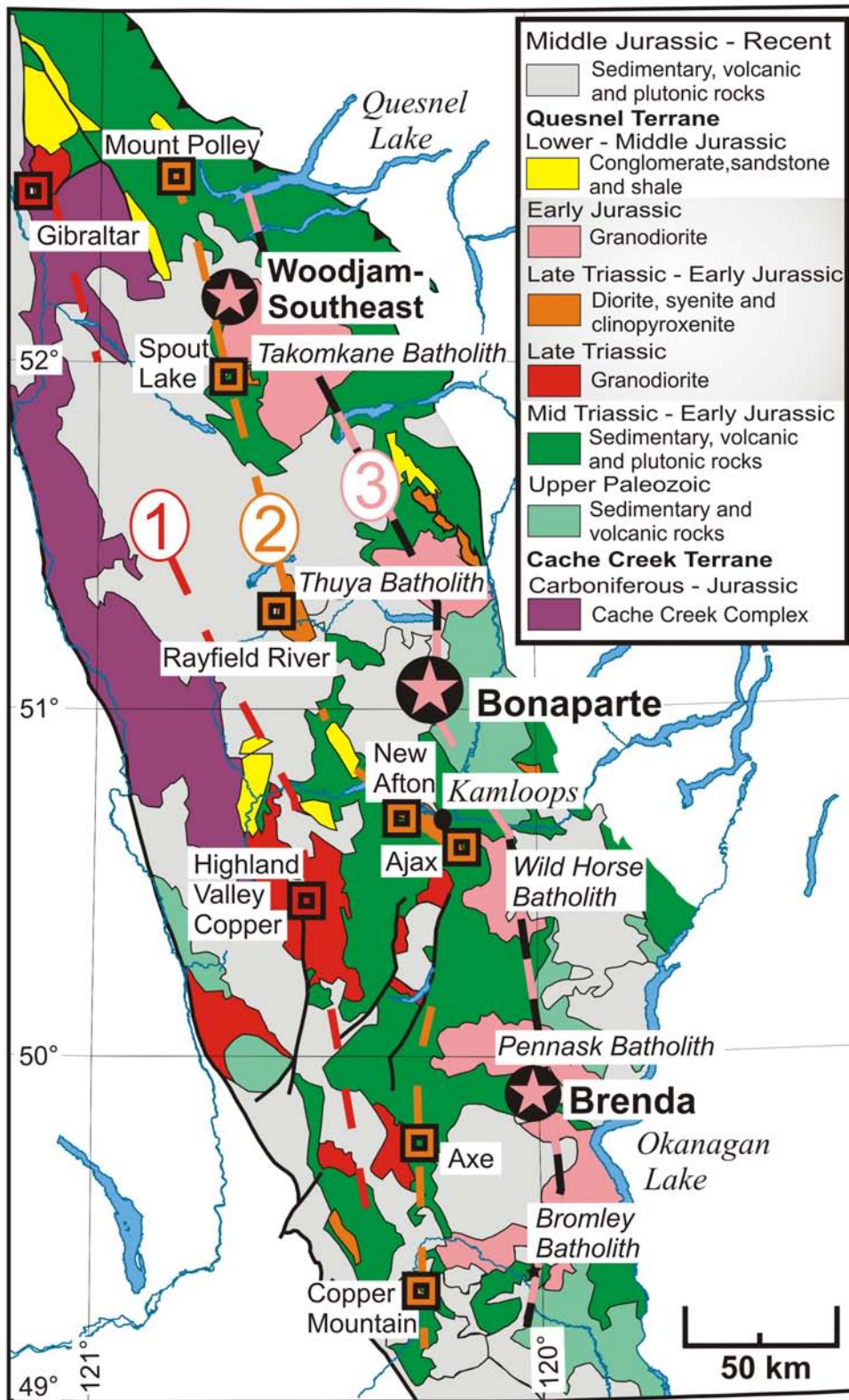


Fig. 2. Generalized geology of southern Quesnellia and Cu-Mo±Au deposits. Mesozoic arc plutons align along the length of southern Quesnellia to define three, north-trending, temporally distinct belts that get younger to the east: 1) Late Triassic; 2) Late Triassic – Early Jurassic; and 3) Early Jurassic. Discrete porphyry copper mineralizing events are directly linked to each of these magmatic episodes. The Bonaparte deposit lies in the tract of Early Jurassic plutons (Wildhorse-Takomkane plutonic suite), midway between the Brenda and Woodjam-Southeast deposits (modified after Massey et al., 2005).

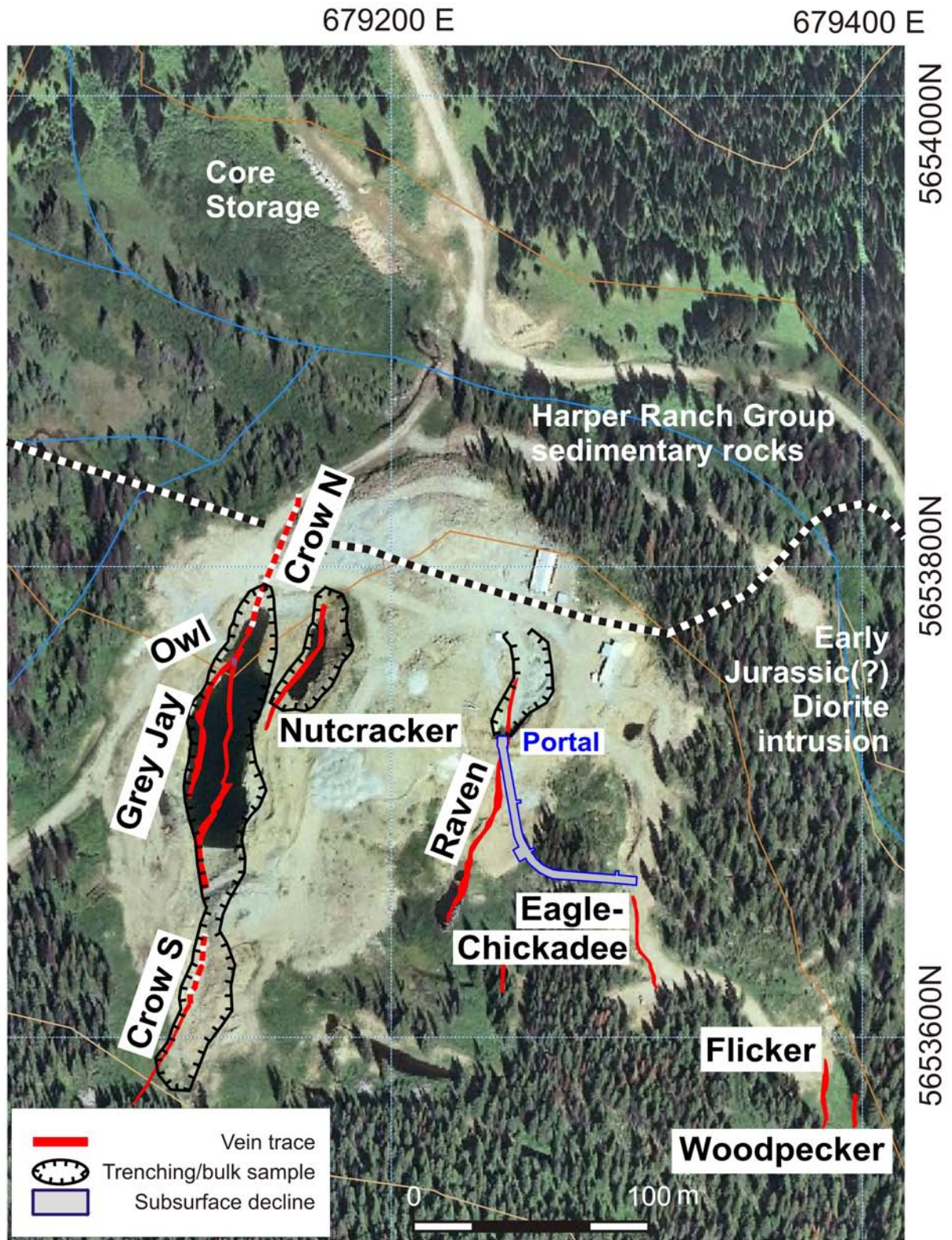


Fig. 3. Location of the main quartz veins at the “Discovery Zone” on the Bonaparte developed prospect showing surface trenches, bulk sample locations, and the surface projection of the decline (after Beaton, 2011). The dashed line indicates the approximate contact between the dioritic intrusive complex and hornfelsed sedimentary country rocks of the Harper Ranch Group.

Wildhorse-Takomkane magmatic belt (Breitsprecher et al., 2010). To test this correlation, we collected samples of quartz diorite and monzodiorite for U-Pb zircon geochronology, and a sample of sericite-altered intrusion associated with quartz-carbonate veins and gold mineralization to determine cooling ages using the Ar^{40} - Ar^{39} method. This work is ongoing; results will be presented as they come available.

Herein we present mapping, sampling, and petrographic data to establish the geological history of the Bonaparte property and the paragenesis of alteration and mineralization. Historically, exploration at Bonaparte has focussed on quartz vein networks. Based on similarities in metal and alteration assemblages and an assumed Early Jurassic age, we pose the question: “does this vein-related mineralization represent the upper level of a Brenda or Woodjam porphyry copper-gold deposit?”. Samples collected for isotopic age determination will provide some of the first tentative answers.

2. Access and history of development

The Bonaparte gold mine is approximately 38 km north of Kamloops, B.C., straddling map sheets 92I/16W & 92P/1W, at about $51^{\circ} 02' N$ and $128^{\circ} 28' W$ (Fig. 1). Access is by way of a 24 km-long paved road north from Kamloops and then by an additional 24.7 km-long series of well-maintained gravel logging roads (Jamieson-Wentworth Creek and Bob Lake).

The first recorded mineral exploration on the Bonaparte property was by Amoco Canadian Petroleum Company Ltd., between 1969 and 1973 (Neugebauer, 1973). Their search for molybdenum culminated in the drilling of two diamond-drill holes, which met with discouraging results. In 1984, regional geochemical sampling by Minequest Exploration Associates Ltd. revealed anomalous gold and arsenic values in stream, soil, and graphitic and siliceous sedimentary rocks. Follow-up work resulted in the discovery of auriferous quartz float (Gourlay, 1985). Drilling in 1986 confirmed in-situ gold mineralized veins hosted by diorite (Peatfield, 1986).

In 1986, the Hughes-Lang Group of companies optioned the property and carried out geological mapping, stripping, trenching, and 4674 metres of diamond drilling. They succeeded in intersecting veins with gold values (multiple grams of gold per tonne over less than meter thicknesses; Gosse, 1987; 1988) but the mineralization was highly irregular.

In 1994, Beaton Engineering purchased the property and optioned it to Claimstaker Resources Ltd. At that time a 3700 tonne bulk sample was removed from the Grey Jay and Crow veins and shipped to the Cominco smelter at Trail, B.C. It yielded ~98 kg of gold, equivalent to a grade of 26.5 g/t Au (Beaton, 2011). Additional work between 1994 and 1995 by Claimstaker Resources included 25 diamond-drill holes totalling 1185 m. The claims reverted back to Beaton Engineering in 1997, and in 1998, Orko Gold Corporation purchased the property and completed

23 diamond-drill holes totalling 1171.3 m (Livgard, 1998). Additional trenching and diamond drilling were completed by North American Gems Inc. in 2003 (Beaton, 2011).

In 2009, Encore Renaissance Resources Corp. acquired an option to purchase 60% of the property. As part of the option agreement, Encore Renaissance agreed to extract a permitted 10,000 tonne test sample, in part from a decline to be driven on the Raven vein (Fig. 3). A total of 364.61 tonnes of this vein material was shipped to Kinross Gold's mill in Washington State in September of 2009. The material, most of which was derived from surface trenching north of the decline portal, yielded ~5 kg of gold, equivalent to 16.28 g/t. Underground developments to date have produced a 3 by 3 m 15% decline that is 161 m long (Fig. 3; Beaton, 2011).

3. Regional setting

The oldest rocks at the Bonaparte property include a succession of rusty-weathering, graphitic, and siliceous sedimentary rocks of uncertain age. They have been correlated with the Carboniferous to Permian Harper Ranch Group (Massey et al., 2005) which, at this latitude, are basement to Mesozoic volcanic and sedimentary rocks of the Quesnel terrane (Fig. 2). The Harper Ranch Group rocks were hornfelsed during emplacement of a composite quartz diorite to monzodiorite porphyritic intrusion and dike complex, which is mineralized. These intrusive rocks have been correlated with the Early Jurassic Eakin Creek suite of the Late Triassic to Middle Jurassic Thuya batholith (Anderson et al., 2010; Schiarizza and Israel, 2001), which is part of the regional Early Jurassic Wildhorse-Takomkane plutonic suite of Breitsprecher et al. (2010). Harper Ranch rocks are exposed as inliers near the southeastern margin of an extensive sheet of Chilcotin Group flood basalts (Miocene) that form much of the Bonaparte Plateau.

4. Property geology

The country rock consists of dark, rusty-weathering, polydeformed argillaceous sedimentary rocks of the Harper Ranch Group. These rocks crop out north of the “Discovery Zone” (Fig. 3). At least three discrete intrusive phases cut the Harper Ranch Group rocks; all are overprinted by late hydrothermal quartz and quartz-carbonate veins. Relative ages of the intrusions are readily established from cross-cutting relationships. Brown quartz diorite is the oldest and the most intensely foliated, lineated, and altered. It is cut by the moderately to unfoliated and typically moderately to weakly altered monzodiorite. Aplitic dikes cut the monzodiorite and are unfoliated.

4.1.1. Quartz diorite

The oldest intrusive phase is mafic quartz diorite porphyry (‘dark matrix porphyry’ of Peatfield, 1986). It is coarse grained with white plagioclase, altered hornblende, and distinctive, sparse blue quartz eyes. Plagioclase crystals are stubby, euhedral, and display oscillatory zoning; crystal glomerocrysts comprise up to 25% of the

rock. Matrix minerals are fine-grained prismatic hornblende (20%), and intra-crystalline plagioclase-feldspar \pm quartz containing minor to trace biotite, apatite, titanite, magnetite and pyrite (Fig. 4a). The diorite is blocky to slabby weathering, where most intensely foliated and lineated. It is typically biotite-altered and brown, but green where least altered. Black and brown xenoliths of hornfelsed argillaceous country rock are common.

The degree of alteration is directly related to the intensity of foliation development. In weakly foliated diorite, the hornblende is replaced by patchy biotite and chlorite. In well foliated rocks, biotite \pm chlorite pseudomorph hornblende. In shear zones, hornblende has been totally replaced by fine-grained biotite-quartz-white mica-carbonate and opaque minerals that define micrometre-thick lamellae that wrap around porphyroclasts of plagioclase (Fig. 4b). In strongly foliated sections plagioclase phenocrysts are rounded and saussuritized to an assemblage of epidote + clinozoisite + white mica.

4.1.2. Monzodiorite

Holocrystalline biotite-hornblende monzodiorite to granodiorite is white to pinkish grey weathering (rusty where pyritic) and grey to greenish-grey on fresh surfaces (Fig. 4c). It is typically medium grained. Quartz comprises \sim 20% of the rock, locally as rounded quartz eyes and matrix. Up to 10% of the rock is biotite, both as euhedral books and replacements of hornblende. Hornblende and K-feldspar occur as sparse, out-sized crystals up to 1 cm long. Chloritized mafic xenoliths are common, comprising several percent of some outcrops; where less altered, the xenoliths can be recognized as having been originally composed of fine-grained hornblende and biotite.

4.1.3. Granite - aplite

Grey to tan, quartz- and plagioclase-phyric granite dikes are the youngest intrusive phase. They are unfoliated, typically less than 5 cm thick, spaced 10's of cm to 1 m apart, and cut foliation at a high angle. In hand sample, the groundmass is fine grained, and contains minor biotite, and sparse 0.5-1 mm, rounded quartz and euhedral plagioclase phenocrysts ($<$ 10%), except at chilled margins (Figs. 4d, e). Sodium cobaltinitrite staining reveals that about 40-45% of the groundmass is K-feldspar. In thin section, the aplite consists of very fine-grained ($<$ 0.2 mm) interlocking crystals of quartz and K-feldspar and rare interstitial biotite (Fig. 4d). Disseminated pyrite and chalcopyrite grains are concentrated in the monzodiorite at the contact with aplite, but apparently not within the aplite that we sectioned (Fig. 4e).

5. Structure

Paleozoic sedimentary rocks are folded and foliated; the foliation is cut by a crenulation cleavage. Intrusive rocks cut and thermally metamorphose the structures in the sedimentary rocks and are cut by shear zones.

The main workings ("Discovery Zone") occupy a north-trending, greenschist grade, mylonitic shear zone. Rocks in the shear zone display discrete, meter-wide zones with a well developed fabric that is locally accompanied by a prominent down-dip (east) lineation. The foliation is defined by biotite, quartz, white mica, and carbonate laminae. Preliminary analysis of kinematic indicators including displaced broken grains and feldspar porphyroclasts with sigma- and delta-type geometries (Fig. 4b) suggest an east side-up (reverse) sense of movement. Medial to the shear zones in the plutonic rock are north-trending, (\sim 026 $^{\circ}$) east-dipping, decimetre- to metre-thick auriferous quartz veins that continue along strike for up to 250 m (Fig. 3). Younger brittle faults and carbonate-altered quartz veins cross-cut the mylonitic fabric and attest to ongoing hydrothermal alteration and mineral deposition.

6. Alteration

Within the area of the main workings, pyritic, carbonaceous, and calcareous siltstone is locally hornfelsed to pyroxene-diopside facies in some xenoliths, although biotite hornfels is more common for the country rock surrounding the intrusion. East of the main workings, monzodiorite is altered along quartz-lined fractures to a propylitic assemblage of epidote-chlorite-magnetite-pyrite \pm actinolite. Locally, irregular patches of very fine grained biotite overprints this assemblage.

Both the quartz diorite and monzodiorite are biotite-altered, but this alteration is especially prevalent and pervasive in the older quartz diorite. Synkinematic potassic alteration is manifested as secondary biotite and orthoclase within gaps between fragments of extended plagioclase porphyroclasts or as a replacement of hornblende.

K-feldspar "pinking" and magnetite veins are conspicuously absent in the areas visited during our work, which included a cursory look at core in collapsed racks. Preliminary lithogeochemistry, thin section, and off-cut staining also indicate low potassium feldspar content for unaltered quartz diorite and quartz monzodiorite. However, positive sodium cobaltinitrite staining of the "grey" aplite suggests it may be a late potassium-rich phase, and that potassium enrichment does not necessarily impart pink colouration.

Carbonate \pm pyrite introduced along fractures and quartz vein margins has altered and bleached both quartz diorite and quartz monzodiorite. Sparry calcite fills open spaces between euhedral quartz crystals and is locally accompanied by disseminated arsenopyrite \pm gold and perhaps bismuth tellurides (Fig. 5). Probably closely following or accompanying carbonate alteration are discrete narrow zones of carbonate-quartz-pyrite and coarse well-formed books of muscovite. This last alteration type is not widespread or well endowed with sulphide mineralization, but does attest to an evolving hydrothermal system likely related to the intrusive complex.

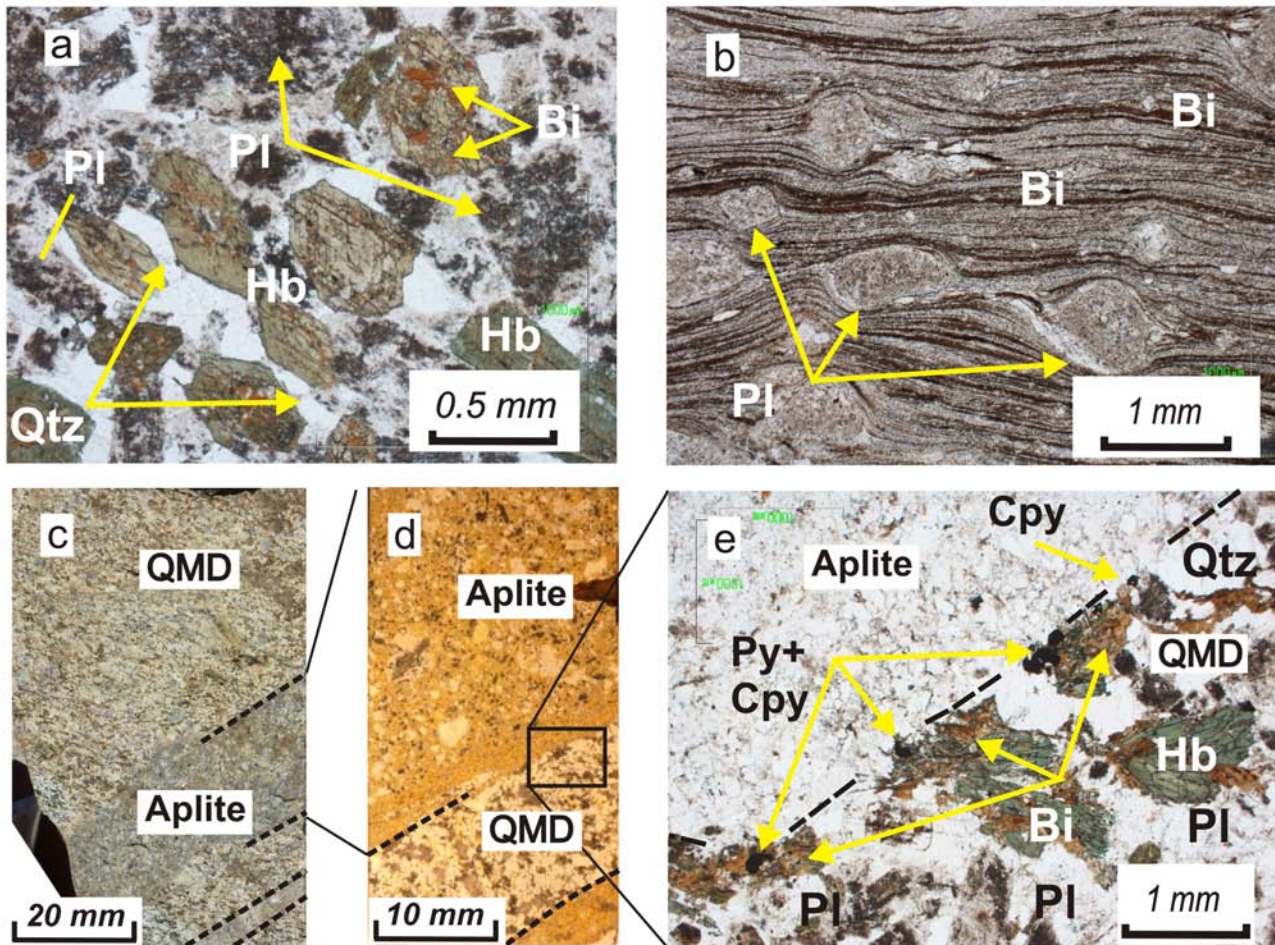


Fig. 4. “Discovery Zone” quartz diorite photomicrographs. **a)** Weakly altered (hornblende replaced by biotite) quartz diorite porphyry, plane polarized light. **b)** Mylonitic quartz diorite footwall to Owl vein displays delta- and sigma-type plagioclase porphyroclasts indicating top to the left movement (in outcrop: up-dip, westward thrust sense), plane polarized light. Mylonitic fabric is defined by laminae of biotite-quartz-sericite-carbonate and opaque minerals. View is to the north, perpendicular to foliation, and containing the mineral lineation. **c)** Thin section offcut showing quartz monzodiorite intruded by aplite. **d)** Offcut stained with sodium cobaltinitrite to highlight K-feldspar (yellow); note chilled contact of aplite. **e)** Photomicrograph in plane polarized light of contact zone between quartz monzodiorite and aplite showing biotite alteration of hornblende and concentration of pyrite and chalcopyrite (sulphides are opaque). Abbreviations: Pl, plagioclase; Hb, hornblende; Qtz, quartz; QMD, quartz monzodiorite; Py, pyrite; Cpy, chalcopyrite.

Secondary muscovite has been separated from alteration vein envelopes cutting the monzodiorite for $^{40}\text{Ar}/^{39}\text{Ar}$ isotopic analysis to determine its cooling age.

7. Mineralization

High-grade gold at the Bonaparte property has been demonstrated by bulk sampling and previously reported geochemical results (Lee, 1989; Livgard, 1998), and our petrographic analyses (Fig. 6d) and analytical results (see below). Porphyry molybdenum mineralization is reported within and adjacent to the porphyritic hornblende quartz diorite and biotite-hornblende quartz monzodiorite plug. However, drilling and surface sampling to date have returned very low molybdenum values (McClintock, 1987).

The “Discovery Area” (Fig. 3) is 300 m wide and 350 m long. It contains at least eight semi-parallel veins and areas of quartz stockwork. These have been variably

exposed at surface by past trenching or defined by drilling. The eight veins include; the Grey Jay, Owl, Crow, Nutcracker, Raven, Eagle-Chickadee, Flicker and Woodpecker. To date, 112 diamond-drill holes totalling over 6784 meters have been completed (Beaton, 2011). The drilling was almost entirely restricted to the Crow, Nutcracker and Grey Jay vein systems to a maximum depth of ~250 m. Most holes were drilled at -45° , effectively testing the intrusion only to a depth of 212 m from surface.

Gold mineralization is hosted in a series of eight north-trending, east-dipping quartz veins (Figs. 3, 6a). The veins cut biotite-altered and silicified diorite porphyry, with the possible exception of the Crow N that is shown extending north into Harper Ranch sedimentary rocks (Beaton, 2011). According to Peatfield (1986) these major veins crosscut the quartz stockwork and therefore

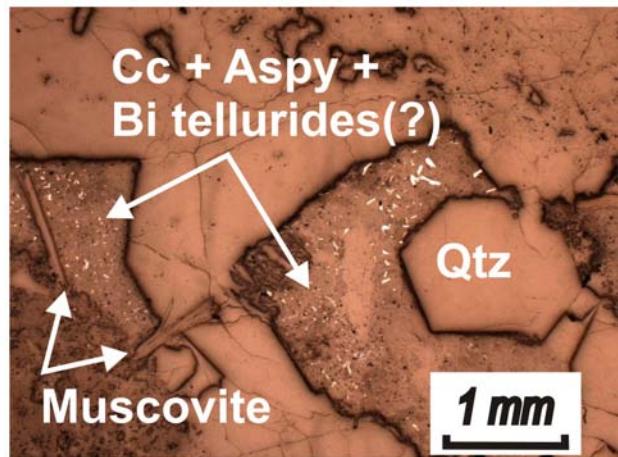


Fig. 5. Plane polarized reflected light photomicrograph of white mica in mineralized quartz-carbonate vein collected from stockpiled ore. Late stage calcite fills open spaces between euhedral quartz crystals. Fine bright white needles of arsenopyrite and possibly bismuth tellurides intergrown with calcite. Abbreviations: Qtz, quartz; Cc, calcite; Aspy, arsenopyrite; Bi, bismuth.

post-date the molybdenum mineralization. Gold grade is generally correlated with sulphide content in the veins (Leitch, 1988; Gosse, 1988); however, restriction of gold mineralization to the quartz veins has not been confirmed. Disseminated chalcopyrite is prevalent in the brown quartz diorite adjacent to the “Crow vein zone”, especially near its contact with younger monzodiorite. A grab sample (MMI12-16-2) of disseminated mineralization from this location returned values of 0.12% Cu, 0.26 g/t Au and 2.2 g/t Ag (Table 1). Chalcopyrite is reported together with molybdenite in silicified zones at the intrusive-country rock contact (Livgard, 1998).

Primary sulphides at Bonaparte include pyrite, pyrrhotite, chalcopyrite, arsenopyrite, (Figs. 6b, c, d.) sphalerite, bismuth-tellurides (Fig. 5) and molybdenite. Scanning electron microscopy has been used to identify gold-, lead- and bismuth- tellurides and native gold of high fineness (no copper and only minor silver, Leitch, 1988). Gangue minerals recognized in thin section include quartz, chlorite, epidote, carbonate, hematite, and white mica.

Peatfield (1986) reported 30 meters of polyolithic breccia intersected in DDH NTM86-004 (85.4-115.0 m). Breccia fragments include argillite, hornfels, and intrusive and vein quartz. Sulphides (pyrite, pyrrhotite, ±chalcopyrite) are both in the matrix and fragments, suggesting repeated hydrothermal mineralization and brecciation. Geochemical analyses of this intersection failed to return elevated base or precious metal values (Peatfield, 1986). Nonetheless, this hole is important because it demonstrates the presence of high-level porphyry processes west of the Grey Jay vein and north of the contact with the main intrusion.

8. Summary and conclusions

Our preliminary study reveals the following sequence of events at the Bonaparte property (Fig. 7).

- 1) Deposition of Paleozoic (?) carbonaceous and calcareous mud to fine sandstone.
- 2) One, possibly two phases of deformation.
- 3) Intrusion of quartz diorite and biotite hornfelsing of adjacent country rock.
- 4) Coincident with 3), east-side up motion along north-trending reverse shear zones (mylonitic fabric; stage 4 in Fig. 7) and alteration.
- 5) Continued deformation and intrusion of monzodiorite (stage 5 in Fig. 7). Alteration of diorite to secondary biotite and chlorite assemblages and introduction of disseminated chalcopyrite with gold and silver values (stage 5a in Fig. 7).
- 6) Brittle deformation and dilation adjacent to contact zones with diorite and focusing of quartz-pyrite and chalcopyrite veins.
- 7) Continued brittle deformation and quartz-carbonate-sericite-chalcopyrite-arsenopyrite and -gold veining across early foliation in diorite (stage 7 in Fig. 7). Carbonate alteration along veins/intrusive contact (stage 7a in Fig. 7). Biotite alteration envelope around veins increasing biotite overprint; propylitic alteration of monzodiorite overprinted by biotite alteration.
- 8) Cooling and further brittle deformation with intrusion of porphyritic aplite dikes and sparse open-space quartz-carbonate-pyrite veins.

Previously reported quartz stockwork zones with molybdenum mineralization could not be confirmed. However, shear-hosted gold-chalcopyrite quartz veins have been verified by this study. Ever since gold-mineralized float was first discovered at the Bonaparte in 1985, work has focused primarily on evaluating the potential of the quartz vein mineralization. Nonetheless, the metal and alteration assemblages at Bonaparte are shared by porphyry deposits of the Early Jurassic Takomkane-Wildhorse magmatic belt (i.e. Brenda Cu-Mo porphyry and the Woodjam Au, Cu-Mo porphyry; Fig. 2), inviting speculation that the Bonaparte mineralization discovered to date represents an upper level of a buried porphyry system. This hypothesis is being addressed through ongoing U-Pb zircon and Ar⁴⁰-Ar³⁹ white mica isotopic age determination aimed at testing the assumed Early Jurassic age of the Bonaparte intrusions and synchronicity of gold mineralization.

References cited

- Anderson, R.G., Schiarizza, P., Andrews, G., Breitsprecher, K., Davis, W., Dunne, C.E., Plouffe, A. and Thomas, M.D., 2010. Bedrock, surficial, geophysical and geochemical mapping reveals exploration targets in the Thuya batholith, southern Nicola arc. In: Geological Association of Canada, Targeted Geoscience Initiative 3 Workshop,

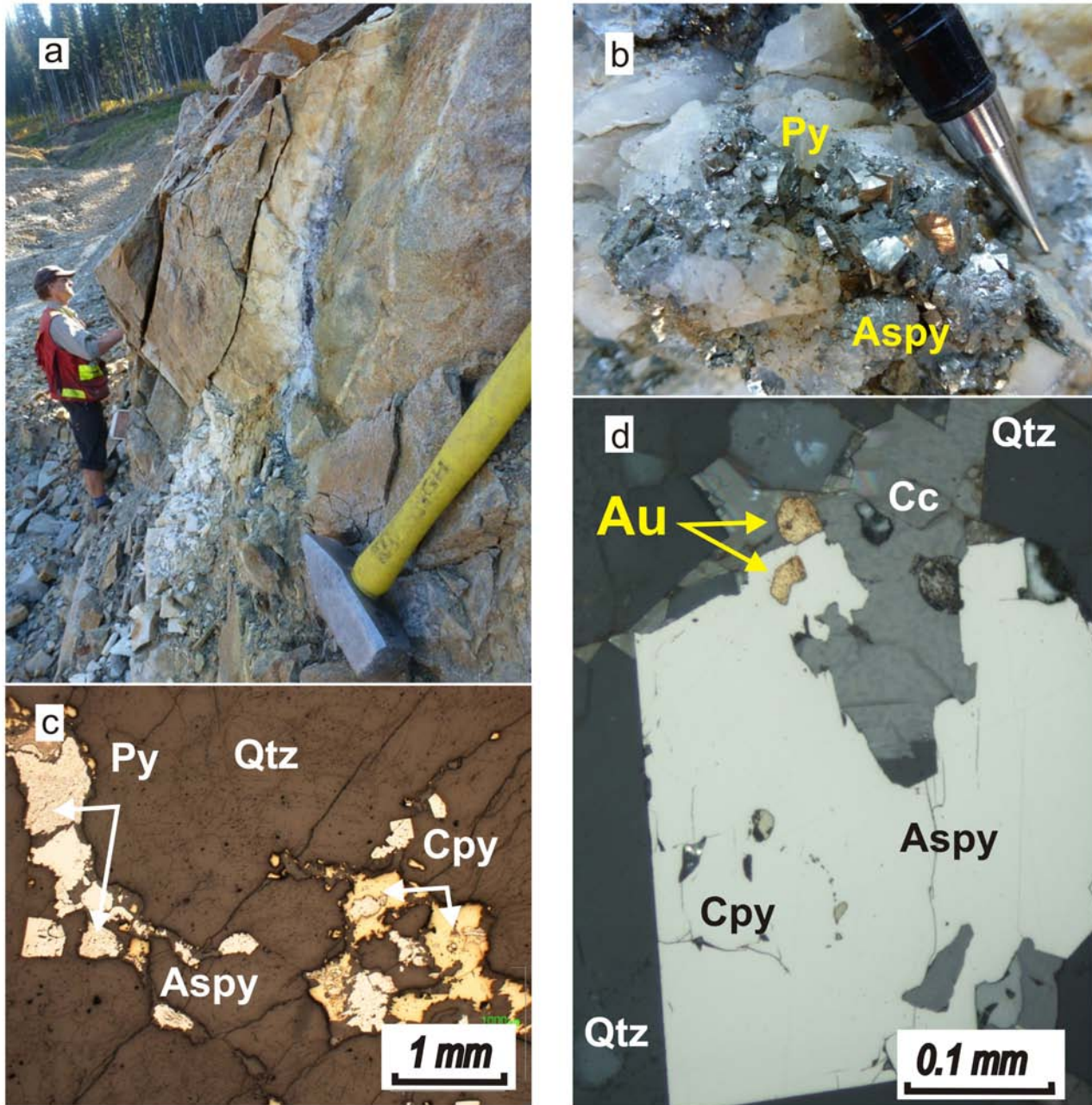


Fig. 6. Quartz vein mineralization. **a)** Biotite-altered, silicified, and mineralized quartz diorite footwall rock to the Crow S vein has been mostly removed from the trench now occupied by geologist, view to south. **b)** Detail of quartz vein in a) showing coarsely crystalline pyrite and arsenopyrite intergrowths. **c)** and **d)** Plane polarized reflected light photomicrographs of mineralized quartz vein material. In **c)**, intergrowth of pale spongy pyrite, brassy chalcopyrite and lesser arsenopyrite (white). In **d)** arsenopyrite crystal with inclusions of chalcopyrite (appearing as very pale yellow against bright background) and irregular contact (? replacement) with carbonate and deposition of gold grains (~25 μ across). Abbreviations: Qtz, quartz; Cc, calcite; Py, pyrite; Aspy, arsenopyrite; Cpy, chalcopyrite; Au, native gold.

Table 1. Selected geochemical results of mineralized samples collected during the 2012 property visit.

Station Number	Easting	Northing	Analyte	Ag	As	Au	Ba	Bi	Ca	Cd	Ce	Co	Cr	Cu	Fe	Hf	K	La	Li	Mg	Mn	Mo
			Unit	PPB	PPM	PPB	PPM	PPM	%	PPM	PPM	PPM	PPM	PPM	PPM	PPM	%	PPM	PPM	PPM	%	PPM
			MDL	2	0.1	0.2	0.5	0.02	0.01	0.01	0.1	0.1	0.5	0.01	0.01	0.02	0.1	0.5	0.1	0.01	1	0.01
12JLO50-30z	679297	5653683		399	8.1	38.3	96.2	0.02	4.03	0.1	5.2	4.8	34.1	131.1	1.55	0.03	0.18	2.5	5.4	0.4	614	5.12
12JLO50-38	679121	5653664		17	0.6	1.8	323.4	<0.02	1.74	0.05	39.4	7	43.3	4.09	3.23	0.32	1.58	20.3	15.6	1.17	718	0.03
12JLO50-39-2	679239	5653736		68	1.6	1.1	61.7	<0.02	1.07	0.02	5.8	8.8	55	111.04	2.13	0.08	0.16	2.9	7.4	0.54	376	4.79
MMI-12-16-2	679117	5653670		2202	9.9	261.3	201.1	0.18	1.46	0.46	36.8	9.8	28.2	1209.52	3.27	0.32	0.96	18.5	8.4	1.01	657	0.14

Station Number	Easting	Northing	Analyte	Na	Nb	Ni	P	Pb	Rb	S	Sb	Se	Sn	Sr	Th	Ti	U	V	W	Y	Zn	Zr
			Unit	%	PPM	PPM	%	PPM	PPM	%	PPM	PPM	PPM	PPM	PPM	PPM	%	PPM	PPM	PPM	PPM	PPM
			MDL	0.001	0.02	0.1	0.001	0.01	0.1	0.02	0.02	0.1	0.1	0.5	0.1	0.001	0.1	2	0.1	0.01	0.1	0.1
12JLO50-30z	679297	5653683		0.05	<0.02	3.3	0.05	1.29	3.4	0.13	1.67	1	<0.1	143.3	0.5	0.00	0.20	12	0.1	5.79	22.6	1.1
12JLO50-38	679121	5653664		0.15	0.14	3.1	0.12	2.12	71.1	0.04	0.1	11.4	0.7	80.5	7.2	0.21	0.80	98	<0.1	7.35	65	6.5
12JLO50-39-2	679239	5653736		0.15	0.05	5.2	0.06	0.77	5.2	0.61	0.13	1.2	<0.1	67.1	0.8	0.07	0.30	28	<0.1	2.44	25.7	1.3
MMI-12-16-2	679117	5653670		0.06	0.1	3	0.12	1.76	32.3	0.6	1.71	11.6	0.6	46.2	7.9	0.14	1.3	88	0.2	8.88	78.2	11.6

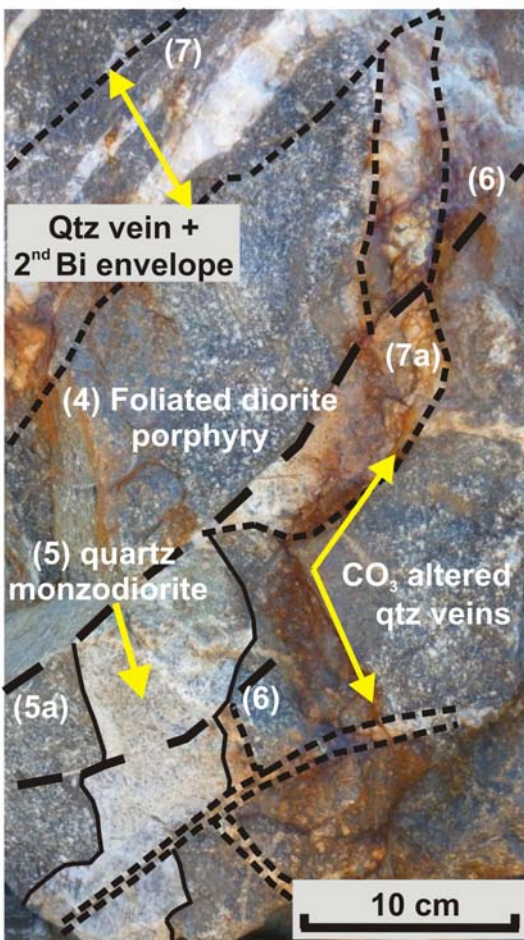


Fig. 7. Partial synopsis of Bonaparte intrusion, strain, alteration, and mineralization history (numbers correspond to events in text). Photograph of foliated brown quartz diorite porphyry (4) and quartz monzodiorite (5). The quartz monzodiorite is chilled along its contact with biotite-altered quartz diorite (5a). Quartz diorite and quartz monzodiorite are crosscut by brittle faults (6). Episodic quartz veining along north-trending lithologic contacts (6a). Extension gashes with introduction of sulphides and gold; enveloped by secondary biotite (7); carbonate alteration along veins/intrusive contacts (7a). Abbreviations: Cc, calcite; Qtz, quartz; Bi, biotite.

March 2010, Vancouver, pp. 52-57. URL accessed November, 2012, http://www.gac-cs.ca/workshops/TGI3/abstracts/GAC_TGI3_workshop_abstracts.pdf.

- Beaton, A.J., 2011. Bonaparte gold underground decline and surface trench bulk-sample project. BC Ministry of Energy, Mines, and Petroleum Resources, Assessment Report 32930, 382 p.
- Breitsprecher, K., Weis, D., Scoates, J.S. and Anderson, R.G., 2010. Targeting mineralized Late Triassic to Early Jurassic plutons in the Nicola arc, southern Quesnel terrane, Canadian Cordillera. In: Geological Association of Canada, Targeted Geoscience Initiative 3 Workshop, Vancouver, pp. 49-51. URL accessed November, 2012, http://www.gac-cs.ca/workshops/TGI3/abstracts/GAC_TGI3_workshop_abstracts.pdf.
- Durfeld, R., 1980. Geology report on the JS mineral claim. BC Ministry of Mines, Energy, Mines, and Petroleum Resources, Assessment Report 8500, 11 p.
- Gosse, R.R., 1987. Bonaparte property Discovery Zone, diamond drilling, trenching and geophysics. BC Ministry of Energy, Mines, and Petroleum Resources, Assessment Report 15757, 235 p.
- Gosse, R.R., 1988. Bonaparte property Discovery Zone, diamond drilling and trenching. BC Ministry of Energy, Mines, and Petroleum Resources, Assessment Report 17206, 380 p.
- Gourlay, A.W., 1985. North Thompson claims - geology and geochemistry. BC Ministry of Energy, Mines, and Petroleum Resources, Assessment Report 13908, 49 p.
- Lee, L.J., 1989. Trenching and drilling on the Bonaparte central property. BC Ministry of Energy, Mines, and Petroleum Resources, Assessment Report 18682, 270 p.
- Leitch, C.H.B., 1988. A polished section and SEM study of Bi- and precious metal tellurides from the Discovery Zone, Bonaparte property. In: BC Ministry of Energy, Mines, and Petroleum Resources, Assessment Report 17206, 380 p.
- Livgard, E., 1998. Summary of past exploration and details of 1998 diamond drilling on the Bonaparte gold property. BC Ministry of Energy, Mines, and Petroleum Resources, Assessment Report 25740, 151 p.
- Logan, J.M., Mihalynuk, M.G., Friedman, R.M., and Creaser, R.A., 2011. Age constraints of mineralization at the Brenda and Woodjam Cu-Mo±Au porphyry deposits –

- An Early Jurassic calc-alkaline event, south-central British Columbia. In: Geological Fieldwork 2010, British Columbia Ministry of Forests, Mines and Lands, British Columbia Geological Survey Paper 2011-1, pp. 129-144.
- Massey, N.W.D., MacIntyre, D.G., Desjardins, P.J. and Cooney, R.T., 2005. Digital geology map of British Columbia: whole Province; BC Ministry of Energy, Mines and Petroleum Resources, British Columbia Geological Survey GeoFile 2005-1.
- McClintock, J.A., 1987. Bonaparte Property West - 1987 geological, geochemical and geophysical report. BC Ministry of Energy, Mines, and Petroleum Resources, Assessment Report 17086, 239 p.
- Neugebauer, H.E.O., 1973. Geochemical report on Rave Group. BC Ministry of Energy, Mines, and Petroleum Resources, Assessment Report 4665, 15 p.
- Peatfield, G.R., 1986. Geology, rock and soil geochemistry, geophysics and diamond drilling on the Bob 1986 group (Bonaparte property). BC Ministry of Energy, Mines, and Petroleum Resources, Assessment Report 15166, 308 p.
- Schiarizza, P. and Israel, S., 2001. Geology and mineral occurrences of the Nehalliston Plateau, south-central British Columbia (92P/7, 8, 9, 10). In: Geological Fieldwork 2000, BC Ministry of Energy, Mines, and Petroleum Resources, British Columbia Geological Survey Paper 2001-1, pp. 1-30.

Geological setting of Late Triassic porphyry Cu-Au mineralization at Miner Mountain, Princeton, southern British Columbia

Mitchell G. Mihalynuk^{1,a} and James M. Logan¹

¹ British Columbia Geological Survey, Ministry of Energy, Mines and Natural Gas, Victoria, BC, V8W 9N3

^a corresponding author: Mitch.Mihalynuk@gov.bc.ca

Recommended citation: Mihalynuk, Mitchell G. and Logan, James M., 2013. Geological setting of Late Triassic porphyry Cu-Au mineralization at Miner Mountain, Princeton, southern British Columbia. In: Geological Fieldwork 2012, British Columbia Ministry of Energy, Mines and Natural Gas, British Columbia Geological Survey Paper 2013-1, pp. 81-96.

Abstract

Porphyry copper style mineralization at Miner Mountain is associated with dioritic intrusions in a predominantly sedimentary arc flank setting, not a predominantly volcanic arc axial setting as has commonly been assumed. It is generally difficult to distinguish epiclastic and pyroclastic (or even flow) units, particularly where altered. Nonetheless, argillaceous beds, limestone layers, and local rounding of clasts in arenites indicate a significant epiclastic component. The mixed sedimentary volcanic setting is akin to the Copper Mountain deposit, ~25 km to the south-southwest. Mineralization that has received the most exploration attention is concentrated on the disrupted western flank of an open syncline that mainly plunges gently to the north. Minor folds and faults produce more locally intense deformation zones. Carbonate-quartz-feldspar alteration predates calcite-chalcopyrite-bornite cementation of fragments in diorite breccias. K-feldspar-magnetite alteration is best developed in mineralized rocks, and these display Au, Pt and Pd enrichments, features typical of British Columbian alkalic porphyry deposits.

Keywords: Miner Mountain, alkalic porphyry copper gold, Nicola Group, Quesnel terrane, Late Triassic, potassic alteration, Copper Mountain intrusive suite

1. Introduction

Geological fieldwork conducted between Merritt and Princeton in 2012 (Fig. 1), forms part of an ongoing province-wide porphyry copper project (Logan and Mihalynuk, 2005). Objectives of this project include defining the geological setting and evaluating the structural and stratigraphic controls on porphyry Cu-Au ±Ag-Mo mineralization in Late Triassic and Early Jurassic arc rocks as an aid to mineral resource evaluation and exploration (Logan and Mihalynuk, 2013). Herein we report on a recent component of the project, including geochemistry, petrography, and geochronology at Miner Mountain, in the southern Nicola belt (Fig. 2). In a companion paper (Mihalynuk and Logan, 2013a, this volume) we provide a similar treatment for mineralization in the Dillard Creek camp, about 20 km north of Miner Mountain.

2. Geological setting

Porphyry copper deposits in British Columbia are predominantly of Late Triassic age and belong to two arc terranes, Quesnel and Stikine (Coney et al., 1980), which extend the entire length of the province. These two terranes share Devonian through Triassic histories and fossil faunas indicating an origin far from the influence of North America. They are now separated along most of their length by a belt of even more exotic oceanic rocks, the Cache Creek terrane. At their northern ends, Stikine and Quesnel terranes appear to merge, Cache Creek terrane disappears, and all three terranes are enveloped by

rocks of pericratonic character; a configuration that has led to the “oroclinal hypothesis” (Mihalynuk et al., 1994). Accordingly, Stikine and Quesnel arc terranes were originally linked and were oroclinally folded (in plan, with a hinge to the north) around the exotic Cache Creek oceanic accretionary complex, most of which accumulated at the Stikine and Quesnel arc trenches. Although Quesnel-Stikine porphyry deposits formed throughout the Late Triassic, one class of porphyry deposits, the Cu-Au alkalic type, formed almost entirely during a remarkable metallogenic epoch near the end of the Triassic, at about 204 Ma (Logan and Mihalynuk, 2013). This event has been attributed to collision of an exotic, extinct arc terrane with the Stikine - Quesnel arc complex. Relics of the colliding arc, known locally as the Kutcho terrane, are now found within the Cache Creek complex. Collision of Kutcho terrane is thought to have interrupted subduction of the Cache Creek ocean plate, causing it to rupture. Hot sub-slab mantle welled up into the rupture and melted parts of the overlying Quesnel-Stikine mantle wedge, especially those metasomatized by metal-rich volatiles exsolved from the subducted Cache Creek ocean plate (Mihalynuk, 2010; Logan and Mihalynuk, 2013). Melts derived by roasting of the metasomatized mantle are inclined to be rich in Cu-Au and Pt-Pd elements (e.g., McInnis et al., 2005). Thus, volcanic strata of Latest Triassic age and coeval intrusive rocks are important targets for porphyry Cu-Au exploration. Such rocks are believed to underlie Miner Mountain (also known as Mt. Miner, Allison Mountain,

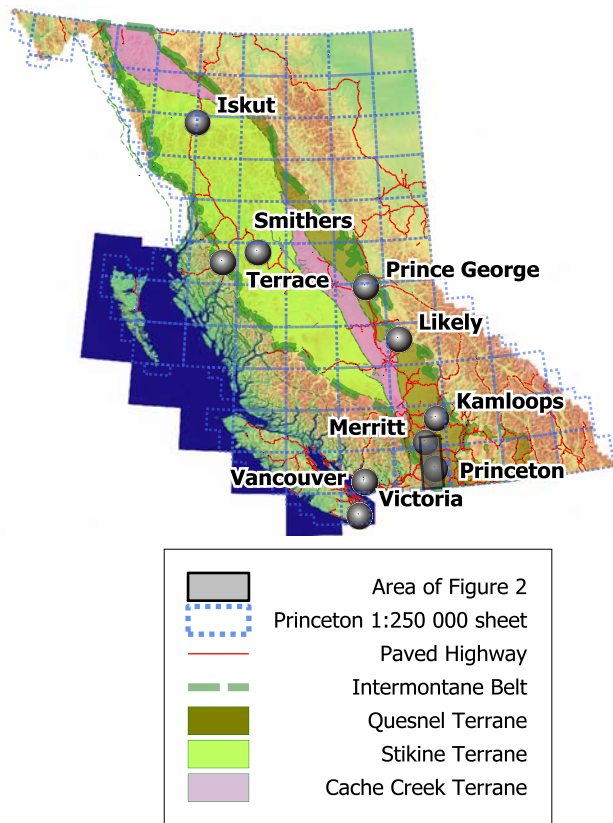


Fig. 1. Tectonic setting of southern Quesnel terrane and study area. Terrane boundaries modified after (Tipper et al., 1981). Area covered by Figure 2 is outlined by transparent grey box.

or Bald Mountain).

Late Triassic Nicola Group arc strata near Princeton are juxtaposed on their west side with Eocene volcanic and sedimentary rocks of the Princeton Basin (Fig. 2). Much of the contact is the north northeast-trending Boundary fault which dips westerly between 45° (Preto, 1979) and 68° (Read, 2000). To the east, the Nicola Group is intruded by the granodioritic Bromley pluton, with an Early Jurassic crystallization age, and to the northeast by the Late Jurassic Osprey Lake intrusion (193 ± 1 Ma and 166 ± 1 Ma respectively; Parrish and Monger, 1992). Approximately 25 km along strike to the south-southwest is the Copper Mountain mine, currently in operation and with past production of more than 650 million kg of Cu, 264 million g Ag and 16 million g Au (MINFILE 092HSE001) and a reported proven and probable reserve of 211 Mt grading 0.36% Cu (Copper Mountain Mining Corporation, 2009). Most mineralization at Copper Mountain is hosted within eastern facies mixed tuffaceous and sedimentary rocks of the Nicola Group (Preto, 1972) and is coeval with intrusive phases between 201 and 205 Ma (Mihalynuk et al., 2010). Mineralization at Miner Mountain is hosted in a potentially correlative volcanosedimentary succession that currently lacks age control. Principal objectives of our field work were to map volcanosedimentary facies

and to sample both volcanic and mineralized intrusive phases for isotopic age determination.

3. Location and access

Miner Mountain property (MINFILE 092HSE203) is on the eastern outskirts of Princeton, about 280 km east of Vancouver, at the junction of highways 3 and 5A. Easy access to the property, only ~5 km from the town's centre, is via an all-season paved and gravel road network to grassy ranchland and a microwave tower. Miner Mountain is a relic of the plateau dissected by the Similkameen River to the south and Allison Creek to the west. Vegetation is sparse, with forested areas of predominantly lodgepole and ponderosa pine, aspen, and fir, and open slopes commonly supporting the growth of prickly pear cacti, owing to the dry climate. With the exception of cliff sections along the incised valleys, the area is easily negotiated by 4x4 vehicles or on foot. Mineralization has been extensively explored in zones southwest, northwest, and north of the Miner Mountain peak.

4. Previous exploration work

Popular mining lore tells of disseminated bornite discovered circa 1914 in diorite at a working face of United Empire Coal Mine's Red Triangle coal deposit on the northwestern flank of Miner Mountain (Dolmage and Campbell, 1963). It is rumoured that as underground mining cut eastward, two coal seams in the Eocene Princeton basin strata were lost at a fault, later named the "Boundary Fault". This west-side-down fault (McMechan, 1983) locally delimits the western flank of the coal-bearing volcano-sedimentary basin, and offsets mineralized Late Triassic rocks towards the surface (Fig. 3). Dismayed by the lack of coal, the miners, who had no interest in the copper they found, abandoned their coal mining effort in 1914, after two years of operation (MINFILE 092HSE218). Most of the coal produced from the Red Triangle deposit is reported to have been sold to British Columbia Portland Cement Company to produce cement from their limestone quarry ~750 m to the south (MINFILE 092HSE169).

Exploration work on Miner Mountain began at least as early as 1905 (Preto, 1975), with the earliest reported assessment work recorded 53 years later (Fahrni, 1958). In 1951, extensive trenching, and diamond drilling by Granby Consolidated Mining, Smelting and Power Co. Ltd. (henceforth "Granby") revealed two disappointing zones of "very low grade" oxidized copper mineralization. As a result, 60 of 66 claims were allowed to revert to the Crown. However, the slopes of Miner Mountain are blanketed in glacial till and alluvium, with less than 1% outcrop (see Fig. 3), so in 1958, Granby conducted magnetic and electromagnetic surveys to look for buried mineralization. Two magnetic spot highs with highly irregular texture were attributed to glacially transported "boulders or slabs of magnetite bearing material which occur close to the surface ..." (p. 17,

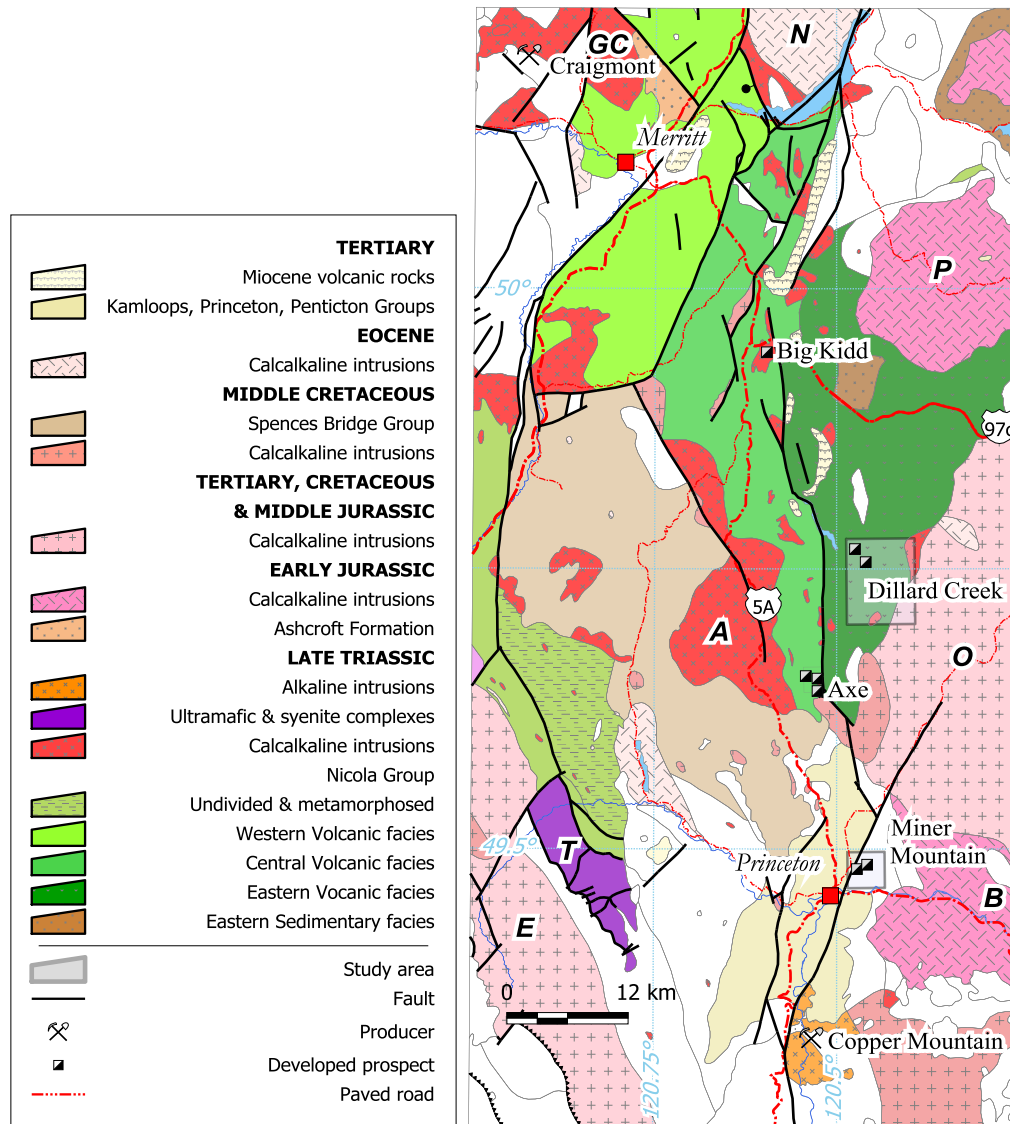


Fig. 2. Geological setting of 2012 field mapping in the Miner Mountain area between Princeton and Merritt. Western, Central and Eastern belts of the Nicola arc as defined by Preto (1979) are shown for reference. Adapted from Massey et al. (2005). Abbreviations denote major plutons: A = Allison Lake, B = Bromley, E = Eagle, GC = Guichon Creek, N = Nicola, O = Osprey Lake, P = Pennask, T = Tulameen.

Fahmi, 1958; Regal 2 claim). Later opinions favoured a gravity slide origin (Dolmage and Campbell, 1963; Preto, 1975; Christopher, 1981; Tribe, 2010) because mineralized blocks of Nicola Group lithologies up to ~10 m across were apparently deposited atop Eocene Princeton Basin strata. Electromagnetic and self potential surveys failed to yield responses that could be unambiguously attributed to in situ mineralization, but weak correlated responses were found south of the old workings (Regal 4 M.C.).

Over the next five decades, work on or adjacent to Miner Mountain included: 1) an aeromagnetic survey by Kennco Explorations (Western) Ltd. (Anderson and Gower, 1959); 2) further geophysical work by Climax Copper Mines N.P.L. (Nicholls and Gregotski, 1963;

Dolmage and Campbell, 1963), Great Slave Mines Ltd. (Cochrane, 1968), and Quintana Minerals Corporation, (Nielsen, 1977); 3) comprehensive exploration, including drilling and construction of an ill-fated copper leaching plant by Joy Mining Ltd. (Taylor, 1988); 4) drilling by Bethlehem Copper Corp. (Taylor, 1988); 5) soil and litho-geochemistry (Livingstone, 1981); 6) soil geochemistry by Mingold Resources Inc. (Taylor, 1988; Reynolds, 1990; and Hopper, 1996); and 7) exploration, including drilling, by Golden Kootenay Resources Inc. and Nustar Resources Inc. (McLeod, 2000; McLeod, 2002). Since 2007, a multi-faceted exploration program has been undertaken by Segor! Resources Inc. (Christopher, 2012).

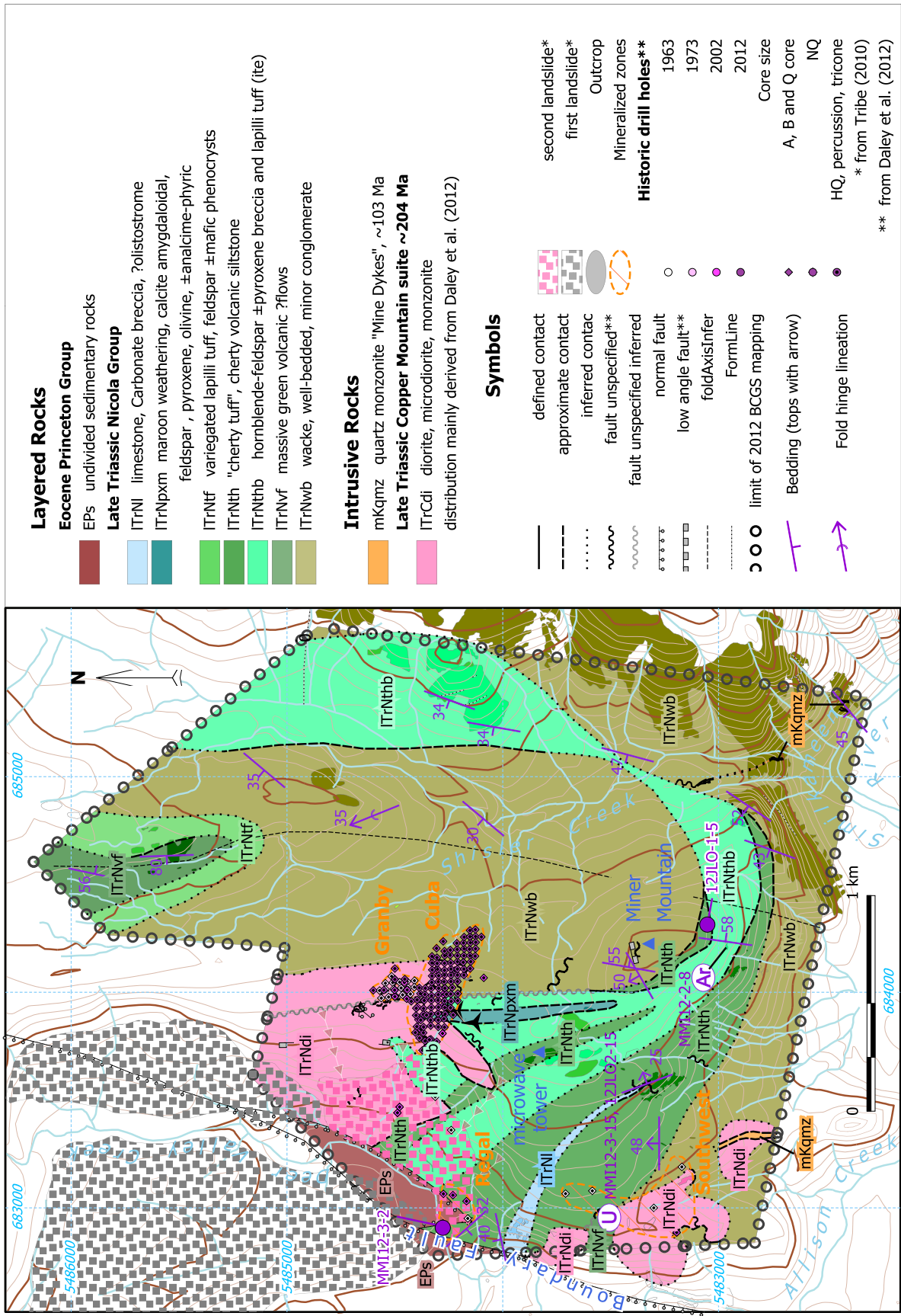


Fig. 3. Geology of Miner Mountain includes new British Columbia Geological Survey mapping, and new property mapping by Sego! Resources (Daley et al., 2012). Distribution of intrusive rocks is based largely upon mapping of trenches by Sego! Resources and others before trenches were reclaimed (prior to 2012).

4.1. Previous systematic mapping

Regional-scale published maps that include contemporary work in the Miner Mountain camp are lacking. Systematic regional mapping in the area dates to that of Rice (1947) and Monger (1989). We present a synopsis of the regional geology of Miner Mountain, parts of which are extracted from compiled property-scale mapping (Daley et al., 2012) and incorporated into Figure 3.

Previous work at Miner Mountain mapped most of the property as underlain by igneous rocks, mainly andesite and diorite. Field observations in 2012 lead us to reinterpret much of the succession as sedimentary, with subordinate volcanic and intrusive rocks. Similar conclusions were drawn by Rodgers (2000) who recognized felsic volcanic rocks interbedded with limestone and calcareous debris flows when the area north of the property was assessed for potential subaqueous volcanogenic massive sulphide mineralization (none was found).

Well-bedded strata are exposed on all flanks of Miner Mountain, but particularly to the south and east (Fig. 3). Alteration commonly obscures primary sedimentary features, and even in the absence of alteration, it can be very difficult to distinguish epiclastic from pyroclastic rocks; for example, a coarse arkose (Fig. 4) from a crystal lithic ash tuff. However, at several localities argillaceous interbeds (Fig. 5), and carbonate layers imply sedimentation in standing bodies of water. This interpretation is supported by petrographic observations of rounding and sorting of volcanic grains (including in graded layers), suggesting aqueous transport and deposition (Fig. 6). However, a coarse monomictic volcanic breccia on the south slope of Miner Mountain is interpreted as an autoclastic flow breccia, and a vesicular flow layer extending from near the microwave tower to the Granby zone have also been mapped. If correctly interpreted, these units confirm the presence of primary volcanic units.

5. Geological units

Miner Mountain is near the boundary between the backarc facies, “eastern belt” comprising predominantly sedimentary rocks and the arc-axis facies or “central belt” comprising predominantly volcanic rocks (terminology of Preto, 1979). This relationship is borne out at the property scale as mineralized diorite cuts predominantly sedimentary rocks. Intercalated with this sedimentary package, are sparse primary volcanic units. Key units are described here, starting with what are interpreted as the lowest, oldest units in the succession. (Discussions of sedimentary grain sizes conform to the Wentworth/ISO scale where sand grains range from 0.063 to 2 mm in diameter. Igneous grain size designations “fine”, “medium”, and “coarse” are divided at 1 mm and 5 mm grain diameters.)



Fig. 4. a) Parallel-stratified coarse arkosic volcanic sandstone. Typical beds are more massive. **b)** Coarse lithic volcanic wacke overlain by indurated siltstone (locally referred to as “cherty tuff”).

5.1. Layered rocks

5.1.1. Volcanic conglomerate to siltstone

The lowest sedimentary unit consists of pebble-cobble conglomerate, sandstone, siltstone (Fig. 4) and rare



Fig. 5. Recessive and rusty, well-bedded argillaceous section with more massively bedded volcanic sandstone above and below. View is easterly along the top of the cliffs south of Miner Mountain. Height of cliff section shown in photo foreground is about 8 metres.

argillite (Fig. 5). Most common are fine- to medium-grained arkosic volcanic sandstone containing 1-3 mm subrounded grains. Outcrops are typically grey- to green- or brown-weathering, blocky, and form cliffs along the south and east parts of the map area. Along the cliff tops of the southern map area, carbonate alteration produces orange-weathering outcrops. Here too is one of the few exposures of black argillite (Fig. 5).

Except in areas with mainly fine-grained rocks, bedding is commonly indistinct, with tabular beds decimetres to metres thick. Siltstone and rare argillaceous beds are laminated on a sub-centimetre scale. Low-angle trough cross-stratification is displayed locally in sandstones, but is rarely well enough developed to permit unambiguous determination of paleoflow directions. Graded bedding is normal, with few exceptions. Scours and soft-sediment deformation structures confirm younging directions. Clasts are derived from volcanic or hypabyssal intrusive protoliths, mainly feldspar and lesser hornblende or pyroxene porphyries, or intraformational sedimentary sources.

Most conglomerate is matrix supported (<10% clasts), although rare crystal-rich (75% 1-3 mm white plagioclase) and volcanic fragment-rich beds are clast-supported. Some laminated siltstone beds are cherty; these are described separately below.

5.1.2. “Cherty tuff”

Pale green to white cherty volcanic siltstone forms blocky to rubbly, angular outcrops. It commonly displays obvious centimetre-scale bedding and may be finely laminated (Fig. 7). Beds may display grading: both normal and lesser reverse grading is developed. Local

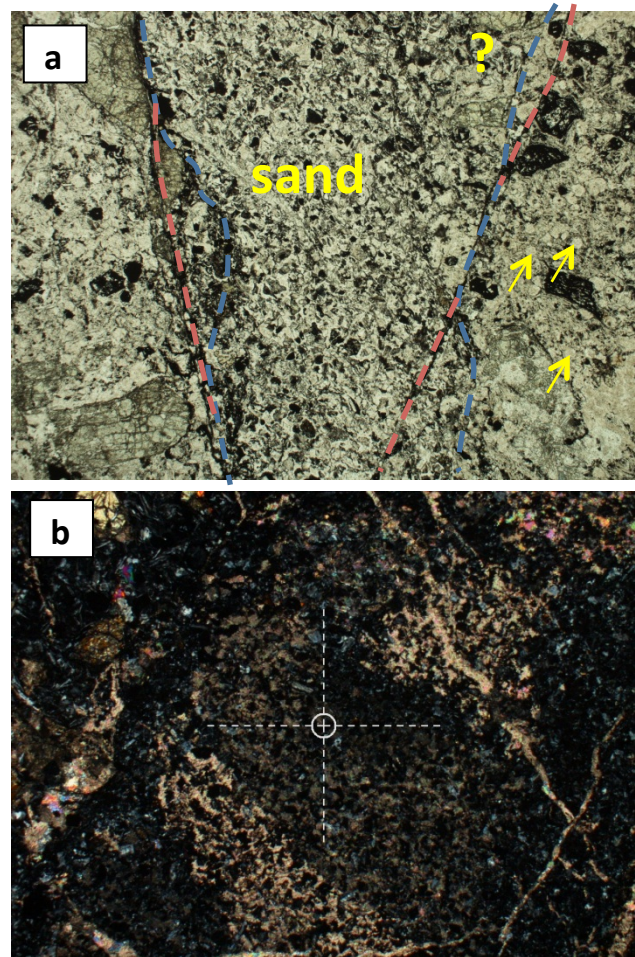


Fig. 6. a) Photomicrograph showing V-shaped infill of immature volcanic sandstone (labelled “sand”) between flow-top breccia fragments. Blue dashed lines mark clast margins and red lines highlight small-scale faults that modify the contacts between the breccia fragments and sandy infill. Note rounding of many of the sand grains, as well as very angular shards (presumably minimally transported). In area identified by “?” the breccia fragment is breaking apart, contributing to the matrix infill. Rounded grains marked by arrowheads within the breccia clasts may be altered analcime. Field of view represents ~4 mm. **b)** Slightly enlarged view of a) in cross polarized light. High birefringence dark and bright domains are optically continuous carbonate cement in which fine sand-sized grains are supported. Irregular carbonate veinlets cut the sandstone. Circle at crosshairs has a radius of 100 μ .

disrupted beds may record synsedimentary faults. Bedding is not accentuated by parallel fractures; instead, fractures commonly intersect bedding at high angles producing angular talus, probably on account of its high level of induration. Staining for potassium shows low but pervasive potassium content, perhaps due to finely disseminated K-bearing mineral phases or diffuse alteration. “Cherty tuff” can be observed as interbeds in coarse sandstone at many localities (Fig. 4b), and on the west flank of Miner Mountain, it is overlain by carbonate clast conglomerate. Farther north, it is overlain by augite-phyric volcanoclastic rocks; at one locality south of Miner Mountain it is intruded by sills of crowded, coarse augite

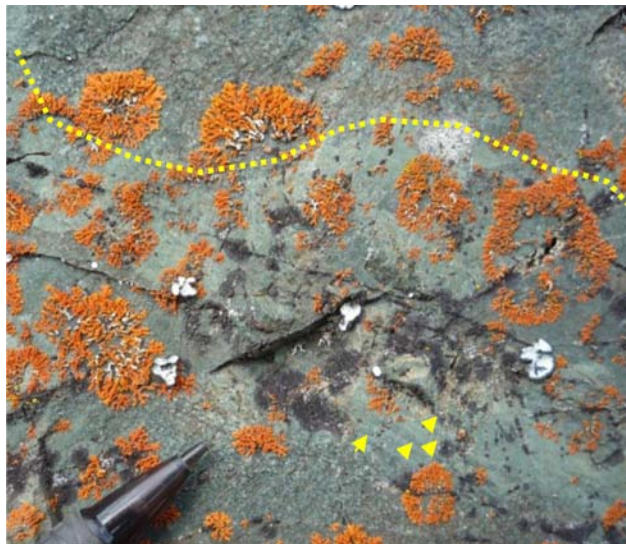


Fig. 7. Sandstone (beneath pencil tip) overlain by mm-scale graded couplets (yellow arrows) of coarse siltstone (dark) to fine siltstone (light), which are overlain by uniform light green "cherty tuff" (fine siliceous siltstone). Top of photo is a bed of coarse sandstone that cuts down into the "cherty tuff" (base of bed highlighted by dotted line).

porphyry more than 1 m thick. "Cherty tuff" occurs at various stratigraphic levels and, therefore, should not be used as a marker horizon. A water lain pyroclastic origin is suspected, with crystal shards, lithic grains, and outsized clasts visible in thin section (Fig. 8).

5.1.3. Limestone

Light grey to maroon hematitic limestone is exposed on steep dip slopes east of Allison creek. It is medium grained where recrystallized. It contains rectangular single carbonate crystals that may be relic crinoids. Limestone beds are massive to irregularly jointed and commonly hematite-stained. Where cut by fracture

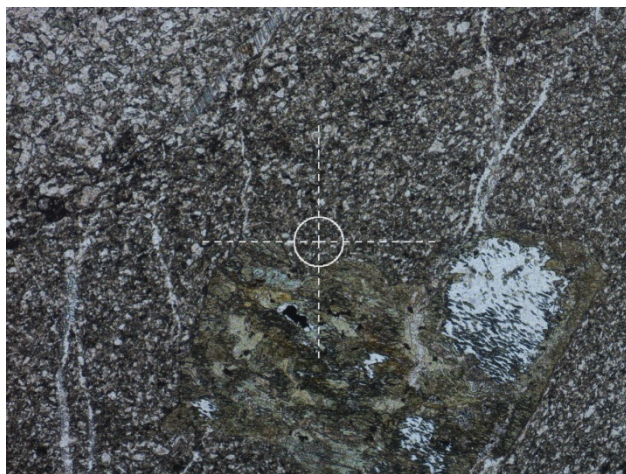


Fig. 8. Photomicrograph of "Cherty tuff" siltstone in plane polarized light. Many silt-sized grains are very angular and crystal shards are common. Bedding, defined by clast size, extends diagonally from middle left to upper right. An outsized clast of foliated, epidote-altered country rock is in the bottom central part of the image. Circle at crosshairs has a radius of 100 μ .

networks, the limestone is replaced by white sparry calcite with maroon to purple hematitic envelopes. At contacts with volcanoclastic rocks, the limestone is dirty green and contains abundant volcanic lithic and crystal fragments; white calcite lenses and vein stockworks, including veinlets of hematite, are also common. Individual limestone beds are 3-5 m thick; it remains unclear if repeated interlayering of three limestone and calcareous, hematitic to green, fine-grained volcanoclastic rock successions are primary or result from structural repetition. Mineralization is locally developed near the bed tops where in contact with volcanic rocks; it occurs as disseminated to blebby magnetite with traces of chalcopyrite. A 10 m thick quartz microdiorite cuts the unit (see following).

5.1.4. Carbonate breccia and conglomerate

At least one broken, irregular layer of carbonate and conglomerate, crops out sporadically on the west flank of Miner Mountain 1 km from the peak. In this layer, angular limestone clasts are slightly deformed, probably flattened, and are mixed with green or red oxidized volcanic detritus. Overlying and underlying medium- to coarse-volcanic sandstone layers are carbonate cemented. Interlayered with the base of this calcareous section are well-exposed outcrops of cherty siltstone. Perhaps only 2 m in maximum thickness and discontinuous along strike (both thickness and continuity are exaggerated on Figure 3), this carbonate breccia unit is important because it demonstrates a probable subaqueous origin (like the limestone unit described above); in this case likely as an olistostrome. No macrofossils were found in the clasts. At one locality, an undisturbed carbonate layer is up to 15 cm thick (Fig. 9).

5.1.5. Polymictic lapilli tuff

Grey to pale orange-weathering and massive to thickly bedded lapilli tuff is characterized by variegated, angular to subrounded lapilli clasts floating in an arkosic wacke matrix (Fig. 10). Plagioclase may comprise 30-40% of the matrix, and also occurs as phenocrysts together with 20-30% hornblende and/or pyroxene crystals that range between 2 and 6 mm long. Fragments include: fine aphyric black basalt; plagioclase-phyric basalt; augite and plagioclase-phyric basalt; and altered pink hypabyssal diorite. Alteration includes: epidote flooding of the matrix and plagioclase; hematite dusting of plagioclase and along fractures; and K-feldspar flooding of the matrix plus replacement of some clasts. Magnetite and chalcopyrite are sparsely disseminated; malachite patches are common on fracture surfaces. Zones of calcite as veinlets and breccia infills postdate lithification.

5.1.6. Pyroxene-phyric volcanic breccia

A coarse mafic fragmental unit can be traced along the southern and eastern portions of the map area. It is pale green and contains dark, coarse-grained hornblende and pyroxene-porphyry blocks and lapilli within a crystal-rich tuff matrix. Breccia layers are 10s of metres thick and



Fig. 9. Light grey to white carbonate layer extends from above head of hammer to lower right corner of the photo. Adjacent rocks are, in part, cemented by carbonate.



Fig. 10. Polymictic lapilli tuff cut by late calcite veins.

are overlain by bedded sedimentary rocks. Elsewhere, sections of basaltic andesite, decimetres thick, contain 2-4 mm hornblende phenocrysts as the predominant mafic mineral and occur together with subhedral 1-2 mm pyroxene crystals. Both breccia types also contain plagioclase (1-2 mm, 10-20%), which is especially abundant in hornblende-phyric varieties. Disseminated magnetite is also common, giving the unit a relatively high magnetic susceptibility (~ 20 to 45×10^{-5} SI). Locally, the unit is cut by white centimetre-thick quartz veins. Alteration of the fine-grained matrix and phenocrysts by chlorite and/or epidote and pyrite is pervasive, whereas patches and fracture controlled epidote \pm pyrite and magnetite are only locally developed. It is unknown if the alteration represents a broad propylitic alteration halo, or greenschist-grade metamorphism.

5.1.7. Hornblende-feldspar porphyry

Dark grey, blocky and indurated acicular hornblende-feldspar-phyric breccia and lapilli tuff (Fig. 11) is a mappable unit ~ 20 m thick, best exposed on the south flank of Miner Mountain. Layers containing both medium-grained euhedral hornblende and lesser coarse augite ($\sim 15\%$ combined) are generally less than a metre thick. Petrographic analysis shows that hornblende in these layers have cores of pyroxene. Plagioclase is relatively fresh, although turbid, and displays strong oscillatory zoning.

Along the eastern part of the map area the hornblende porphyry crops out as a well jointed, massive, 25 m thick flow with a blocky weathering flow-top breccia that passes upwards into hornblende plagioclase phyric lapilli tuff.

Locally the mafic minerals are vitreous, but more commonly they are chlorite-epidote \pm actinolite-altered along with the feldspar and matrix. Medium-grained plagioclase is generally more abundant than hornblende crystals, especially in crystal rich layers. Staining shows that the alteration mineral assemblage includes K-feldspar. Where the unit contains vitreous hornblende, it was sampled for $^{40}\text{Ar}/^{39}\text{Ar}$ dating (sample MMI12-2-8; Table 1).



Fig. 11. Hornblende-phyric breccia displays acicular hornblende with trachytic alignment in direction of arrow, and patches of green-yellow epidote alteration.

Table 1. Major oxide analyses from Inductively Coupled Plasma-Mass Spectroscopy following lithium metaborate fusion of sample. Analyses performed at Activation Laboratories, Lancaster, Ontario. All values reported are weight %. UTM coordinates are zone 10, North American Datum 1983. See (Mihalynuk and Logan, 2013b) for a digital table of the complete suite of elements analyzed.

StatNum	Unit	UTME	UTMN	SiO ₂	Al ₂ O ₃	Fe ₂ O _{3(T)}	MnO	MgO	CaO	Na ₂ O	K ₂ O	TiO ₂	P ₂ O ₅	LOI	Total
12JLO-1-5		684314	5483052	51.22	16.26	9.67	0.192	4.02	9.1	3.37	1.52	0.903	0.37	2.1	98.72
12JLO-3-31	ITrNth	685028	5485107	66.11	17.63	2.92	0.072	0.96	4.14	5.12	2.46	0.258	0.12	1.18	101
MMI12-2-8	ITrNhb	684236	5482960	52.28	17.6	9.38	0.163	4.15	8.02	3.33	2.28	0.831	0.36	1.85	100.2
MMI12-3-15	ITrCdi	682955	5483506	54.86	15.69	4.96	0.083	2.66	7.03	6.5	0.94	0.488	0.46	6.53	100.2
Std MRG-1				38.59	8.43	17.42	0.167	13.26	14.72	0.71	0.18	3.705	0.07	1.45	98.71
STD WGB-1				48.83	10.91	6.33	0.135	9.14	16.34	2.15	0.91	0.885	0.09	3.8	99.51
				0.01%	0.01%	0.01%	0.001%	0.01%	0.01%	0.01%	0.01%	0.001%	0.01%	%	0.01%

5.1.8. Pyroxene-phyric flow rocks

An ochre-coloured basalt flow unit crops out east of the microwave tower. Also known as the “brick red unit”, it is maroon to tan or dark grey on weathered and fresh surfaces, and is typically fine grained and sparsely amygdaloidal. Phenocryst content varies markedly along strike to include coarse-grained augite (\pm hornblende, to 10% combined), glomeroporphyritic feldspar (up to 20%), and greasy green relics after olivine. Petrographic analysis reveals rounded crystals <1 mm in diameter that are interpreted as analcime, altered to a low birefringence mineral aggregate (Fig. 6a). Amygdules are less than 1 cm in diameter and comprise ~10% of the basalt. They are composed of calcite, commonly rimmed by epidote. This unit is chlorite altered, with late brittle fractures containing hematite and calcite and patchy epidote replacements of feldspar and mafic minerals. Its brecciated upper contact may interfinger with fine sandstone (Fig. 6a) or dust tuffite.

Similar rocks comprise some of the structurally highest rocks mapped on the property. These are augite-phyric flows and breccia that grade upwards into monomictic augite-phyric breccia and interlayered massive flows. They occur within the core of a shallowly north-plunging syncline near the northern limit of the map area.

5.2. Intrusive rocks

We describe the intrusive stocks and major dikes by relative age, from oldest to youngest. Volumetrically minor dikes, typically displaying variable contents of pyroxene, hornblende, and plagioclase phenocrysts, are not included. Some rocks formerly described as “microdiorite” on property maps can be shown to be arkosic volcanic sandstones with graded bedding. Small hornblende porphyry intrusions probably have irregular outlines, and are difficult to portray accurately on Figure 3 due to inadequate exposure.

5.2.1. Porphyritic diorite

Diorite, and locally quartz diorite, occurs at several localities, but some of the best exposures are of a 10 m

thick dike that cuts the limestone unit. This dike is a quartz-bearing leucocratic diorite with a fine-grained salt and pepper texture. White, equant plagioclase crystals (1-2 mm) comprise much of the rock (~45%); it also contains weakly chlorite-altered hornblende (0.5-1 mm, 30%) and intergranular quartz (5-10%). Hornblende is altered to lath-shaped clots of chlorite 2-3 mm across (10-15%); orthoclase is 3-5 mm (~5%), and white plagioclase (overprinted by green epidote alteration, 2-3 mm, 30%). Fine-grained hematite disseminations likely replace magnetite. Trachytic fabric is well displayed on some surfaces.

Northwest of Miner Mountain, along the property access road, are low, rubbly outcrops, probably of microdiorite. However, the moderate degree of alteration and broken outcrop precludes positive identification in the field.

On the southwest flank of Miner Mountain, outcrops and trenches expose tan, green and orange-weathering hornblende diorite. Petrographic analyses of a sample of mineralized diorite shows pervasive brecciation such that most individual plagioclase crystals are floating in a comminuted matrix that is altered or cemented by calcite-feldspar-quartz- \pm chalcopyrite or fine white mica, (or various combinations thereof). Plagioclase crystals display corroded margins and may be bent or show other optical evidence of strain. Whether this brecciation is due to deep-seated hydromagmatic fracturing (e.g., breccia pipe) or to interaction with wet sedimentary country rocks (e.g. peperite) has not yet been determined (see also “Mineralization” section).

5.3. Mine dikes

Also known as “Candy Stripe dykes” where well exposed along strike to the south-southwest, in the open pits of the Copper Mountain mine, the mine dikes are composed of distinctive, white to orange-weathering, quartz-feldspar-porphyritic rhyolite (Fig. 12). Coarse K-feldspar, coarse quartz eyes, and altered mafic minerals comprise ~20%, 3-5%, and ~2-3% of the rock respectively. These dikes form swarms with individual tabular bodies typically 5-10 metres thick. In the Miner



Fig. 12. Quartz-eye feldspar porphyry; correlated with the ~103 Ma Mine Dykes at Copper Mountain.

Mountain area, they appear to be restricted mainly to the Shisler Creek valley and ridges to the east (Fig. 3).

5.4. Depositional setting

Volcanic and sedimentary rocks in the Miner Mountain area were likely deposited in an arc flank setting. Very immature volcanoclastic input during arc construction eventually built out to override the flanking sedimentary basin to the east. Intrusion of mineralized diorite may have locally interacted with the wet sedimentary pile, causing the ubiquitous brecciation in the intrusions.

6. Lithochemistry

Samples collected for major oxide and trace element analysis were selected to represent the diorite and hornblende and pyroxene-phyric breccia units in the Miner Mountain study area. Major oxide analyses are reported in Table 1. Major and trace element analyses are available in downloadable format from Mihalynuk and Logan (2013b).

Following the classification of Peccerillo and Taylor (1976), and assuming that these porphyritic units are representative of their source magmas, the breccia units are high-K calcalkaline basalt (12JLO-1-5) or andesite (MMI12-2-8), and the porphyritic diorite is calcalkalic (MMI12-3-15) and compositionally equivalent to a basaltic andesite. Because the ratio of Na_2O to K_2O is near unity, the breccia units are shoshonites when their

non-normalized compositions are considered in total-alkalis – silica space (not shown; LeBas et al., 1986). However, when compared to the trace element alkalinity index Nb/Y (Pearce, 1996), neither the breccia units nor diorite are especially alkaline. Low Nb likely arises from the strong arc signature with deep Nb depletion, as shown on the primitive mantle – normalized spider diagram (Sun and McDonough, 1989) of Figure 13c. Other arc characteristics include Ta and Ti depletion and enrichment in large ion lithophile elements shown on the left side of the diagram (e.g., Cs, Rb, Ba, K, Sr). Lack of an Eu anomaly suggests that feldspar was not a residual phase in the source area, nor was it removed from the crystallizing melt. All units are uniformly light rare earth element enriched as compared to chondrite values (Fig. 13d; Sun and McDonough, 1989), and all display a common parentage (Figs. 13c and 13d).

7. Mineralization

The four main zones of mineralization on the property that have received most of the exploration development are Regal, Granby, Southwest, and Cuba (Fig. 3). We have few new observations to report as most mineralization is poorly exposed and the aim of our brief study was to establish regional geologic setting, not mineral resource potential. However, first impressions of the broad propylitic alteration zone (chlorite-epidote-actinolite-pyrite \pm quartz-calcite) are favourable and K-feldspar-magnetite alteration is locally intensely developed. Secondary biotite is rare. For detailed descriptions of mineralization the reader is directed to the many Assessment Reports cited herein, especially drill core logs.

7.1. Regal zone

Mineralization of the Regal zone (Fig. 3) is particularly intriguing. It is a blanket of chaotic, mineralized intrusive blocks. Copper oxides within this blanket are reported to grade to 1% Cu (Dolmage and Campbell, 1963); historical production includes construction of a leaching plant (Anonymous, 1972) in an attempt to leach oxidized mineralization, which was apparently unsuccessful (Taylor, 1988). This chaotic debris has been consistently interpreted as a landslide deposit (Dolmage and Campbell, 1963; Tribe, 2010). Drill holes are reported to penetrate through the oxide blanket into till and underlying Eocene Princeton Group volcano-sedimentary strata, and the occurrence of mineralization diagonally up-slope of the Regal zone (in the Granby “crush zone”; see below; Fig 3), appears to support this interpretation (Dolmage and Campbell, 1963). However, during our brief examination we did not observe in situ Cu mineralization in rocks of the Granby zone that matched the mineralized blocks in the Regal zone.

We did sample a mineralized block from the Regal zone (Fig. 3). The block, ~0.5 m in diameter, sat in colluvium atop undisturbed till, within ~0.5 m of underlying bedrock of presumed indurated Nicola Group volcano-sedimentary rock; clearly not the poorly lithified,

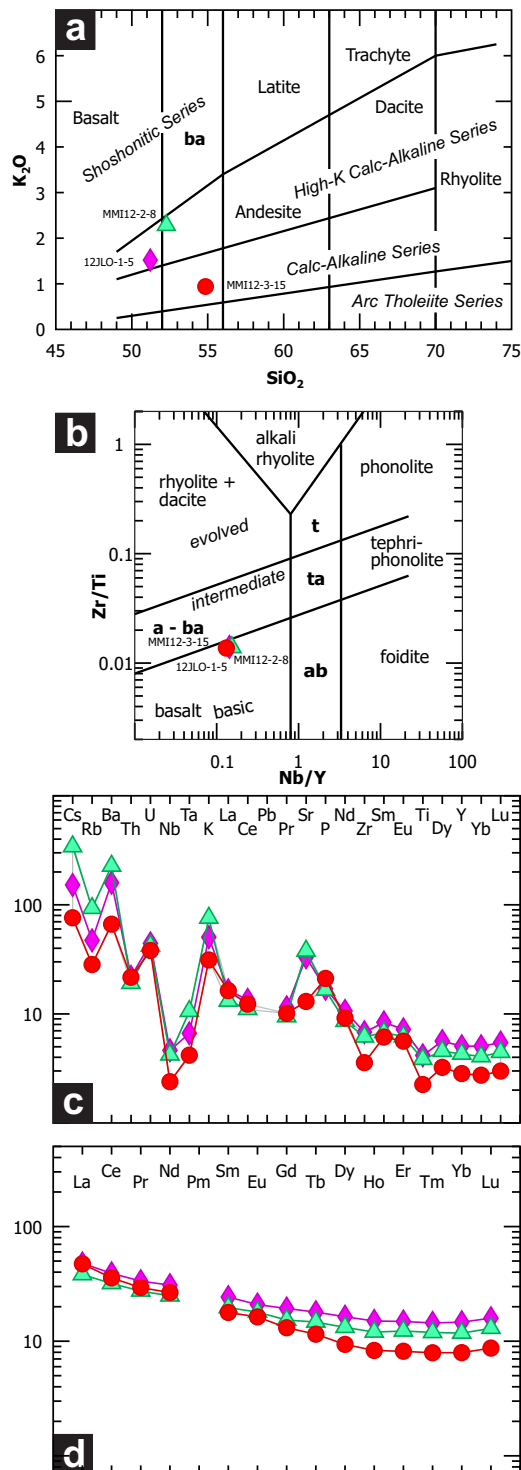


Fig. 13. Geochemical character of diorite (solid circle) and coarse breccia with predominantly feldspar-hornblende-pyroxene (diamond) or feldspar-hornblende (triangle). **a)** plot of K_2O versus SiO_2 , fields after Peccerillo and Taylor (1976), with oxides normalized with removal of components lost on ignition (LOI, see Table 1). **b)** Zr/Ti versus Nb/Y with fields after Pearce (1996). **c)** Primitive mantle normalized spider diagram and **d)** chondrite-normalized rare earth element plot using normalization factors of Sun and McDonough (1989). Abbreviations: a = andesite, ab = alkali basalt, ba = basaltic andesite, t = trachyte, ta = trachy-andesite.

dark red-brown, coaly Princeton Group strata that crop out ~100 m to the southwest. Both the style of mineralization and alteration of this block are similar to the Southwest zone. This block displays pervasive matrix flooding by calcite and white K-feldspar/albite (Fig. 14), but the original plagioclase crystals are relatively unaltered, although fractured. Chalcopyrite is uniformly distributed between the corroded margins of the feldspar crystals (Fig. 14c). Post-mineralization brecciation seems to have had little effect on destruction or beneficiation of mineralization. Analysis of the block yielded >1% copper (Table 2; MMI12-3-2b compare with 12JLO2-15 from the Southwest zone).

It is worthwhile to question again the origin of the mineralized blocks comprising the Regal zone. Could they have been derived from immediately up-slope, in an area that has received no drilling and very limited trenching (Fig. 3)? Could mineralized monzonite of the Southwest zone extend to this area?

7.2. Southwest zone

Host rocks for the Southwest zone mineralization (Fig. 3) are described above (see section 5.2.1. Porphyritic diorite). Stringers and veins and coarse blebs of chalcopyrite occur in rusty diorite in a >5 m zone exposed by trenching. Chalcopyrite is also disseminated in the matrix and as a replacement of mafic minerals. Broken outcrop may weather orange where cut by limonitic calcite-coated fractures, commonly with malachite staining. Alteration minerals include epidote as patchy matrix flooding veins, and together with calcite on most fractures. K-feldspar/albite rims plagioclase and floods the matrix (Fig. 15). A propylitic alteration assemblage of chlorite-epidote-calcite and disseminated pyrite (<1%, fine-grained) near the stock contact is overprinted by potassium alteration with introduction of chalcopyrite. Calcite and hematite occur along late fractures, in some instances with chalcopyrite (Fig. 15). Microscopic analysis of mineralized porphyry reveals that brecciation has produced corroded and sutured, but relatively unaltered plagioclase, like at the Regal zone (see above). Intercrystalline spaces are occupied by secondary calcite, feldspar, quartz, magnetite (oxidized to hematite/goethite), and chalcopyrite (Fig. 15). Despite evidence of widespread oxidation of magnetite to hematite, this unit is relatively magnetic, averaging 3.4×10^{-5} SI. It has been sampled for U-Pb isotopic age determination (MMI12-3-15, Table 1).

7.3. Cuba zone

Mineralization at the Cuba Zone does not crop out. It is a discovery made mainly through testing a geophysical anomaly using percussion drilling (Christopher, 2012). Figure 3 shows the known extent of Cuba Zone mineralization in the subsurface.

7.4. Granby zone

Mineralization at the Granby zone is also covered by glacial till. A westward continuation of the Granby Zone is the shallow, high grade, “crush zone” that does crop out

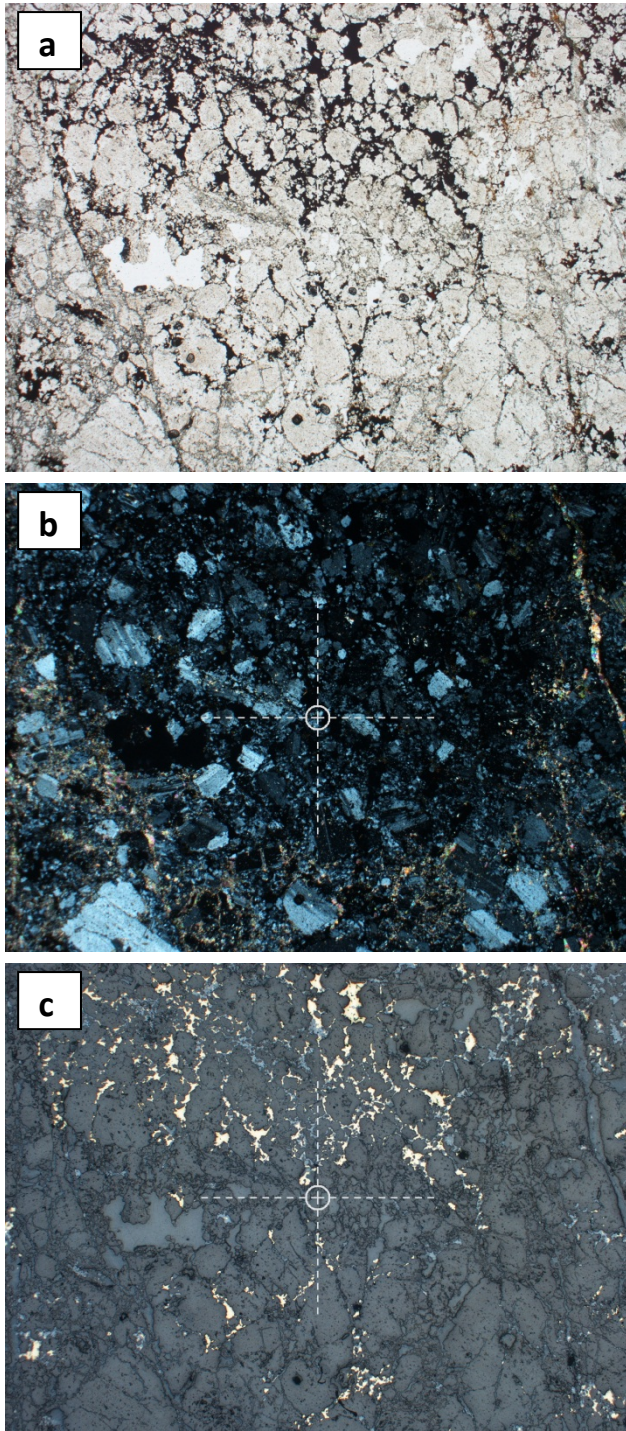


Fig. 14. Photomicrographs of Regal zone block showing the same field of view. **a)** In plane polarized light, brecciated feldspar porphyry shows corroded grain margins and intergranular calcite and fine-grained K-feldspar and albite. **b)** Cross polarized light showing high birefringence of intergranular calcite and calcite veinlet on right. **c)** Plane polarized reflected light showing disseminated yellow chalcopyrite mantled by bright grey and medium grey Fe-oxide/hydroxide minerals (mainly goethite and hematite) that probably formed during interaction with meteoric waters (dark grey minerals are non-reflective silicates). Calcite and isotropic epoxy have lower relief than silicate minerals. Circle at crosshairs has a radius of 100 μ .

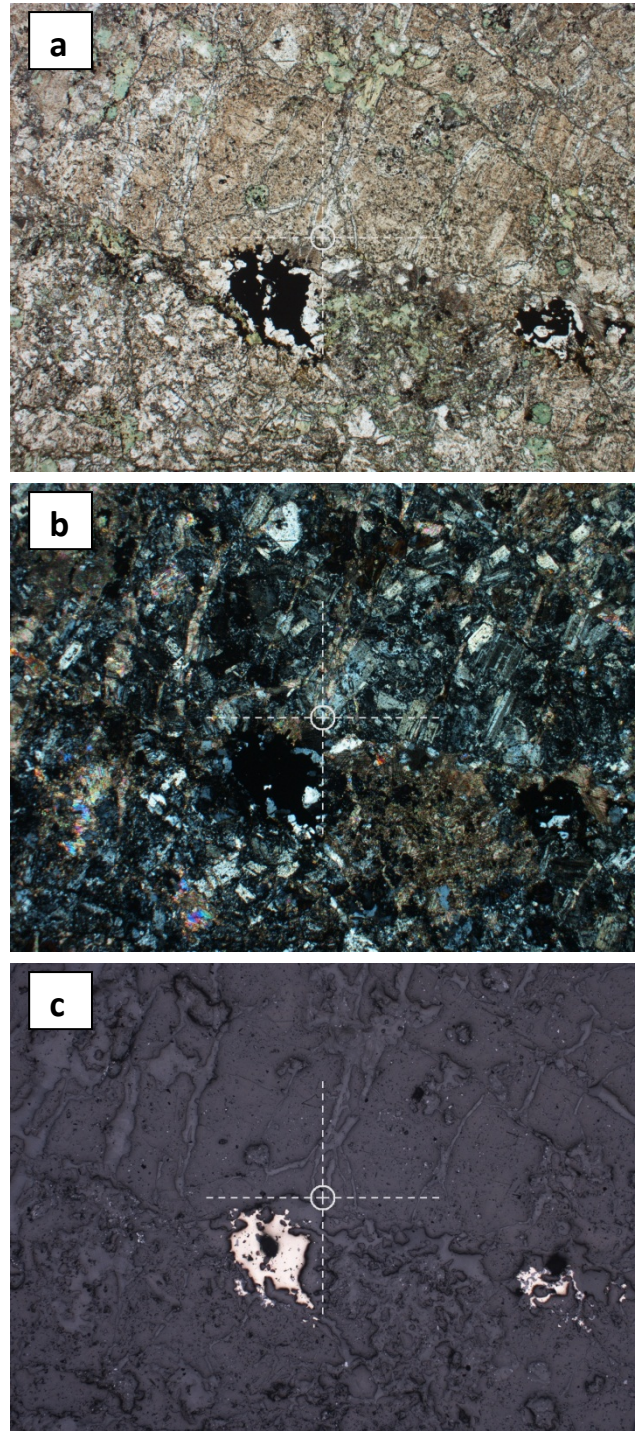


Fig. 15. Photomicrographs of mineralized porphyritic monzodiorite in Southwest zone. **a)** Plane polarized light view of dusty feldspar phenocrysts and matrix extensively cut by calcite veinlets. Chlorite alteration is widespread, but especially around opaques. **b)** Cross polarized light view shows trachytic alignment of plagioclase and admixture of high birefringence calcite with chlorite, and extensive calcite veinlets. **c)** Plane polarized reflected light view showing yellow chalcopyrite and minor domains of purple bornite alongside low relief patches of chlorite. Hematite occurs as fine dusting of bright blue-grey specks. Calcite veinlets are also visible as low relief linears. All images are the same field of view. Circle at crosshairs has a radius of 100 μ .

Table 2. Base metal and Pt, Pd analytical values from select samples. Analyses performed by Inductively Coupled Plasma – Mass Spectroscopy (ICP-MS) at Acme Analytical Laboratories Ltd., Vancouver. For a full suite of elements analyzed see Mihalynuk and Logan (2013b). Det. Lim. = detection limit. Coordinates are UTM zone 10, North America Datum 1983.

StatNum	UTME	UTMN	Mo	Cu	Pb	Zn	Ag	Fe	As	Au	Sb	Bi	Ca	P	Mg	Na	K	S	Hg	Pd	Pt
			Det. Lim.	0.01	0.01	0.01	0.1	2	0.01	0.1	0.2	0.02	0.02	0.01	0.001	0.01	0.001	0.01	0.02	5	10
			ppm	ppm	ppm	ppm	ppb	%	ppm	ppb	ppm	ppm	%	%	%	%	%	%	ppb	ppb	ppb
12JLO-2-15	682954	5483511	0.5	8899	2.37	24.3	997	3.16	2.7	3.5	0.04	0.09	4.32	0.154	1.6	0.066	0.1	0.67	10	45	3
MMI12-3-2	682908	5484278	0.28	288	5.37	51.2	229	5.01	1.8	26.1	0.16	0.15	7.73	0.133	1.99	0.019	0.09	2.53	14	11	6
MMI12-3-2b	682908	5484278	5.58	>10000	1.96	3.4	1938	2.19	2.2	42.9	0.49	0.37	2.88	0.112	0.19	0.067	0.07	0.58	21	15	4
MMI12-4-12	684661	5482763	0.64	116	2.57	56.9	60	3.97	19.9	9.4	0.26	0.04	4.44	0.168	2.34	0.047	0.18	0.05	15	<10	8
Std WGB-1			0.85	7204	11.27	79.4	3046	7.98	3.8	181.1	0.86	0.29	1.71	0.058	2.56	0.007	0.02	3.04	154	431	212
Std BCGS till 1999			0.85	202	236.64	352.5	1752	7.35	66.9	62	11.12	0.28	0.36	0.119	2.74	0.004	0.05	<0.02	371	<10	<2
Std GSBtill99			0.73	183	220.27	334.4	1660	7.34	61.9	27.1	7.86	0.22	0.35	0.114	2.84	0.01	0.05	<0.02	295	<10	<2
Std DS9			15.24	111	140.49	345.5	1981	2.34	28.4	140	5.69	8.03	0.74	0.09	0.62	0.085	0.4	0.17	224	135	405
Std DS9			12.97	113	130.1	312.9	1793	2.38	27	108.8	5.25	5.94	0.72	0.087	0.63	0.083	0.41	0.17	206	124	332

in a trench west of the main Granby Zone. At this locality, intensely fractured siliceous, and clay-altered rocks with veinlets of cryptocrystalline quartz contain substantial disseminated and veinlet chalcopyrite and malachite staining.

7.5. Mineralization geochemistry

PGE analysis was a focus of work by Nustar Resources Inc., (McLeod, 2000) who found that gold, palladium, and to a lesser extent, platinum, correlate with copper grade. Analyses reported here also show elevated Pd, up to 45 ppb, and to a lesser extent Pt in mineralized samples (Table 2, compare 12JLO-2-15 from the Southwest zone with BCGSStill99 standard). Elevated Pd and Pt seems to be a hallmark of the alkalic family of porphyry Cu-Au deposits in British Columbia (Nixon and Laflamme, 2002; Nixon, 2003), although Pt-Pd content does not always correlate with Cu content (Nixon, 2003).

8. Structure

Miner Mountain and the adjoining ridge to the north are near the core of an open syncline with regionally shallow north plunges, although some bedding orientations suggest local steep to moderate plunges. Strata maintain constant strike and dip on the eastern limb, but the western limb (west of Miner Mountain) is disrupted by multiple faults that cut bedding at high angles (Fig. 16a). Across these faults, bedding has rotated to variable degrees, such that dip directions vary along strike (Fig. 3). This regional fold has an unknown age relative to apparent small-scale folds intersected by drill core.

Near the bottom of vertical drillhole DDH MM09-11 is a folded tuff or tuffaceous sedimentary rock with a poorly developed, subhorizontal spaced cleavage (Fig. 16b). Petrographic analysis of this cleavage indicates evidence of minimal recrystallization and reorientation, opening the possibility of a soft sediment origin. It is possible that the fold was formed by syndepositional slumping. However, in the same drill hole, discrete subhorizontal ductile shear zones are consistent with significant subhorizontal shortening (or extension) which

could be related to the folds in drill core. Subvertical, quasi-ductile fabric in bornite-chalcopyrite-clay mineralization (Fig. 16a) indicates that some tectonic fabrics developed during or subsequent to mineralization. Given the incompetent nature of the mineralization, the fabric developed therein could have formed at low differential stresses.

Cherty tuff west of Miner Mountain peak is cut by brittle-ductile shears. These shears dip moderately to the northeast and may be related to southwest-directed thrusting (Fig. 17). Unfortunately, unambiguous shear sense indicators were not observed.

Previous mapping outlined the approximate trace of the Boundary Fault along the western side of the map area. This is a steep to moderately west-dipping fault that forms part of the eastern margin of the Eocene Princeton Basin. Its orientation and offset is consistent with the history of Eocene east-west extension across southern British Columbia. We expect that related, subsidiary structures are present, but were unable to confidently identify any.

9. Geochronology

We are unaware of any age determinations from geological units in the area mapped around Miner Mountain. In an effort to provide age context for the stratigraphic section and mineralized intrusions we have collected and submitted samples for ⁴⁰Ar-³⁹Ar age determination of the hornblende porphyritic breccia and U-Pb determination of the mineralized porphyritic diorite (see Fig. 3 for sample locations). Results are pending.

10. Summary

A six man-day mapping program was conducted in the area around Miner Mountain. Field observations, confirmed by petrographic work, necessitate a reinterpretation of the geological setting of Miner Mountain. Host rocks of the deposit appear to have been deposited mainly in a subaqueous arc flank setting not a subaerial arc axis setting as previously mapped. This setting is more like that of the Copper Mountain deposit, 25 km to the south-southwest. Quartz-deficient intrusions

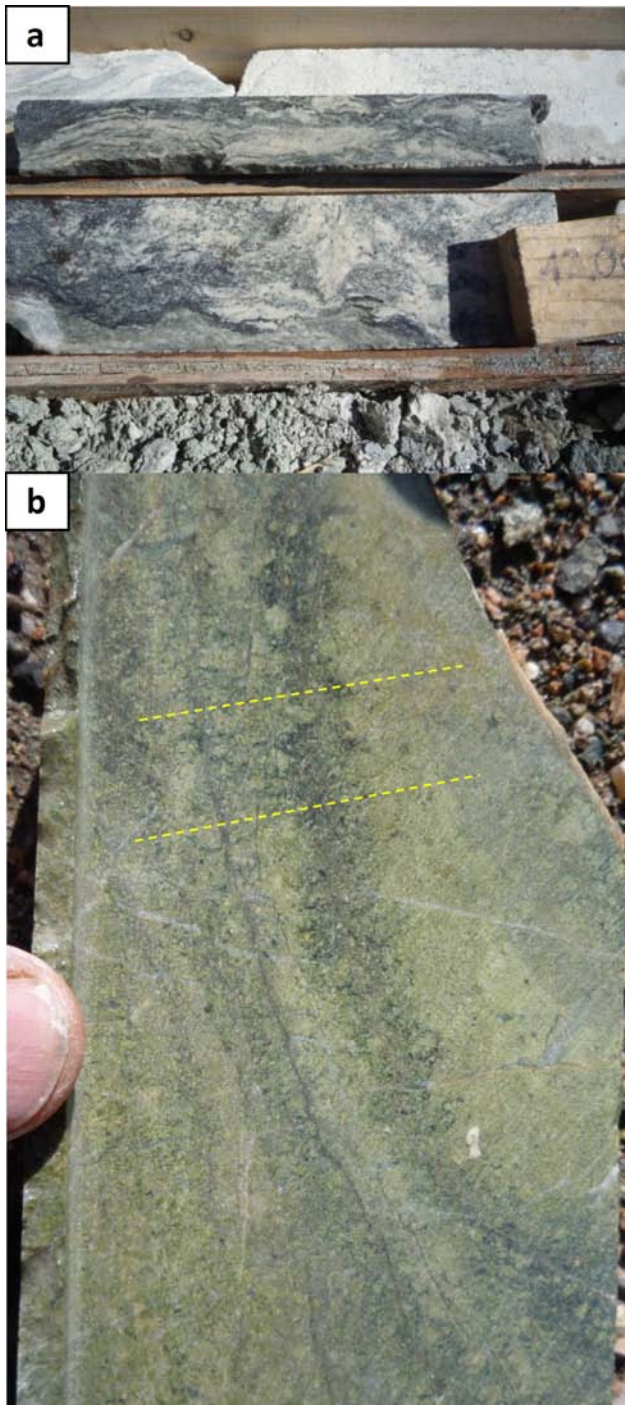


Fig. 16. a) Ductile fabric developed within siliceous, bornite-rich clay alteration zone. **b)** Strong epidote-chlorite alteration of folded tuffaceous rock possibly preserving a weak axial planar fabric as highlighted by yellow lines.

and a K-feldspar-magnetite alteration overprint of a more widely-developed propylitic mineral assemblage are typical of alkalic porphyry mineralization. Copper mineralization with elevated platinum-group element content also support an alkalic association; however, secondary quartz within mineralized diorite breccia is atypical of a British Columbia-type quartz deficient alkalic porphyry system (Logan and Mihalynuk, 2013).



Fig. 17. Low angle brittle shear zone within section containing "cherty tuff" and aphanitic, dark green rocks of probable volcanic origin.

Lack of biotite in the alteration assemblage may indicate that only high levels of the alteration system have been so far exhumed. Mineral exploration at Miner Mountain is ongoing. For latest exploration results refer to the company website, currently www.SegoResources.com.

Acknowledgments

Fieldwork was conducted following an informative orientation by Sego! Resources Inc. CEO J-P. Stevenson and explorationists A. Watson, D. Takagawa and C. Kauss. We thank V. Preto and S. Rowins for insightful reviews of an early draft of this paper, and L. Aspler for careful editorial analysis which significantly improved the final version.

References Cited

- Anderson, J.D., and Gower, J., 1959. Report on the geological, geochemical and geophysical surveys on the F.H. Group, BC Department of Mines and Petroleum Resources, Assessment Report 318, 25 p.
- Anonymous, 1972. GE. Geology, Exploration and mining in British Columbia, 1971. British Columbia Department of Mines and Petroleum Resources, p. 275.
- British Columbia Geological Survey, 2012. MINFILE – British Columbia mineral deposits database: British Columbia Ministry of Energy, Mines and Natural Gas (<http://minfile.gov.bc.ca/>).
- Christopher, P.A., 1981. Geological and prospecting report on the G.E. 1 and G.E. 3 claims, Princeton area, B.C. BC Ministry of Energy, Mines and Petroleum Resources, Assessment Report 10565, 8 p.
- Christopher, P.A., 2012. Technical report on the Miner Mountain copper-gold property, British Columbia, Public NI43-101 Report for Sego! Resources Inc., 63 p.
- Cochrane, D., 1968. Geophysical report on the G.E. and Vi mineral claims, Bald (Holmes) Mountain property, Princeton, BC. BC Department of Mines and Petroleum Resources, Assessment Report 1721, 35 p.
- Coney, P.J., Jones, D.L., and Monger, J.W.H., 1980. Cordilleran suspect terranes. *Nature*, 288, 329-333.
- Copper Mountain Mining Corporation, 2009, Copper Mountain production plan and reserves updated. Copper Mountain

- Mining Corporation press release, July 28, 2009 (http://www.cumtn.com/all_news/090728_Production_Plan_Reserves_Updated.pdf).
- Daley, S.P., Kauss, C., Takagawa, D., and Preto, V.A., 2012. Bedrock geology Miner Mountain, Princeton, B.C., unpublished map, Sego! Resources Inc., 1:2500 scale.
- Dolmage, V., and Campbell, D.D., 1963. Report on geology of Climax Copper Co. property, Princeton, B.C. (Unpublished company report #1), Property File. BC Department of Mines and Petroleum Resources.
- Fahrni, K., 1958. Geophysical Investigation of 22 claims of the Regal Group of mineral claims. BC Department of Mines and Petroleum Resources, Assessment Report 251, 21 p.
- Hopper, D.H., 1996. Geochemical report on the Concha claim group. BC Department of Mines and Petroleum Resources, Assessment Report 24070, 27 p.
- LeBas, M.J.L., Maitre, R.W.L., Streckeisen, A., and Zanettin, B., 1986. A chemical classification of volcanic rocks based on the total alkali-silica diagram. *Journal of Petrology* 27, 745-750.
- Livingstone, K.W., 1981. Geochemical survey report on the Old Baldy property, Princeton, B.C. BC Ministry of Energy, Mines and Petroleum Resources, Assessment Report 9634, 7 p.
- Livingstone, K.W., 1982. Lead-zinc geochemistry report, Old Baldy property, Princeton, B.C.. BC Ministry of Energy, Mines and Petroleum Resources, Assessment Report 10379, 8 p.
- Logan, J.M. and Mihalynuk, M.G., 2005. BC's 200 million year old porphyry Cu-Au deposits – an alkaline advantage, In: Association for Mineral Exploration British Columbia, Mineral Exploration Roundup, program with abstracts, pp. 13-15.
- Logan, J.M., and Mihalynuk, M.G., 2013. Tectonic controls on Early Mesozoic paired alkaline porphyry deposit belts (Cu-Au ± Ag-Pt-Pd-Mo) within the Canadian Cordillera. *Economic Geology*, in press.
- McInnes, B.I.A., McBride, J.S., Evans, N.J., Lambert, D.D., and Andrew, A.S., 1999. Osmium isotope constraints on ore metal recycling in subduction zones. *Science*, 286, 512-516.
- McLeod, J.W., 2000. Report on the Miner Mountain project. BC Ministry of Energy, Mines and Petroleum Resources, Assessment Report 26296, 28 p.
- McLeod, J.W., 2002. Magnetometer survey and rock exposure mapping report on the Miner Mountain property. BC Ministry of Energy, Mines and Petroleum Resources, Assessment Report 26902, 26 p.
- McMechan, R.D., 1983. Geology of the Princeton Basin. Province of British Columbia, Ministry of Energy, Mines, and Petroleum Resources, Paper 1983-3, 52 p.
- Mihalynuk, M.G., 2010. Recipe for Cu-Au-Ag ± Mo porphyry deposits: Ingredients from the northern Cordilleran terranes. In: Geological Association of Canada Copper Porphyry Workshop, Geological Association of Canada, Vancouver, BC, Canada.
- Mihalynuk, M.G., and Logan, J.M., 2013a. Geological setting of Late Triassic porphyry Cu-Au mineralization at the Dillard-Primer prospects near Merritt. In: Geological Fieldwork 2012, BC Ministry of Energy, Mines and Natural Gas, British Columbia Geological Survey, Paper 2013-1, (this volume).
- Mihalynuk, M.G., and Logan, J.M., 2013b. Lithochemical data from porphyry environments between Princeton and Merritt, BC Ministry of Energy, Mines and Natural Gas, Geofile 2013-in press.
- Mihalynuk, M.G., Logan, J.M., Friedman, R.M., and Preto, V.A., 2010. Age of Mineralization and "Mine Dykes" at Copper Mountain alkaline copper-gold-silver porphyry deposit (NTS 092H/07), South-central British Columbia. In: Geological Fieldwork 2009, BC Ministry of Energy, Mines and Petroleum Resources, British Columbia Geological Survey, Paper 2010-1, 163-171.
- Mihalynuk, M.G., Nelson, J., and Diakow, L.J., 1994. Cache Creek terrane entrapment - oroclinal paradox within the Canadian Cordillera. *Tectonics*, 13, 575-595.
- Monger, J.W.H., 1989. Geology, Hope, British Columbia. Geological Survey of Canada, Map 41-1989, 1:250 000 scale.
- Nicholls, E., and Gregotski, E., 1963. Report on induced polarization survey, Princeton, BC. BC Department of Mines and Petroleum Resources, Assessment Report 488, 18 p.
- Nielsen, P.P., 1977. Geophysical report of the induced polarization survey on the B.T.U. mineral claims. BC Ministry of Energy, Mines and Petroleum Resources, Assessment Report 6336, 19 p.
- Nixon, G.T., 2003. Platinum-group elements in the Afton Cu-Au porphyry deposit, southern British Columbia. In: Geological Fieldwork 2002, BC Ministry of Energy, Mines and Petroleum Resources, British Columbia Geological Survey, Paper 2003-1, pp. 263-290.
- Nixon, G.T., and Laflamme, J.H.G., 2002. Cu-PGE Mineralization in Alkaline Plutonic Complexes BC Ministry of Energy, Mines and Petroleum Resources, British Columbia Geological Survey, Geofile 2002-2.
- Parrish, R.R., and Monger, J.W.H., 1992. New U-Pb dates from southwestern British Columbia. In: Geological Survey of Canada, Radiogenic age and isotopic studies, Report 5, pp. 87-108.
- Pearce, J.A., 1996. A user's guide to basalt discrimination diagrams. Short Course Notes - Geological Association of Canada 12, pp. 79-113.
- Peccerillo, A., and Taylor, S.R., 1976. Rare earth elements in the East Carpathian volcanic rocks. *Earth and Planetary Science Letters*, 32, 121-126.
- Preto, V.A., 1972. Geology of Copper Mountain. British Columbia Department of Mines and Petroleum Resources, British Columbia Geological Survey, Bulletin 59, 87 p.
- Preto, V.A., 1975. GE, VI. In: British Columbia Department of Mines and Petroleum Resources, Geology, Exploration and Mining in British Columbia 1974, pp. 117-118.
- Preto, V.A., 1979. Geology of the Nicola Group between Merritt and Princeton. British Columbia Ministry of Energy, Mines and Petroleum Resources, British Columbia Geological Survey, Bulletin 69, 90 p.
- Read, P.B., 2000. Geology and industrial minerals of the Tertiary basins, south-central British Columbia British Columbia Ministry of Energy, Mines and Petroleum Resources, British Columbia Geological Survey, Geofile 2000-3.
- Reynolds, P., 1990. Geochemical report on the TNT claim. BC Ministry of Energy, Mines and Petroleum Resources, Assessment Report 20221, 23 p.

- Rice, H.M.A., 1947. Geology and mineral deposits of the Princeton map-area, British Columbia, Geological Survey of Canada, Memoir 243, 136 p.
- Rodgers, G. 2000. Geological and geochemical report JR 1-25 mineral claims, Rafter-F Ranch area, Princeton, B.C. BC Ministry of Energy, Mines and Petroleum Resources, Assessment Report 26305, 59 p.
- Sun, S.S., and McDonough, W.F., 1989. Chemical and isotopic systematics of oceanic basalts; implications for mantle composition and processes. Geological Society Special Publication 42, 313-345.
- Taylor, K.J., 1988. Soil geochemistry report for assessment on TNT claims, Princeton area, B.C. BC Ministry of Energy, Mines and Petroleum Resources, Assessment Report 17715.
- Tribe, S., 2010. Miner Mountain terrain study. Unpublished company report, Carta Exploration Ltd., 7 p.

Geological setting of Late Triassic porphyry Cu-Au mineralization at the Dillard Creek property near Merritt, southern British Columbia

Mitchell G. Mihalynuk^{1,a} and James M. Logan¹

¹ British Columbia Geological Survey, Ministry of Energy, Mines and Natural Gas, Victoria, BC, V8W 9N3

^a corresponding author: Mitch.Mihalynuk@gov.bc.ca

Recommended citation: Mihalynuk, Mitchell G. and Logan, James M., 2013. Geological setting of Late Triassic porphyry Cu-Au mineralization at the Dillard Creek property near Merritt, southern British Columbia. In: Geological Fieldwork 2012, British Columbia Ministry of Energy, Mines and Natural Gas, British Columbia Geological Survey Paper 2013-1, pp. 97-113.

Abstract

Porphyry copper mineralization in dioritic intrusive rocks that cut a volcanosedimentary section of the Nicola Group (Late Triassic) is exposed on the rolling hillsides and logging clearcuts at the Dillard Creek property, ~45 km southeast of Merritt. Three high-level tabular dioritic bodies display both potassic and calcic alteration assemblages. Two of the bodies (at the Primer South and Dill Lake prospects) are on the opposite limbs of a gently north-plunging syncline, and are partly elongated east-west. Although these bodies appear to form centres from which sets of moderately to steeply dipping diorite to quartz monzodiorite dikes (1 - >10 m wide) cut across the syncline, it remains unclear if they represent discrete stocks or sites of particularly high dike concentration. Geochemical and petrographic similarities between a hornblende-pyroxene volcanic breccia unit in the upper, predominantly epiclastic, part of the Nicola Group and the mineralized intrusions suggest emplacement of the latter shortly after a transition from mainly volcanic deposition, characterized by pyroxene (augite) units, to mainly epiclastic sedimentation. The apparent change in magma composition may signal increases in volatile and potassium content of the source region, chemical changes that enhance the Cu-Au fertility of the magma. Copper sulphides have commonly been liberated from the volcano-magmatic pile during low-grade metamorphism, demonstrating the high potential for Cu concentration by an efficient hydromagmatic system.

Keywords: Dillard Creek property, Dill Lake, Primer, copper gold porphyry, Nicola Group, Late Triassic, Quesnel terrane, potassic alteration, calcic alteration, litho geochemistry, Osprey Lake batholith, Pennask batholith, Kingsvale Group

1. Introduction

Field investigations in the Dillard Creek area between Merritt and Princeton (Fig. 1) in 2012, are part of the ongoing, province-wide porphyry copper project (Logan and Mihalynuk, 2005a). Project objectives include defining the geological setting and determining the structural and stratigraphic controls on porphyry Cu-Au ±Ag-Mo mineralization in Late Triassic and Early Jurassic arc rocks as an aid to mineral resource evaluation and exploration in the province. We report herein on fieldwork, petrography, and geochemistry of bedrock that underlies developed prospects near the headwaters of Dillard Creek (Fig. 2). In a companion paper (Mihalynuk and Logan, this volume), we provide a similar treatment for mineralization at Miner Mountain on the outskirts of Princeton, about 30 km south of Dillard Creek (see also Logan and Mihalynuk, 2013a, this volume).

2. Geological setting

Striking alignment of porphyry copper deposits along the magmatic axes of two arc terranes, Quesnel and Stikine (Coney et al., 1980) creates well-defined exploration targets in British Columbia. These arcs have the same Devonian through Triassic histories, including a remarkable metallogenic event: a pulse of metal-laden magmatism near the end of the Late Triassic, creating a

rich endowment of porphyry Cu-Au ±Ag-Pt-Pd deposits (Mihalynuk, 2010; Logan and Mihalynuk, 2013b). Tectonic events giving rise to this mineralizing pulse are discussed by Mihalynuk and Logan (this volume) and detailed in (Logan and Mihalynuk, 2013b). Herein we focus on the structural and stratigraphic setting of mineralization at the Dill Lake, Primer South, and Primer North developed prospects (Fig. 3; MINFILE 092HNE191, 55, 56). These prospects, at the headwaters of Dillard Creek, have collectively been referred to as the Dillard Creek property (Pringle, 1969). Late Triassic Nicola Group volcanosedimentary rocks that contain mineralization at the Dillard Creek property are interpreted to span the Late Triassic porphyry-forming event, based on correlation with layered and intrusive rocks to the west (Preto, 1979; Monger, 1989).

Younger rocks also occur in the map area (Fig. 3): granite of the Middle Jurassic Osprey Lake batholith intrude Nicola Group strata, and both are overlain by felsic volcanic rocks of the Cretaceous Spences Bridge Group (Monger, 1989; Massey et al., 2005).

3. Access and previous work

The Dillard Property can be reached by Highway 3 to Princeton, about 280 km east of Vancouver, then by following the Princeton-Summerland Road (8.5 km

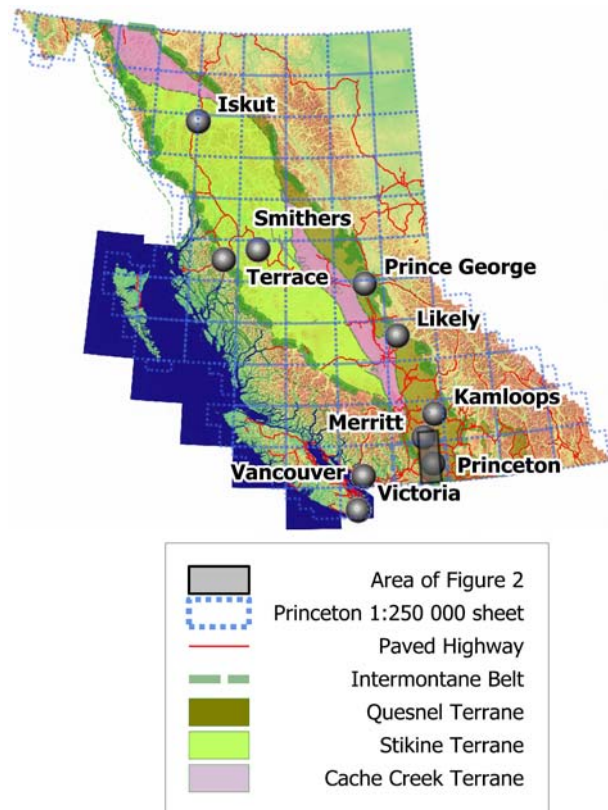


Fig. 1. Tectonic setting of southern Quesnel terrane and study area. Terrane boundaries modified after Tipper et al. (1981). Area of Figure 2 is shown by transparent grey box.

northeast) to the gravel Hembrie Mountain road and forest service roads (28 km north). Alternative access is via Highway 5 to Merritt, 260 km northeast of Vancouver, and then Highway 5A for 38 km southeast to the Loon Lake Road and gravel forest service roads that continue 20 km south to Dillard Lake. Most of the area is rolling and forested or clearcut (Fig. 4), with local steep rocky bluffs along glacial meltwater channels or modern valley sides.

Published maps covering the Dillard Property area at a scale appropriate for mineral exploration are lacking. Systematic regional mapping in the area dates to that of Rice (1947) and Monger (1989). The latter 1:250 000-scale map shows that the area is underlain by undivided “Eastern volcanic facies” mafic pyroclastic rocks and flows of the Nicola Group. Preto (1979) similarly defined the “Eastern Belt” west and northwest of the Dillard Property as submarine volcanic sedimentary rocks, lahar and basalt flows with comagmatic stocks. Mineral exploration in the area has resulted in a series of property-scale maps (e.g., Chapman, 1970; Guttrath, 1980) and drill hole logs (Tully, 1970).

4. Dillard Creek area geology

Field observations in 2012 reveal a north-trending syncline in which various stratigraphic levels of the Late Triassic Nicola Group section are exposed, much like the Miner Mountain area to the south (Mihalynuk and Logan, this volume) and perhaps related to broad folds east of

Missezula Lake as recognized by Preto (1979). Layered rocks are cut by small dioritic intrusive “stocks” having irregular outlines, and associated with significant copper-gold mineralization, although, in the case of the Primer South and Dill Lake prospects, these “stocks” are, at least in part, concentrations of porphyritic dikes. Younger intrusions include the western edge of the Middle Jurassic Osprey Lake batholith and an isolated piece of the Early Jurassic Pennask batholith. The youngest rocks are previously unmapped exposures of rhyolite correlated with the Cretaceous Spences Bridge Group mapped ~3 km to the south (Massey et al., 2005). Alternatively, these rocks could belong to the Eocene Princeton Group. A sample has been collected for isotopic age determination.

Figure 3 draws upon the results of our reconnaissance mapping, and compiles mapping (Chapman, 1970; Guttrath, 1980) and drill core logging (Tully, 1970) from assessment reports. In cases where rock types logged at the top of the holes disagree with early mapping, we incorporate the drill hole data. This is particularly an issue in the Primer North area where rocks were previously mapped as undifferentiated Nicola Group andesites, but were logged as “feldspar porphyry”, in agreement with our field observations. Major improvements in access and number of outcrops exposed from road construction during recent logging aided our mapping.

On Figure 3, dikes are shown to extend for up to 2.5 km. The width of individual dikes is exaggerated; as portrayed, the dikes represent sets having the same orientation, with individual dikes 1 - >10 m thick. The composite tabular nature of the intrusions can be seen in the drill logs from Tully (1970). Some inclined drill holes at Primer South cut more than 300 m of nearly continuous intrusion.

4.1. Layered rocks

Below we describe volcanic and sedimentary rocks in order of inferred ages, from oldest to youngest. We are unaware of any fossil or isotopic age data from rocks in this area, although the Nicola Group strata clearly extend beyond the map area to where their age is better defined.

4.1.1. Coarse augite porphyry breccia

Crowded, coarse augite porphyries, the hallmark unit of the Nicola Group, are widespread in the study area. The porphyries constitute clasts in volcanic breccias and lesser lapilli tuffs, but are also in rare autobrecciated flows up to several metres thick. This unit is basaltic in composition, with SiO₂ contents of less than 52% (Table 1, e.g., 12JLO-5-54). Both fresh and weathered outcrops are typically green because of ubiquitous chlorite and epidote alteration (Fig. 5). However, surfaces where the weathered rind has not been removed by erosion can take on a tan, light grey, or even cream colouration. Outcrops are typically angular and blocky, but may appear pockmarked and hackly where thermally altered, due to clots of resistant secondary minerals. Euhedral black or dark green pyroxene can comprise up to 25% of the rock, and is accompanied by subequal amounts of plagioclase,

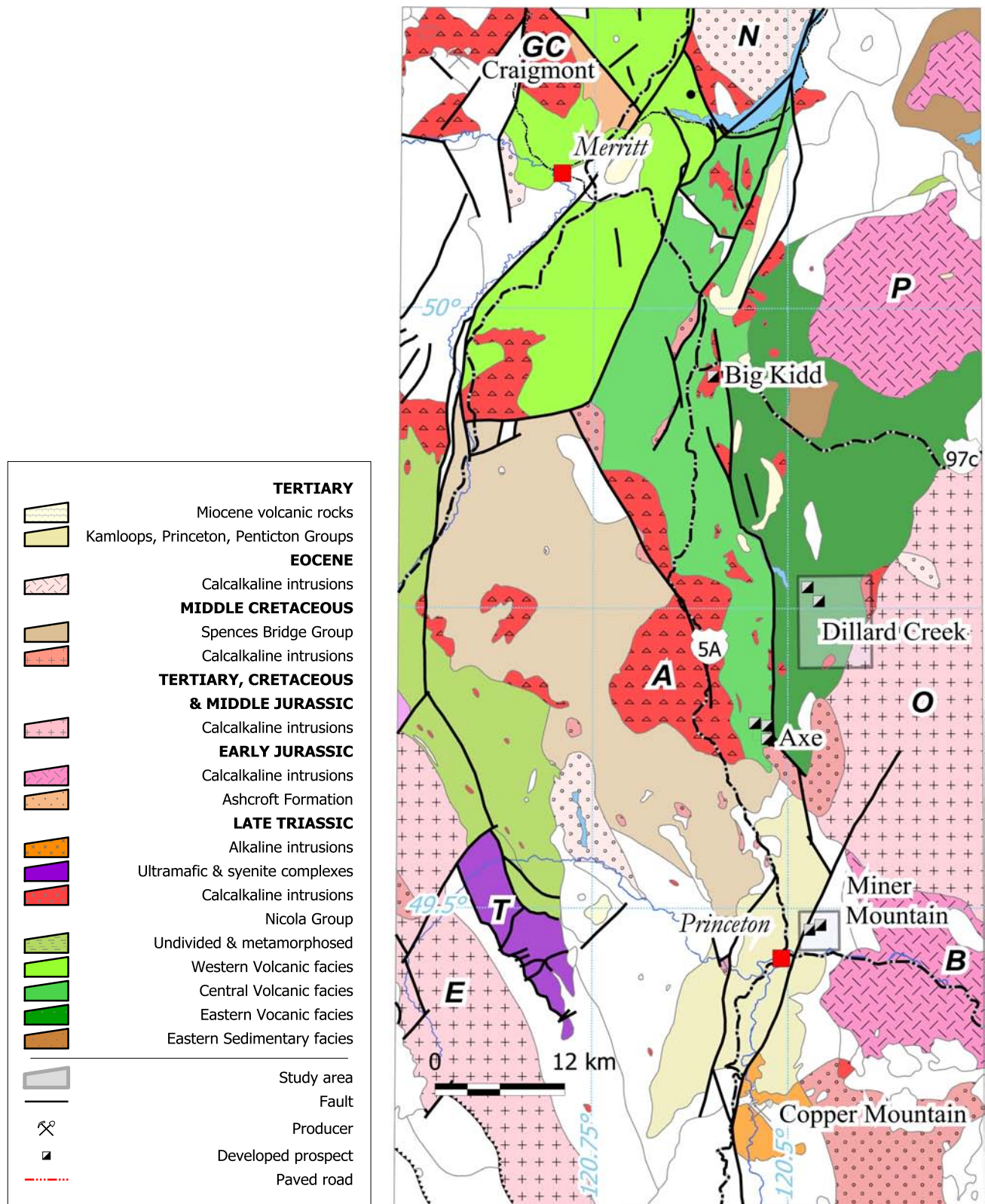


Fig. 2. Geological setting of 2012 field mapping in the Dillard Creek area between Princeton and Merritt (also shown is the Miner Mountain area; see Mihalynuk and Logan, this volume). Extents of Preto's Eastern Belt (mafic submarine volcanic and sedimentary rocks), Central Belt (arc axis, mafic volcanic and coeval intrusive rocks) and Western Belt (intermediate to felsic volcanic and sedimentary rocks) are shown for reference, as adapted from Massey et al. (2005). Abbreviations denote major plutons: A = Allison Lake, B = Bromley, E = Eagle, GC = Guichon Creek, N = Nicola, O = Osprey Lake, P = Pennask, T = Tulameen.

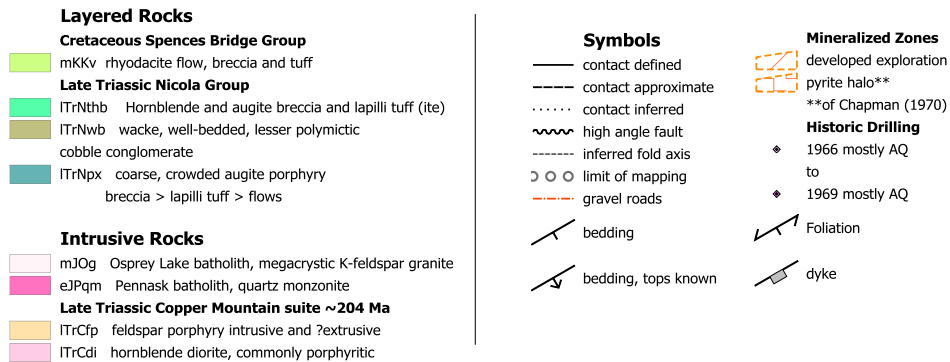
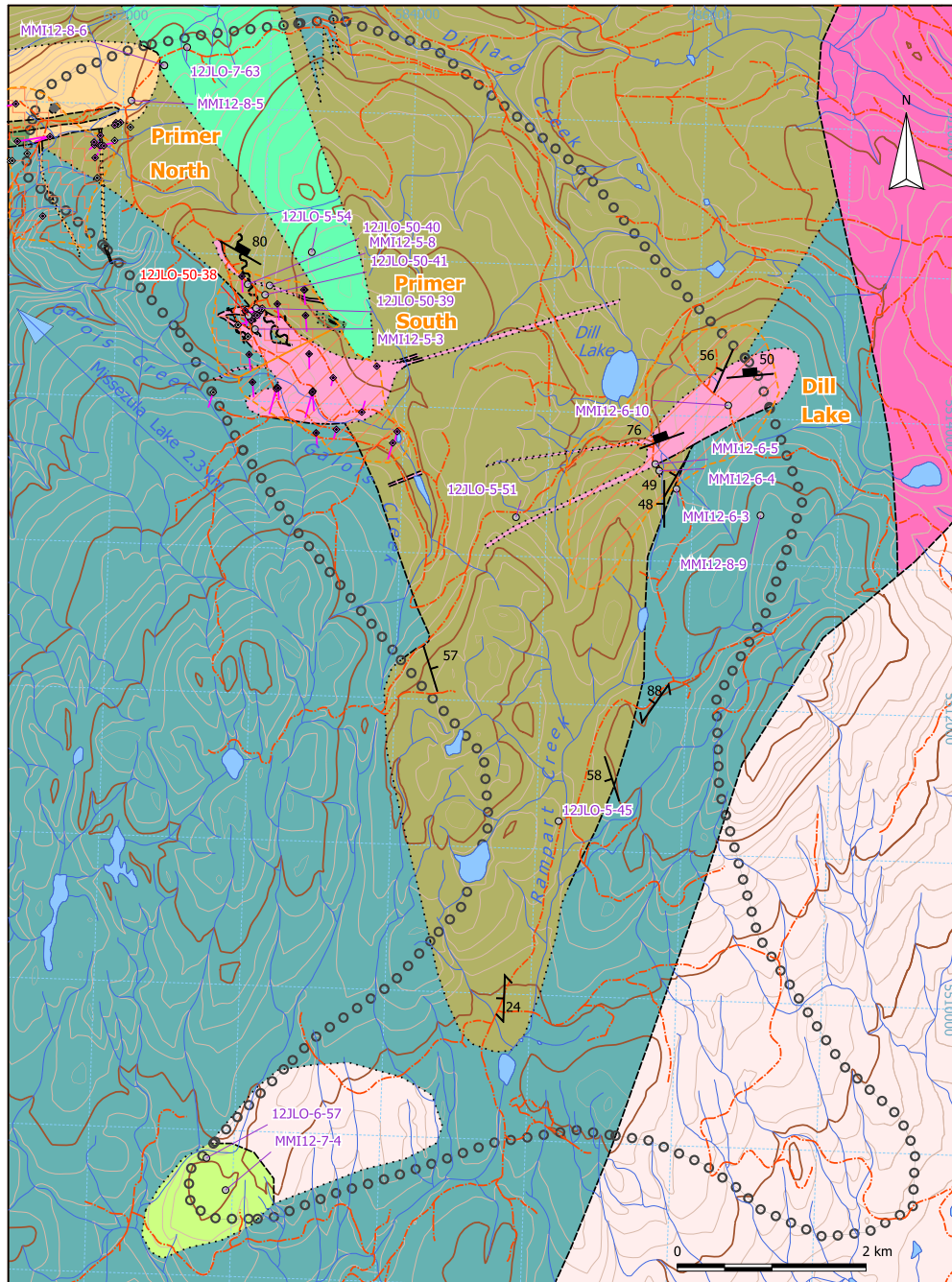


Fig. 3. Preliminary geology of the Dillard group of properties (Primer North, Primer South, Dill Lake); includes information compiled from Chapman (1970) and Gutrath (1980) and drill core logs from Tully (1970). Continuity and width of dikes may be exaggerated. Contacts with the Osprey Lake and Pennask batholiths are modified from Monger (1989).



Fig. 4. View from the eastern Dill property towards the west. Dill Lake (DL) is hidden in foreground valley on the right, with the Primer South property in the mid distance (PS, with patchy relics of forest).

which is altered to calcite, white mica, and prehnite, and 10% fine-grained magnetite that may be altered to hematite. Chlorite, calcite, and epidote veins are common.

4.1.2. Hornblende-pyroxene porphyry

A layer of hornblende-rich pyroxene breccia interrupts the epiclastic succession above the main pyroxene-porphyry unit. It is of unknown extent, but is assumed to wedge out laterally into epiclastic strata to the south. Its northern extent is entirely unconstrained by our mapping. Coarse euhedral pyroxene and euhedral to anhedral hornblende occur in subequal abundances of 15-20% each. Hornblende is commonly embayed to sieve-textured, apparently in disequilibrium with the melt in which it travelled prior to solidifying. Both matrix and clasts appear to be of the same composition, thus we interpret the bed as a pyroclastic deposit, although an epiclastic mass flow origin cannot be ruled out.

4.1.3. Epiclastic unit

An abrupt upward change from mainly pyroclastic to mainly epiclastic rocks is displayed in outcrops along the main haul road south of Dill Lake. The epiclastic rocks display prominent planar bedding (Fig. 7a), water escape structures, local synsedimentary slumps, and rare possible bioturbation structures. A lower unit, probably derived directly from underlying porphyries, comprises predominantly monomictic conglomerate to fine sandstone containing comminuted augite-phyric basalt fragments (Fig. 7a). An upper polymictic conglomerate unit contains augite-porphyry clasts and in similar proportions clasts also derived from the arc: hornblende and feldspar porphyries; hypabyssal intrusive rocks (diortite and monzonite); and sedimentary intraclasts (Fig. 7b). Our map coverage was insufficient to show subdivision of the epiclastic unit with any confidence.

4.1.4. Rhyolite breccia (Spences Bridge Group?)

Previously unmapped, mauve, pink, and tan flow-banded rhyolite breccia forms low outcrops scattered over more than 1 km² of a new logging clearcut in the southern

part of the area (Fig. 3). Breccia clasts contain fine- to medium-grained oxyhornblende ±biotite (3%), rectangular sections of beta-quartz (1%), and plagioclase ±sanidine (up to 15% combined) phenocrysts in an aphanitic to very finely granular groundmass (devitrified glass?) (Fig. 8). In unaltered outcrops the feldspars appear fresh, but mafic minerals are rimmed by clay alteration. Chalcedonic quartz lines flattened vesicles that are typically less than 5 mm across.

The rhyolite is locally pyritic, and oxidation of pyrite has produced a strong acid alteration and bleaching. Where the pyritic rock is exposed in road cuts it is highly weathered, and stained red (hematite) or yellow (jarosite?). Very low magnetic susceptibilities seem typical. Geochemical analysis of a single grab sample returned negligible base and precious metal values, but elevated As values of 158 ppm (Table 2, 12JLO6-57). Another small outlier of young intermediate to felsic volcanic rocks is in the northwest corner of the map area. There, brown, scaly-weathering, highly vesicular volcanic rocks likely form a thin veneer atop altered porphyry.

The rhyolite unit is interpreted as a series of coalescing flow domes. We include these occurrences in the Spences Bridge Group to maintain a nomenclature consistent with the nearest post-Jurassic felsic volcanic package. However, some volcanic units within the Eocene Princeton Group are also rhyolite (Church, 1973). We collected a sample for isotopic age determination in order to resolve the uncertainty (MMI12-7-4; Fig. 3).

4.2. Intrusive rocks

Intrusive rocks in the map area are correlated with suites of rocks that range from Late Triassic to Middle Jurassic. Of the intrusive rocks in the Dillard Lake area, only those correlated with the Middle Jurassic Osprey Lake batholith are demonstrably continuous with a well-dated body (166 ±1 Ma; Parrish and Monger, 1992). A wedge-shaped area in the northeast corner of the map area is underlain by intrusive rocks that are interpreted as an isolated part of the Early Jurassic Pennask batholith

Table 1. Major oxide analyses from Inductively Coupled Plasma – Mass Spectroscopy following lithium metaborate fusion of sample. Analyses performed at Activation Laboratories, Lancaster, Ontario. All values reported are weight %. Coordinates are UTM zone 10, North America Datum 1983.

StatNum	Unit	UTME	UTMN	SiO ₂	Al ₂ O ₃	Fe ₂ O _{3(T)}	MnO	MgO	CaO	Na ₂ O	K ₂ O	TiO ₂	P ₂ O ₅	LOI	Total
12JLO-5-54	ITrNpx	683327	5515033	48.33	15.81	10.51	0.257	4.93	7.98	3.04	3.65	0.743	0.57	3.93	99.74
12JLO-7-63	ITrNpx	682425	5516407	52.09	16.22	8.14	0.167	4.63	8.15	2.13	3.81	0.733	0.33	3.34	99.74
MM112-5-3	iTrCdi	682956	5514493	58.57	17.02	5.72	0.032	4.16	2.43	3.35	2.45	0.628	0.33	5.26	99.95
MM112-5-8	iTrCdi	683045	5514796	55.43	16.51	7.31	0.101	3.74	6.22	3.75	2.93	0.639	0.31	2.48	99.42
MM112-7-4	mKkv	682953	5508591	72.89	14.66	1.32	0.016	0.46	2.6	4.14	2.9	0.431	0.15	1.37	100.9
MM112-8-5	ITrCfp	682055	5516029	50.86	16.38	8.67	0.172	5.99	7.51	3.55	1.92	0.666	0.31	4.77	100.8
MM112-8-6	ITrNthb	682272	5516277	50.48	17.29	9.45	0.176	4.95	8.78	2.12	3.41	0.731	0.34	2.75	100.5
MM112-8-6b	ITrNthb	682272	5516277	50.2	17.15	9.42	0.175	4.92	8.84	2.1	3.37	0.728	0.36	2.76	100
MM112-8-9	ITrNpx	686467	5513337	49.24	13.34	10.92	0.221	8.11	11.91	2.42	1.43	1.104	0.29	1.34	100.3
Std MRG-1				38.59	8.43	17.42	0.167	13.26	14.72	0.71	0.18	3.705	0.07	1.45	98.71
Std WGB-1				48.83	10.91	6.33	0.135	9.14	16.34	2.15	0.91	0.885	0.09	3.8	99.51
			Det.				0.001	0.01							
			Limit	0.01%	0.01%	0.01%	%	%	0.01%	0.01%	0.01%	0.001%	0.01%	%	0.01%



Fig. 5. Typical augite-phyric volcanic breccia of the Nicola Group. Augite crystals are more obvious on some strongly weathered surfaces (Fig. 6).

(Massey et al., 2005), which has a U-Pb zircon age of ~195 Ma (Logan et al., 2011). Ages of other intrusive rocks are inferred on the basis of association and relative geological relationships.

4.2.1. Copper Mountain suite hornblende diorite

Hornblende diorite (to quartz monzodiorite) intrusions that cut Nicola Group strata have been the focus of mineral exploration in the Dillard Creek area. In part, these intrusions consist of a series of easterly trending dikes, some of which extend for up to 2.5 km (if intermittently exposed sections of dike along trend belong to the same body). The dikes are typically moderately to steeply dipping (both north and south), and may be 1 m to more than 10 m wide. Depicted schematically in Figure 3, are the two southern mineralized intrusions at Primer South and Dill Lake, which seem to be areas where hornblende diorite dikes are concentrated. The intrusion at Primer North is a hornblende-feldspar porphyry of a different character (see below).

Where unaltered, the hornblende diorite forms blocky light to dark grey outcrops. It is medium- to coarse-grained, with black hornblende (10-20%) and vitreous, zoned feldspar (70-80%). Isolated hornblende and feldspar crystals are up to 2 cm long. Fine, irregular, commonly embayed grains of magnetite comprise ~3% of the rock. Some variants are quartz monzodiorite. For example, where orthoclase is more abundant than

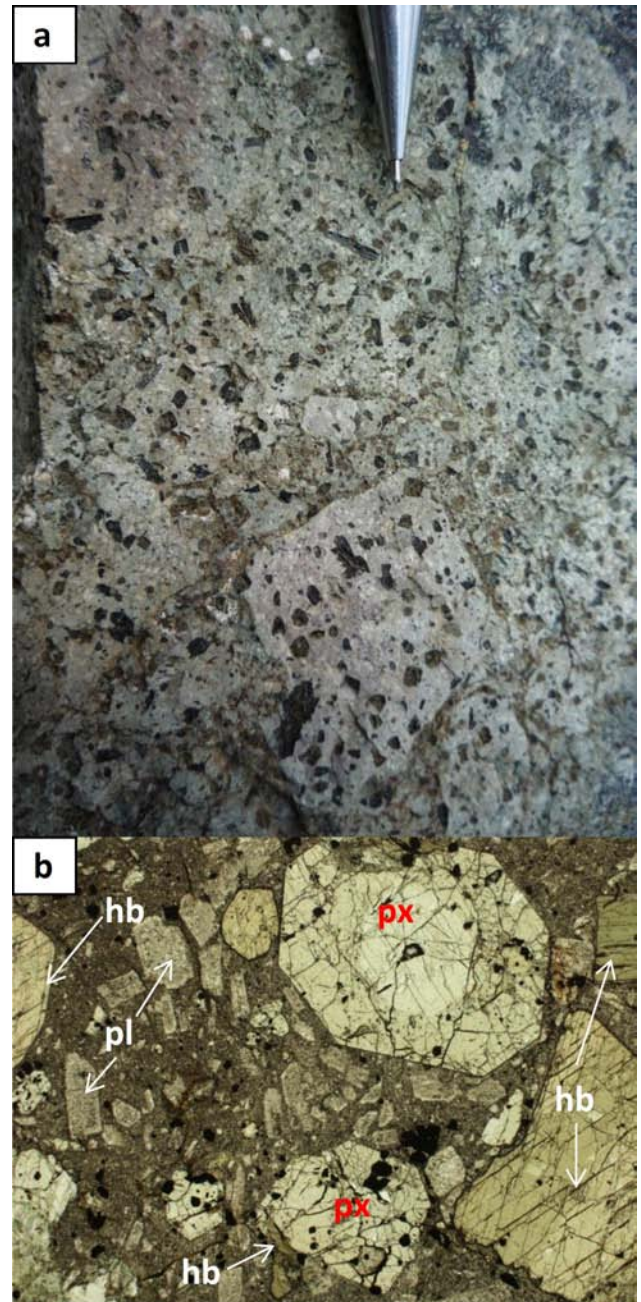


Fig. 6. Coarse zoned pyroxene and hornblende-phyric breccia in outcrop **a**) and in thin section **b**). In **b**), hb = hornblende and px = zoned pyroxene; note pyroxene at bottom centre partly engulfs a hornblende crystal. Turbid plagioclase is medium grained in a devitrified matrix with fine granular opaque minerals. Field of view is 4 mm.

plagioclase, and where the little matrix that exists in the holocrystalline intrusions is quartz, it comprises as much as 10% of the rock. Porphyritic intrusions can be crowded or sparsely populated with 1-10 mm subhedral hornblende laths and 2-5 mm plagioclase (and sanidine?) in a devitrified groundmass dusted with magnetite. A trachytic alignment of the crystals is common in both holocrystalline and porphyritic variants. Where mineralized, chalcopyrite is disseminated, and most broken samples contain a paper thin chalcopyrite veinlet

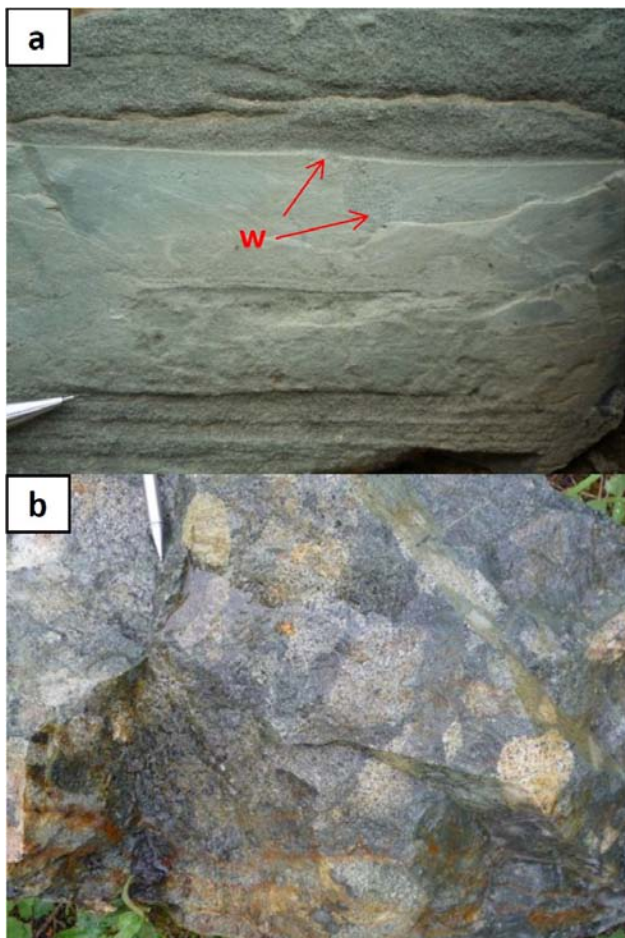


Fig. 7. Epiclastic unit. **a)** Well-bedded sandstones derived from augite-porphry volcanic units (W = possible bioturbation or water escape features). **b)** Coarse polymictic conglomerate containing clasts of hypabyssal hornblende-feldspar porphyry-like units that cut the underlying augite porphyry breccia unit.

or two. Rounded xenoliths of pyroxene-phyric volcanic rock are common. Magnetic susceptibilities range between 20 and 45×10^{-5} SI (and higher or lower where altered).

At the Dill Lake prospect, coarse trachytic plagioclase- and hornblende-phyric monzodiorite intrudes thinly bedded and bleached, pyritic (1-2%) sandstone. The monzodiorite is white weathering and massive to well jointed. Euhedral, white stubby plagioclase phenocrysts are 3-5 mm in size. Hornblende is 2-3 mm long and, together with the intrusive groundmass, is altered to epidote, actinolite, chlorite, quartz and pyrite (~1%) (Fig. 9). Disseminated magnetite is common and magnetic susceptibilities range between 17 and 35×10^{-5} SI.

On the west side of Primer South is an area of a few 100 m² with sparse outcrops of medium- to coarse-grained pyroxene-hornblende gabbro with 50% coarse plagioclase and hornblende (after pyroxene?) in a fine-grained, white, feldspathic groundmass. Gossanous “veins” up to 15 cm thick contain traces of malachite and



Fig. 8. Rhyolite breccia clasts containing oxyhornblende (±biotite)-quartz-plagioclase ±sanidine-porphyrific rhyolite. This unit is mapped as the mid-Cretaceous Spences Bridge Group, but could be part of the Eocene Princeton Group.

are probably weathered-out pyrite with minor chalcopyrite. This gabbro is interpreted as a border phase, intrusive-country rock hybrid. Magnetic susceptibilities are near 100×10^{-5} SI.

Like other workers (e.g., Preto, 1979; Monger, 1989; and authors of most assessment reports cited herein) we assume these intrusions equivalent with the Late Triassic Copper Mountain suite. We collected a sample with fresh hornblende for ⁴⁰Ar/³⁹Ar isotopic age determination (MMI12-5-8) to test this correlation. These intrusions cut both the augite porphyry units and the lower epiclastic package, but also appear to have provided detritus for polymictic conglomerates higher in the Nicola Group stratigraphy. On this basis, they should be Late Triassic in age, broadly time equivalent to mineralizing intrusions at Copper Mountain (Mihalynuk et al., 2010). If the mineralized intrusions at Dill Lake and Primer South did form as a dense concentration of dikes, this mode of occurrence is different than the discrete stocks at Copper Mountain. However, significant copper mineralization associated with dike concentrations is not unprecedented in British Columbia. One good example of an alkalic porphyry Cu-Au deposit where the mineralizing intrusions are dike-like, is the massive Galore Creek deposit in northwestern part of the province.

Table 2. Base metal and Pt, Pd analytical values from samples collected in the Dillard Creek area, away from localities obviously sampled previously. Analyses performed by Inductively Coupled Plasma – Mass Spectroscopy (ICP-MS) at Acme Analytical Laboratories Ltd., Vancouver. For a full suite of elements analyzed see Mihalynuk and Logan (2013b). Coordinates are UTM zone 10, North America Datum 1983.

StatNum	UTME	UTMN	Mo	Cu	Pb	Zn	Ag	Ni	Fe	As	Au	Sb	Bi	V
12JLO-5-45	685153	5511196	0.15	125.55	3.13	27.3	121	4.8	2.48	1.9	1.4	0.1	0.22	83
12JLO-5-51	684790	5513267	77.38	29.34	1	10.6	308	4.9	2.97	3.1	4.9	0.15	0.17	94
12JLO-6-57	682815	5508807	14.64	41.84	0.88	18.8	25	4.2	1.22	158.3	<0.2	0.1	0.11	31
12JLO-8-81	677388	5503059	0.34	3689.06	1.2	57.7	648	7.3	3.12	4.8	337.5	0.32	<0.02	109
MM112-6-3	685884	5513498	0.48	333.28	3.09	69.9	1125	22.1	3.25	6.1	135.2	0.1	0.46	101
MM112-6-4	685762	5513618	0.32	350.86	4.84	71.3	223	14.2	3.02	2.8	7.2	0.27	0.05	145
MM112-6-5	685733	5513664	3.08	715.9	16.52	58.3	708	11.1	1.93	3.5	18.1	0.21	0.19	93
MM112-6-10	686220	5514083	0.05	29.44	1.35	10.5	99	11.1	2.38	1.9	73.9	0.14	0.18	91
MM112-6-10b	686220	5514083	0.13	281.28	1.86	14.7	431	11.6	2.33	2.7	67	0.29	0.32	79
12JLO50-30	685019	5484773	5.12	131.1	1.29	22.6	399	3.3	1.55	8.1	38.3	1.67	0.02	12
12JLO50-38-3	682908	5514583	0.03	4.09	2.12	65	17	3.1	3.23	0.6	1.8	0.1	<0.02	98
12JLO50-39	682958	5514637	4.79	111.04	0.77	25.7	68	5.2	2.13	1.6	1.1	0.13	<0.02	28
Std WGB-1			0.85	7204.1	11.27	79.4	3046	3418.4	7.98	3.8	181.1	0.86	0.29	59
Std BCGS till1999			0.85	202.65	236.64	352.5	1752	293.2	7.35	66.9	62	11.12	0.28	135
Std BCGS till1999			0.73	183.46	220.27	334.4	1660	214.2	7.34	61.9	27.1	7.86	0.22	103
STD DS9			15.24	111.43	140.49	345.5	1981	40.6	2.34	28.4	140	5.69	8.03	54
STD DS9			12.97	113.43	130.1	312.9	1793	41.3	2.38	27	108.8	5.25	5.94	41
			ppm	ppm	ppm	ppm	ppb	ppm	%	ppm	ppb	ppm	ppm	ppm
		det. Limit	0.01	0.01	0.01	0.1	2	0.1	0.01	0.1	0.2	0.02	0.02	2

Table 2. Continued.

StatNum	UTME	UTMN	Ca	P	La	Cr	Mg	Na	K	S	Hg	Se	Pd	Pt
12JLO-5-45	685153	5511196	0.88	0.086	6.6	59.1	0.68	0.092	0.38	<0.02	<5	<0.1	<10	<2
12JLO-5-51	684790	5513267	2.44	0.19	3.6	24.8	0.48	0.04	0.05	1.96	33	0.6	21	7
12JLO-6-57	682815	5508807	0.08	0.037	3.5	26.9	0.04	0.065	0.1	0.67	<5	<0.1	<10	<2
12JLO-8-81	677388	5503059	0.79	0.102	2.8	19.8	1.36	0.051	0.1	0.03	14	2.3	<10	<2
MM112-6-3	685884	5513498	0.82	0.136	3.5	40.5	1.48	0.064	1.04	0.69	9	0.8	<10	4
MM112-6-4	685762	5513618	0.98	0.134	1.8	48	1.54	0.093	0.46	0.04	24	0.2	<10	4
MM112-6-5	685733	5513664	0.89	0.141	7.4	34.2	0.98	0.06	0.11	0.07	29	0.5	<10	2
MM112-6-10	686220	5514083	1.15	0.119	1.9	52.6	0.43	0.168	0.41	2.01	250	0.9	<10	2
MM112-6-10b	686220	5514083	0.94	0.124	2.1	35.2	0.56	0.098	0.16	1.05	281	2.4	<10	4
12JLO50-30	685019	5484773	4.03	0.053	2.5	34.1	0.4	0.049	0.18	0.13	21	0.6	<10	<2
12JLO50-38-3	682908	5514583	1.74	0.116	20.3	43.3	1.17	0.149	1.58	0.04	16	0.2	<10	<2
12JLO50-39	682958	5514637	1.07	0.057	2.9	55	0.54	0.15	0.16	0.61	8	1.4	<10	<2
Std WGB-1			1.71	0.058	3.2	275.5	2.56	0.007	0.02	3.04	154	14.2	431	212
Std BCGS tii11999			0.36	0.119	14.4	265.8	2.74	0.004	0.05	<0.02	371	0.7	<10	<2
Std BCGS ti111999			0.35	0.114	13.4	236.7	2.84	0.01	0.05	<0.02	295	0.7	<10	<2
STD DS9			0.74	0.09	15.5	132.3	0.62	0.085	0.4	0.17	224	6	135	405
STD DS9			0.72	0.087	12.5	115.6	0.63	0.083	0.41	0.17	206	5.6	124	332
			%	%	ppm	ppm	%	%	%	%	ppb	ppm	ppb	ppb
		det. Limit	0.01	0.001	0.5	0.5	0.01	0.001	0.01	0.02	5	0.1	10	2



Fig. 9. Chlorite-epidote altered porphyritic diorite displays pale green epidote vein selvage alteration overprinted on a broader K-feldspar flush. Dark green-black vein in centre of photo is chlorite-actinolite-pyrite with minor chalcopyrite.

4.2.2. Feldspar porphyry intrusives and flows?

Coarse hornblende- and medium-grained feldspar porphyry forms blocky outcrops at the Primer North prospect. A strong trachytic fabric is generally displayed. The rock may be relatively fresh, cut by widely spaced epidote and calcite veins, or pervasively pyritic \pm biotite-flooded and indurated. Where altered, granular feldspar comprises \sim 70% of the rock, together with 15% fine-grained secondary biotite (and chlorite) and up to 5% pyrite in clots and veins up to 5 mm thick. Alteration masks contacts between the porphyry and surrounding pyroxene-bearing tuffite. Even at fresh exposures, we were unable to unequivocally determine whether this unit represents flows or a hypabyssal intrusion. We correlate this unit with the Copper Mountain suite, following earlier interpretations, but careful mapping and geochronologic work are needed to verify this assumption.

4.2.3. Monzonite dikes

At the Primer North property a series of orange to pink or white felsic dikes cut indurated, hornfelsed, pyritic epiclastic country rocks. They are steep, north-trending, 1.5 - $>$ 3.5 m wide, and display sharp, chilled contacts. Medium-grained, salmon pink feldspar comprises \sim 40% of the rock within an altered white groundmass; where less altered, the feldspars are white in

a pink groundmass. In either case, mafic minerals are totally replaced by clots of chlorite.

4.2.4. Osprey Lake granite

Osprey Lake batholith is a large composite intrusive complex that extends from the map area to ridges west of Okanagan Lake, \sim 70 km away. As expected for a body of this size, the country rocks display a strong thermal-metamorphic halo, which extends for at least 0.5 km from its western contact into the study area.

Typical outcrops of Osprey Lake granite are white to pinkish-grey and rounded to blocky. Conspicuous K-feldspar megacrysts up to 5 cm (20%) are supported by a groundmass of medium- to coarse-grained plagioclase, orthoclase, and grey quartz (Fig. 10). Megacrysts have zones outlined by hornblende microlytes and exterior zones that are white albite (?). Medium-grained biotite forms 3-5 mm euhedral to subhedral books. It constitutes \sim 10% of the rock, and medium-grained hornblende comprises \sim 6%. Equant plagioclase and pinkish matrix K-feldspar comprises \sim 60% of the rock volume. Accessory minerals identifiable in hand sample include euhedral, honey brown titanite (0.5-1%) and magnetite. Xenoliths of hornblende diorite are common. Magnetic susceptibilities range between 20 and 38×10^{-5} SI.

4.2.5. Rhyolite dikes

Decimetre wide dikes of white to pale pink, quartz-eye porphyry rhyolite intrude hornblende diorite at the Primer South prospect. The rock is characteristically flow-banded, fine grained, and contains miarolitic cavities. Relict 1-2 mm biotite and oxidized pyrite crystals are visible in a pervasive quartz-sericite-pyrite- and clay-altered groundmass. Unlike intrusions of presumed Late Triassic age, malachite was not visible within or adjacent to the dike contacts. Magnetic susceptibility values are very low.

These felsic dikes are lithologically similar to the rhyolite flows identified in the southern part of the map area, and may represent feeders to the Cretaceous Spences Bridge Group.

5. Litho geochemistry

Representative samples were collected from the Dillard Creek area for major oxide and trace element analysis with a bias towards the mafic part of the Late Triassic stratigraphy: hornblende and pyroxene-phyric breccia units and diorite. Major oxide analyses are reported in Table 1; major and trace element analyses are available in downloadable format from Mihalynuk and Logan (2013b). Select major oxide and trace element concentrations are shown on Figure 11.

Most pyroxene porphyry samples, and all of the hornblende-pyroxene tuff samples, fall within the shoshonitic basalt series, based on the K_2O versus SiO_2 classification of Peccerillo and Taylor (1976; Fig. 11a). Diorite samples belong to the high-K calcalkaline series, and their volcanic equivalents range from basalt (MMI12-8-5) to andesite (MMI12-5-3). The Spences Bridge



Fig. 10. Distinctive zoned K-feldspar megacrysts in Osprey Lake batholith.

rhyolite sample is shown by the star in Figures 11a and 11b. Na_2O contents of all mafic volcanic rocks exceed 2 weight % (represented by green bars on Fig. 11a), so that on the Total alkalis - silica space ($\text{Na}_2\text{O} + \text{K}_2\text{O}$ vs. SiO_2 , not shown) they are also classified as alkaline ($>5\%$ $\text{Na}_2\text{O} + \text{K}_2\text{O}$) over the range of basalt to basaltic andesite (LeBas et al., 1986).

In contrast, application of the trace element alkalinity index Nb/Y (Pearce, 1996) shows that the mafic volcanic units are not alkaline (Fig. 11b). In some environments, this discrepancy could be attributed to addition of alkalis during alteration, an especially likely event in volcanic rocks deposited in a submarine environment, as has been interpreted regionally (e.g., Preto, 1979). In this case however, the low Nb/Y index arises from the deep Nb-Ta depletion: a strong arc signature, as shown on the Primitive Mantle – normalized spider diagram (Sun and McDonough, 1989) of Figure 11c. Samples collected from hornblende diorite intrusive units that cut the basalts, display the same range of Nb/Y as do samples of Nicola Group from elsewhere, including units known to contain analcime (Preto, 1979; shown as grey triangles with olive outlines on Fig. 11b). Thus, the intrusions are interpreted as comagmatic with the basalts, a contention supported by clasts of hornblende diorite within strata intercalated with the volcanic units.

Other geochemical features of arc basalt include Ti depletion and enrichment in large ion lithophile elements

shown on the left side of Figure 11c (e.g., Cs, Rb, Ba, K, Sr). These rocks lack a Eu anomaly (Figs. 11c, d), suggesting that feldspar was neither a residual phase in the source area, nor was it removed from the crystallizing melt. All units are uniformly light rare earth element (LREE) enriched compared to chondrite values (Fig. 13d; Sun and McDonough, 1989) and show similar parentage (Figs. 11c, d). However, a systematic increase in heavy rare earth elements in hornblende-bearing samples may indicate magmatic contributions from a region that sequesters HREE, perhaps garnet-bearing metasomatized mantle. Shaded fields on both Figures 11c and 11d are those of mafic volcanic and dioritic rocks in the Miner Mountain area. They are nearly identical in geochemical character to the rocks at Dillard Creek, but show a definite relative LREE enrichment.

6. Alteration and mineralization

Early mapping of alteration zones at the Dillard Creek property (Chapman, 1970), partly delimited zones of pyrite (Fig. 3). These zones are superimposed on regional prehnite-pumpellyite grade metamorphic mineral assemblages (prehnite and/or pumpellyite and epidote-chlorite-albite) that are typically developed in the augite porphyries and derived volcaniclastic rocks of the Nicola Group (Fig. 12). Our mapping was insufficiently detailed to permit delineation of authigenic mineral zones. However, different alteration assemblages are associated with different intrusive phases. Hornblende diorite (to quartz monzonite) at Dill Lake and Primer South display both calcic and potassic alteration assemblages including actinolite-epidote-magnetite-calcium carbonate-pyrite-chalcopyrite \pm quartz, and K-feldspar-biotite-magnetite-chalcopyrite \pm pyrite (with minor inclusions of pyrrhotite) (Fig. 13).

Calcic alteration assemblages are predominant near trenches at the Primer South and Dill Lake prospects. Potassic alteration is subordinate and apparently younger, although timing is not well established. Secondary biotite and chalcopyrite assemblages at Primer South are cut by quartz veinlets containing carbonate, sulphides, and (?) gold values (e.g., MMI12-6-3, Table 2). Gold is also associated with quartz carbonate veins cutting albite-actinolite-epidote-pyrite- altered hornblende diorite in the area around Dill Lake (Cormier, 1990; Table 2).

In addition, carbonate alteration of some dikes is intense (Fig. 12b) and includes calcite (\pm Mg and Fe carbonates?) - pyrite \pm white mica \pm quartz. At Primer South, carbonate alteration seems to be related to a specific suite of dikes, but nowhere did we see the same dikes pass from an intensely altered to unaltered state. And because all carbonate-altered dikes seem to contain relicts of both hornblende and plagioclase, they cannot be distinguished, on this basis, from the other mineralized diorite dikes.

7. Structure

Bedding orientations and the distribution of volcanic and sedimentary facies outline a broad syncline that plunges gently and opens to the north. Outcrops in the

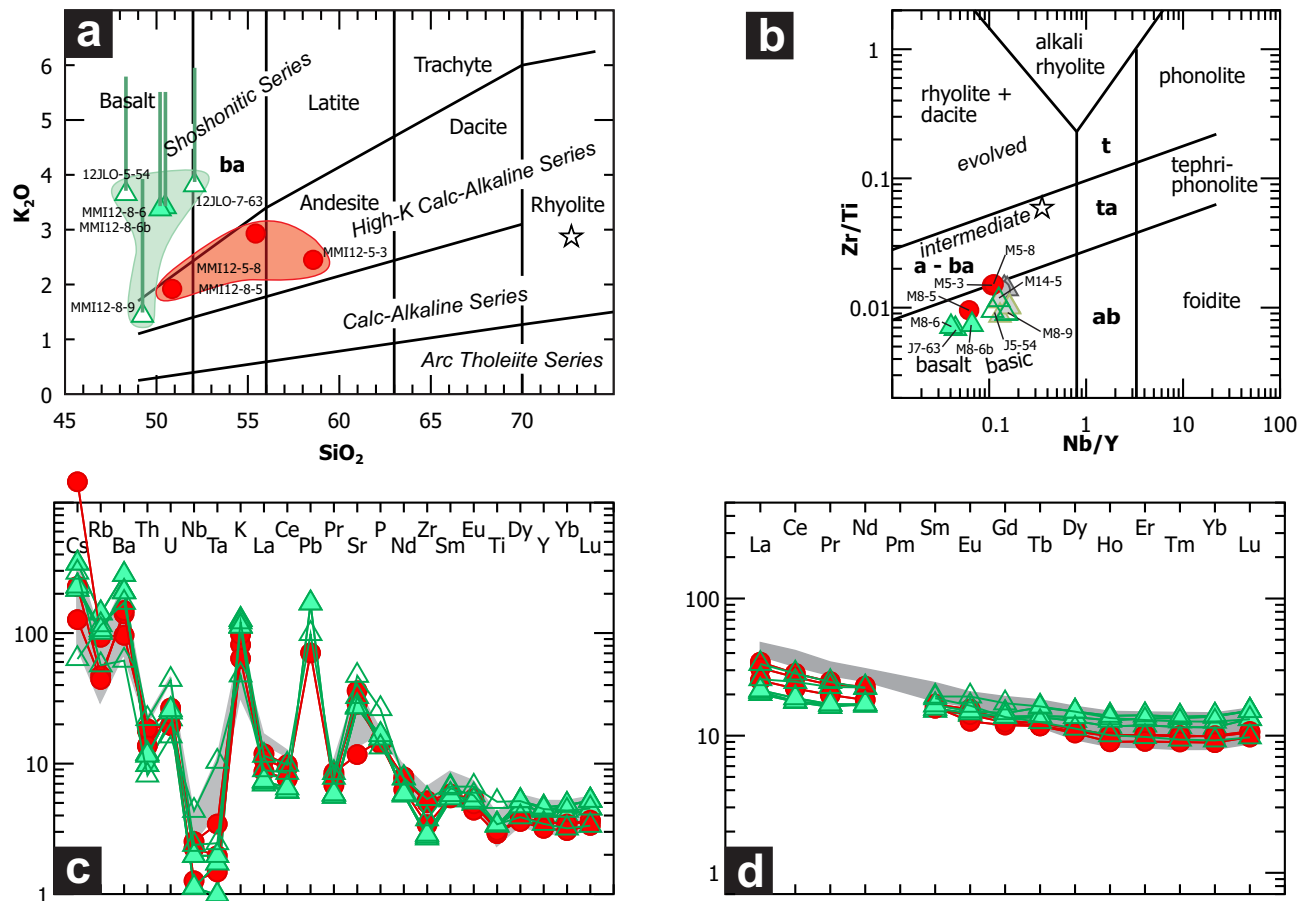


Fig. 11. Geochemical character of pyroxene-phyric basalt (open triangle), hornblende-pyroxene-phyric basalt (green-filled triangle), diorite (solid red circle, includes hornblende-feldspar porphyry of Primer North, MMI12-8-5), and Spences Bridge Group rhyolite (star), are shown by **a**) Plot of K_2O versus SiO_2 , fields after (Peccerillo and Taylor, 1976), with oxides normalized with removal of components lost on ignition (LOI – see Table 1). **b**) Zr/Ti versus Nb/Y with fields after (Pearce, 1996). **c**) Primitive mantle normalized spider diagram and **d**) Chondrite-normalized rare earth element plot, using normalization factors of (Sun and McDonough, 1989). Abbreviations: a = andesite, ab = alkali basalt, ba = basaltic andesite, t = trachyte, ta = trachyandesite. Grey fields on c) and d) and dark grey-outlined grey symbols on b) are from similar rocks in the Miner Mountain area (Mihalynuk and Logan, this volume), olive-outlined grey symbols in b) are from analcime-bearing Nicola Group basalt (analcime identified by Preto, 1979).

hinge zone display a strong, near-vertical foliation indicating an upright fold. A shallow foliation near the southern limits of mapping is imparted by intrusion of the Osprey Lake batholith and partly defined by growth of garnet, epidote and hornblende.

Steeply dipping brittle fault zones are common, but the limited exposures do not provide opportunities to assess the amount or sense of offset. Slickenside orientations reveal no clear regional trends. If dikes can be traced for kilometres, as we infer on Figure 3, horizontal offsets on faults at high angles to the dikes must be minimal within the map area.

8. Summary

Dillard Creek property is located within the submarine volcanic and sedimentary “Eastern Belt” of (Preto, 1979). Mineralized intrusive centres at Dill Lake, Primer South and Primer North are all related to irregular

or east-west elongated hornblende feldspar porphyry or holocrystalline diorite to quartz monzodiorite bodies.

These bodies intrude both the east and west flanks of a gently north-plunging syncline. The Dill and Primer South bodies appear to have been centres from which moderately to steeply dipping dikes cut across the syncline. It is uncertain however, if the bodies are continuous “stocks” or sites of high dike concentration. Hypabyssal dioritic clasts within the sedimentary succession may indicate pencontemporaneous unroofing of the shallow (?) dioritic intrusions or erosion of their eruptive equivalents.

A transition from pyroxene to hornblende-pyroxene-phyric volcanic strata may mark an increase in the water and potassium content of the arc magma source. Presence of hornblende might indicate that the pyroxene-dominated arc magma was recharged from a more hydrated and potassium-rich source region or by a more evolved

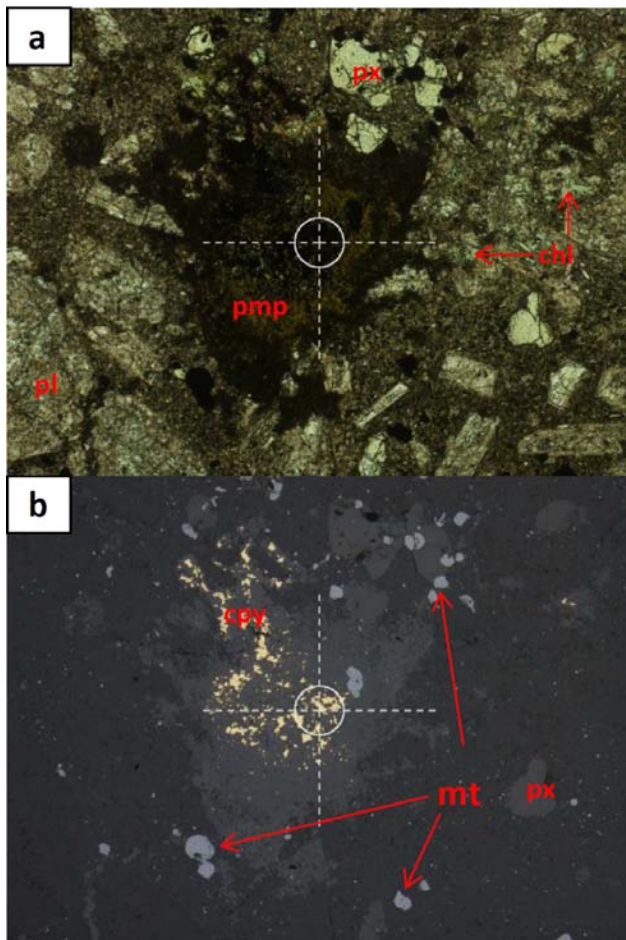


Fig. 12. **a)** Hornblende-pyroxene-feldspar porphyry with secondary chlorite (chl) and a patch of pumpellyite (pmp) with minor intergrown epidote at the centre of the photomicrograph. Plagioclase phenocrysts (pl) are made turbid by calcite and white mica alteration (in plane polarized light). In other samples, prehnite alters feldspars. **b)** The same field of view as in a) in reflected light shows chalcopyrite intergrowth with pumpellyite as an indication of the copper content of this rock, mobilized during low-grade metamorphism. Light grey rounded grains are magnetite; smooth dark grey crystals are pyroxene. Radius of the circle at crosshairs is 100 μ .

magma permitting growth or introduction of hornblende, followed by loss of volatiles and destabilization of hornblende. This same pyroxene to hornblende-bearing transition occurs at Miner Mountain (Mihalynuk and Logan, this volume) and other Late Triassic porphyry camps such as at the Iron Mask (Logan and Mihalynuk, 2005b) and Mount Polley (Logan and Mihalynuk, 2005c), and may be an important indicator of changing arc chemistry and fertility. Because of its potential importance to mineral exploration, we would like to establish whether or not this chemical change is coeval with the mineralizing epoch along the Late Triassic arc. Based on the appearance of hornblende-pyroxene-phyrlic volcanic strata in the predominantly epiclastic upper part of the Nicola Group, this chemical change may have occurred at about the same time as emplacement of the mineralized plutons at the Dillard Creek property. As a

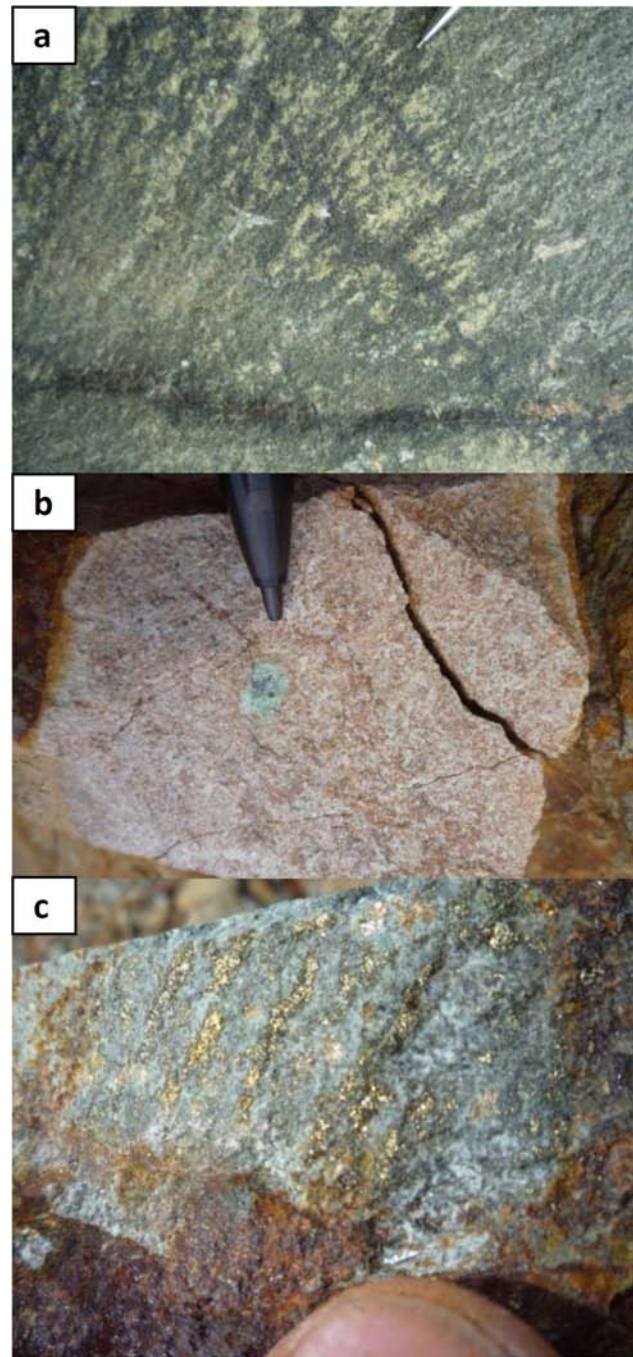


Fig. 13. Three styles of alteration and mineralization on the Dillard Creek property. **a)** Chlorite lined joints and thin veins \pm epidote and medial chalcopyrite. **b)** Strong carbonate alteration of trachytic? diorite. Parts of this same outcrop contain zones with secondary biotite alteration (see Fig. 14a). **c)** Within 50 m of the sample shown in Figure 14a, altered diorite is cut by secondary actinolite-magnetite-chalcopyrite veins (rusty material at bottom, see photomicrograph 14b, c). The irregular fracture surface obliquely intersects chalcopyrite and pyrite veinlets. A $\sim 7\mu$ gold inclusion was found in an irregular crystal of pyrite from this locality (Fig. 15). Sample is from near the collars of DDH 1966-1 and DDH 1991-8 (Tully, 1970; Fig. 3).

preliminary test, we have collected samples for isotopic age determinations to establish if the two events are synchronous. Both pyroxene- and pyroxene-hornblende-

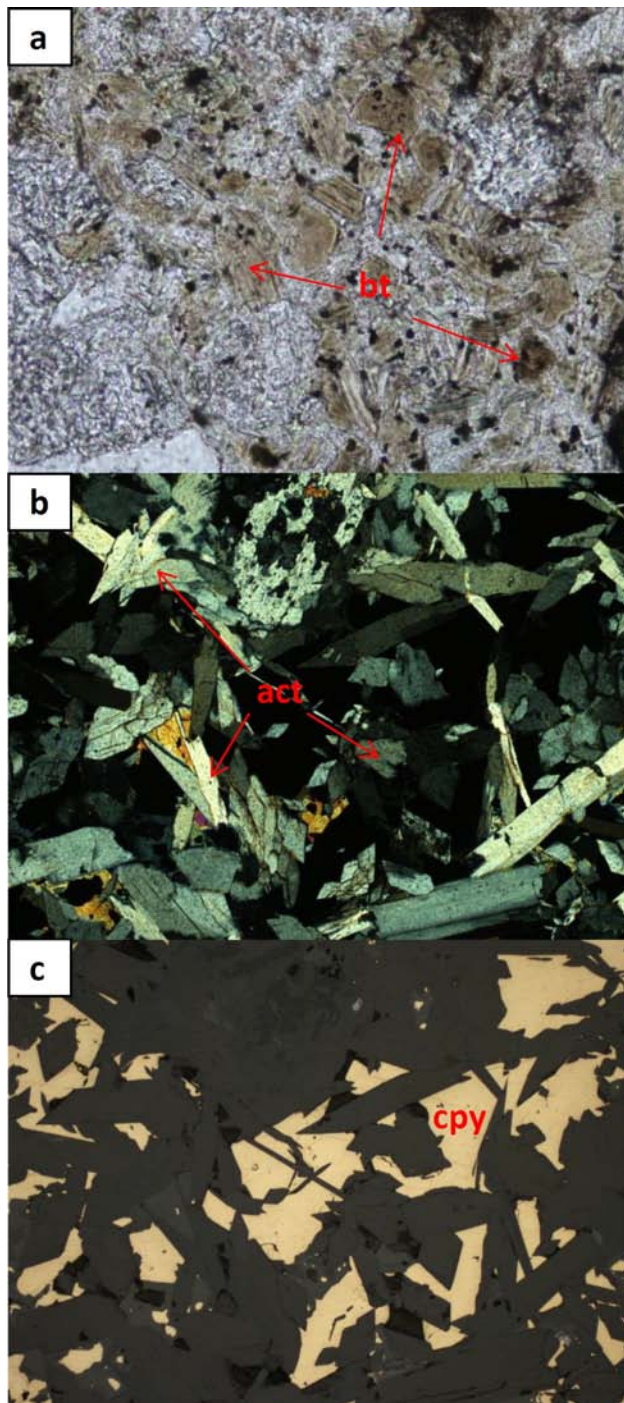


Fig. 14. Photomicrographs of mineralization at the Primer South from petrographic mounts cut from a hand sample like that shown in Figure 13c. **a)** Fine grained, brown booklets of secondary biotite partly altered to chlorite from sample MMI12-5-3, **b)** Cross polarized light view of sample MMI12-5-4 displays prisms and needles of euhedral actinolite intergrown with chalcopyrite (cpy) shown in reflected light in **c)**. Same field of view in all photos is 2 mm.

phyric volcanic strata show evidence of copper liberated during low grade regional metamorphism.

Copper-gold mineralization is associated with both potassic and calcic alteration of the dioritic intrusive

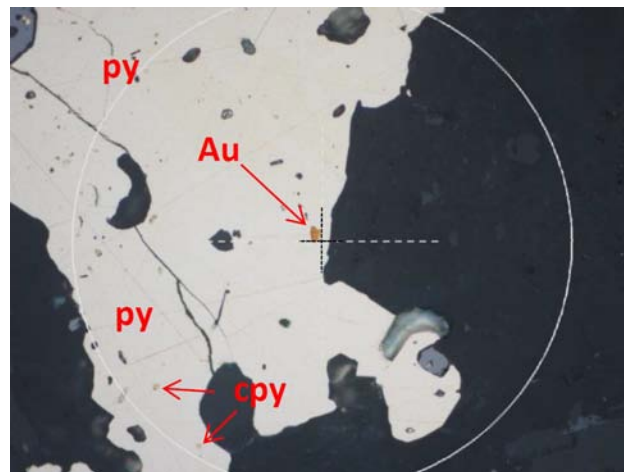


Fig. 15. Bright yellow-orange inclusion of gold (Au) in an irregular pyrite crystal (at crosshairs). Chalcopyrite (cpy) inclusions about half the size of the gold appear pale yellow in comparison, especially against the bright pyrite background (Sample MMI12-5-4, Primer South). Radius of the circle surrounding crosshair is 100 μ .

centres. Key mineral associations are K-feldspar-biotite-magnetite (and sulphides) and actinolite-epidote-calcite (and sulphides). Elevated gold values have been reported from mainly the eastern part of the property, although pyrite from the Primer South prospect, in the south-central part of the property, contains inclusions of gold (Fig. 16).

Acknowledgments

We thank T. Schroeter for pointing out the lack of base-line regional geological mapping information in the Dillard Creek area, and for sharing unpublished geochemical data (none included here). This paper was improved substantially by careful reviews by P. Schiarizza and L. Aspler.

References cited

- Church, B.N., 1973. Geology of the White Lake Basin. British Columbia Ministry of Energy, Mines and Petroleum Resources, British Columbia Geological Survey Bulletin 61, 141 p.
- Chapman, D.A., 1970. Geological reconnaissance report in Tectonic analysis of fracture density and geochemical report on the Dillard Creek property. British Columbia Ministry of Energy and Mines, British Columbia Geological Survey Assessment Report 2356, 8 p.
- Coney, P.J., Jones, D.L., and Monger, J.W.H., 1980. Cordilleran suspect terranes. *Nature*, 288, 329-333.
- Cormier, 1990. 1989 geochemical, geophysical and trenching report on the Dill claim: British Columbia Ministry of Energy, Mines and Petroleum Resources, British Columbia Geological Survey Assessment Report 19593, 21 p.
- Gutrath, G.C., 1980. Outcrop geology report, Prime claim group. British Columbia Ministry of Energy, Mines and Petroleum Resources, British Columbia Geological Survey Assessment Report 7521, 8 p.
- LeBas, M.J.L., Maitre, R.W.L., Streckeisen, A., and Zanettin, B., 1986. A chemical classification of volcanic rocks

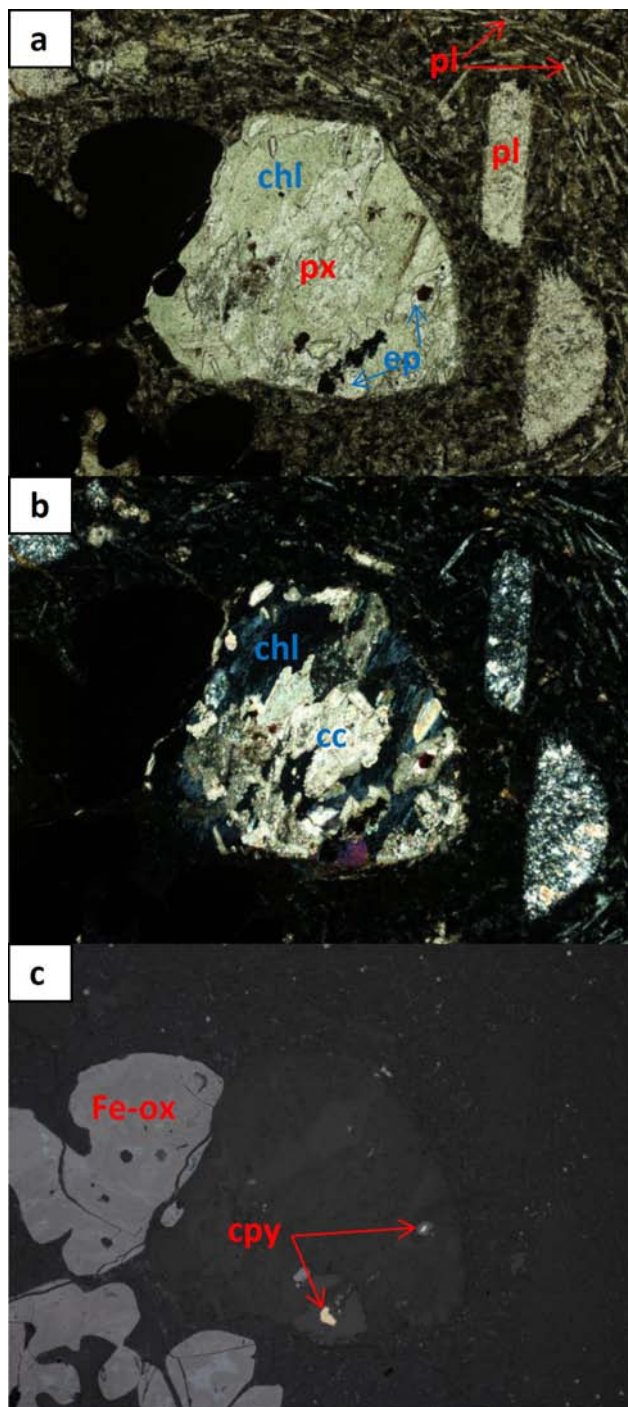


Fig. 16. Altered augite porphyry basalt in **a**) Plane polarized light displays a well-developed trachytic flow fabric (outlined by plagioclase microlites) that wraps around the pyroxene phenocrysts at the centre of the photo. Light green area is Fe-rich chlorite that displays anomalous blue interference colours in **b**) Cross polarized light. Much of the pyroxene is replaced by calcite (cc, high birefringence). Plagioclase phenocrysts are replaced by fine-grained? prehnite. **c**) In plane reflected light, bright yellow chalcopyrite is associated with epidote in altered pyroxene. Amoeboid grains on left are intergrowths of Fe-oxide and hydroxide minerals displaying an internal botryoidal fabric. Same field of view for all images; width is ~4 mm.

based on the total alkali-silica diagram. *Journal of Petrology* 27, 745-750.

- Logan, J.M. and Mihalynuk, M.G., 2005a. BC's 200 million year old porphyry Cu-Au deposits – an alkaline advantage, In: Association for Mineral Exploration British Columbia, Mineral Exploration Roundup, program with abstracts, pp. 13-15.
- Logan, J.M., and Mihalynuk, M.G., 2005b. Porphyry Cu-Au deposits of the Iron Mask Batholith, southeastern British Columbia. In: *Geological Fieldwork 2004*, British Columbia Ministry of Energy and Mines, British Columbia Geological Survey Paper 2005-1, pp. 271-290.
- Logan, J.M., and Mihalynuk, M.G., 2005c. Regional geology and setting of the Cariboo, Bell, Springer and Northeast Porphyry Cu-Au zones at Mount Polley, south-central, British Columbia. In: *Geological Fieldwork 2004*, British Columbia Ministry of Energy and Mines, British Columbia Geological Survey Paper 2005-1, pp. 249-270.
- Logan, J.M. and Mihalynuk, M.G., 2013a. Bonaparte gold: another 195 Ma Au-Cu porphyry deposit in southern British Columbia? In: *Geological Fieldwork 2012*, British Columbia Ministry of Energy, Mines and Natural Gas, British Columbia Geological Survey Paper 2013-1, (this volume).
- Logan, J.M., and Mihalynuk, M.G., 2013b. Tectonic controls on Early Mesozoic paired alkaline porphyry deposit belts (Cu-Au ± Ag-Pt-Pd-Mo) within the Canadian Cordillera. *Economic Geology*, in press.
- Logan, J.M., Mihalynuk, M.G., and Friedman, R.M., 2011. Age constraints of mineralization at the Brenda and Woodjam Cu-Mo+/-Au Porphyry deposits - An Early Jurassic calcalkaline event, south-central British Columbia. In: *Geological Fieldwork 2010*, British Columbia Ministry of Energy, Mines and Petroleum Resources, British Columbia Geological Survey Paper 2011-1, pp. 129-144.
- Massey, N.W.D., MacIntyre, D.G., Desjardins, P.J., and Cooney, R.T., 2005. Digital Geology Map of British Columbia. British Columbia Ministry of Energy, Mines and Petroleum Resources, British Columbia Geological Survey Open File 2005-1; URL accessed November, 2012, <http://www.empr.gov.bc.ca/Mining/Geoscience/PublicationsCatalogue/GeoFiles/Pages/2005-1.aspx>.
- Mihalynuk, M.G., 2010. Recipe for Cu-Au-Ag ±Mo porphyry deposits: Ingredients from the northern Cordilleran terranes. In: *Copper Porphyry Workshop*, Geological Association of Canada, Vancouver, BC, Canada.
- Mihalynuk, M.G., and Logan, J.M., 2013a. Geological setting of Late Triassic Cu-Au porphyry mineralization at Miner Mountain, Princeton. In: *Geological Fieldwork 2012*, British Columbia Ministry of Energy, Mines and Natural Gas, British Columbia Geological Survey Paper 2013-1, (this volume).
- Mihalynuk, M.G., Logan, J.M., 2013b. Lithogeochemical data from porphyry environments between Princeton and Merritt, BC Ministry of Energy, Mines and Natural Gas, Geofile 2013, in press.
- Mihalynuk, M.G., Logan, J.M., Friedman, R.M., and Preto, V.A., 2010. Age of mineralization and "Mine Dykes" at Copper Mountain alkaline copper-gold-silver porphyry deposit (NTS 092H/07), South-Central British Columbia. In: *Geological Fieldwork 2009*, BC Ministry of Energy, Mines and Petroleum Resources Paper 2010-1, pp. 163-171.

- Monger, J.W.H., 1989. Geology, Hope, British Columbia. Geological Survey of Canada, Map 41-1989, scale 1:250 000.
- Parrish, R.R., and Monger, J.W.H., 1992. New U-Pb dates from southwestern British Columbia. In: Geological Survey of Canada, Radiogenic age and isotopic studies; Report 5, 87-108.
- Pearce, J.A., 1996. A user's guide to basalt discrimination diagrams. Short Course Notes - Geological Association of Canada 12, pp. 79-113.
- Peccerillo, A., Taylor, S.R., 1976. Rare earth elements in the East Carpathian volcanic rocks. *Earth and Planetary Science Letters*, 32, 121-126.
- Preto, V.A., 1979. Geology of the Nicola Group between Merritt and Princeton. British Columbia Ministry of Energy, Mines and Petroleum Resources, British Columbia Geological Survey Bulletin 69, 90 p.
- Pringle, D., 1969. Tectonic analysis of fracture density and geochemical report on the Dillard Creek property. British Columbia Ministry of Energy and Mines, British Columbia Geological Survey Assessment Report 2356, 91 p.
- Rice, H.M.A., 1947. Geology and mineral deposits of the Princeton map-area, British Columbia Geological Survey of Canada, Memoir 243, 136 p.
- Sun, S.S., McDonough, W.F., 1989. Chemical and isotopic systematics of oceanic basalts; implications for mantle composition and processes. *Geological Society Special Publication* 42, pp. 313-345.
- Tipper, H.W., Woodsworth, G.J., and Gabrielse, H., 1981. Tectonic assemblage map of the Canadian Cordillera and adjacent parts of the United States of America. Geological Survey of Canada, Map 1712A, scale 1:2 000 000.
- Tully, D., 1970 Report on diamond drill and geochemical results on Dillard Creek property. British Columbia Ministry of Energy and Mines, British Columbia Geological Survey Assessment Report 2354, 108 p.

Geology, U-Pb geochronology, and geochemistry of the Miocene Pheno Mountain complex, Hoodoo Mountain area, British Columbia

A. Zagorevski^{1,a}, C. Dziawa², R.M. Friedman³ and M.G. Mihalynuk⁴

¹ Geological Survey of Canada, 601 Booth St., Ottawa, ON, K1A 0E8

² Department of Earth Sciences, Carleton University, Ottawa, ON, K1S 5B6

³ Pacific Centre for Isotopic and Geochemical Research, Department of Earth and Ocean Sciences, University of British Columbia, Vancouver, BC, V6T 1Z4

⁴ British Columbia Geological Survey, Ministry of Energy, Mines and Natural Gas, Victoria, BC, V8W 9N3

^a corresponding author: azagorev@nrcan.gc.ca

Recommended citation: Zagorevski, A., Dziawa, C., Friedman, R.M. and Mihalynuk, M.G., 2013. Geology, U-Pb geochronology, and geochemistry of the Miocene Pheno Mountain complex, Hoodoo Mountain area, British Columbia. In: Geological Fieldwork 2012, British Columbia Ministry of Energy, Mines and Natural Gas, British Columbia Geological Survey Paper 2013-1, pp. 115-125.

Abstract

The Pheno Mountain complex comprises rhyolite, trachyte and intrusive quartz feldspar porphyry that form extrusive and hypabyssal portions of a volcanic complex. A subvolcanic quartz feldspar porphyry with columnar jointing and brecciated margins underlies petrographically identical volcanic rocks. It yielded a 7.78 ± 0.01 Ma U-Pb zircon crystallization age, which is interpreted to constrain the age of the Pheno Mountain complex. Both the volcanic and hypabyssal rocks are characterized by high Nb/Y, Nb, Y, and Zr suggesting that they formed in a within-plate setting by fractional crystallization from an alkali basalt parent. These data support correlation of the Pheno Mountain complex with the Neogene to Quaternary Northern Cordilleran Volcanic Province. However, in contrast to the coeval Mount Edziza and Level Mountain volcanic centres, magmatism in the Pheno Mountain complex does not appear to be preceded by construction of a basaltic shield.

Keywords: Northern Cordilleran Volcanic Province, silica-saturated, felsic magmatism, alkaline rhyolite, peralkaline trachyte, upper Miocene, U-Pb geochronology, geochemistry

1. Introduction

The Neogene to Quaternary Northern Cordilleran Volcanic Province (NCVP) comprises predominantly alkaline volcanic rocks that extend from northwestern British Columbia to the Yukon-Alaska Border (Fig. 1). The NCVP erupted during dextral-oblique transtension of North America (Edwards and Russell, 2000). Over most of its geographical extent, the NCVP is dominated by short-lived, monogenetic mafic volcanic centres (see review in Edwards and Russell, 2000). A few centres, such as Level Mountain and Mount Edziza (Fig. 1), were long-lived and polygenetic. Well-dated strata of the Mount Edziza Complex, for example, indicate that the alkaline magmatism lasted from 7.5 Ma to Recent (Souther, 1992).

The NCVP extends through the Hoodoo Mountain Area (104/B14), where the conspicuous Late Quaternary (periods and epochs follow Gradstein et al. 2012) phonolitic Hoodoo Mountain Volcano erupted as recently as 9 Ka (Edwards et al., 2002). Neogene to Early Quaternary rocks have not been previously identified in this area. Mihalynuk et al. (2012) identified sections of volcanic and hypabyssal porphyritic rocks near Pheno Mountain (Pheno Mountain complex) ~ 15 km northwest

of Hoodoo Mountain (Fig. 2). Petrographic and geochemical data presented herein support that the volcanic and hypabyssal components of the Pheno Mountain complex are co-genetic. They are likely derived from fractional crystallization of a common alkali basalt parent. Our data demonstrate that Pheno Mountain complex is significantly older than the Hoodoo Mountain complex and is broadly coeval with the Late Miocene felsic volcanic rocks of the Mount Edziza, Level Mountain, and Heart Peaks complexes (Fig. 1).

2. Pheno Mountain complex

The Hoodoo Mountain region (104/B14) is characterized by mountainous terrain largely covered by the Andrei Glacier Icefield (Fig. 2). It is mainly underlain by Carboniferous to Jurassic volcanic, sedimentary and plutonic rocks that characterize the Stikine terrane (see Mihalynuk et al., 2011; Mihalynuk et al., 2012). These Mesozoic and older rocks are intruded by Eocene plutons of the Coast Plutonic Complex (Logan and Koyanagi, 1994) and are unconformably overlain and intruded by Neogene and younger rocks of the Northern Cordilleran Volcanic Province, such as the Late Quaternary phonolitic Hoodoo Mountain Volcano (Kerr, 1948; Edwards et al., 2002).

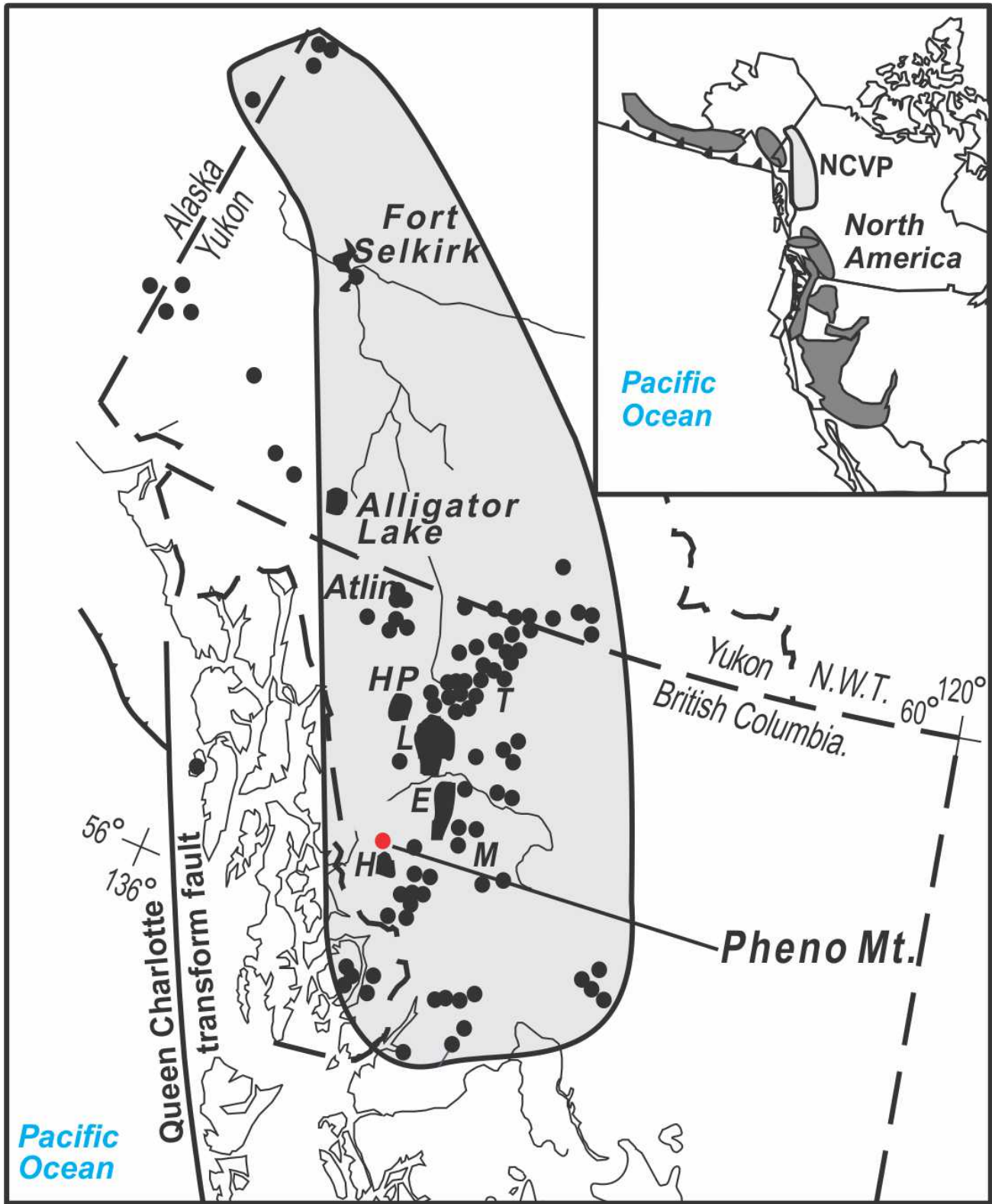


Fig. 1. Distribution of Neogene and Quaternary volcanic rocks of the Northern Cordilleran volcanic province (from Edwards and Russell, 2000) with location of the Pheno Mountain volcanic centre. E – Mount Edziza, H – Hoodoo Mountain, HP – Heart Peaks, L – Level Mountain, M – Maitland, T – Tuya. Inset: Location of the NCVP with respect to other Neogene and Quaternary volcanic rocks in western North America

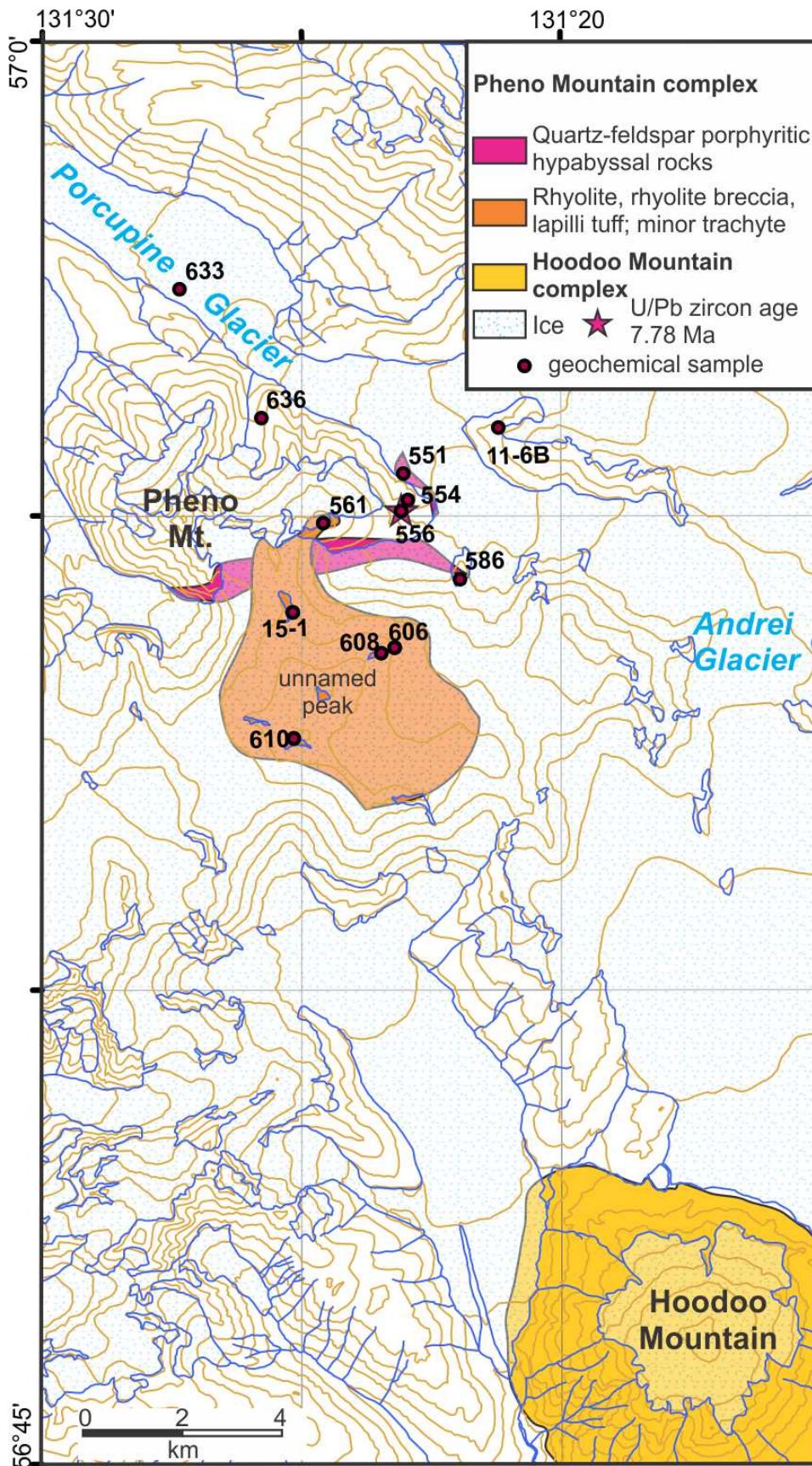


Fig. 2. Distribution of Neogene to Quaternary volcanic rocks in the Hoodoo Mountain area (modified from Mihalyuk et al., 2012).

The Pheno Mountain complex (Mihalynuk et al., 2012) is dominated by felsic to intermediate volcanic and hypabyssal rocks that are locally cut by mafic dikes. Exposures of the Pheno Mountain complex occur 15 km north-northwest of Hoodoo Mountain and Porcupine Glacier wraps north side of complex, about 1 km southeast of Pheno Mountain summit (Fig. 2). Large, rounded, rusty weathering boulders of the Pheno Mountain complex are common in the southern lateral moraine of Porcupine Glacier (Fig. 3a).

2.1. Volcanic rocks

Pheno Mountain complex volcanic rocks cap an unnamed peak 5 km SE of Pheno Mountain (Figs. 2, 3a-c). They predominantly comprise light blue-green to rusty, vesicular, quartz and feldspar porphyritic, rhyolitic lapilli tuff, tuff breccia, banded flows, and flow breccia (Fig. 3d). Dense pyroclasts commonly exhibit flow banding, coalesced spherulites, and perlite (Figs. 3e, f). Quartz phenocrysts (<3 mm, 5%) are euhedral to rounded and commonly embayed. Feldspar phenocrysts (<3 mm, <10%) locally contain zones of melt inclusions and are commonly altered. Some samples display granophyric intergrowth between quartz and alkali feldspar. Rare chloritized pseudomorphs suggest replacement of a mafic phenocryst phase, likely pyroxene (Fig. 3e). The vesicles are mostly open, though some are lined with opaque minerals or partly filled with chlorite.

2.2. Trachytic rocks

Feldspar porphyritic, macroscopically banded, trachytic rocks occur to the north of the main rhyolitic volcanic centre. The contact between the trachyte and rhyolite is obscured by extensive felsenmeer. Rhyolite and trachyte are interlayered (Fig. 3c); however, it is unclear whether trachytes are flows or sills. Trachyte does occur as 1 m wide, north-trending dikes (Fig. 2). Trachyte contains glomeroporphyritic or granophyric, locally sieve-textured feldspar (<10 mm). Clinopyroxene is locally present. One sample contains abundant fine grained, strongly coloured, pleochroic blue amphibole typical of peralkaline suites (Fig. 4d).

2.3. Felsic hypabyssal rocks

Felsic hypabyssal rocks are common near Pheno Mountain, immediately to the north of the volcanic rocks (Figs. 2, 3a, b). Other areas to the east, west and south are largely obscured by ice or were inaccessible during mapping. Petrographically similar north-trending dikes occur 13 km south of Pheno Mountain and felsic dikes are common in cliff exposures near Pheno Mountain, suggesting that hypabyssal magmatism was likely extensive. Felsic hypabyssal rocks are dominated by quartz and feldspar porphyritic, holocrystalline, granophyric felsic dikes (Figs. 4a, b). Euhedral to rounded and embayed quartz (<5 mm) comprises <20% of most dikes. Euhedral, lath-shaped, locally sieve-textured feldspar phenocrysts (generally <5 mm up to 2 cm) generally comprise 20-25% of these rocks. Rarely, feldspar forms glomeroporphyritic aggregates. Some

samples contain hematite, calcite and/or chlorite-filled vesicles. The dikes locally display brecciated margins and columnar jointing; both suggest shallow depth of emplacement (Fig. 3b inset).

2.4. Mafic dikes

Feldspar porphyritic, pilotaxitic, vesicular mafic dikes cut the felsic hypabyssal rocks. Feldspar phenocrysts are euhedral to rounded and sieve-textured (Fig. 4c). Calcite and chlorite-filled amygdalae are commonly up to 1 cm, although rare vesicles are >5 cm. Some feldspar crystals show distinct albite twinning. The fine-grained matrix is altered, mostly to chlorite and carbonate.

3. Geochronology

U-Pb geochronology was conducted at the Pacific Centre for Isotopic and Geochemical Research (PCIGR), University of British Columbia (Vancouver) using chemical abrasion thermal ionization mass spectrometry (CA-TIMS) procedure that is modified from Mundil et al. (2004), Mattinson (2005) and Scoates and Friedman (2008). Rock samples were processed using standard mineral separation procedures, followed by hand picking of zircons in alcohol. The clearest, crack and inclusion-free grains were selected, photographed, and annealed in quartz glass crucibles at 900°C for 60 hours. Annealed grains were transferred into 3.5 mL PFA screw-top beakers, ultrapure HF (up to 50% strength, 500 µL) and HNO₃ (up to 14 N, 50 µL) were added and caps are closed finger tight. The beakers were placed in 125 mL PTFE liners and about 2 mL HF and 0.2 mL HNO₃ of the same strength as acid within beakers containing samples were added to the liners. The liners were then slid into stainless steel Parr™ high pressure dissolution devices, which were sealed and heated to a maximum of 200°C for 8-16 hours (typically 175°C for 12 hours). Beakers were removed from liners and zircon was separated from leachate. Zircons were rinsed with >18 MΩ.cm water and subboiled acetone. Then 2 mL of subboiled 6N HCl was added and beakers were set on a hotplate at 80°-130°C for 30 minutes and again rinsed with water and acetone. Masses were estimated from the dimensions (volumes) of grains. Single grains were transferred into clean 300 µL PFA microcapsules (crucibles), and 50 µL 50% HF and 5 µL 14 N HNO₃ were added. Each was spiked with a ²³³⁻²³⁵U-²⁰⁵Pb tracer solution (EARTHTIME ET535), capped and again placed in a Parr liner (8-15 microcapsules per liner). HF and nitric acids in a 10:1 ratio, respectively, were added to the liner, which was then placed in a Parr high pressure device for 40 hours at 240°C. The resulting solutions were dried on a hotplate at 130°C, 50 µL 6N HCl was added to the microcapsules, and fluorides were dissolved in high pressure Parr devices for 12 hours at 210°C. HCl solutions were transferred into clean 7 mL PFA beakers and dried with 2 µL of 0.5 N H₃PO₄. Samples were loaded onto degassed, zone-refined Re filaments in 2 µL of silicic acid emitter (Gerstenberger and Haase, 1997).

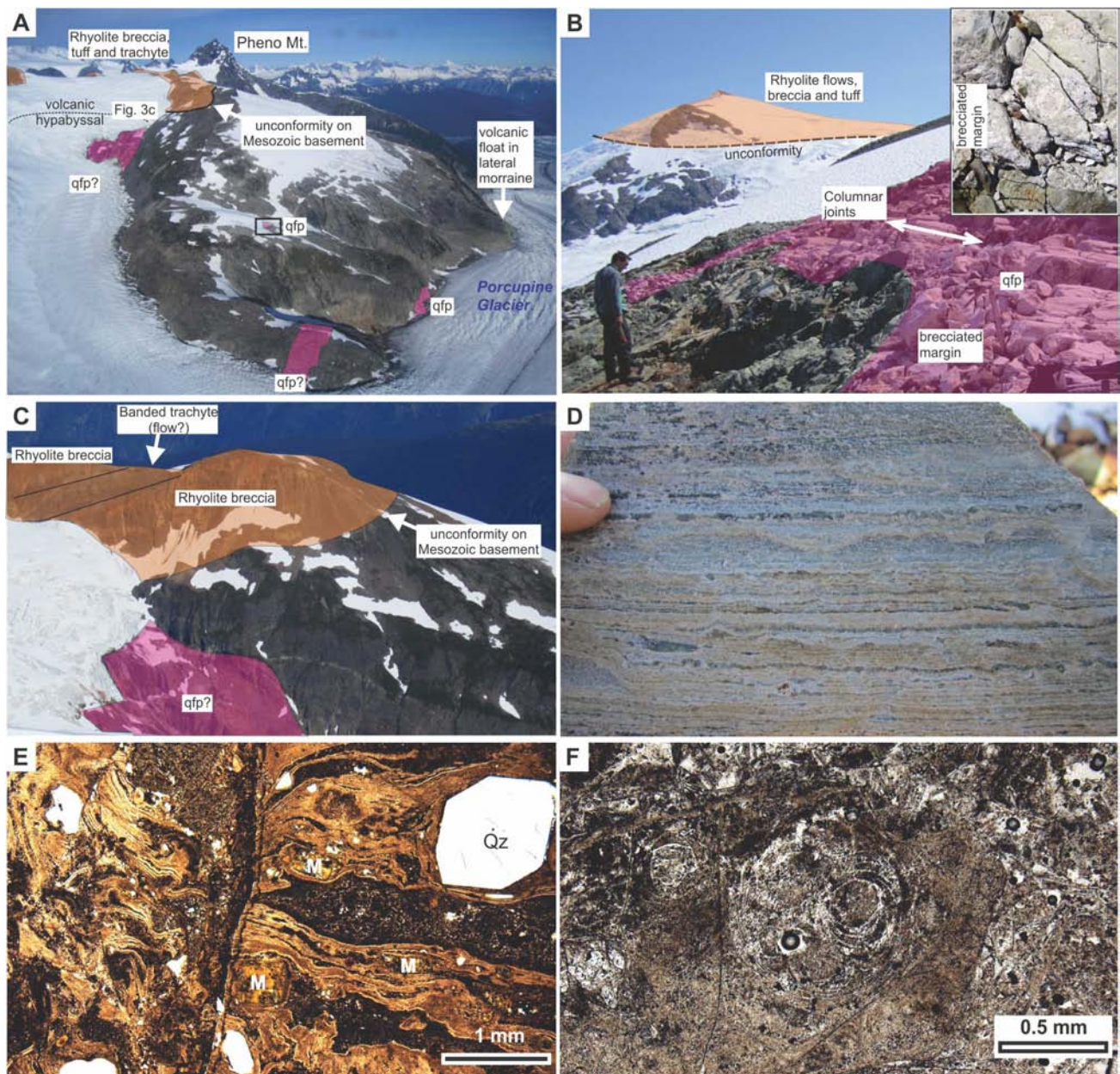


Fig. 3. Representative photographs of the Pheno Mountain complex. **a)** Relationships of Mesozoic basement with intrusive quartz and feldspar porphyric (qfp) and volcanic rocks, view to the WNW. Box marks the location of outcrop in **b)**. **b)** Dated locality (see Fig. 2) with intrusive columnar-jointed quartz and feldspar porphyry (foreground), view to the SW. Unnamed peak in the background is underlain by rhyolitic flows and breccia. Inset: margin of columnar-jointed dike displays fragmental texture, scale card graduations are 1 cm. **c)** Relationship between quartz and feldspar porphyry (qfp), rhyolite breccia and trachyte. Trachyte forms a banded, tabular body within rhyolitic rocks and may represent a flow or a sill, view to the N. Arrow identifying unconformity points to the same location as in Fig. 3a. **d)** Flow banded rhyolite with coalesced spherulites. **e)** Flow banded quartz (Qz)-phyric rhyolite with relict mafic phenocrysts (M). **f)** Perlitic fractures in rhyolite.

Isotopic ratios were measured on a modified single collector VG-54R or 354S (with Sector 54 electronics) thermal ionization mass spectrometer equipped with analogue Daly photomultipliers. Analytical blanks were 0.2 pg for U and 0.5 pg for Pb. U fractionation was determined directly on individual runs using the

EARTHTIME ET535 mixed $^{233-235}\text{U}$ - ^{205}Pb isotopic tracer and Pb isotopic ratios were corrected for fractionation of 0.23%/atomic mass unit, based on replicate analyses of NBS-982 reference material and the values recommended by Thirlwall (2000). Data reduction employed the Excel-based program of Schmitz and Schoene (2007). Standard concordia diagrams were constructed and weighted

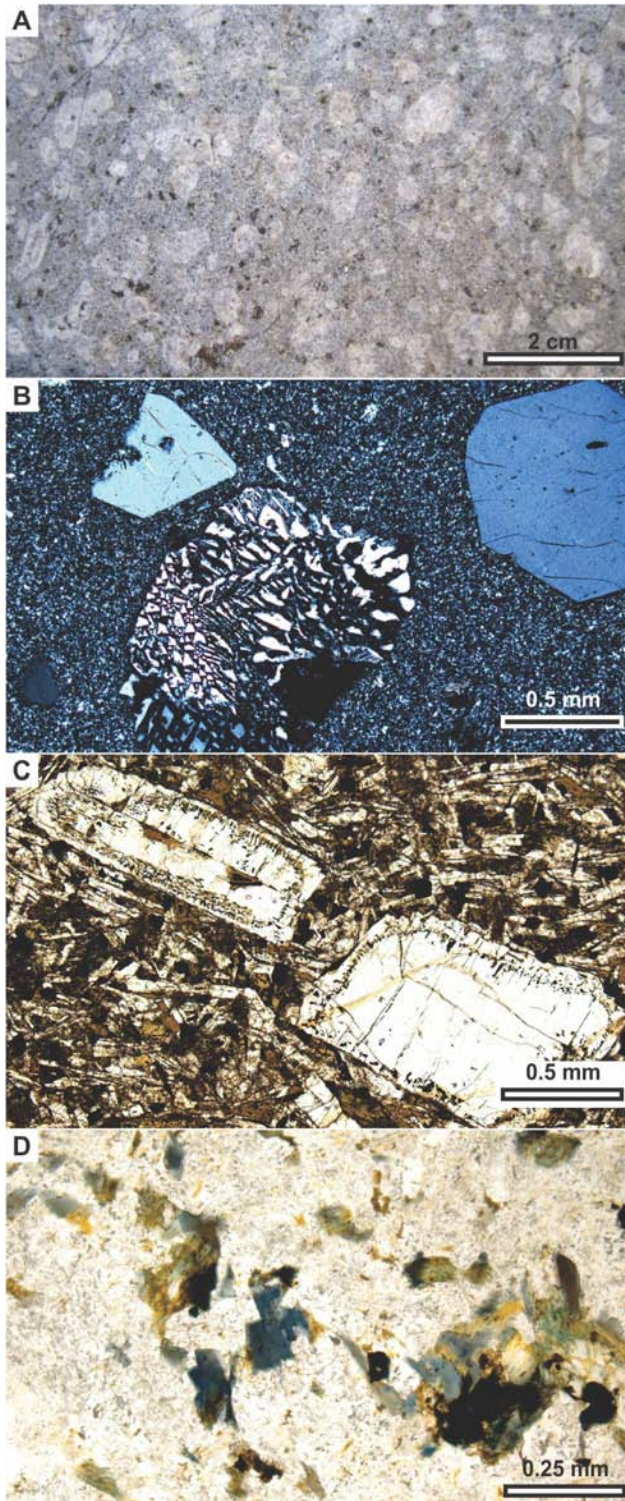


Fig. 4. Representative photographs of the Pheno Mountain complex. **a)** K-feldspar and quartz-phyric dike along the Porcupine Glacier. **b)** Photomicrograph of the dated quartz feldspar porphyry with granophyric crystals. **c)** Sieve-textured feldspar in mafic dike. **d)** Pleochroic, blue amphibole in trachyte dike.

$^{206}\text{Pb}/^{238}\text{U}$ age (2σ) calculated using Isoplot (Ludwig,

2003). Unless otherwise noted all errors are quoted as 2σ (95% confidence). Isotopic dates were calculated with the decay constants $\lambda_{238}=1.55125\text{E}-10$ and $\lambda_{235}=9.8485\text{E}-10$ (Jaffey et al., 1971).

3.1. Sample description and interpretation

A steep ridge south of Porcupine Glacier (Fig. 2) is dominated by bedded, moderately dipping, Mesozoic volcanogenic conglomerate and sandstone. The Mesozoic volcanogenic rocks are cut at a high angle to bedding by steep rhyolitic dikes. One dike exhibits well developed shallowly plunging columnar jointing that is perpendicular to the steep dike margin. Brecciation along the margin of this dike suggests very shallow level of emplacement (Fig. 3b). A sample from this dike (ZE11-556a; N56.91732, W131.38604) comprises light blue-green quartz and feldspar porphyritic, granophyric rhyolite. The sample yielded well-faceted, 150-200 μm stubby prismatic zircon grains with melt and apatite inclusions (Fig. 5 inset). Five single zircon grains were analyzed using CA-TIMS (Fig. 5). The three youngest grains yielded overlapping concordant data with a weighted $^{206}\text{Pb}/^{238}\text{U}$ age of 7.78 ± 0.01 Ma (MSWD = 0.52), which is interpreted to record the crystallization age of the columnar-jointed rhyolite dike. Two grains yielded $^{206}\text{Pb}/^{238}\text{U}$ ages of 7.92 ± 0.02 and 8.47 ± 0.01 Ma suggesting presence of an inherited, Cenozoic to Mesozoic component (Table 1).

4. Geochemistry

Sixteen samples of Pheno Mountain complex volcanic and hypabyssal rocks were screened for whole rock geochemical analysis using portable XRF (see Mihalynuk et al., 2012). The samples were trimmed to remove zones of weathering and alteration using a diamond saw. Major and trace elements were analyzed

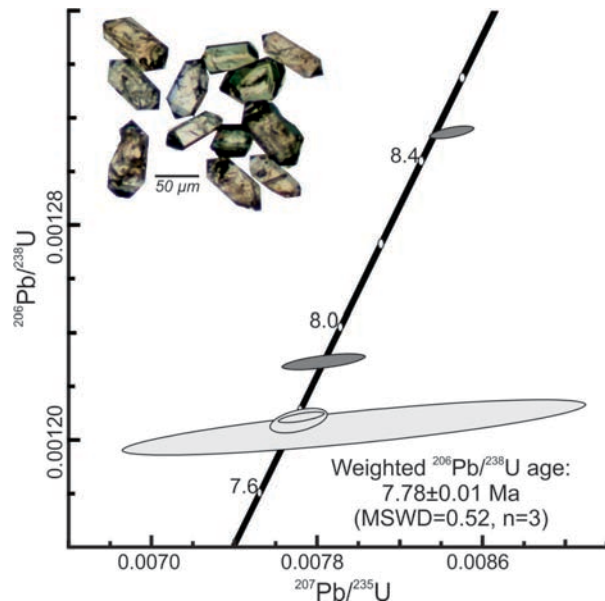


Fig. 5. U-Pb zircon concordia diagram of quartz feldspar porphyry. Inherited fractions are indicated by dark grey ellipses. Inset: Representative photomicrograph of analyzed zircon.

Table 1. U-Pb CA-TIMS analytical data for sample ZE11-556.

Sample	Compositional Parameters										Radiogenic Isotope Ratios						Isotopic Ages						
	Wt. mg	U ppm	Th ppm	Pb ppm	$x(10^{-13})$	$\frac{^{206}\text{Pb}^*}{^{206}\text{Pb}}$ mol %	$\frac{\text{Pb}^*}{\text{Pb}_c}$ (pg)	$\frac{^{206}\text{Pb}}{^{206}\text{Pb}}$ (f)	$\frac{^{206}\text{Pb}}{^{206}\text{Pb}}$ (g)	$\frac{^{206}\text{Pb}}{^{206}\text{Pb}}$ (g)	% err	$\frac{^{207}\text{Pb}}{^{235}\text{U}}$ (e)	% err	$\frac{^{206}\text{Pb}}{^{238}\text{U}}$ (g)	% err	$\frac{^{207}\text{Pb}}{^{206}\text{Pb}}$ (i)	corr. coef.	$\frac{^{207}\text{Pb}}{^{206}\text{Pb}}$ (i)	\pm	$\frac{^{206}\text{Pb}}{^{238}\text{U}}$ (j)	\pm	$\frac{^{206}\text{Pb}}{^{238}\text{U}}$ (h)	\pm
A	0.0051	1177	0.318	1.5	0.2987	97.24%	10	0.70	673	0.104	0.046335	1.138	0.007717	1.229	0.001208	0.149	0.649	15.09	27.19	7.81	0.10	7.78	0.01
B	0.0063	1379	0.310	1.9	0.4710	97.71%	12	0.90	813	0.102	0.046643	0.979	0.008454	1.064	0.001315	0.159	0.588	31.01	23.34	8.55	0.09	8.47	0.01
C	0.0093	1121	0.324	2.7	0.5173	77.39%	1	12.46	82	0.110	0.048025	11.072	0.007973	11.645	0.001204	0.719	0.808	100.49	260.45	8.06	0.94	7.76	0.06
D	0.0112	1123	0.321	1.4	0.6251	98.34%	17	0.87	1121	0.105	0.046302	1.373	0.007704	1.497	0.001207	0.325	0.475	13.35	32.83	7.79	0.12	7.77	0.02
E	0.0491	162	0.342	0.2	0.4015	97.84%	13	0.72	857	0.111	0.046196	2.043	0.007827	2.166	0.001229	0.215	0.609	7.84	48.90	7.92	0.17	7.92	0.02

- (a) A, B etc. are labels for fractions composed of single zircon grains or fragments; all fractions annealed and chemically abraded after Mattinson (2005) and Scoates and Friedman (2008).
- (b) Nominal fraction weights estimated from photomicrographic grain dimensions, adjusted for partial dissolution during chemical abrasion.
- (c) Nominal U and total Pb concentrations subject to uncertainty in photomicrographic estimation of weight and partial dissolution during chemical abrasion.
- (d) Model Th/U ratio calculated from radiogenic $\frac{^{206}\text{Pb}}{^{206}\text{Pb}}$ / $\frac{^{206}\text{Pb}}{^{206}\text{Pb}}$ ratio and $\frac{^{207}\text{Pb}}{^{235}\text{U}}$ age.
- (e) Pb* and Pb_c represent radiogenic and common Pb, respectively; mol % $\frac{^{206}\text{Pb}^*}{^{206}\text{Pb}}$ with respect to radiogenic, blank and initial common Pb.
- (f) Measured ratio corrected for spike and fractionation only. Mass discrimination of 0.23%/amu based on analysis of NBS-982; all Daly analyses.
- (g) Corrected for fractionation, spike, and common Pb; up to 8 pg of common Pb was assumed to be procedural blank: $\frac{^{206}\text{Pb}}{^{206}\text{Pb}}$ / $\frac{^{206}\text{Pb}}{^{206}\text{Pb}}$ = 18.50 ± 1.0%; $\frac{^{207}\text{Pb}}{^{206}\text{Pb}}$ / $\frac{^{206}\text{Pb}}{^{206}\text{Pb}}$ = 15.50 ± 1.0%.
- (h) Errors are 2-sigma, propagated using the algorithms of Schmitz and Schoene (2007) and Crowley et al. (2007).
- (i) Calculations are based on the decay constants of Jaffey et al. (1971). $\frac{^{206}\text{Pb}}{^{206}\text{Pb}}$ / $\frac{^{206}\text{Pb}}{^{206}\text{Pb}}$ ages corrected for initial disequilibrium in $\frac{^{230}\text{Th}}{^{238}\text{U}}$ using Th/U [magma] = 3.

Isotopic dates are calculated the decay constants $\lambda_{238} = 1.55125\text{E}-10$ and $\lambda_{235} = 9.8485\text{E}-10$ (Jaffey et al. 1971).

using ICP-ES and ICP-MS following lithium metaborate/tetraborate fusion and nitric acid digestion (analytical package 4A4B) at ACME Laboratories (Vancouver, British Columbia). Whole-rock data are grouped on the basis of petrography (Table 2; Fig. 6).

4.1. Geochemistry results

Rhyolitic volcanic and hypabyssal rocks are characterized by high SiO₂ (72.3 to 80 wt.%), K₂O (2.2 to 7.5%), high Zr/Ti, high Nb/Y ratios and a peraluminous character. They plot in rhyolite and alkali rhyolite fields on discrimination plots (Figs. 6a, b). Most of the felsic rocks are characterized by high Zr (576 to 3110 ppm) and low Zr/Nb ratio (6.6 to 10.3). Heavy rare earth element (HREE) concentrations are 40 to 200 times chondritic values and LREE are moderately to strongly enriched (La/Yb - 3.2 to 13.1). Nb/Nb* ratios are variable (0.65 to 1.95). However, in many samples, Nb is enriched relative to La. Eu is strongly depleted (Eu/Eu* - 0.10 to 0.25) in both volcanic and hypabyssal samples, whereas Sr is highly depleted in volcanic samples (Sr 4.8 to 8.8 ppm). The dated sample (ZE11-556) exhibits a strong positive Ce anomaly (Ce/Ce* = 2.5), a strong negative Eu anomaly (Eu/Eu* = 0.04), and has a lower Zr/Hf ratio than other felsic samples (18 compared to 39).

Trachytic rocks (SiO₂ 59.8 to 61.8%) are characterized by lower Zr/Ti and similar Nb/Y ratios as the felsic rocks (Fig. 6b). They plot in the trachyte field on the TAS plot (Fig. 6a). They are characterized by high Zr (359 to 471 ppm) and low Zr/Nb ratio (7.5 to 8.5). They exhibit similar extended trace element profiles as the felsic rocks, but have generally lower absolute trace element abundances and a smaller Eu anomaly (Eu/Eu* - 0.63 to 0.78). The trachytic samples possess similar Zr/Hf ratios ($\mu = 40$) as the felsic rocks ($\mu = 39$). The sample that contains blue amphibole (ZE11-586) is acmite normative.

The mafic dike has high TiO₂ (2.5 wt.%) and Fe₂O_{3 total} (13.45 wt%), and plots near the boundary of the alkali basalt field (Fig. 6b). It exhibits similar extended trace element profile as the felsic and trachytic rocks, but has lower absolute trace element abundances and lacks Eu, Ti, and Sr depletion (Eu/Eu* = 1.03).

5. Summary and discussion

Regional mapping in the Hoodoo Mountain area identified a new felsic volcanic centre related to the Neogene to recent Northern Cordilleran Volcanic Province (Mihalynuk et al., 2012). The Pheno Mountain complex consists mainly of silica-saturated volcanic and hypabyssal rocks with minor metaluminous to peralkaline trachyte and alkali basalt. The petrography, geochemistry, and spatial co-occurrence of the felsic volcanic rocks and the stratigraphically underlying (Figs. 2, 3, 7) quartz and feldspar porphyritic hypabyssal rocks suggest that the rocks of the Pheno Mountain complex are co-genetic and represent parts of the same Miocene volcanic centre. Trachytic rocks are locally interlayered with the felsic volcanic rocks and may be either coeval or younger,

depending on whether the relationship is stratigraphic or intrusive. The age of the mafic and trachytic dikes is only constrained as younger than the hypabyssal porphyries.

Trace element geochemistry supports including the volcanic and hypabyssal rocks in the same magmatic suite. Both rocks are characterized by similar Nb/Ti ratios but different Zr/Ti ratios (Fig. 6b) suggesting that the compositional range resulted from fractionation of a parental magma similar to the mafic dike. This interpretation is supported by deeper Eu* anomalies with increasing Zr/Ti ratios (not shown), which suggest feldspar fractionation. The dated sample has similar characteristics, but contains a positive Ce anomaly, a more pronounced Eu anomaly, and overall lower LREE than other samples. These characteristics are easiest attributed to fractionation of LREE-rich phases, such as apatite, or volatile-mediated mobility of LREE complexes in a shallow magma chamber.

Trace element characteristics such as strongly enriched Nb, Zr, and Y (Figs. 6d, e) are all typical of within-plate magma suites (Fig. 6c) that form predominantly by fractionation of alkali basalt parental magma (e.g., Souther, 1992; Edwards et al., 2002; Macdonald, 2012). However, in contrast to typical within-plate highly fractionated peralkaline rhyolites, the Pheno Mountain complex rhyolite and hypabyssal quartz and feldspar porphyries display an alkalinity and alumina-saturation index typical of peraluminous rocks ($Al/(Na+K) > 1$ and $Al/(Ca+Na+K) \geq 1$).

The alkalinity index is very sensitive to mobility of alkali elements, whether in a shallow magma chamber, during cooling (e.g., Noble, 1970) and/or due to post-emplacement fluid-rock interaction. Many of our samples show evidence of fluid interaction (replacement of matrix and infilling of amygdalae). Our samples also display non-systematic variation in concentrations of Na₂O and K₂O (Table 2), suggesting mobility of elements used in alkalinity and alumina-saturation indexes. Relict pyroxene phenocrysts (Fig. 3e) are most consistent with metaluminous suites. Phenocrysts typical of peraluminous rocks have not been observed. Alkaline affinity of the Pheno Mountain complex is supported by a high Nb/Y ratio that is typical of alkaline to peralkaline rhyolites (Fig. 6b) and by the presence of blue amphibole (Fig. 4d) and normative acmite in one trachytic dike.

U-Pb dating of zircon separated from a subvolcanic Pheno Mountain complex quartz feldspar porphyry yielded a crystallization age of 7.78 ± 0.01 Ma. This age is significantly older than the ~85 to 9 Ka Hoodoo Mountain complex (³⁹Ar/⁴⁰Ar whole rock ages: Edwards et al., 2002) precluding the tentative correlation of Mihalynuk et al. (2012). The NCVP mainly comprises alkaline mafic rocks; evolved volcanic rocks are rare (see Edwards and Russell, 2000 and references therein). However, rhyolite has been documented at Level Mountain (Hamilton, 1981) and Mount Edziza (Souther, 1992). Both of these complexes erupted felsic volcanic rocks in the Late Miocene, following construction of coalesced basaltic

Table 2. Whole Rock geochemistry of the Pheno Mountain complex.

Sample ¹	Rhyolite								Quartz feldspar porphyry				Mafic	Trachyte		
	15-1A	15-1C	606A	606B	608	610A	610B	633 ⁵	551	554	556A	636A	556B	11-6B ⁶	561	586 ⁶
N ²	56.899	56.899	56.893	56.893	56.892	56.877	56.877	56.956	56.924	56.919	56.917	56.933	56.917	56.932	56.915	56.906
W ²	131.421	131.421	131.388	131.388	131.392	131.420	131.420	131.457	131.385	131.384	131.386	131.431	131.386	131.355	131.411	131.367
SiO ₂	78.39	76.15	72.28	74.70	75.55	75.53	79.15	79.96	74.32	74.31	77.73	73.29	39.35	59.80	61.40	61.82
Al ₂ O ₃	7.82	8.94	11.33	10.44	10.80	10.85	9.89	7.32	12.11	11.25	11.59	9.67	17.18	15.44	14.29	14.30
Fe ₂ O ₃	7.38	6.72	6.79	6.09	4.75	4.27	2.87	4.21	3.51	5.14	1.54	7.44	13.45	9.03	8.14	8.84
MgO	0.01	0.02	0.06	0.09	0.02	0.02	BD	0.01	0.09	0.16	0.07	0.07	3.15	0.28	0.08	0.36
CaO	0.04	0.02	0.08	0.09	0.12	0.16	0.06	0.06	0.14	0.09	0.11	0.89	11.80	0.60	2.28	2.13
Na ₂ O	0.14	0.14	0.15	0.17	0.28	1.46	4.03	1.78	3.70	0.13	2.64	2.38	2.40	4.77	2.96	5.10
K ₂ O	4.32	5.55	7.54	6.73	5.86	6.16	2.24	3.08	5.11	5.52	5.47	3.99	0.77	5.74	6.87	5.58
TiO ₂	0.26	0.30	0.39	0.36	0.25	0.25	0.20	0.21	0.27	0.30	0.08	0.32	2.50	1.05	0.62	0.71
P ₂ O ₅	0.01	0.02	0.04	0.03	BD ⁴	0.01	BD	0.02	0.03	0.02	BD	0.02	0.47	0.32	0.11	0.14
MnO	0.12	0.13	0.13	0.12	0.06	0.08	BD	0.06	0.06	0.06	0.03	0.13	0.20	0.22	0.23	0.24
LOI	1.20	1.70	1.00	1.00	1.90	0.90	1.30	2.50	0.50	2.50	0.70	1.20	8.40	2.50	2.80	0.60
Sum	99.70	99.64	99.79	99.83	99.58	99.72	99.80	99.16	99.85	99.45	99.93	99.45	99.69	99.71	99.83	99.86
Ba (ppm)	16	11	52	55	13	28	38	18	205	1468	39	66	458	1350	614	335
Cs	0.50	0.90	0.50	0.70	2.80	1.20	0.70	1.00	0.90	1.60	1.40	1.10	2.30	2.20	5.50	0.60
Ga	36.8	43.5	47.0	41.7	42.1	35.0	38.2	22.3	34.1	36.8	23.2	50.6	21.6	30.4	28.9	32.6
Hf	37.3	43.2	30.1	22.7	45.2	31.5	28.0	83.4	15.2	42.3	8.1	50.0	3.6	12.1	8.4	9.6
Nb	162	221	132	143	200	140	121	302	57	171	77	205	21	55	46	49
Pb	45.0	35.8	14.7	6.8	36.4	32.5	18.1	77.8	5.2	26.1	11.3	20.4	2.1	7.8	10.9	7.4
Rb	148	213	232	243	220	256	98	120	116	186	206	189	13	103	98	64
Sr	4.8	3.7	8.5	7.8	5.4	8.8	7.9	5.7	18.7	365	29.2	44.9	816	142.4	36.1	37.4
Ta	11.5	13.4	8.5	7.4	12.9	9.2	8.3	21.1	3.7	11.2	6.4	12.6	1.5	3.4	2.5	3.4
Th	25.5	28.1	18.2	13.8	27.1	26.8	25.7	56.6	11.2	28.2	30.5	37.4	1.7	8.2	5.9	5.8
U	6.1	11.7	6.2	3.3	10.9	8.8	10.0	22.1	4.8	11.6	13.6	13.4	0.5	3.2	1.3	2.2
Zr	1442	1872	1081	949	1893	1211	1096	3110	576	1627	148	2016	162	471	359	368
Y	144	201	108	98	199	149	110	453	71	166	71	255	29	63	48	56
La	126.1	71.3	64.9	44.1	198.5	190.2	40.4	432.7	60.3	101.7	14.1	212.2	21.4	48.1	60.3	47.6
Ce	201.4	154.0	121.6	93.0	398.4	311.3	80.0	844.6	126.6	216.9	74.1	448.0	44.6	106.5	99.5	101.5
Pr	34.82	20.62	18.08	11.12	52.86	42.22	9.60	106.60	16.74	28.36	3.68	51.86	6.15	13.80	14.56	13.58
Nd	130.6	84.7	68.7	44.1	202.5	155.6	34.8	420.3	66.1	107.2	13.3	206.9	28.3	55.2	55.5	54.4
Sm	28.88	24.95	15.08	9.74	40.48	29.17	7.83	86.26	13.92	23.57	4.01	44.86	6.19	12.54	10.99	11.95
Eu	1.60	1.69	1.19	0.85	1.85	0.94	0.31	4.11	0.95	1.04	0.06	2.62	2.06	3.14	2.54	2.38
Gd	26.74	30.35	14.39	11.23	36.90	27.06	10.30	86.40	13.17	23.11	5.69	47.19	6.06	11.98	9.83	11.21
Tb	4.43	5.66	2.67	2.37	5.95	4.07	2.19	13.29	2.19	4.13	1.38	8.05	0.90	1.91	1.65	1.78
Dy	28.34	34.95	19.48	16.32	35.13	26.62	17.49	86.69	13.56	29.18	10.19	45.82	5.34	12.70	9.21	10.75
Ho	5.39	7.33	3.91	3.59	6.90	4.97	3.84	15.87	2.64	5.88	2.26	10.45	0.99	2.29	1.77	1.97
Er	14.39	21.56	12.05	11.17	19.92	14.34	11.98	45.55	7.38	18.38	7.17	27.18	2.75	6.47	4.96	5.86
Tm	2.31	3.19	1.86	1.66	2.96	2.21	1.86	6.39	1.17	2.79	1.16	4.28	0.38	0.95	0.77	0.86
Yb	15.57	20.71	12.45	10.73	19.57	14.57	12.56	41.47	7.23	18.78	8.36	25.90	2.38	6.05	5.11	5.64
Lu	2.16	3.01	1.81	1.65	2.64	2.00	1.76	5.50	1.07	2.63	1.14	3.86	0.38	0.89	0.80	0.87
Ce/Ce ^{*3}	0.75	0.98	0.87	1.03	0.95	0.85	1.00	0.96	0.98	0.99	2.52	1.05	0.95	1.01	0.82	0.98
Eu/Eu [*]	0.18	0.19	0.25	0.25	0.15	0.10	0.11	0.15	0.21	0.14	0.04	0.17	1.03	0.78	0.75	0.63
Nb/Nb [*]	0.96	1.66	1.29	1.95	0.92	0.66	1.26	0.65	0.74	1.08	1.25	0.78	1.17	0.94	0.82	1.00

1. Sample numbers 11-6B, 15-1A, 15-1c are preceded by MMI-11; all other samples are preceded by ZE11. 2. Geographic coordinates, NAD 83, decimal degrees

3. Chondrite-normalized values (Sun and Macdonough, 1989) Ce*=(La_n*Pr_n)^{0.5}; Eu*=(Sm_n*Gd_n)^{0.5}; Nb*=(Th_n*La_n)^{0.5}. 4. BD - Below Detection; 5 - boulder; 6 - dike

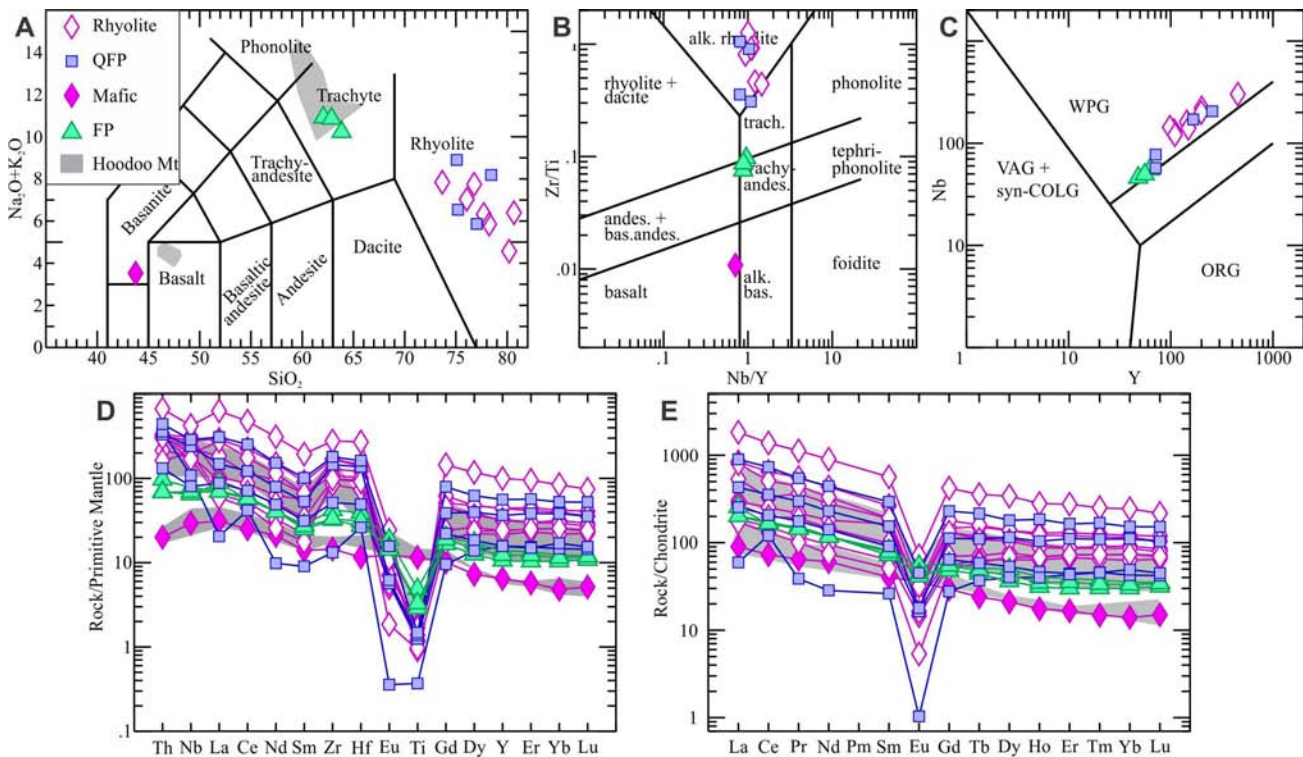


Fig. 6. Geochemical characteristics of the Pheno Mountain complex. **a)** TAS plot (Le Maitre et al., 1989); QFP – quartz feldspar porphyritic dikes, FP – feldspar porphyry. **b)** Pearce (1996) rock type plot. **c)** Felsic discrimination plot (Pearce et al., 1984). **d)** and **e)** Extended trace element plots. Normalization factors from Sun and McDonough (1989). Fields of Hoodoo Mountain complex are plotted for reference (from Edwards et al., 2002)

shields (Hamilton, 1981; Souther, 1992; Edwards and Russell, 2000). The Pheno Mountain complex is temporally equivalent to silica-saturated metaluminous to peralkaline rhyolitic rocks at Level Mountain and Mount Edziza, but apparently erupted directly onto Mesozoic basement, without construction of an extensive basaltic shield (Fig. 7). The lack of eruptive basaltic products thus presents a bit of a conundrum for the generation of these highly fractionated melts. Whereas it is possible that the Late Miocene Mount Edziza complex was much more laterally extensive than at present (Fig. 1), it is unlikely to

have been the source of the rhyolite in the Pheno Mountain complex as the present edge of the Mount Edziza complex is more than 60 km distant (Fig. 1). It is more likely that the Pheno Mountain complex was either sourced from a distinct, fractionating magma chamber or formed by low degree partial melting of the lower crust.

6. Conclusions

The Pheno Mountain complex comprises high Nb, Zr rhyolite, quartz feldspar porphyry and trachyte that unconformably overlie deformed Mesozoic to Paleozoic

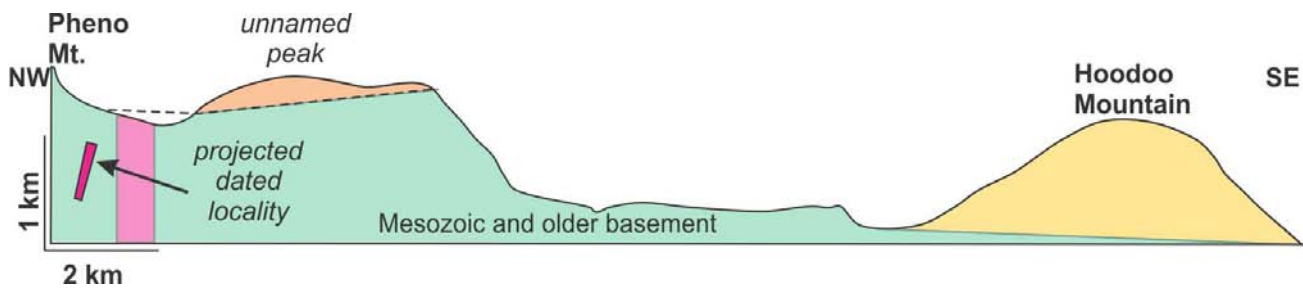


Fig. 7. Schematic NW-SE cross-section showing the relationship between Hoodoo Mountain and Pheno Mountain complexes (2x vertical exaggeration).

basement of Stikine terrane. The 7.78 Ma U-Pb zircon age confirms that the Pheno Mountain complex forms part the Neogene to Quaternary Northern Cordilleran Volcanic Province (Edwards and Russell, 2000). Because most of the NCVP was dated using K-Ar, Rb/Sr and fission track methodology (e.g., Hamilton, 1981; Souther, 1992; Evenchick and Thorkelson, 2005), which are sensitive to post-crystallization alteration and heating, the ca. 7.78 Ma age provides one of the best constraints on the NCVP felsic magmatism. Whole rock geochemistry indicates that different components of the complex are comagmatic, resolving ambiguities in field relationships. Whereas, most of NCVP is characterised by basaltic magmatism with minor felsic volcanic rocks, the Pheno Mountain complex appears unique in that it is not intimately linked to a major basaltic shield-building event.

Acknowledgments

This is a contribution to the Geological Survey of Canada Geomapping for Energy and Minerals Program (Multiple Metals Northwest Cordillera project; Geological Survey of Canada contribution #20120328). C. Evenchick, T. Hamilton, and L. Aspler are gratefully acknowledged for careful reviews that improved this paper.

References cited

- Edwards, B.R., and Russell, J.K. 2000. Distribution, nature, and origin of Neogene-Quaternary magmatism in the northern Cordilleran volcanic province, Canada. *Geological Society of America Bulletin*, 112, 1280-1295.
- Edwards, B.R., Russell, J.K., and Anderson, R.G. 2002. Subglacial, phonolitic volcanism at Hoodoo Mountain Volcano, northern Canadian Cordillera. *Bulletin of Volcanology*, 64, 254-272.
- Evenchick, C.A., and Thorkelson, D.J. 2005. Geology of the Spatsizi River map area, north-central British Columbia. *Geological Survey of Canada Bulletin* 577, 277 p.
- Gerstenberger, H., and Haase, G. 1997. A highly effective emitter substance for mass spectrometric Pb isotope ratio determinations. *Chemical Geology*, 136, 309-312.
- Gradstein, F.M., Ogg, J.G., Schmitz, M., Ogg, G., 2012, *The Geologic time scale*, Elsevier.
- Hamilton, T.S. 1981. Late Cenozoic alkaline volcanics of the Level Mountain Range, northwestern British Columbia: Geology, petrology, and paleomagnetism. University of Alberta, Edmonton, 490 p.
- Jaffey, A.H., Flynn, K.F., Glendenin, L.E., Bentley, W.C., and Essling, A.M. 1971. Precision Measurement of Half-Lives and Specific Activities of ^{235}U and ^{238}U . *Physical Review C* 4, 1889-1906.
- Kerr, F.A. 1948. Lower Stikine and western Iskut River areas, British Columbia. *Geological Survey of Canada Memoir* 246, 94 p.
- Le Maitre, R., Bateman, P., Dudek, A., Keller, J., Lameyre, J., Le Bas, M., Sabine, P., Schmid, R., Sorensen, H., Streckeisen, A., Woolley, A., and Zanettin, B. 1989. A classification of igneous rocks and glossary of terms: Recommendations of the International Union of Geological Sciences Subcommittee on the Systematics of igneous rocks Blackwell, Oxford, 193 p.
- Logan, J.M., and Koyanagi, V.M. 1994. Geology and mineral deposits of the Galore Creek area (104G/3, 4). Ministry of Energy, Mines and Petroleum Resources, British Columbia Geological Survey Bulletin 92, 95 p.
- Ludwig, K.R., 2003, *Isoplot 3.09 - A geochronological toolkit for Microsoft Excel*: Berkeley Geochronology Center, Special Publication No. 4.
- Macdonald, R. 2012. Evolution of peralkaline silicic complexes: Lessons from the extrusive rocks. *Lithos*, 152, 11-22.
- Mattinson, J.M. 2005. Zircon U-Pb chemical abrasion (CA-TIMS) method; combined annealing and multi-step partial dissolution analysis for improved precision and accuracy of zircon ages. *Chemical Geology*, 220, 47-66.
- Mihalyuk, M., Zagorevski, A., and Cordey, F. 2012. Geology of the Hoodoo Mountain area (NTS 104B/14). *Geological Fieldwork 2011*, British Columbia Ministry of Energy and Mines, British Columbia Geological Survey Paper 2012-1, 45-67.
- Mihalyuk, M., Logan, J., Zagorevski, A., and Joyce, N. 2011. Geology and mineralization in the Hoodoo Mountain area (NTS 104B/14E). *Geological Fieldwork 2010*, British Columbia Ministry of Energy and Mines, British Columbia Geological Survey Paper 2011-1, 37-63.
- Mundil, R., Ludwig, K.R., Metcalfe, I., and Renne, P.R. 2004. Age and timing of the Permian Mass Extinctions: U/Pb Dating of Closed-System Zircons. *Science*, 305, 1760-1763.
- Noble, D.C. 1970. Loss of sodium from crystallized comendite welded tuffs of the Miocene Grouse Canyon Member of the Belted Range Tuff, Nevada. *Geological Society of America Bulletin*, 81, 2677-2688.
- Pearce, J.A. 1996. A user's guide to basalt discrimination diagrams. In: *Trace element geochemistry of volcanic rocks: Applications for massive sulphide exploration*. D. A. Wyman (Ed.), Geological Association of Canada, Short Course 12, 79-113.
- Pearce, J.A., Harris, N.B.W., and Tindle, A.G. 1984. Trace element discrimination diagrams for the tectonic interpretation of granitic rocks. *Journal of Petrology* 25, 956-983.
- Schmitz, M.D., and Schoene, B. 2007. Derivation of isotope ratios, errors, and error correlations for U-Pb geochronology using ^{205}Pb - ^{235}U - ^{233}U -spiked isotope dilution thermal ionization mass spectrometric data. *Geochemistry, Geophysics, Geosystems*, 8, Q08006, 20 p.
- Scoates, J.S., and Friedman, R.M. 2008. Precise age of the platiniferous Merensky Reef, Bushveld Complex, South Africa, by the U-Pb ID-TIMS chemical abrasion ID-TIMS technique. *Economic Geology*, 103, 465-471.
- Souther, J.G. 1992. The late Cenozoic Mount Edziza volcanic complex, British Columbia. *Geological Survey of Canada, Memoir* 420, 319 p.
- Sun, S.S., and McDonough, W.F. 1989. Chemical and isotopic systematics of oceanic basalts; implications for mantle composition and processes. *Geological Society Special Publication* 42, 313-345.
- Thirlwall, M.F. 2000. Inter-laboratory and other errors in Pb isotope analyses investigated using a ^{207}Pb - ^{204}Pb double spike. *Chemical Geology*, 163, 299-322.

Geological setting of the Lonnie niobium deposit, British Columbia, Canada

Simandl, G.J.^{1,2,a}, Reid, H.M.¹ and Ferri, F.¹

¹ British Columbia Geological Survey, Ministry of Energy, Mines and Natural Gas, Victoria, BC, V8W 9N3

² University of Victoria, School of Earth and Ocean Sciences, Victoria, BC, V8P 5C2

^a corresponding author: George.Simandl@gov.bc.ca

Recommended citation: Simandl, G.J., Reid, H.M., and Ferri, F., 2013. Geological setting of the Lonnie niobium deposit, British Columbia, Canada. In: Geological Fieldwork 2012, British Columbia Ministry of Energy, Mines and Natural Gas, British Columbia Geological Survey Paper 2013-1, pp. 127-138.

Abstract

The Lonnie Nb deposit lies along the Wolverine fault, which is related to the Manson Creek fault system. It is the third-most developed Nb prospect in British Columbia. Unlike the larger Aley Carbonatite and Upper Fir deposits, where the Nb and Nb+Ta zones are carbonatite-hosted, historical work suggests that the highest Nb grades at the Lonnie complex are in quartz-free feldspathic rocks. The carbonatite (metacarbonatite) zones also contain significant concentrations of Nb. Limited sampling carried out in 2012, including 12 samples from the Lonnie deposit, agrees with the historical findings: the highest Nb value (>2500 ppm) is from one of three quartz-free feldspathic samples; the next highest values (1670 and 1210 ppm) are from two of five carbonatite samples. The 2012 sampling indicates that the metacarbonatites have chondrite-normalized REE patterns that are similar to the quartz-free feldspathic rocks, fenites, and nearby limestone; however, they have the highest REE concentrations. Fenitization extends for more than 30 metres southwestward into the host rock, perpendicular to the strike of the Lonnie mineralization and projection of the Wolverine fault. Carbonatite emplacement predates 4 periods of tectonic activity and the metamorphic peak. Pyrochlore is the main Nb-bearing mineral within the aegirine carbonatite. However, its paucity in quartz-free feldspathic rocks, suggests the presence of minerals of the columbite series or fersmite, a possibility that remains to be tested by microprobe analysis. Projection of the Wolverine fault zone, probably the main Nb metallogenic in the area, was shifted northeast to reflect results of a recent magnetic survey. Geochemical anomalies identified by Rara Terra Minerals Corp. at the Vergil carbonatite, less than 5 km northwest of the Lonnie complex, lie along the reinterpreted projection of the Wolverine fault.

Keywords: Niobium, quartz-free feldspathic rocks, carbonatite, fenite, pyrochlore, columbite series minerals

1. Introduction

Niobium (Nb) is a strategic metal that is mainly used for the production of steel and superalloys (e.g., Simandl et al., 2012). The global Nb supply for 2011 is estimated at 63 000 tonnes of contained Nb. Brazil (58 000 tonnes) and Canada (4400 tonnes) are the main producing countries (Papp, 2012). Carbonatites and their weathered equivalents are the main sources of Nb (Mariano, 1989a, b; Birket and Simandl, 1999; Simandl et al., 2012). Most carbonatites are found in stable cratonic settings, commonly along ancient rift zones (Wolley and Kjarsgaard, 2008; see Gwalani et al., 2010 and references therein for summaries of recent research on carbonatites and alkaline rocks). British Columbia carbonatite-related deposits straddle the western margin of ancestral North America, in the British Columbia alkaline province (Fig. 1, inset; Pell, 1994), which also hosts numerous other potential specialty metals deposits (Birkett and Simandl, 1999). In British Columbia, carbonatites and their host rocks have been affected by several periods of tectonic activity and overprinted by medium- to high-grade metamorphism.

Niobium mineralization associated with the Lonnie metacarbonatite (MINFILE 093N 012) represents the

third-most developed Nb prospect in British Columbia (after the Aley and Upper Fir deposits). The Lonnie deposit, the smallest of the three, lies 220 kilometres northwest of Prince George and approximately 7 kilometres east of the Manson Creek settlement (Fig. 1, inset). Discovered in 1953, Lonnie was stripped and drilled by Northwest Exploration Limited (Thompson, 1955; Hankinson, 1958). Since then it has been intermittently investigated by a number of individuals and companies (Vaillancourt and Payne, 1979). Currently, the deposit is being investigated by Rara Terra Minerals Corp, which recently conducted airborne geophysical and soil surveys (Helmel, 2012).

This deposit was chosen as part of the specialty metals component of the 2012 Targeted Geoscience Initiative 4 (TGI4) because: 1) the paragenesis, mineralogy, and mineral chemistry of this complex has not been investigated by modern laboratory methods; and 2) much of the mineralization is considered to be in feldspar-rich lithologies, which contrasts with the Aley and Upper Fir deposits. The main objective of this component of TGI4 is to reduce the knowledge gaps currently hampering the exploration for, and development of, specialty metal deposits. This study describes the

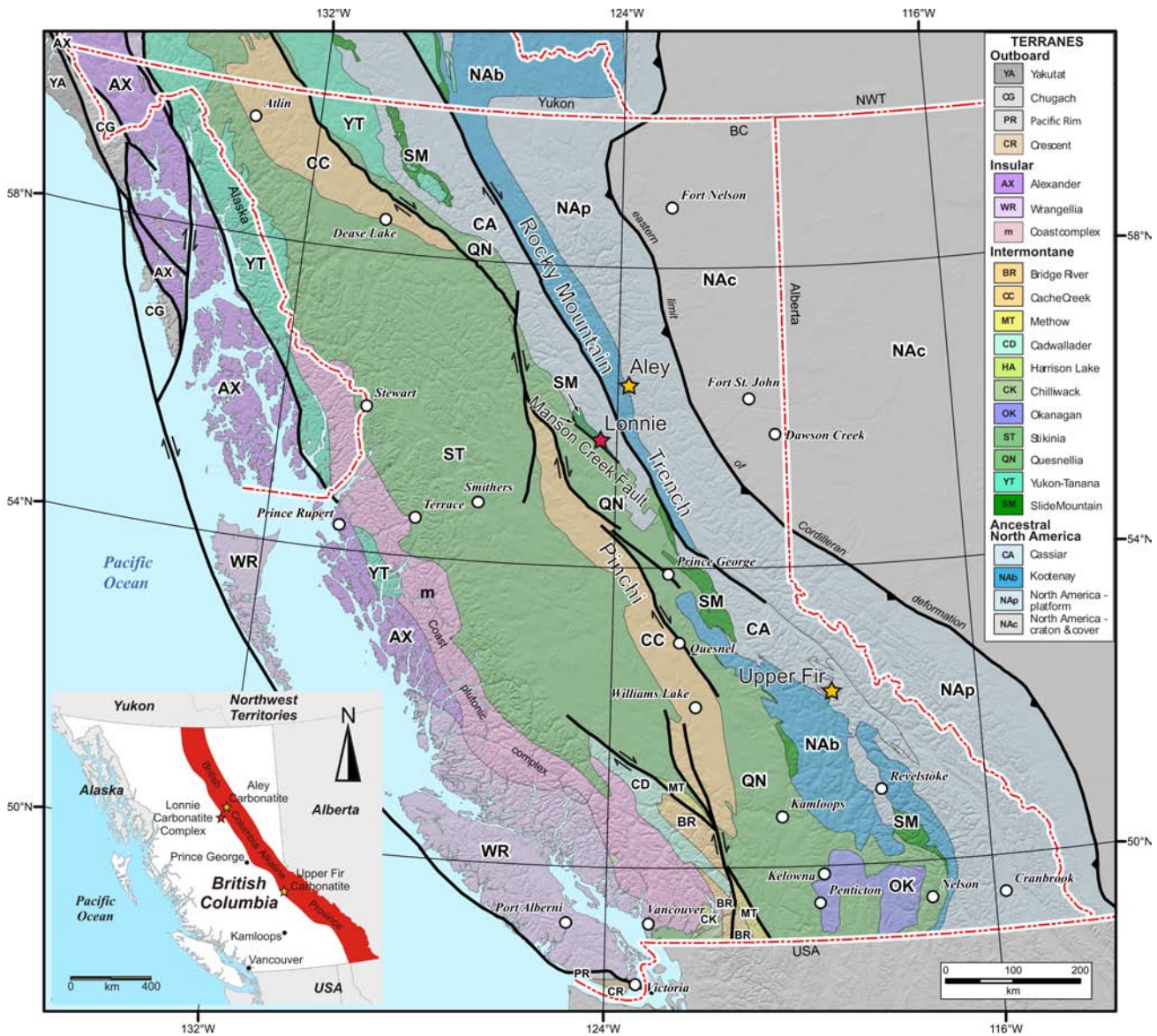


Fig. 1. Location and tectonic setting of the Lonnie carbonatite complex. Towns and major settlements are represented by white circles. Modified from Colpron and Nelson (2011).

regional tectonic setting of the Lonnie deposit and presents the preliminary results of detailed sampling in 2012.

2. Geological setting

The Lonnie carbonatite belongs to a series of metacarbonatites, syenite complexes, and other alkaline rocks of the British Columbia alkaline province, which follows the Rocky Mountain Trench (e.g., Pell, 1994; Simandl et al., 2012). It is in the southern Omineca Mountains, which straddle the boundary between the Intermontane and Omineca Belts. The Lonnie metacarbonatite outcrops along the projection of the Wolverine fault (Fig. 2), an extensional structure that is sub-parallel to the nearby dextral, transcurrent Manson

Creek fault zone (Fig. 1). The Manson Creek fault zone is a 1-5 km wide, near-vertical system of anastomosing transcurrent faults considered to be part of the Rocky Mountain Trench system, separating the Quesnel Terrane from the Slide Mountain and Cassiar terranes (Ferri and Melville, 1994). We modified the projection of the Wolverine fault zone, shifting it an average of 700 m to the northeast, to fit both previously available geological constraints and results from a recent magnetic survey conducted by Rara Terra (Helmel, 2012). Following this modification, it appears that the Vergil carbonatite occurrence (MINFILE 093N 174), less than 5 km northwest of the Lonnie complex, and a number of geochemical soil anomalies located by Rara Terra, also align along the reinterpreted projection of the Wolverine

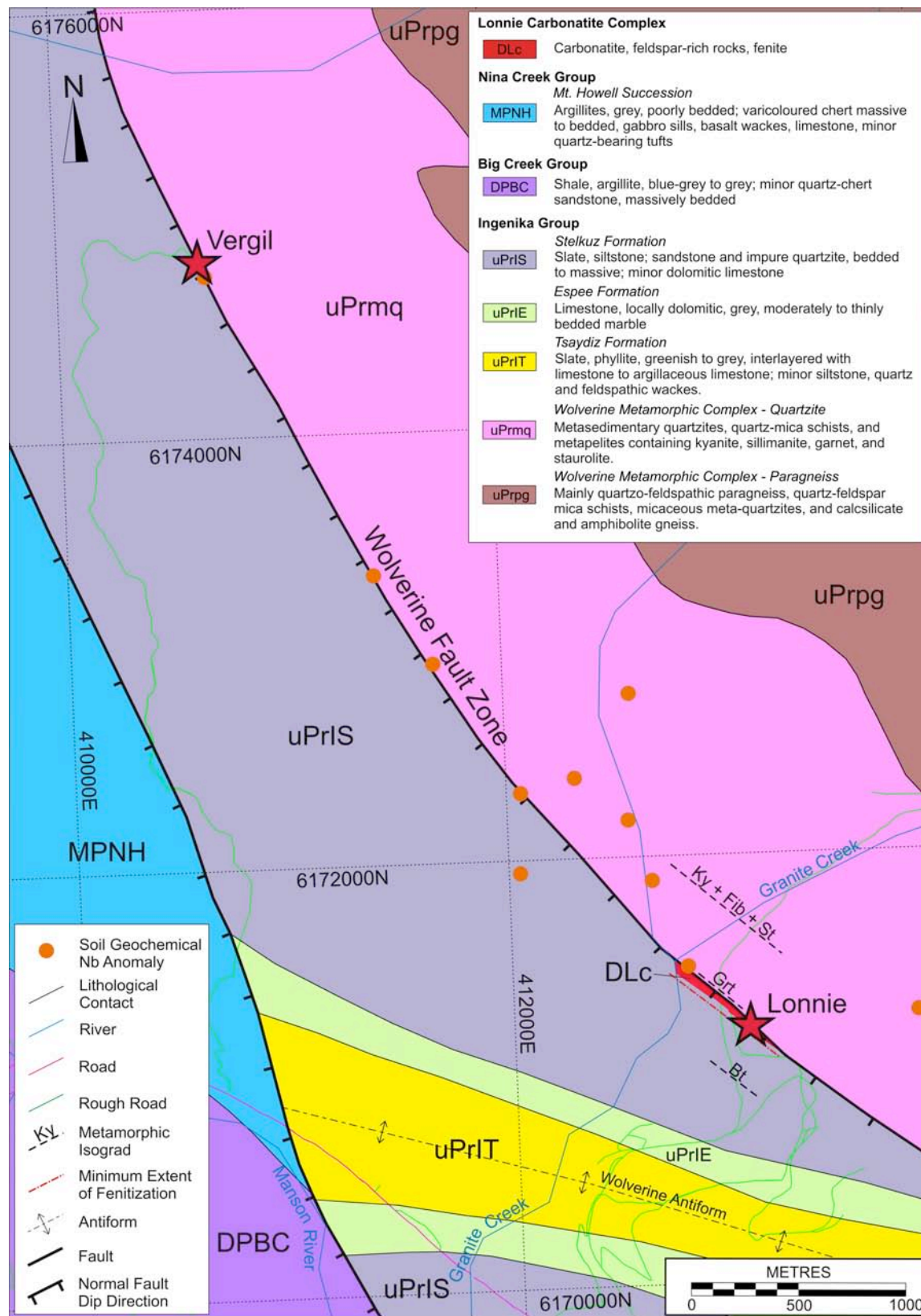


Fig. 2. Regional map of the Lonnie carbonatite complex. Abbreviations of metamorphic index minerals are placed on the high-grade side of the isograd; Bt = biotite, Grt = garnet, Ky = kyanite, St = staurolite, and Fib = fibrolite. Most geochemical soil anomalies (Nb and Total REE) and a strong magnetic signature (Helmel, 2012) coincide with the most likely projection of the Wolverine fault zone. Modified from Ferri and Melville (1994).

fault (Fig. 2).

The Wolverine fault zone represents the boundary between polydeformed, amphibolite grade (garnet, staurolite, kyanite, and fibrolite-bearing) rocks of the Wolverine metamorphic complex to the northeast, and less metamorphosed strata of the upper Proterozoic Ingenika Group and the Paleozoic Nina Creek and Big Creek groups to the southwest (Fig. 2; Ferri and Melville 1994). In the Lonnie Creek area, the fault is probably manifested as multiple splays rather than a single strand as shown on Figure 2. For example, fault gouge more than 1 metre thick is exposed less than 40 m northeast of the projection of the Wolverine fault. The northeastern contact of the Lonnie carbonatite complex is not exposed. However, southwest of the fault, carbonatite-related fenitization was observed to have survived metamorphic overprint.

The Wolverine metamorphic complex is composed of amphibolite facies rocks of the Ingenika Group. Metasedimentary rocks outcropping less than 540 metres north of the Wolverine fault contain white mica, biotite, garnet, staurolite, fibrolite, and kyanite (Figs. 3-5).

Near the Lonnie deposit, southwest of the Wolverine fault zone, are Upper Proterozoic siliciclastic and carbonate rocks of the Stelkuz Formation, a lower to middle Paleozoic continental succession (Big Creek Group), and upper Paleozoic oceanic rocks of the Nina Creek Group. In addition, a series of excellent marker units, such as the upper Proterozoic Espee Formation, outline megascopic geological structures (Fig. 2). All of these rocks were affected by lower grade metamorphism, indicated by: phyllitic and slaty textures; the appearance of sericite, chlorite, and biotite; and an absence of garnet in gneiss (Fig. 6).

2.1. Age relationship between carbonatite emplacement and deformation

The Lonnie complex is considered to have been emplaced during the Late Devonian to Early Mississippian, before regional deformation. This timing is based on U-Pb zircon data from carbonatite samples at both the Lonnie and Vergil occurrences, including a discordant U-Pb age of ~340 Ma, and Pb-Pb ages of 351-365 Ma (Pell, 1987; 1994). Rukhlov and Bell (2010) reported a similar U-Pb zircon crystallization age (~360 Ma) from a composite sample of British Columbia alkaline province rocks that included Vergil carbonatite material.

Four penetrative phases of deformation (D1, Early to Middle Jurassic; D2, Middle to Late Jurassic; D3, Early to Middle Cretaceous; and D4, Late Cretaceous to Early Tertiary) have been identified in metamorphic rocks of the area based on interference, crosscutting relationships, structural styles, and relationships to metamorphism (Ferri and Melville, 1994). The metamorphic peak appears to postdate D1 and predate D2, the Wolverine antiform was created during D3, and development of the Wolverine and Manson Creek fault systems and

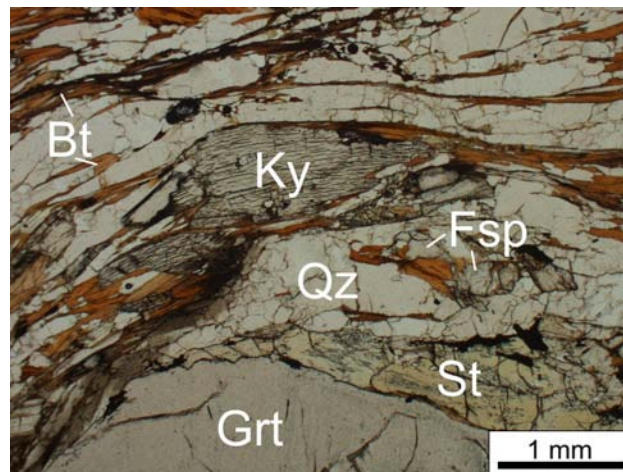


Fig. 3. Garnet (Grt), staurolite (St), and kyanite (Ky) metapelite from the Wolverine complex. Quartz (Qz), biotite (Bt) and feldspar (Fsp) are also present. (Plane-polarized light).

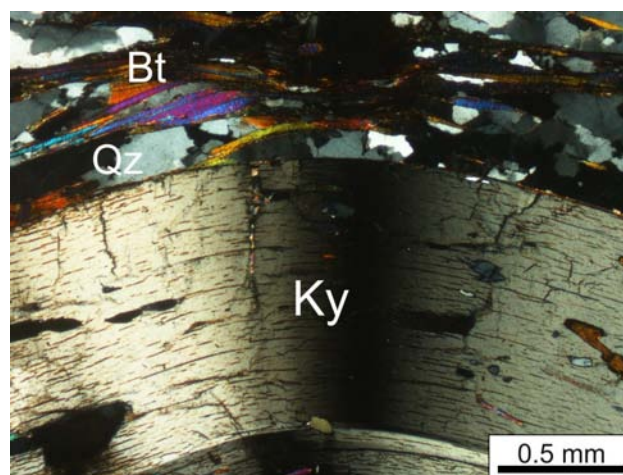


Fig. 4. Bent kyanite (Ky) crystal from the Wolverine complex showing wavy extinction, indicating that kyanite predates at least the last deformation (D4). Groundmass consists mainly of biotite (Bt) and quartz (Qz). (Cross-polarized light).

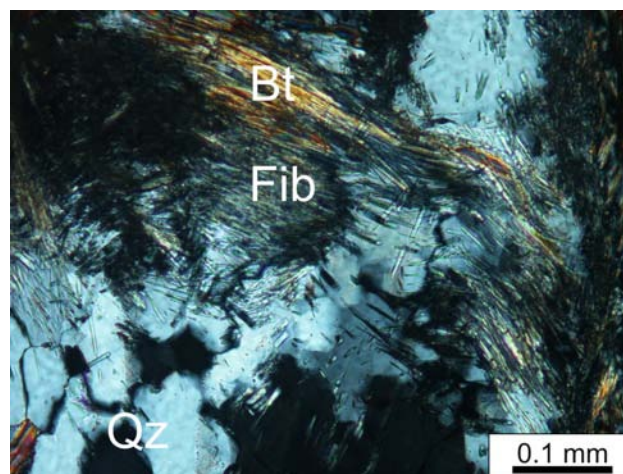


Fig. 5. Fibrolite (Fib) growing on biotite (Bt) in quartz (Qz) groundmass. This mineral is common in rocks approaching the sillimanite stability field. (Cross-polarized light).

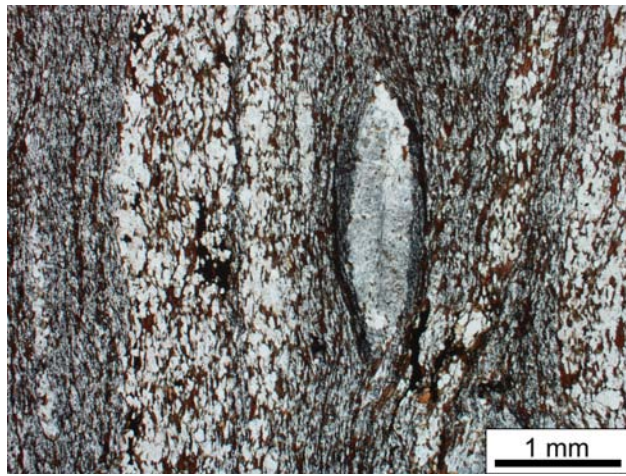


Fig. 6. Biotite-quartz-feldspar gneiss in the hanging wall, 25 metres from the Lonnie complex. Pale grey minerals are quartz and feldspar; biotite is reddish-brown. Darker grey bands are finer-grained, and contain micron-scale opaque minerals. (Plane-polarized light).

emplacement of most of the intrusions in the Wolverine complex was during D4 (Ferri and Melville, 1994). K-Ar geochronological studies, described in detail by Ferri and Melville (1994), indicate that the Wolverine metamorphic complex remained hot until early Tertiary times, when it was rapidly uplifted. Unless the zircon that was dated was inherited by the ascending carbonatite from continental crustal rocks or underlying subducting oceanic crust, the Lonnie carbonatite complex pre-dates all four phases of deformation. The alignment of the Vergil and Lonnie complexes along the projection of the Wolverine fault suggests that this fault may have been a plane of weakness for at least 350 million years (since the emplacement of carbonatites in an extensional regime) and could have been reactivated several times, with most of the displacement along this plane occurring during the Late Cretaceous to Early Tertiary D4 deformation event.

The steep metamorphic gradient, in agreement with primary sedimentary features partly preserved in the limestones and phyllites southwest of the Wolverine fault, in contact with the Wolverine metamorphic complex, is explained by inferred lateral or vertical step-like offsets parallel to the Manson Creek/Wolverine fault system. Fluid movement along this fault zone cannot explain this steep, asymmetric metamorphic gradient. Southwest of the Lonnie carbonatite complex and Wolverine fault, carbonatite-related fenitization has survived metamorphic overprint; however, the northeastern contact of the Lonnie complex is not exposed, is absent, or has been rendered unrecognizable due to metamorphism.

3. Deposit geology

The Lonnie carbonatite complex has been traced by trenching over a length of approximately 650 metres, with widths of up to 50 metres. It strikes 120E/60SW (Hankinson, 1958; Rowe, 1958). It consists of biotite-bearing sövite, aegerine-amphibole sövite, and a variety of quartz-free feldspathic rocks. These feldspathic rocks

have Na-plagioclase contents corresponding to syenite monzonite or monzodiorite, according to the IUGS classification of Streikenson (1978) and Le Maitre (2002). The geochemical classification scheme of Wilson (1989) categorizes these rocks as syenites.

The map produced by K.C. Campbell on behalf of Northwestern Exploration Ltd. in 1955 has been reproduced many times (e.g., Hankinson, 1958; Rowe, 1958; Halleran, 1980; Pell, 1987) and will not be shown here. Instead, our examination and sampling concentrates on a single, relatively well exposed vertical section over 40 metres long and approximately 5 metres high, oriented nearly perpendicular to the strike of the Lonnie complex (Fig. 7).

Host rocks of the Lonnie complex are strongly fenitized on the southwest side of the Wolverine fault (see section 3.4). In general, the degree of fenitization decreases with increasing distance from the complex. The 1955 trenching program (pre- NI-43-101) outlined a zone 530 metres long and approximately 17 metres wide grading 0.21% Nb₂O₅ (Rowe, 1958; Chisholm, E.O., 1960). In this zone, the Na-amphibole-bearing carbonatite assayed 0.16% Nb₂O₅ over 6 metres. Feldspathic rocks averaged 0.23% Nb₂O₅ over nearly 10 metres.

Furthermore, the central portion of this zone averaged 0.3% Nb₂O₅ across 8.3 metres over a length of 283 metres (Rowe, 1958). In summary, assuming that the laboratory digestion (see section 4) of both pyrochlore and columbite series minerals was complete, the feldspathic rocks have higher Nb content than the carbonatites.

3.1. Biotite-rich calcite carbonatite

Biotite-bearing calcite carbonatite (biotite sövite, Fig. 8) is beige on weathered surfaces and pale gray on fresh surfaces. It reacts strongly with HCl, and is locally moderately magnetic. Most of this unit is sheared and highly friable (Fig. 9). Where the carbonatite is intact, it is mottled and displays well-developed planar fabrics. It consists of calcite (>75%, 25 mm) with deformed twin planes, biotite (~20%, 1-6 mm) which is locally crenulated, potassium and plagioclase feldspar (2-15%, ~1 mm), subhedral to anhedral apatite (2-10%, 1-3 mm), pyrochlore (0-0.5%, <2 mm), pyrite in form of cubes (<0.5%, <2 mm) or as anhedral grains (<0.5 mm) with hematite rims, and other opaque minerals (<2%, <1 mm) consisting mainly of magnetite. Columbite series minerals [(Fe,Mn)(Nb,Ta)2O6] or fersmite may also be present. Vestiges of small aegirine grains (<0.1%, <0.2 mm) were observed in thin section. Biotite near the carbonatite-syenite contact locally forms platy crystals up to 15 cm in the largest dimension and approaching 1 cm in thickness. Pyrochlore has been identified, and is found locally in biotite (Fig. 10). Where carbonatite forms enclaves in feldspathic rocks, the biotite appears strongly chloritized, and laths of opaque minerals are abundant. Chemical analyses of representative biotite-rich calcite carbonatite are provided in Table 1.

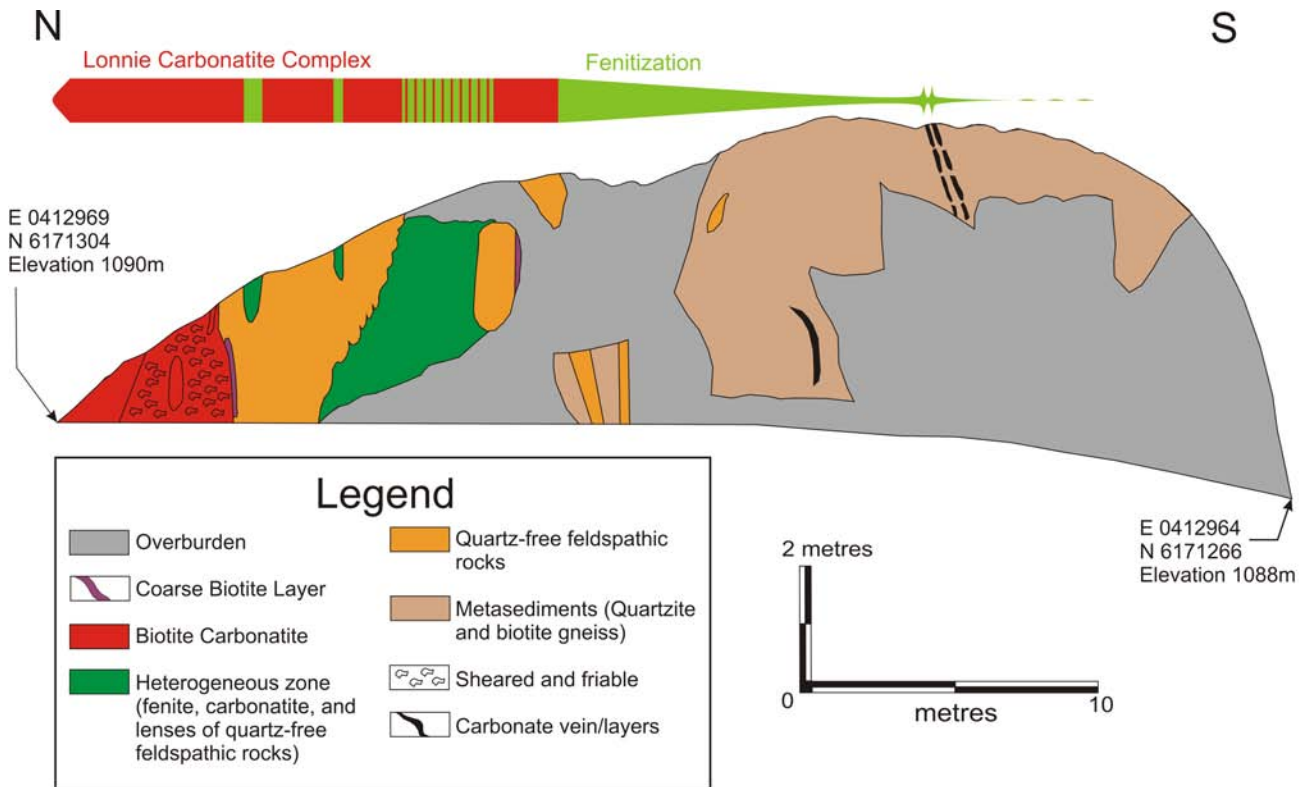


Fig. 7. Vertical section of the Lonnie complex, looking east. Fenitization and the modal ratio of aegirine to Na-amphibole decreases with increasing distance from the complex.

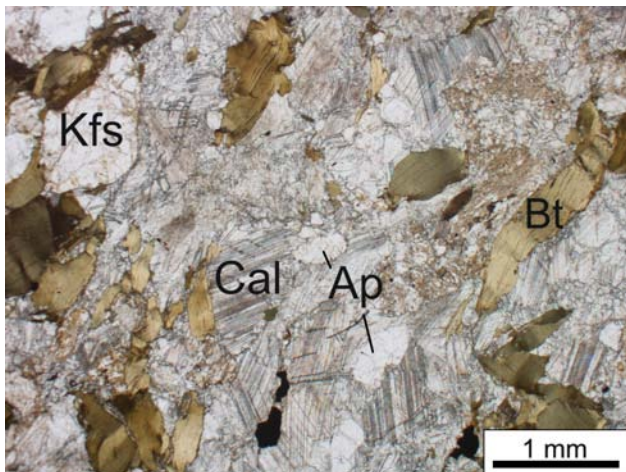


Fig. 8. Biotite-rich calcite carbonatite, containing potassic feldspar (Kfs), calcite (Cal), apatite (Ap), and biotite (Bt). (Plane-polarized light).



Fig. 9. Friable biotite-rich calcite carbonatite. Marker for scale.

3.2. Aegirine ± Na amphibole-bearing carbonatite

Aegirine ± Na amphibole-bearing carbonatite is mostly pale beige to grey on the weathered surfaces and white to pale-gray on fresh surfaces. It is typically massive; local macroscopic fabrics are weakly developed. This carbonatite also reacts strongly with HCl. It is interlayered with fenite rocks approximately 5 metres from the main biotite carbonatite exposure. It consists

predominantly of calcite (>75%, <5 mm) and aegirine (2-20%, 0.5-6 mm), with accessory pyrochlore (<3%, <1 mm), apatite (<5%, <2 mm), and feldspars (<3%, <2 mm); it may also contain Na-amphiboles (<0.5-5%, <5 mm) displaying strong blue-green pleochroism in thin section. Pyrochlore appears to be the main niobium-bearing mineral. It is subhedral, commonly containing carbonate inclusions. Zoning is caused by preferential concentrations of small (<0.003 mm) dark inclusions and separate colour variations are probably caused by

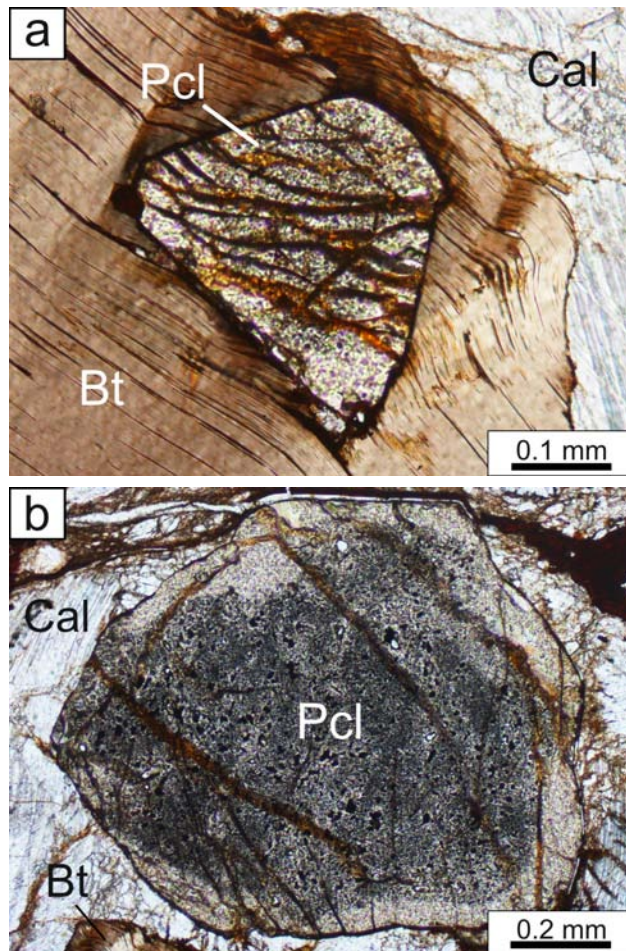


Fig. 10. Biotite-rich calcite carbonatite. **a)** Pyrochlore (Pcl) growing in biotite (Bt). **b)** Pyrochlore growing in calcite (Cal). (Plane-polarized light).

variations in chemical composition (Fig. 11). Opaque minerals, mostly anhedral (<0.5%, <2 mm) are also present. Electron microprobe analysis is needed to confirm the presence of columbite series minerals or fersmite. Pyrite accounts for a small proportion of opaques (<0.05%, 0.05 mm). Chemical analyses of representative samples are in Table 1.

3.3. Quartz-free feldspathic rocks

Leucocratic, quartz-free feldspathic rocks are brown on weathered surfaces and pale gray on fresh surfaces (Fig. 12). They are massive, but locally display layering, and are cut by fractures and micro-fractures filled by brown Fe oxides or carbonate. They consist mainly of feldspar displaying deformed twin planes (>80%, <1 cm), biotite – commonly showing a kinked texture – (<5%, <6 mm), calcite (<5%, <2 mm), and opaques (probably hematite and/or columbite filling fractures and interstitial spaces). Sparse grains of pyrite (<0.01%, <0.05 mm) have been largely converted to Fe oxides. Some of these rocks are characterized by small, untwinned feldspars (<0.3 mm) along the interstitial boundaries of large feldspar crystals (1.5-2.5 mm). Locally, carbonates fill interstitial spaces. Where carbonate invades along

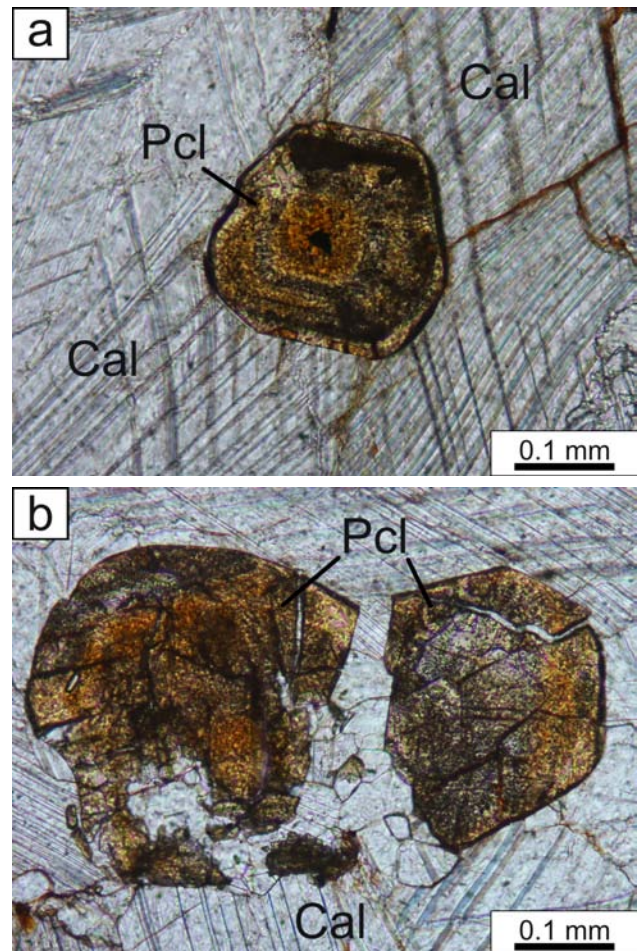


Fig. 11. Zoned pyrochlores (brown) in aegerine-dominated sövite carbonatite. **a)** Shows zoning parallel to the nearly euhedral outline of the crystal. **b)** Pyrochlore, fractured and partially resorbed. (Plane-polarized light).

fractures, biotites are strongly altered. Samples collected in 2012 contain trace microscopic pyrochlore (<0.01%, <0.1 mm). High Nb values suggest that Nb is concentrated in opaque minerals, probably belonging to the columbite series or fersmite. Zircons can be observed in some hand specimens and in all thin sections. One sample, consisting predominantly of plagioclase (>85%), also contains white mica (<1%, <4 mm). These rocks are probably, at least in part, the result of fenitization.

3.4. Fenites

The zone of fenitization associated with the Lonnie meta-carbonatite extends for at least 33 metres southwestward into the host rock, and the degree of fenitization decreases with increasing distance from the complex. Within or immediately adjacent to the complex or related carbonatite dikes, the fenite is brown or green on weathered surfaces, medium green on fresh surfaces (Fig. 13), and massive to crudely layered. In thin section, fenites display distinct layering and typically contain alkali feldspar (40-80%, <2 mm) and aegerine (10%-50%, <4 mm), with Na-amphibole (<10%, <4 mm) and accessory quartz and calcite. Fenitization within or

Table 1. Major and trace element analyses of samples from the Lonnie carbonatite complex and surrounding area (see section 4 for description of analytical methods).

Rock Type:	Biotite Carbonatite					Aegirine Carbonatite			Quartz-free Feldspathic Rocks			Fenites		Fenitized Metasediments*		Limestone
Sample:	LO-12-09	LO-12-10	LO-12-10A	LO-12-14C	LO-12-14E	LO-12-12	LO-12-13	LO-12-15 ¹	LO-12-14B	LO-12-14D	LO-12-16	LO-12-17 ²	LO-12-19			
<i>wt%</i>																
SiO ₂	21.5	6.38	1.72	22.4	35	61.4	62.9	62.6	53.2	50.4	77.4	49.7	2.39			
Al ₂ O ₃	9.83	1.78	0.5	1.58	3.58	17.15	17.45	17.55	7.84	7.68	7.29	9.59	0.47			
Fe ₂ O ₃	5.53	5.39	1.82	10.45	12.9	0.32	0.5	0.83	13.15	12.05	4.72	6.73	0.18			
CaO	33.2	47.2	54.5	34.9	21.5	2.99	1.21	4.52	9.12	11.35	1.43	16.25	60.6			
MgO	1.96	2.1	0.95	0.78	1.27	0.06	0.05	0.06	1.75	1.64	1.09	1.18	0.66			
Na ₂ O	1.5	0.21	0.11	4.49	6.84	5.79	5.52	11	7.89	8.37	5.02	5.98	0.03			
K ₂ O	2.88	0.54	0.28	0.84	1.29	6.88	7.44	0.25	2.62	1.45	1.73	1.46	0.11			
TiO ₂	0.65	0.36	0.1	0.45	0.43	0.01	0.05	0.04	0.78	0.75	0.57	0.54	0.02			
MnO	0.28	0.69	0.69	0.57	0.48	0.05	0.04	0.07	0.37	0.39	0.14	0.5	0.01			
P ₂ O ₅	2.28	2.02	0.68	3.23	0.54	0.07	0.37	1.18	1.75	2.14	0.1	0.47	0.01			
SrO	0.81	1.6	1.88	0.98	0.72	0.12	0.07	0.2	0.18	0.29	0.04	0.55	0.46			
LOI	17.5	33.3	38.1	18.45	17.2	2.87	1.13	-0.11	2.04	2.97	0.35	8.63	36.3			
Total	97.92	101.57	101.33	99.12	101.75	97.71	96.73	98.19	100.69	99.48	99.88	101.58	101.24			
S	0.24	0.04	0.07	<0.01	<0.01	<0.01	<0.01	0.01	<0.01	0.02	0.05	0.08	<0.01			
C	6.29	9.35	11.25	6.38	4.37	0.64	0.23	0.65	1.34	1.82	0.24	3.35	11.7			
<i>ppm</i>																
V	105	51	18	704	533	<5	12	5	404	354	114	135	<5			
Cr	<10	<10	<10	10	30	<10	<10	10	70	70	90	70	10			
Co	7	7.7	1.2	1.7	2.5	<0.5	<0.5	<0.5	8.8	7.1	8.6	8.7	0.5			
Ni	<5	<5	<5	5	7	<5	<5	<5	29	26	23	31	<5			
Cu	<5	<5	<5	<5	<5	<5	<5	<5	<5	<5	11	9	<5			
Zn	94	91	32	63	81	5	8	6	188	144	94	70	16			
Ga	18.4	18.5	8.1	21.2	21.4	33	33.3	75.4	45.1	48.5	14.5	20.9	0.8			
Rb	110	69.2	18.9	20.5	26.3	98.6	132.5	4.7	73.1	35.7	56.8	32	2.2			
Zr	130	30	<20	280	350	330	5000	3370	150	110	360	220	<20			
Nb	312	1210	131.5	1670	291	617	>2500	939	236	140	369	193	1.3			
Mo	<2	<2	<2	<2	<2	<2	4	<2	<2	<2	169	25	<2			
Ag	<1	<1	<1	<1	<1	<1	<1	<1	<1	1	<1	<1	<1			
Sn	1	1	<1	10	12	<1	5	1	7	8	2	6	<1			
Cs	1.97	1.68	0.39	0.13	0.12	0.21	0.82	0.1	0.24	0.16	0.27	0.28	0.07			
Ba	2300	1250	1260	607	709	3120	4200	135	243	272	380	439	316			
Hf	1.5	0.5	<0.2	3.9	5.4	3.5	48	39.7	1.4	1.4	8.4	4.9	<0.2			
Ta	3.2	1	0.1	7.4	1.2	12.8	63.4	6	1.6	1.1	1.1	0.9	<0.1			
W	<1	1	<1	1	1	1	12	1	1	1	<1	1	<1			
Tl	1.1	1	0.8	<0.5	1.3	0.8	0.9	1.5	0.6	<0.5	2.4	3.5	1.3			
Pb	20	26	22	103	33	11	14	43	38	128	54	40	19			
Th	8.56	12.9	3.24	21.7	28	14.75	69	47	436	230	50.1	33.9	0.93			
U	3.03	2.21	0.18	46.7	7.91	51	39.6	8.41	3.14	2.26	3.55	4.72	1.38			
F	1900	2530	730	2420	940	90	360	840	1820	2070	1320	1340	110			
La	328	570	489	506	354	69	147.50	383	172.50	205	54.30	176	3.70			
Ce	580	1000	889	809	537	113.50	265	662	283	335	95.50	332	6.90			
Pr	58.50	103	90.60	77.80	49.20	10.95	24.60	65	28.10	33.50	10.15	35.60	0.75			
Nd	188	320	289	239	142.50	31.80	71.10	194.50	85.20	104.50	32.90	118	2.50			
Sm	30.20	52.20	48.40	36.20	20.20	4.31	9.02	26	12.90	16.05	5.75	22.80	0.44			
Eu	9.05	15.60	14.70	10.65	5.81	1.22	2.41	6.73	3.58	4.81	1.61	6.50	0.13			
Gd	25.50	43.60	38.90	29.30	15.90	3.32	6.51	17.85	9.78	13.65	5.61	21.50	0.40			
Tb	3.18	5.46	5.17	3.65	2.05	0.41	0.76	1.97	1.17	1.64	0.74	3.08	0.05			
Dy	13.90	25.10	23.90	16.35	9.37	1.82	3.18	8.11	5.10	7.11	3.63	15.85	0.28			
Ho	2.42	4.46	4.24	2.87	1.68	0.32	0.58	1.34	0.85	1.20	0.67	3.10	0.05			
Er	6.09	11.35	11.15	7.37	4.47	0.85	1.60	3.46	2.09	2.98	1.87	8.84	0.15			
Tm	0.83	1.62	1.59	1.05	0.66	0.14	0.27	0.51	0.31	0.45	0.31	1.38	0.02			
Yb	4.37	9.11	9.03	5.85	3.98	0.74	1.60	3.01	2.07	2.74	1.92	8.03	0.13			
Lu	0.68	1.49	1.49	0.98	0.72	0.13	0.29	0.53	0.45	0.56	0.36	1.33	0.02			
Y	59.10	113.50	122.50	70.10	44.20	8.50	12.7	33.50	21.50	27.40	16.40	86	1.50			
ΣREE	1250.72	2162.99	1916.17	1746.07	1147.54	238.51	534.42	1374.01	607.10	729.19	215.32	754.01	15.52			
ΣREY	1309.82	2276.49	2038.67	1816.17	1191.74	247.01	547.12	1407.51	628.60	756.59	231.72	840.01	17.02			
Ce/Yb	132.72	109.76	98.44	138.29	134.92	153.37	165.62	219.93	136.71	122.26	49.73	41.34	53.07			
Nb/Ta	97.50	1210.00	1315.00	225.67	242.50	48.20	39.43	156.50	147.50	127.27	335.45	214.44	26.00			

Lower detection limit for major elements and LOI is 0.01%. Lower detection for REE: (0.5 ppm), Ce (0.5 ppm), Pr (0.03 ppm), Nd (0.1 ppm), Sm (0.03 ppm), Eu (0.03 ppm), Gd (0.05 ppm), Tb (0.01 ppm), Dy (0.05 ppm), Ho (0.01 ppm), Er (0.03 ppm), Tm (ppm), Yb (0.03 ppm), Lu (0.01 ppm) and Y (0.5 ppm).

*Fine-grained biotite quartz feldspar gneiss and quartzites

¹Primarily composed of albite

²Quartzite with carbonate veins



Fig. 12. Quartz-free, Nb-bearing feldspathic rocks. Marker for scale.



Fig. 13. Aegirine carbonatite–fenite contact. Carbonatite is grey, fenite is rusty brown.

immediately adjacent to the complex is characterized by aegirine, with subordinate Na-amphibole (Fig. 14). In one sample, where carbonatite layers are in contact with feldspar, aegirine is particularly coarse (>5 mm). In addition, within fine, feldspar-rich layers, aegirine creates a net-like texture. Carbonatite forms the northern extremity of the rock exposure. As distance from the complex increases, aegirine becomes confined to minor distinct bands, commonly adjacent to carbonatite veinlets, and Na-amphibole becomes the main indicator of fenitization (Fig. 7). Trace amounts of interstitial opaque minerals (including pyrite) are present.

The first outcrops northeast of the biotite carbonatite are quartz-rich schists characterized by white mica and, at least locally, garnet. It is possible that the fenitization zone was truncated by faulting, is simply narrower than 34 metres, or, less likely, that the alkalis were incorporated into white micas (muscovite), potentially forming phengite ($\text{KA}_2(\text{AlSi}_3\text{O}_{10})(\text{OH})_2$) or paragonite ($\text{NaAl}_3\text{Si}_3\text{O}_{10}(\text{OH})_2$). Electron microprobe analyses are required to determine the chemical composition of these micas.

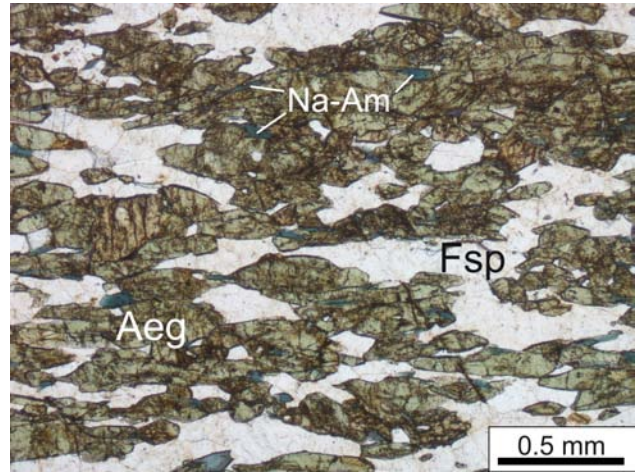


Fig. 14. Aegirine fenite consisting of green aegirine (Aeg), white feldspar (Fsp), blue Na-amphiboles (Na-Am). (Plane-polarized light).

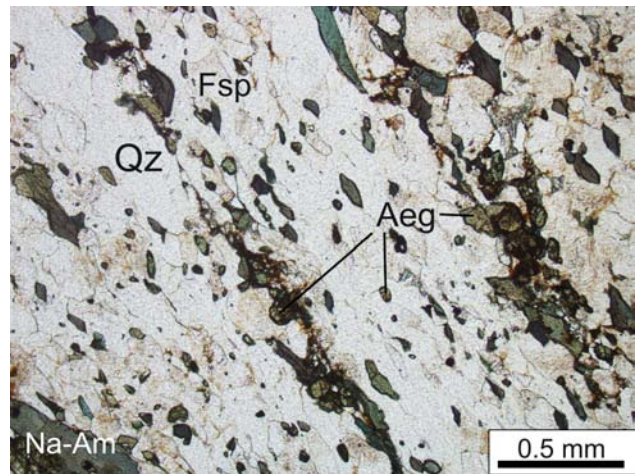


Fig. 15. Fenitized quartzite, 8 metres from the Lonnie complex. Contains quartz (Qz), feldspar (Fsp), small aegirines (Aeg), and strongly pleochroic Na-amphiboles (Na-Am). (Plane-polarized light).

3.5. Fine-grained biotite-quartz-feldspar gneiss and quartzite (metasedimentary rocks)

Fine-grained biotite gneiss is exposed near the southern end of the outcrop. This rock is medium to dark brown on weathered surfaces and medium grey on fresh surfaces. It is difficult to break, tending to separate along planes of weakness 2-20 centimetres apart. Grain size varies within individual gneiss layers. The main leucocratic constituents are quartz ($\approx 25\%$, 0.03-1.4 mm), potassium feldspar ($\approx 20\%$, 0.03-1 mm), and plagioclase ($\approx 25\%$, <1 mm). The proportions of these minerals are difficult to estimate, but collectively they account for more than 60% of the rock. The main ferromagnesian mineral is biotite (<10-30%, <0.4 mm in longest dimension). White mica (<2%, <0.5 cm) is also present along some of the planes coexisting with biotite. Pyrite is present as irregular, oriented, coplanar grains concentrated along the fine-grained layers (<2%, <1 mm). Some of the pyrite grains are fresh; others are partly or entirely converted to hematite. Chalcopyrite is present as

a trace mineral (<0.05%, <0.2 mm), mainly within pyrite. The layers with the finest grains appear to contain dust-like particles of an opaque mineral, probably pyrite and iron oxides. No pyrochlore or minerals belonging to columbite series were observed in this rock. Chemical analyses of these rocks are provided in Table 1, and supports the absence of Nb-bearing ore minerals.

With increasing quartz content, fine-grained biotite gneiss grades into quartzofeldspathic gneiss and quartzite (Fig. 15). The quartzofeldspathic gneiss has a similar appearance and physical properties to the biotite gneiss. However, closer to the carbonatite than the biotite gneiss, it is fenitized. This quartzofeldspathic gneiss is brown on weathered surfaces, gray on fresh surfaces and displays layering and fissility similar to the biotite gneiss. It contains mainly quartz (>40%, <1.4 mm) and alkali feldspar (~40%, <1 mm). Na-amphibole (~5-15%, <0.9 mm) and aegirine (~5-15%, <0.6 mm) are other major constituents. Aegirine tends to be confined to a few bands associated with trace plagioclase and calcite, particularly on the boundaries of calcite veins. Interstitial opaques comprising <1% of the quartzite are locally poikilitic, enclosing small feldspar grains.

4. Lithochemochemistry

Five carbonatite, three quartz-free feldspathic rocks, two fenites, two fenitized metasediments, and a limestone sample (collected nearby to provide background for carbonatite analyses) were analysed (Table 1). The chemical analyses were done by ALS Laboratories in Vancouver. All samples were ground using a steel mill. Major element chemistry was determined using lithium metaborate fusion followed by Inductively Coupled Plasma Emission Spectrometry (ICPES). Loss on ignition (LOI) was determined during the sample fusion (at 1000°C). Total carbon and sulphur were determined using the LECO combustion method. Most of the trace elements were analyzed by lithium metaborate fusion followed by Inductively Coupled Plasma Mass Spectrometry (ICPMS).

These samples show a significant variation in the concentrations of specialty metals (Table 1). The REE content of carbonatites is much higher than in nearby limestone (Fig. 16). The chondrite-normalized REE element pattern of metacarbonatites, quartz-free feldspathic rocks, amphibole (\pm pyroxene)-bearing fenites, and other rocks are similar. None of the samples that were analysed have pronounced Eu anomalies and, as expected, Lonnie carbonatites have higher REE concentrations than associated quartz-free feldspathic rocks and fenites. Based on the geochemical classification diagram of Wilson (1989), the quartz-free feldspathic rock can be geochemically classified as syenites (Fig. 17). These observations suggest that all rock types close to the Lonnie complex were affected by carbonatite-related fluids.

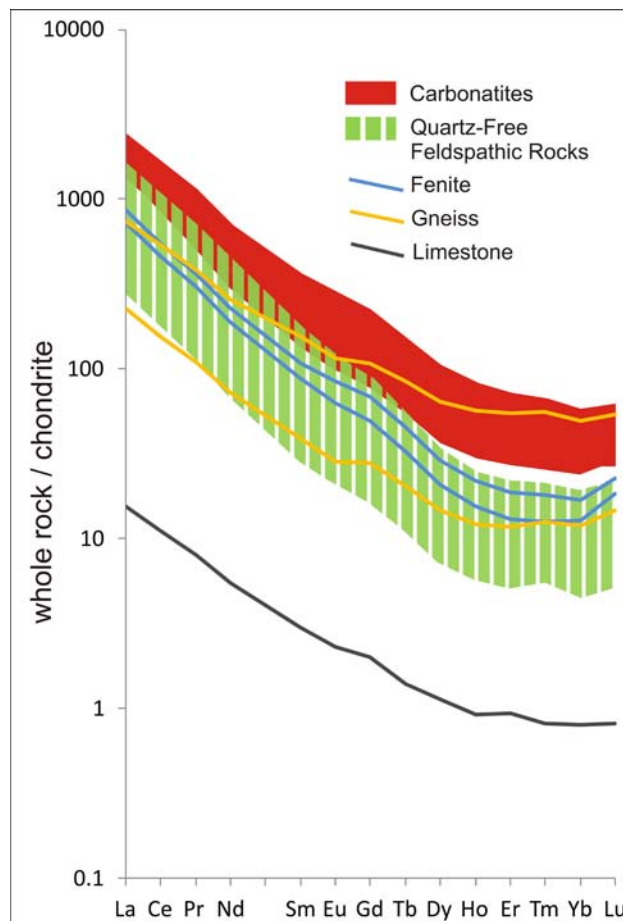


Fig. 16. REE spider plot for samples from the complex and surrounding rocks. Chondrite normalized using values from McDonough and Sun (1995).

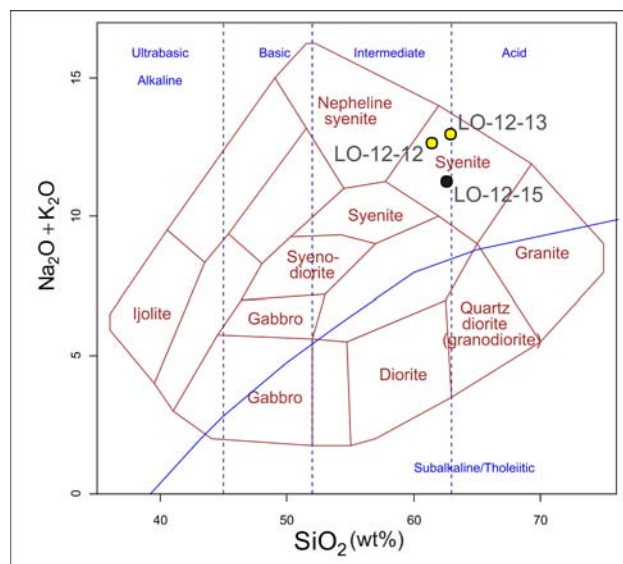


Fig. 17. Quartz-free feldspathic rocks plotted on the TAS diagram for plutonic rocks of Wilson (1989). Samples represented by yellow circles are composed primarily of potassium feldspar. The sample represented by the black circle consists primarily of plagioclase.

4.1. Soil Geochemistry

A cursory examination of geochemical soil survey results conducted in the area by Rara Terra indicates that several Nb and total REE (including Y) anomalies coincide with the projection of Wolverine fault system (Fig. 2). This observation further confirms the importance of the Wolverine fault system as a potential metallotect.

5. Summary

Unlike the larger Aley Carbonatite and Upper Fir deposits, where the Nb and Nb+Ta zones are carbonatite-hosted, historical work at the Lonnie deposit, which lies along the Wolverine fault zone, suggests that, although the carbonatite zones contain significant concentrations of Nb, the highest Nb grades are associated with quartz-free feldspathic rocks. Fenitization extends for more than 30 metres southwestward into the host rock, perpendicular to the strike of the Lonnie mineralization and the Wolverine fault zone. Niobium is probably contained mostly in pyrochlore and unidentified opaque minerals (probably columbite series minerals or fersmite). Electron microprobe analyses are required to positively identify Nb-bearing minerals, and determine the composition of potential indicator minerals. Carbonatites of the Lonnie complex have similar chondrite-normalized REE patterns to related quartz-free feldspathic rocks and fenites; however, they have the highest REE concentrations.

Based on the combination of new aeromagnetic data of Rara Terra Minerals Inc., and previously recognized geological controls, we have moved the projection of the Wolverine fault zone northeastward. The revised projection now connects the Lonnie and Vergil Nb-bearing complexes. The Wolverine Fault Zone probably reflects movement along an old zone of weakness that provided structural control for the emplacement of Nb mineralization in the Lonnie–Vergil area.

Detailed ore and gangue mineralogy, mineral chemistry, and paragenesis based on samples collected during 2012, are currently unavailable. These samples will be examined in a future study using electron microprobe and laser ablation ICP-MS technologies, and the results will be merged with data from other specialty metals-bearing deposits. The results of this research, together with ongoing studies on the tectonic, regional, and deposit-scale controls of other specialty metal deposits, will be used to define parameters permitting vectoring towards high-grade mineralization on regional and deposit scales.

Acknowledgments

The authors wish to thank Alex Kaul and Rebecca Stone for their assistance in the field, as well as preliminary drafting by Alex Kaul. This project received funding and support from Targeted Geoscience Initiative 4 (2010-2015), a Natural Resources Canada program carried out under the auspices of the Geological Survey of Canada. A review by John Veltheer (Rara Terra Minerals Corp.) is greatly appreciated.

References

- Birkett, T.C. and Simandl, G.J., 1999. Carbonatite-associated deposits. In: Simandl, G.J., Hora, Z.D., and Lefebvre, D.V. (Eds.), *Selected British Columbia Mineral Deposit Profiles, Vol. 3: Industrial Minerals and Gemstones*. British Columbia Ministry of Energy, Mines and Petroleum Resources, British Columbia Geological Survey, Open File 1999-10.
- Chisholm, E.O., 1960. Lonnie columbian deposit. British Columbia Ministry of Energy and Mines property file <<http://propertyfile.gov.bc.ca/showDocument.aspx?&docid=138373>> accessed October 2012.
- Colpron, M., Nelson, J.L., 2011. A digital atlas of terranes for the northern Cordillera. British Columbia Ministry of Energy and Mines, British Columbia Geological Survey, GeoFile 2011-11.
- Ferri, F., Melville, D.M., 1994. Bedrock geology of the Germansen Landing – Manson Creek area, British Columbia. British Columbia Ministry of Energy, Mines and Petroleum Resources, British Columbia Geological Survey, Bulletin 91, scale 1:100 000.
- Gwalani, L.G., Moore, K. and Simonetti, A., 2010. Carbonatites, alkaline rocks and the mantle: a special issue dedicated to Keith Bell. *Mineralogy and Petrology*, 98, 5-10.
- Halleran, A.A.D., 1980. Petrology, mineralogy and origin of the niobium-bearing Lonnie carbonatite complex of the Manson Creek area, British Columbia. Unpublished B.Sc. thesis, University of British Columbia, 41 p.
- Hankinson, J.D., 1958. The Lonnie group columbian deposit, Unpublished B.Sc. thesis, University of British Columbia, 32 p.
- Helmel, A., 2012. Rara Terra Minerals receives soil geochemical survey results from Lonnie Project. Press release <<http://www.raraterra.com/investors/news/2012/mar27/>> accessed December 2012.
- Le Maitre, R.W., 2002. *Igneous rocks: A classification and glossary of terms, recommendations of International Union of Geological Sciences Subcommittee on the Systematics of Igneous Rocks*. Cambridge University Press, 236 p.
- Mariano, A.N. 1989a. Economic geology of rare earth minerals. In: Lipman B.R. and McKay G.A. (Eds.) *Geochemistry and Mineralogy of Rare Earth Elements: Reviews in Mineralogy, Volume 21*, pp. 303-337.
- Mariano, A.N. 1989b. Nature of economic mineralization in carbonatites and related rocks. In: Bell, K. (Ed.) *Carbonatites: Genesis and Evolution*. Unwin Hyman, London, pp. 149-176.
- McDonough, W.F., and Sun, S.-s., 1995. The composition of the Earth. *Chemical Geology*, 120, 223-253.
- Papp, J.F., 2012. Niobium (columbium). In: *Mineral Commodity Summaries 2012*; United States Geological Survey, 110-111.
- Pell, J., 1987. Alkaline ultrabasic rocks in British Columbia. B.C. Ministry of Energy, Mines and Petroleum Resources, British Columbia Geological Survey, Open File 1987-17, 109 p.
- Pell, J., 1994. Carbonatites, nepheline syenites, kimberlites and related rocks in British Columbia. British Columbia Ministry of Energy, Mines and Petroleum Resources, British Columbia Geological Survey, Bulletin 88, 136 p.

- Rowe, R.B., 1958. Niobium (columbium) deposits of Canada. Geological Survey of Canada, Economic Geology Series 18, 103 p.
- Rukhlov, A.S., and Bell, K., 2010. Geochronology of carbonatites from the Canadian and Baltic Shields, and the Canadian Cordillera: clues to mantle evolution. *Mineralogy and Petrology*, 98, 11–54.
- Simandl, G.J., Prussin, E. A., Brown, N., 2012. Specialty metals in Canada. British Columbia Ministry of Energy and Mines, British Columbia Geological Survey, Open File 2012-7, 48 p.
- Streckeisen, A.L., 1978. IUGS Subcommittee on the Systematics of Igneous Rocks, classification and nomenclature of volcanic rocks, lamprophyres, carbonatites and melilite rocks, recommendations and suggestions. *Neues Jahrbuch für Mineralogie, Abhandlungen*, 141, 1-14.
- Thompson, R.M., 1955. Lonnie. British Columbia Department of Mines, Minister of Mines Annual Report 1954, A96-A97.
- Vaillancourt, P. and Payne, J.G., 1979. Diamond drilling report on the Lonnie/Pitch claims, Manson Creek area, Omineca Mining Division. British Columbia Ministry of Energy, Mines and Petroleum Resources, Assessment Report 7515, 13 p.
- Wilson, M., 1989. Igneous petrogenesis, a global tectonic approach. Unwin Hyman, London, 466 p.
- Woolley, A.R. and Kjarsgaard, B.A., 2008. Carbonatite occurrences of the world; map and database. Geological Survey of Canada, Open File 5796, scale 1:19 000 000.

The Riddle Creek prospect, an unusual example of Sr-Ba-REE-F mineralization outside the Alkaline Province, British Columbia, Canada

Trofanenko, J.^{1,a}, Williams-Jones, A.E.¹, Simandl, G.J.^{2,3} and Reid, H.M.²

¹ McGill University, Department of Earth and Planetary Sciences, Montreal, QC, H3A 0G4

² British Columbia Geological Survey, Ministry of Energy, Mines and Natural Gas, Victoria, BC, V8W 9N3

³ University of Victoria, School of Earth and Ocean Sciences, Victoria, BC, V8P 5C2

^a corresponding author: joel.trofanenko@gmail.com

Recommended citation: Trofanenko, J., Williams-Jones, A.E., Simandl, G.J., and Reid, H.M., 2013. The Riddle Creek prospect, an unusual example of Sr-Ba-REE-F mineralization outside the Alkaline Province, British Columbia, Canada. In: Geological Fieldwork 2012, British Columbia Ministry of Energy, Mines and Natural Gas, British Columbia Geological Survey Paper 2013-1, pp. 139-148.

Abstract

The Riddle Creek prospect is an unusual occurrence of Sr-Ba-REE-F mineralization in the Okanagan Valley of British Columbia. It is hosted by alkaline volcanoclastic and sedimentary rocks of the Tertiary Penticton outlier, which are interpreted to have formed adjacent to a "Kula-Farallon" slab window, and lies west of the Alkaline Province, hosting the bulk of the known REE mineralization in the province. Macroscopically, the REE-mineralized rocks are fine grained, brown to purple and are contained in a narrow, steeply dipping zone, interpreted to be a shear zone. The surrounding rocks are fine-grained greyish green porphyries comprising anorthoclase and pyroxene in a largely devitrified matrix (Yellow Lake rhomb porphyry). Contacts between the fresh and mineralized rocks are sharp and are most evident by a change in colour from green through yellow and gray, to pale purple (weak mineralization), and dark purple (strong mineralization). This colour change provides an excellent vector to the mineralization. Rocks hosting the REE have been intensely altered, and consist mainly of small fragments of sericitized anorthoclase set in a matrix of purple fluorite, subordinate barite-celestite, and minor dolomite, quartz, and hematite. Alteration was accompanied by major losses of silica, alumina and alkalis (Na+K) and large additions of calcium, fluorine, barium, strontium, and sulphur (sulphate). Unlike most REE deposits, the rare earth elements are not concentrated in a REE-rich phase such as, bastnäsite-(Ce) or monazite-(Ce). Instead, the REE occur mainly as a minor component in barite-celestite and, to a much lesser extent, in fluorite. The prospect is light-REE enriched with a La/Lu ratio of 359 compared to 153 in the unaltered porphyry. The TREO concentration of seven mineralized samples averages 0.7 wt.% and ranges between 0.6 and 0.8 wt.%. Cerium and lanthanum concentrations reach 0.4 wt.% and 0.3 wt.%, respectively. A preliminary model is proposed in which the REE (preferentially the light-REE) were mobilized as chloride complexes by a fluorine-sulphate-bearing hydrothermal fluid of possible magmatic origin and were deposited due to mixing with an external calcium-(strontium-barium)-bearing fluid in a shear zone. The Riddle Creek Sr-Ba-REE-F showing demonstrates the potential for REE exploration opportunities outside the Alkaline Province, particularly in "slab window" tectonic settings of the type represented in the Penticton Tertiary outlier.

Keywords: Riddle Creek, Rare Earth Element prospect, alkaline volcanics, hydrothermal concentration, shear zone, REE-enriched barite-celestite, REE chloride complex, fluid mixing

1. Introduction

The Riddle Creek prospect is an unusual Sr-Ba-REE-F occurrence in the Okanagan Valley, approximately 16 km west of Summerland, outside the British Columbia Alkaline Province, which hosts most of the known rare earth element (REE) mineralization in British Columbia (Fig. 1). The area of the prospect has been explored intermittently since the 1970s for uranium and precious metals. However, its REE potential was recognized relatively recently (Morrison, 2001; Church, 2007; Simandl et al., 2012). The prospect is characterized by low concentrations of U and Th, and is not spatially associated with any U-Th mineralization. Further study may elucidate why this REE prospect is nearly uranium-free, despite its location in a uranium district. Herein we present field, petrographic, SEM, and geochemical data to better document mineralization on the property.

2. Geologic setting

The nature and distribution of REE prospects in British Columbia have been documented in specialty metals compilations (Simandl et al., 2011, 2012). These publications show that the prospects occur predominantly in the NW-SE-trending British Columbia Alkaline Province (Fig. 1), which is largely confined to the Rocky Mountain Trench (Pell, 1994; Simandl, 2011). The Riddle Creek Sr-Ba-REE-F prospect is an exception, and occurs west of this igneous province in alkaline rocks of the Challis-Kamloops belt of south central British Columbia (Church, 2002 and references therein). This belt formed adjacent to a "Kula-Farallon" slab window, and includes the Tertiary Penticton outlier, which comprises the Springbrook, Marama, White Lake, and Marron formations (Church, 1973; Dostal et al., 2003; Church, 2007). The Marron Formation hosts the Riddle REE



Fig. 1. Location of the Riddle Creek Sr-Ba-REE-F prospect.

mineralization, and consists of predominantly Tertiary volcanic rocks that are considered to be coeval with the nearby Coryell syenite plutons (Church, 1971; Church, 1973; Currie, 1976; Souther, 1991). The REE mineralization occurs in the Yellow Lake rhomb porphyry of the Marron Formation (Fig. 2), which consists of anorthoclase and pyroxene phenocrysts in a largely devitrified matrix (Fig. 3). In the area of the prospect, exposure is poor (Fig. 4). However, trenching (Fig. 5) has revealed that the mineralized rocks are in a narrow, steeply dipping zone (Figs. 6 and 7) interpreted to have formed by shearing.

3. Petrography

Near the REE-mineralized zone, fresh rocks of the Yellow Lake rhomb porphyry are greyish-green; weakly altered rocks are light purple. The unaltered rocks contain phenocrysts of primary anorthoclase (40-60%), and rare hornblende (<1%) in a devitrified matrix of clinopyroxene (15-25%), anorthoclase (5-15%), apatite (1-5%), and hornblende and biotite (<1%). Anorthoclase forms subhedral grains up to 0.1 mm long and is commonly replaced by dolomite (20%) and radiating blades of albite (cleavelandite). Outside the shear zone, the Yellow Lake rhomb porphyry shows evidence of propylitic alteration in the form of epidote (1-5%), chlorite (1-5%), and pyrite (1-5%). Within the shear zone, the rocks have been strongly altered. This alteration is evident mainly as secondary fluorite and barite-celestite, which are restricted to the matrix, and dolomite, which also occurs as a rare sieve-textured alteration of anorthoclase. The only primary rock-forming minerals remaining are anorthoclase and rare hornblende and biotite. The altered rocks are purple cataclastic rocks consisting of fine-grained to microcrystalline sericitized anorthoclase (25%), fluorite (20-35%), barite-celestite (15-25%), dolomite (5-15%), lesser quartz (5%), hematite (1-5%), rare biotite (<1%) and hornblende (<<1%). Anorthoclase occurs as angular

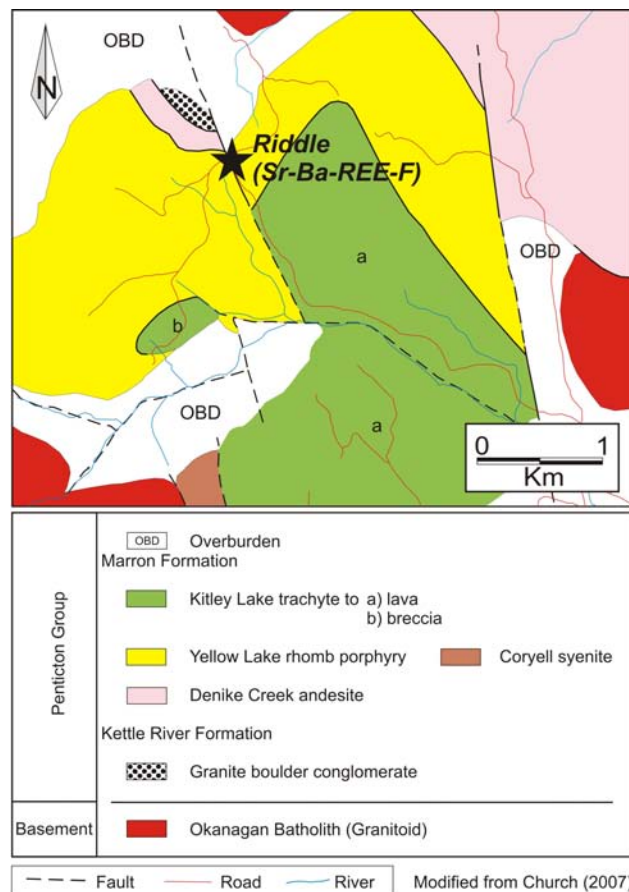


Fig. 2. Geological setting of Riddle Creek Sr-Ba-REE-F prospect (at 49.562 N, 119.888 W). After Church (2007).

to sub-rounded brecciated grains (40 to 600 μm in diameter) in a fine-grained, foliated matrix of fluorite, barite-celestite, dolomite, and quartz (Fig. 8). Hematite occurs as small reddish crystals (10 μm). Based on their cataclastic textures, these foliated rocks are interpreted to represent a shear zone. The high permeability of these rocks resulted in the shear zone becoming a conduit for the passage of hydrothermal fluids and the associated alteration and concentration of the REE.

4. REE mineralogy

No minerals in which REEs are major components were identified, despite a careful search using a SEM equipped with an energy dispersive detector. However, barite-celestite, which occurs as angular grains up to 200 μm in diameter in a fine-grained matrix of fluorite, was shown to contain elevated concentrations of lanthanum and cerium (Fig. 9). The fluorite also contains significant amounts of these elements, but in lower concentrations than in the barite-celestite. Quantitative analyses will be conducted in the near future to determine the REE contents of these minerals.

5. Geochemistry

Twenty-four samples of the Yellow Lake rhomb porphyry and the REE mineralized zone were analysed by ALS Laboratories in Vancouver for bulk and trace element compositions. All samples were ground using a



Fig. 3. Fresh surface of the Yellow Lake rhomb porphyry.



Fig. 4. Riddle Creek prospect. The measuring tape coincides with the base line of Fig. 5.

steel mill. The major element chemistry was determined using lithium metaborate fusion followed by Inductively Coupled Plasma Emission Spectrometry (ICPES). Loss on ignition (LOI) was determined during the sample fusion (at 1000°C). Total carbon and sulphur contents were determined using the LECO combustion method. The other trace elements were analyzed by lithium metaborate fusion followed by Inductively Coupled Plasma Mass Spectrometry (ICPMS). Sample locations are plotted on Fig. 5, and results of the analyses are summarized in Table 1 and illustrated in Figures 10-13.

An immobile element diagram (Winchester and Floyd, 1977) was used to provide information on the

primary nature of the rocks (Fig. 10). Based on their Zr/Ti and Nb/Y ratios, both the Yellow Lake rhomb porphyry and the REE-mineralized zone classify mainly as trachyte and trachyandesite. However, the REE-mineralized samples have higher Zr/Ti ratios, and more of them plot in the trachyte field.

The alteration history of these rocks was traced on a Total Alkali-Silica (TAS) diagram. As expected from their trachyte or trachyandesite composition, all the samples analyzed plot in the alkaline field (Fig. 11). The Yellow Lake rhomb porphyry has been altered; hydrothermal fluids have modified its composition by leaching alkalis and silica in a roughly constant ratio (Fig. 11). Thus, compositions of the Yellow Lake rhomb porphyry are displaced from the trachyandesite field to fields of more mafic alkaline rocks. The same observation applies to the REE-mineralized rocks, except that the leaching was more extreme, yielding rocks with very low alkali and silica contents. This latter alteration reflects pervasive replacement of the host rock by fluorite and barite-celestite. In addition to undergoing extreme leaching of the alkalis and Si, the REE-mineralized rocks experienced extreme leaching of Al and Mg, and moderate leaching of Fe (Table 1 and Fig. 12). These losses were compensated by large additions of Ba, Sr, Ca, F, and sulphate.

The chondrite-normalized REE profiles of samples of the Yellow Lake rhomb porphyry and the REE-mineralized zone are very similar, although the overall REE contents of the REE-mineralized samples are significantly higher (Fig. 13). Both sets of profiles are characterized by light rare earth enrichment and the absence of a europium anomaly. The REE-mineralized samples however, are more enriched in the light REE with a La/Lu ratio of 359 compared to 153 in the Yellow Lake rhomb porphyry. The TREO (Total Rare Earth Oxide) concentration of the seven REE-mineralized samples averages 0.7 wt.% and ranges between 0.6 and 0.8 wt.%. Cerium and lanthanum concentrations reach 0.4 wt.% and 0.3 wt.%, respectively. The absence of a europium anomaly suggests that there was little fractionation of plagioclase during evolution of the magma.

A correlation matrix was generated to evaluate relationships of Ce with elements in the host rocks that may have influenced its concentration (Table 2). As Ce was demonstrated to be an important trace element in barite-celestite, we expected a high correlation coefficient for the Ce-Ba pair. The correlation coefficient for this pair however, is relative modest (0.61). In contrast, the correlation coefficient for the pair Ce-Sr is 0.95. This suggests that Ba must also be present in significant concentrations in another REE-poor mineral, possibly celsian ($\text{BaAl}_2\text{Si}_2\text{O}_8$), a conclusion that is consistent with the relatively modest correlation coefficient of 0.57 between Ba and Sr. Cerium concentration also correlates strongly with that of F (correlation coefficient of 0.87) and Ca (correlation coefficient of 0.81), consistent with the observation that the fluorite contains elevated

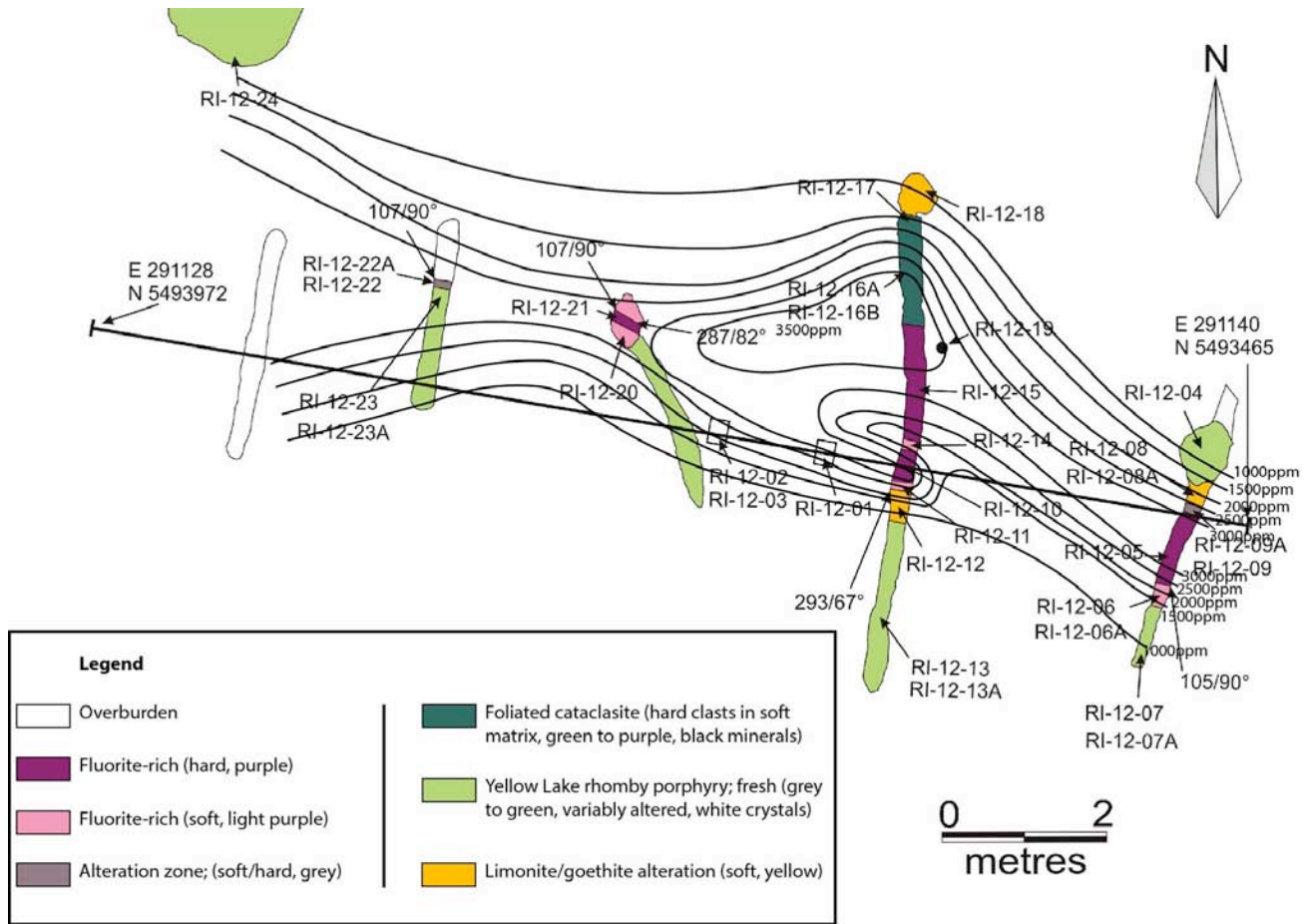


Fig. 5. Geology of the Riddle Creek Sr-Ba-REE-F prospect and isopachs of Ce concentration. The contour interval is 500 ppm.



Fig. 6. Central dark purple rock (mineralized zone; sample RI-12-10), adjacent pale purple rock (weakly mineralized contact zone; sample RI-12-11 and RI-12-14), and outer greyish green zone (fresh porphyry; sample RI-12-12). Pocket knife and measuring tape for scale. See Fig. 5 for sample locations.



Fig. 7. Contact between soft, pale purple and yellow zones; pencil for scale.

Table 1. Chemical composition of mineralized zone and host rocks.

	Detection Limit	RI-12-04	RI-12-05	RI-12-06	RI-12-07	RI-12-08	RI-12-09	RI-12-10	RI-12-11	RI-12-12	RI-12-13	RI-12-13A	RI-12-14
%													
SiO ₂	0.01	50.3	4.83	38.3	42.6	50.4	17.35	3.02	41.7	43.2	47.9	48.3	30.7
Al ₂ O ₃	0.01	14.95	0.58	12.1	13.3	15.3	4.25	0.61	14.95	13.8	13.95	15.7	11.7
Fe ₂ O ₃	0.01	6.47	2.36	7.06	4.93	6.26	2.75	2.19	9.29	5.15	6.03	6.82	8.29
CaO	0.01	6.05	19.8	6.1	6.61	3.02	14.5	20.9	4.64	6.19	6.2	5.5	6.91
MgO	0.01	3.85	0.36	2.63	3.05	3.28	1.4	0.3	3.56	3.27	3.39	3.62	2.26
Na ₂ O	0.01	2.46	<0.01	0.22	0.42	1.77	<0.01	<0.01	0.36	0.45	0.62	0.69	0.1
K ₂ O	0.01	3.75	0.15	3.23	3.73	4	0.87	0.14	3.77	3.68	3.91	4.28	3.34
Cr ₂ O ₃	0.01	0.01	0.01	0.02	0.01	0.02	0.01	<0.01	0.02	0.02	0.01	0.01	0.01
TiO ₂	0.01	0.97	0.05	0.81	0.91	1.01	0.28	0.04	1.01	0.93	0.91	1.05	0.77
MnO	0.01	0.16	0.18	0.09	0.13	0.17	0.09	0.06	0.13	0.13	0.12	0.12	0.12
P ₂ O ₅	0.01	1.31	4.14	2.79	1.76	1.43	4.37	4.84	1.49	1.62	1.57	1.45	3.2
SrO	0.01	0.58	22	5.9	4.12	0.75	14.3	20.3	2.25	2.94	2.45	1.18	6.24
BaO	0.01	0.71	14.1	5.11	2.37	0.81	13.25	15.4	1.43	1.71	1.59	0.63	6.96
LOI	0.01	8.13	5.12	10.25	12.25	9.44	7.09	2.12	11.45	12.1	9.86	9.82	10.6
Total		99.7	73.68	94.61	96.19	97.66	80.51	69.92	96.05	95.19	98.51	99.17	91.2
C	0.01	0.8	1.07	0.06	0.79	0.27	0.09	0.09	0.41	0.79	0.85	0.66	0.13
S	0.01	0.19	9.29	2.83	1.68	0.26	7.27	9.77	0.87	1.13	0.98	0.35	3.52
F	0.01	0.41	7.18	1.88	0.83	0.54	6.14	10.05	0.95	0.79	0.67	0.63	2.21
ppm													
Nb	1	59.6	114.5	80.3	68.8	64.2	114	117.5	61.3	63.5	66.9	65.7	105
Th	1	46.9	25.2	50.5	46.7	47.8	36.8	29.2	44.7	46.5	46.4	51.9	44.9
U	1	7.51	30.2	20.5	14.75	12.15	35.1	27.1	17.8	12.85	14	9.81	45.5
Zr	10	330	20	280	310	340	120	30	310	320	330	370	300
La	0.5	275	2360	944	520	408	2320	2660	409	434	467	314	1315
Ce	0.5	475	3010	1335	790	633	3010	3420	638	691	741	563	1625
Pr	0.03	54.5	251	123.5	77.2	69.1	257	284	63.5	69	73.8	59.5	145.5
Nd	0.1	189	684	380	249	233	726	781	204	223	236	197.5	403
Sm	0.03	25.9	60.9	42.1	29.7	30.1	67.3	69.7	24.9	27.9	29.2	26.8	45.3
Eu	0.03	6.03	16.8	10.1	7.52	7.39	18.7	20.4	6.21	6.83	7.23	6.24	12.75
Gd	0.05	13.45	20.2	17.35	14.25	14.85	23.2	23.7	12.15	13.85	13.65	14.05	20.3
Tb	0.01	1.39	1.97	1.78	1.45	1.5	2.22	2.29	1.29	1.42	1.39	1.43	1.98
Dy	0.05	5.87	8.47	7.8	6.13	6.54	9.83	9.8	5.6	6.13	6.17	6.19	8.04
Ho	0.01	0.96	1.36	1.27	1.02	1.08	1.61	1.61	0.92	1	1.01	1.01	1.3
Er	0.03	2.26	3.18	2.99	2.41	2.56	3.82	3.81	2.2	2.35	2.44	2.38	3.17
Tm	0.01	0.29	0.46	0.41	0.33	0.34	0.54	0.54	0.3	0.31	0.32	0.31	0.48
Yb	0.03	1.82	3.17	2.62	2.1	2.18	3.82	3.83	1.87	2	2.08	1.89	3.11
Lu	0.01	0.28	0.56	0.42	0.33	0.32	0.69	0.72	0.3	0.3	0.31	0.28	0.5
Y	0.5	27.4	47.4	39.5	30.4	30.9	54.4	55.7	27.1	29	30	28.3	45.1
ΣREY		1079.15	6469.47	2908.84	1731.84	1440.86	6499.13	7337.1	1397.34	1508.09	1611.6	1222.88	3630.53

Table 1. Continued.

	Detection Limit	RI-12-15	RI-12-16A	RI-12-16B	RI-12-17	RI-12-18	RI-12-20	RI-12-22	RI-12-23	RI-12-23A	RI-12-24	RI-12-26	RI-12-28
%													
SiO ₂	0.01	9.15	14.7	20.3	40.1	43.7	21.4	5.5	48.2	49.8	50.6	54.6	55
Al ₂ O ₃	0.01	2.66	1.6	5.9	14.8	19.15	8.07	0.31	14.4	14.55	15.2	16.45	16.05
Fe ₂ O ₃	0.01	3.28	1.88	3.85	8.01	7.25	6.96	2.3	7.33	7.04	7	6.27	6.32
CaO	0.01	17.25	8.15	10.35	4.56	2.12	11.4	18.85	6.63	6.28	7.13	4.53	5.55
MgO	0.01	0.87	0.39	1.4	2.8	1.65	1.72	0.21	3.11	2.94	4.32	3.33	3.62
Na ₂ O	0.01	<0.01	<0.01	<0.01	0.37	0.29	<0.01	<0.01	1.33	1.54	3.16	4.06	4.61
K ₂ O	0.01	0.92	0.17	1.32	4.79	3.79	2.36	0.05	4.33	4.43	4.23	4.3	4.53
Cr ₂ O ₃	0.01	0.01	0.01	0.01	0.02	0.02	0.01	0.01	0.01	0.01	0.01	0.01	0.01
TiO ₂	0.01	0.17	0.04	0.28	0.98	1.17	0.51	0.02	0.97	0.98	0.96	0.98	0.93
MnO	0.01	0.07	0.05	0.16	0.6	0.03	0.08	0.06	0.16	0.14	0.15	0.11	0.09
P ₂ O ₅	0.01	4.43	1.88	5.8	2.76	2.5	3.97	4.38	1.18	1.31	1.1	1.12	0.94
SrO	0.01	17.85	21	12.45	2.56	2.55	10.5	21.4	0.78	0.63	0.46	0.45	0.38
BaO	0.01	14.25	19.85	14.1	4.64	1.74	10.05	14.5	0.47	0.39	0.36	0.4	0.34
LOI	0.01	2.79	3.25	6.05	9.41	13.4	8.91	2.59	9.5	8.86	6.77	3.78	2.76
Total		73.7	72.97	81.97	96.4	99.36	85.94	70.18	98.4	98.9	101.45	100.39	101.13
C	0.01	0.07	0.04	0.09	0.06	0.14	0.12	0.38	0.92	0.81	0.88	0.13	0.07
S	0.01	8.67	10.65	7.08	1.59	1.24	5.37	9.94	0.18	0.12	0.02	0.02	0.01
F	0.01	7.87	4.06	2.38	1	0.85	4.39	8.1	0.59	0.52	0.3	0.31	0.22
<i>Ppm</i>													
Nb	1	90.5	58.9	109.5	85.4	70.9	118.5	96.6	57.7	55.8	56.1	58.7	84.6
Th	1	34.8	28	46.4	51.2	55.3	39.4	26.7	46.4	44.8	44.2	46.9	61
U	1	29.6	67	54.1	39.2	45.8	28.5	26.3	8.06	7.15	7.65	8.9	12.7
Zr	10	110	100	150	240	140	160	<20	310	290	320	340	410
La	0.5	2500	2990	2720	1080	468	1940	2540	260	254	211	222	214
Ce	0.5	3170	3570	3450	1495	748	2500	3150	461	463	400	419	391
Pr	0.03	269	296	297	139.5	70	217	267	45.9	47.3	44.1	46.7	41.9
Nd	0.1	758	788	830	392	233	581	730	164	170	150.5	158	142.5
Sm	0.03	70.2	67.7	76.6	45.8	29.3	58.1	62.6	24.2	24.6	21.1	22.2	19.75
Eu	0.03	16.75	15.85	19.35	11.7	6.49	15	17.5	5.2	5.07	4.89	5.07	4.53
Gd	0.05	25	23.7	30.3	23.8	14.8	25.3	25.1	13.6	13.05	10.95	11.25	10.7
Tb	0.01	2.48	2.44	2.98	2.41	1.55	2.48	2.46	1.4	1.33	1.16	1.18	1.18
Dy	0.05	9.82	9.82	11.4	9.18	6.43	9.15	9.05	5.62	5.36	5.09	5.17	5.29
Ho	0.01	1.64	1.68	1.95	1.57	1.11	1.56	1.51	0.96	0.88	0.82	0.84	0.89
Er	0.03	4.11	4.52	4.9	3.98	2.91	3.93	3.84	2.38	2.2	1.97	2.02	2.15
Tm	0.01	0.62	0.74	0.7	0.53	0.41	0.57	0.58	0.31	0.28	0.26	0.26	0.29
Yb	0.03	4.48	5.62	4.61	3.44	2.64	3.71	3.71	1.94	1.76	1.66	1.62	1.84
Lu	0.01	0.83	1.11	0.82	0.53	0.39	0.61	0.65	0.28	0.25	0.24	0.24	0.27
Y	0.5	51.5	53.5	58.7	45.9	31.8	48	44.1	25.3	24.3	22.9	23.5	23.9
ΣREY		6884.43	7830.68	7509.31	3255.34	1616.83	5406.41	6858.1	1012.09	1013.38	876.64	919.05	

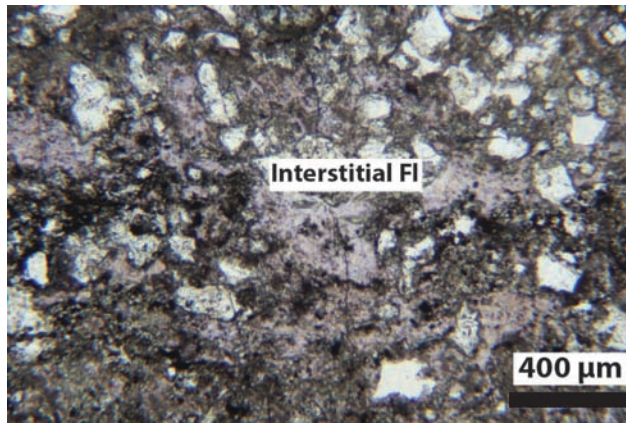


Fig. 8. Subhedral anorthoclase grains (grey) suspended in a pinkish fluorite-rich matrix (Sample RI-12-05).

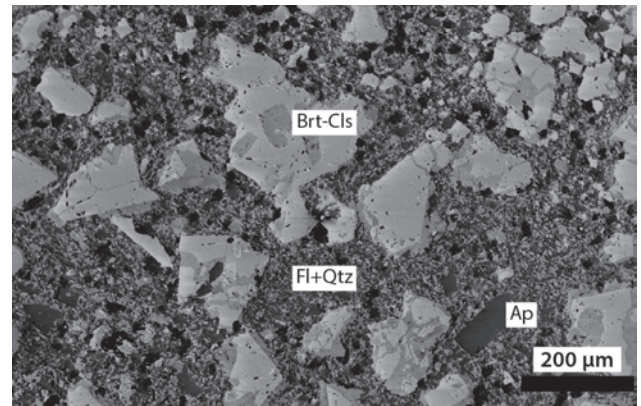


Fig. 9. SEI of sample RI-12-05 showing euhedral barite-celestite grains suspended in a fine-grained matrix of fluorite and silica.

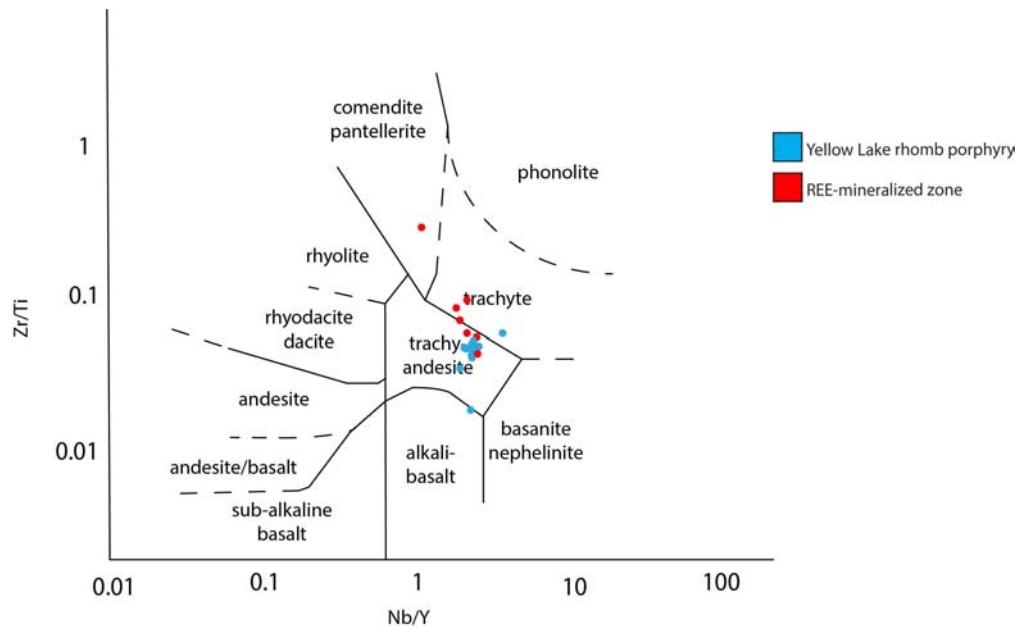


Fig. 10. Immobility element classification of the Yellow Lake rhomb porphyry and the REE-mineralized zone. Samples of both plot in the trachyte and trachyandesite fields. The Zr/Ti values of the REE-mineralized samples are elevated relative to those of the Yellow Lake rhomb porphyry. Modified from Winchester and Floyd (1977).

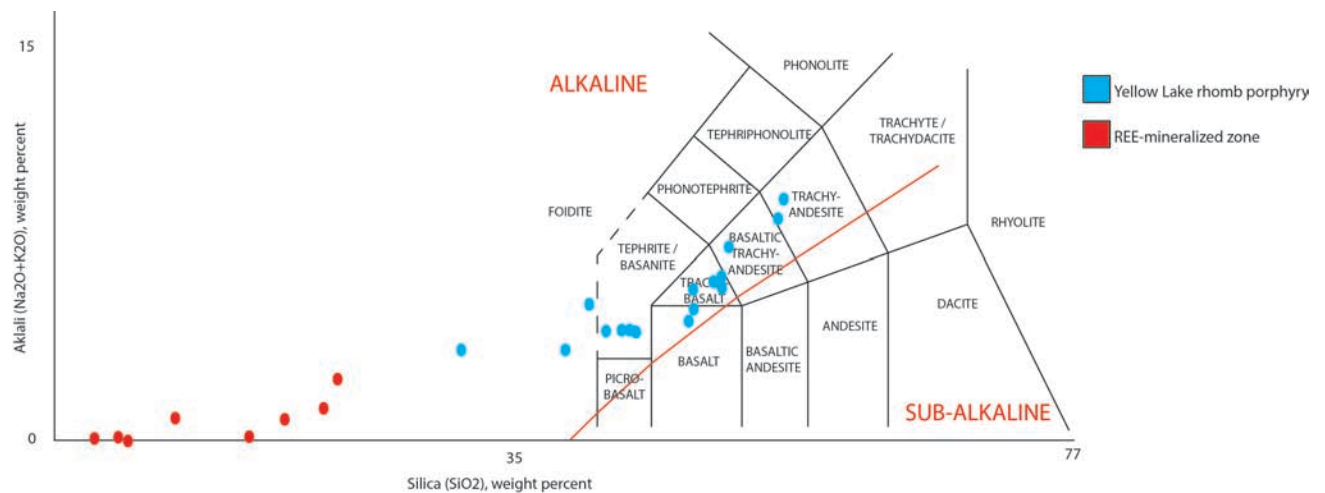


Fig. 11. TAS diagram illustrating the composition of samples of the Yellow Lake rhomb porphyry and the REE-mineralized zone.

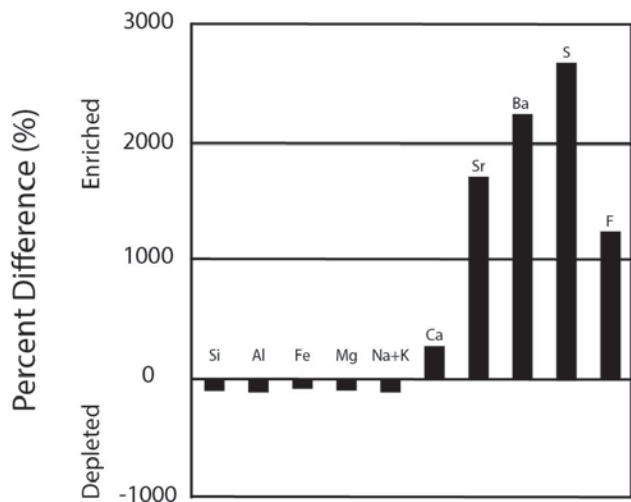


Fig. 12. Mass changes of average mineralized compositions (RI-12-05, RI-12-10, and RI-12-22) with respect to a fresh sample (RI-12-12) obtained from the Yellow Lake rhomb porphyry. Closed system behavior (i.e., constant mass) is assumed.

concentrations of the light REE. Finally, the high correlation coefficient of the Ce-P pair suggests that the rare apatite observed in both the Yellow Lake rhomb porphyry and the REE mineralized zone (Table 2) may have elevated REE contents.

5.1. Spatial distribution of REE

Isopach maps for Ce, Gd, and Y (e.g., Fig. 5) were generated to determine if there was any preferential mobility of individual REE that could be used as a vector towards the mineralization. These maps confirm that the highest REE concentrations coincide with mineralized zone. However, preferential mobility of particular REE was not discerned. The mineralized zone is easily identified by sharp, colour-based contacts from green through yellow and gray (fresh), to pale purple (weak mineralization), and dark purple (strong mineralization). This colour change provides an excellent vector to the mineralization.

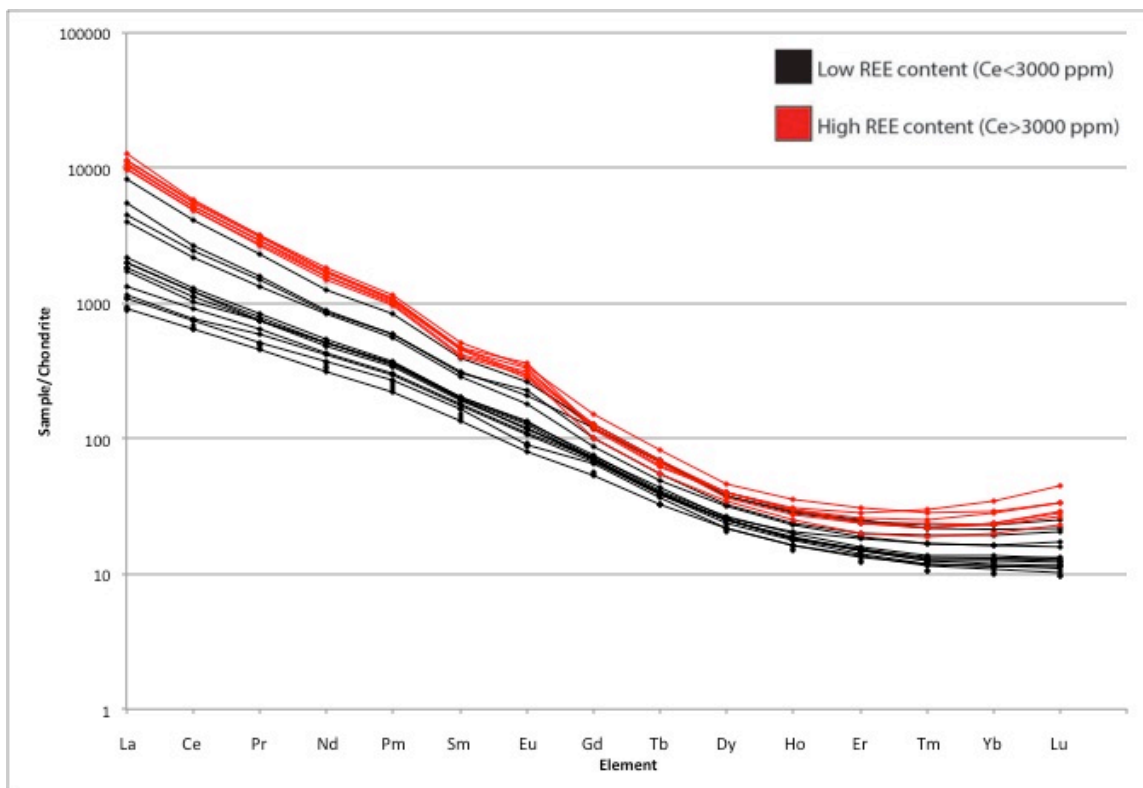


Fig. 13. Chondrite-normalized REE diagram illustrating the relative abundances of the different REE in samples of Yellow Lake rhomb porphyry and the REE-mineralized zone. The chondrite values were obtained from McDonough and Sun (1995).

Table 2. Correlation matrix of selected elements for samples obtained from the Riddle Creek REE prospect.

	Responding Element										
	Ba	Ce	La	Nd	Sm	Yb	Ca	P	Sr	S	F
Ba	1	0.61	0.61	0.62	0.64	0.62	0.37	0.64	0.57	0.99	0.50
Ce	0.61	1	1.00	1.00	0.99	0.93	0.81	0.88	0.95	0.98	0.87
La	0.61	1.00	1	1.00	0.98	0.94	0.80	0.86	0.95	0.98	0.86
Nd	0.62	1.00	1.00	1	0.99	0.93	0.80	0.89	0.94	0.97	0.86
Sm	0.64	0.99	0.98	0.99	1	0.94	0.77	0.91	0.91	0.94	0.84
Yb	0.62	0.93	0.94	0.93	0.94	1	0.57	0.76	0.84	0.89	0.70
Ca	0.37	0.81	0.80	0.80	0.77	0.57	1	0.81	0.88	0.85	0.94
P	0.64	0.88	0.86	0.89	0.91	0.76	0.81	1	0.79	0.78	0.82
Sr	0.57	0.95	0.95	0.94	0.91	0.84	0.88	0.79	1	0.99	0.97
S	0.99	0.98	0.98	0.97	0.94	0.89	0.85	0.78	0.99	1	0.92
F	0.50	0.87	0.86	0.86	0.84	0.70	0.94	0.82	0.97	0.92	1

6. Discussion

The results of the petrographic and geochemical analyses provide insights into the hydrothermal history of the Riddle Creek showing and the possible mechanism of REE enrichment. Mineralization appears to be in a cataclastic shear zone developed at the expense of the Yellow Lake rhomb porphyry (Fig. 10). The evidence of extreme leaching of the alkalis and Mg, and even of an element like Al, which is normally immobile, is strong evidence that the hydrothermal fluid was extremely acid (pH <2); at low pH, dissolution of silica is pH independent but is favoured by high HF activity. A preliminary model is proposed in which the REE (preferentially the light-REE) were mobilized by a fluorine-sulphate-bearing, chloride-rich hydrothermal brine of possible magmatic origin. As HF is strongly associated at low pH, thereby restricting the availability of F⁻, and REE-fluoride mineral solubility is very low, fluoride complexing of the REE is precluded (Williams-Jones et al., 2012). It is therefore proposed that the REE were transported as chloride complexes; such complexes transport the light REE preferentially. Sulphate complexes may also have played a role in REE transport, but would not have contributed to the observed light REE enrichment. Finally, it is proposed that deposition of the REE occurred as a result of mixing of the ore fluid with an external Ca-Sr-Ba-bearing fluid in a shear zone cutting the Yellow Lake rhomb porphyry; the very low solubility of fluorite, barite, and celestite require that their constituent components were transported separately. This mixing increased the pH of the fluid and ore mineral components, leading to supersaturation of barite-celestite and fluorite, and in turn, the concentration of the light REE by incorporating them in their structures.

7. Conclusions

The Riddle Creek Sr-Ba-REE-F prospect demonstrates the potential for REE exploration outside the Alkaline Province, particularly in “slab window” tectonic settings like those represented in the Pentiction Tertiary outlier. Unlike most REE deposits, the rare earth elements are not concentrated in a REE-rich phase such as bastnäsite-(Ce) or monazite-(Ce). Instead, the REE occur mainly as a minor component in barite-celestite and to a much lesser extent in fluorite. The association of REE to fluorite (purple) provides a macroscopically observable colour-based pattern, which may be used as a vector to the ore. The Riddle prospect is also unusual by having anomalously low contents of U and Th relative to other occurrences in the district.

Acknowledgments

The authors wish to thank Alex Kaul and Rebecca Stone for their assistance in the field, and Alex Kaul for his preliminary drafting of the maps. This project received funding and support from Targeted Geoscience Initiative 4 (2010-2015), a Natural Resources Canada program carried out under the auspices of the Geological Survey of Canada.

References cited

- Church, B.N., 1971. The geology of the White Lake basin. In: *Geology, Exploration and Mining in British Columbia, 1970*, British Columbia Department of Mines and Petroleum Resources, pp. 396-402.
- Church, B.N., 1973. *Geology of the White Lake Basin*. British Columbia Department of Mines and Petroleum Resources, British Columbia Geological Survey Bulletin 61, 120 p.
- Church, B.N., 2002. *Geology of the Pentiction Tertiary outlier*. B.C. Ministry of Mines and Energy Resources, British Columbia Geological Survey Geoscience Map 2002-5, scale: 1:50 000.
- Church, B.N., 2007. *Geological and geochemical evaluations of the Riddle Creek Claims, Riddle Creek, Osoyoos Mining Division, British Columbia*. British Columbia Ministry of Energy, Mines and Petroleum Resources, Geological Survey Branch Assessment Report 28970.
- Currie, K.L., 1976. The alkaline rocks of Canada. *Geological Survey of Canada Bulletin* 239, 229 p.
- Dostal, J., Breitsprecher, K., Church, B.N., Thorkelson, D., and Hamilton, T.S., 2003. Eocene melting of Precambrian lithospheric mantle: Analcime-bearing volcanic rocks from the Challis Kamloops belt of south central British Columbia. *Journal of Volcanology and Geothermal Research*, 126, 303-326.
- McDonough, W.F., and Sun, S.-s., 1995. The composition of the Earth. *Chemical Geology*, 120, 223-253.
- Morrison, M.S., 2001. *Geochemical assessment report on the Vent Claim Group Summerland area, Osoyoos Mining Division*; British Columbia Ministry of Energy Mines and Petroleum Resources. Assessment Report 26750, 33 p.
- Pell, J., 1994. *Carbonatites, nepheline syenites, kimberlites and related rocks in British Columbia*. British Columbia Ministry of Energy, Mines and Petroleum Resources, British Columbia Geological Survey, Bulletin 88, 136 p.
- Simandl, G.J., Prussin, E.A., and Brown N., 2011. *Specialty (rare) metals in British Columbia, Canada*. British Columbia Ministry of Energy and Mines, British Columbia Geological Survey GeoFile 2011-10, scale: 1:2 000 000.
- Simandl, G.J., Prussin, E.A., Brown N., Hancock, K. and Meredith-Jones, S., 2012. *Specialty (rare) metal-bearing deposits in British Columbia, with selected examples*. British Columbia Ministry of Energy and Mines, British Columbia Geological Survey GeoFile 2012-2.
- Souther, J.G., 1991. Volcanic Regimes. In: Gabrielse, H., Yorath, C.J. (Eds.), *Geology of the Cordilleran Orogen in Canada*. Geological Survey of Canada, *Geology of Canada* 4 (also Geological Society of North America, vol. G-2), pp. 457-490.
- Williams-Jones, A.E., Migdisov, A.A., and Samson, I.M., 2012. Hydrothermal mobilization of the rare earth elements – a tale of “ceria” and yttria”. *Elements*, 8, 355-360.
- Winchester, J.A., and Floyd, P.A., 1977. Geochemical discrimination of different magma series and their differentiation products using immobile elements. *Chemical Geology*, 20, 325-343.